JOURNAL OF RESEARCH of the National Bureau of Standards
Vol. 86, No. 6, November–December 1981

Contents

Papers Presented in the Asian/Pacific American Heritage Week Program held at the National Bureau of Standards, Gaithersburg, MD, May 4–11, 1979

Library of Congress Catalog Card Number: 63-37059

For sale by the Superintendent of Documents, U.S. Government Printing Office.
Washington, D.C. 20402. Order by SD Catalog
No. C13.22/vol. 86(6). Single copy price $4.25 Domestic: $5.35 Foreign.
Subscription price: $18.00 a year; $4.00 additional for foreign mailing.

UNITED STATES GOVERNMENT PRINTING OFFICE, WASHINGTON: 1981

JOURNAL OF RESEARCH of the National Bureau of Standards
Vol. 86, No. 6, November–December 1981

Turbulence, Plasma Containment, and Galaxies*

C.C. Lin

Massachusetts Institute of Technology, Cambridge, MA 02139

August 5, 1981

These three exciting areas of research, apparently disjointed in content, have similar basic mechanisms in common which can be described by the same mathematical principles, concepts, and methods. Scientific problems will be discussed in all three areas. Emphasis will be placed on galaxies, where observational data are plentiful for checking the theory. A unified mathematical approach applicable to all three areas will then be described.

Key words: density wave; galactic spirals; hydrodynamic instability and turbulence; plasma dynamics; spiral grand design; WASER; winding dilemma.

1. Introduction

Dr. Dillon, Miss Smith, Mr. Tsai, ladies and gentlement, I am indeed honored by your invitation for me to speak on the occasion marking the contribution of American citizens of Pacific and East Asian heritage. I am especially pleased by the fact that I, as a Chinese-American, have been chosen to speak today, May 4th, 1979. For this day marks the 60th anniversay of the celebrated May Fourth Movement, which is generally recognized as the most important milestone of vigorous new cultural developments in modern China.

My talk will be devoted to a discussion of the similarities and differences among the three subjects mentioned in the title. By using these as examples, I also hope to explain the basic theme of an applied mathematician (physical mathematician); that is, the fundamental concepts and mechanisms that show similar mathematical characteristics are also physically similar, and *vice versa*. [These discussions were presented but omitted from this abbreviated record.]

Since my current research work is on the spiral structure of galaxies, I shall begin my discussion with this subject.

2. Galaxies

A galaxy is essentially a collection of stars. Galaxies exhibit a variety of morphological appearances: elliptical, spiral, bar-spiral, and irregular. In figure 1, we show the spiral galaxy M81 in an optical photograph. In figure 2, we show the same galaxy observed in radio-frequency at a wave length of approximately 21 cm. The latter waves are emmitted by hydrogen atoms, which exist in the galaxy (instead of the molecular form) because the medium is so rarefied. We note that the spiral structures observed in optical and in radio frequencies are quite similar. Such spiral structures are observed in many galaxies.

How do we explain these spiral features? Let me first clarify the issues by quoting from the famous Dutch astronomer, Professor Jan Oort, who has been studying galaxies for the past 50 years:

> "In systems with a strong differential rotation, such as is found in all non-barred spirals, spiral features are quite natural. Every structural irregularity is likely to be drawn out into a part of the spiral."

That is, since the galaxy is in a disc form, with a nucleus in the middle, it must be rotating, otherwise self-gravitation would have pulled it together. It turns out that the inner part is rotating faster than the outer part, in such a manner that the liner velocity of rotation is nearly constant. So the inner part, say at the distance of 5 kiloparsecs from the center, is rotating twice as fast as the outer part at 10 kiloparsecs. (One parsec is about 3.3 light years.) Since the inner part rotates faster, any material clump would be stretched out into a part of a spiral structure.

> "But this is not the phenomenon we must consider. We must consider a spiral structure extending over the whole galaxy from the nucleus to its outermost part, and consisting of two arms starting from diametrically opposite points. Although this structure is often hopelessly irregular and broken up, the general form of the large scale phenomenon can be recognized in many nebulae [galaxies]."

*(This is an abbreviated rendition of a lecture delivered at the National Bureau of Standards on May 4, 1979, as a part of the program to mark the Asian/Pacific American Heritage week.)

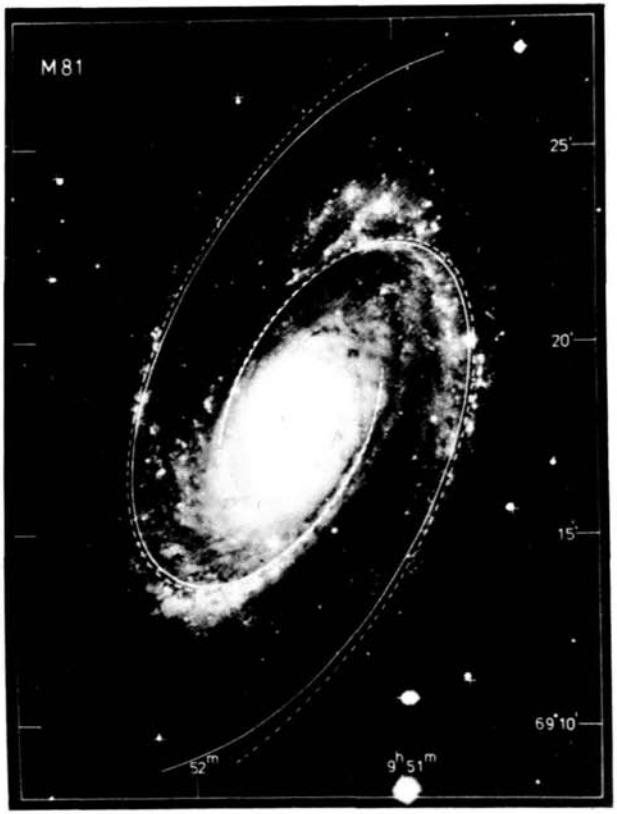

FIGURE 1. The spiral galaxy M81 according to optical observations. The line drawings show the locations of the shock wave in the interstellar medium and the minimum of gravitational potential. Both lie close to the dust lane.

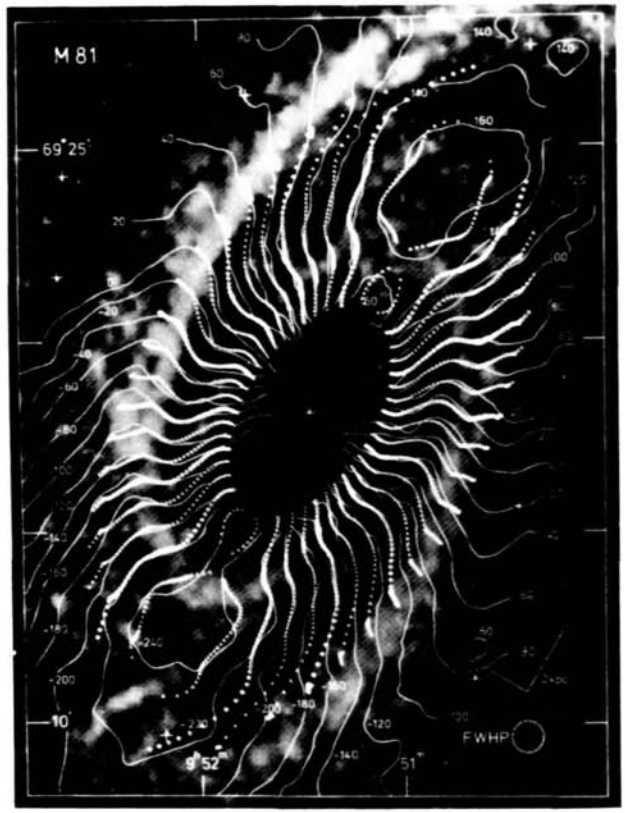

FIGURE 2. The spiral galaxy M81 according to radio observations at 21 cm. wavelength. The line drawings show the iso-velocity lines according to observations and according to theoretical calculations.

This issue is often referred to as the existence of *grand design.*

The other problem is the so-called winding dilemma, i.e., spiral galaxies, especially normal spiral galaxies, are classified by Hubble (see fig. 3) according to the tightness of winding into Sa, Sb, and Sc sprials, Sc being the most open. You might imagine that because of differential rotation, Sc galaxies would soon wind toward Sa, because the inner part is rotating faster, and like a spool of string, would therefore tend to become tighter and tighter with rotation. But this is not observed to be the case. Of course we cannot directly follow the evolution of galaxies in our lifetime: this winding would occur on the order of a few hundred million years. However, we can make a *statistical* study and show that Sc galaxies and Sa galaxies are physically different through the observation of other physical characterisitcs; for example, the gas content in Sc is much higher than in Sa. You can say that Sc galaxies would have their gas formed into stars and then become Sa at the same time. But if that were so, the average mass and the number of stars formed would be so large that Sc galaxies would be much more brilliant than they actually are. Furthermore, the mass distribution is such that there is a very small nucleus in Sc galaxies whereas Sa galaxies have more massive nuclei. It is impossible for mass to accumulate so rapidly because the angular momentum in the system cannot be adjusted so quiclkly. Thus, the evolution from Sc to Sa in a reasonable period of time is ruled out, and they must be rather permanent structures. The question is: If we have material objects arranged like that in an Sc galaxy, why does it not wind down to an Sa structure? This is the so-called *winding dilemma.*

The answer is, as it turns out, that Sc and Sa galaxies have their large scale spiral structure in the form of permanent or nearly-permanent *wave patterns.* These patterns have now been calculated by using a number of methods and the mechanisms for their maintenance have been understood. Waves over a system in differential rotation are well-known in the study of turbulence. Theory of instabilities of this kind goes back to Lord Rayleigh, in 1880, and has been developed over the years. There were mathematical difficulties, so the theory was not fully developed until much later. There were also experimental difficulties, so the

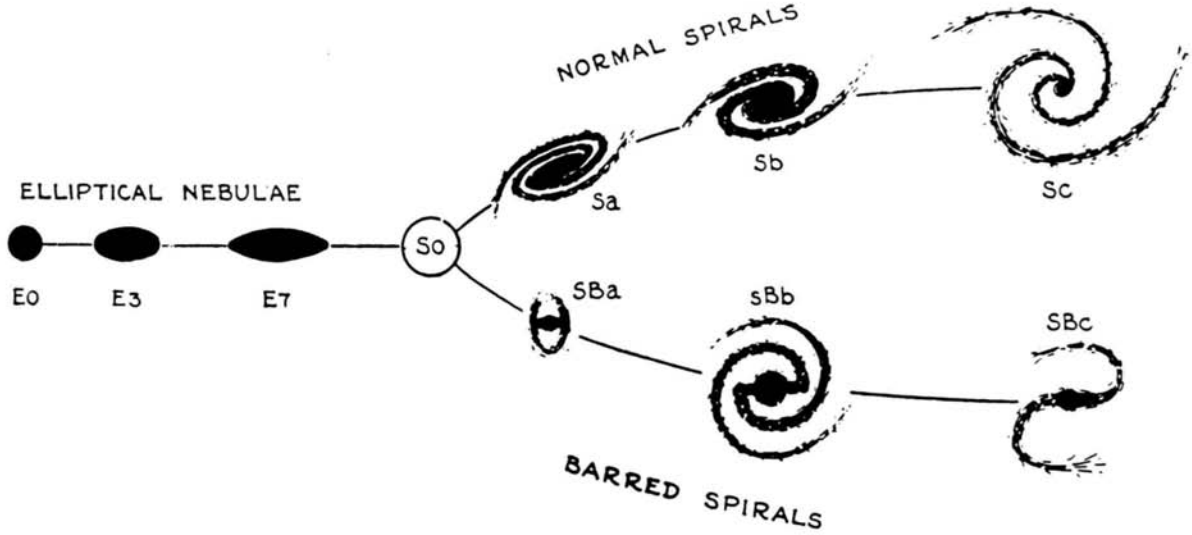

FIGURE 3. Hubble classification of galaxies.

theoretical predictions were not checked until the work at the Bureau of Standards was carried out by Dryden, Schubauer, Klebanoff and their collaborators. It is generally accepted that the calculated instabilities in a sheared boundary layer were verified by these experiments. More recently, in Japan, they have also checked the calculations for the more classical case of flow through a channel. Thus, we are applying these well-known concepts of waves of permanent structure over a system in differential motion (in shear) to the study of galaxies.

The other question is: What are those brilliant stars which mark the waves? How do they behave? They are, as a matter of fact, like the white caps on the ocean: they come and go, they are formed and then they disappear. They are now believed to form out of the interstellar medium (the gas) and then shine brilliantly by burning their nuclear fuel. After exhausting their nuclear fuel, they disappear with a bang, a supernova explosion. Can these things happen over the time period under consideration? Indeed the answer is: Yes! For the time scale for the evolution of such brilliant stars into the supernova state and then into the white dwarfs is one to ten million years, and the time of one period of revolution of the galaxy is about 200 million years. So it is during a small fraction of a period of revolution of the galaxy that the whole phenomena of star formation and star disappearance can occur, and they are no more permanent than the white caps at the crest of waves on the ocean. This is another example where the concepts used to explain the phenomena of turbulence, hydrodynamics, and galaxies get together.

Let me provide some more details. Let us assume the existence of a rotating wave pattern, and imagine ourselves in a moving system in which the wave pattern is fixed (cf. fig. 4). The flow of the interstellar medium follows the arrow, and as it enters the density peak (the gravitational minimum), the material would undergo an oblique shock

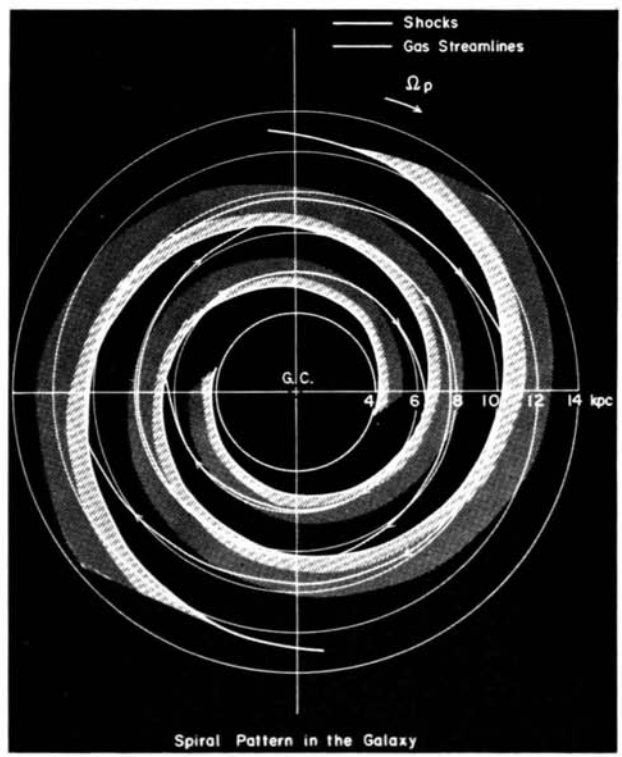

FIGURE 4. Gaseous flow in a galaxy when there is a spiral gravitational field. Streamlines are marked with arrows indicating the direction of gaseous flow. The shocks are the heavy solid lines next to the hatched regions.

which suddenly compresses the material and turns its flow direction. This oblique shock forms a part of the spiral arm. The material passing through the spiral arm follows the arm over a considerable distance, and goes to the next arm where it goes through another shock compression in the same way, and comes around and closes the loop (approximately). So the gas is going around not along a circular path, but in a slightly distorted orbit which has two shocks near the two spiral arms. At these shocks, interstellar medium is compressed, forming stars out of a part of the gas. As the stars emerge from these shocks, they go further and they disappear when their nuclear fuel is burned out. The bright part of this diagram is the region of star formation and star evolution. As the hydrogen gas is compressed by the shock, molecules are formed in the dense clumps of gas. There are also dust particles composed of elements of higher atomic weights. So one would see, at the first sign of compression, a rather dark region—the dust lanes. (See figs.

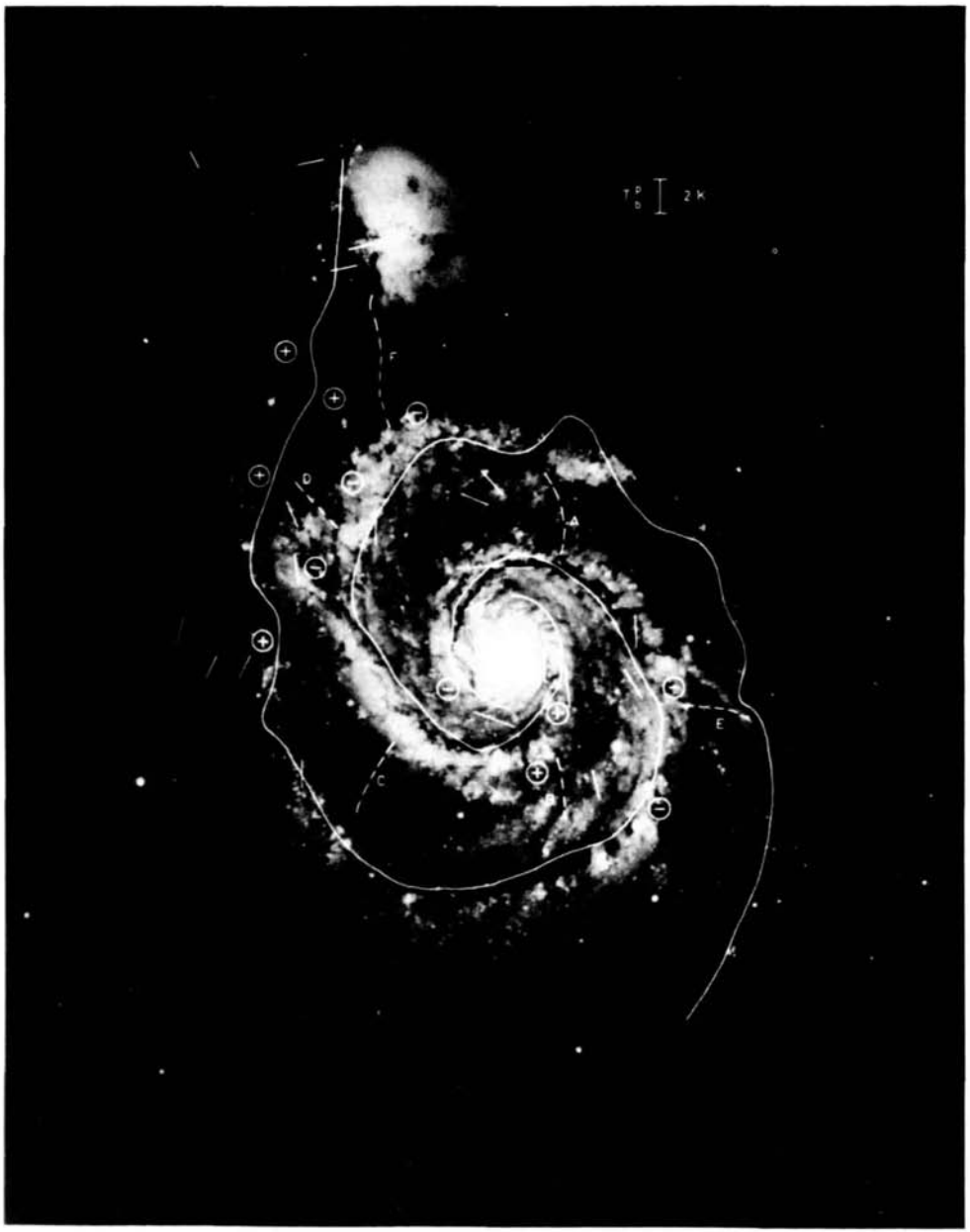

FIGURE 5. LEFT PICTURE: The location of the peak of the synchrotron emission in the right picture is shown and seen to coincide with the location of the dust lane.

1 through 5). This is followed immediately by a region of bright young stars, which are expected to be very bright, and in fact blue in color. This is indeed what is observed. In any case, in the region of compression, one would also expect to see a concentration of atomic hydrogen in the slightly less brightly shaded area.

The young stars stand out well in the galaxy M51 in blue light. These young stars are indeed in a very narrow band because their age is short and they do not move very far before they burn themselves out. Through a study of the nuclear reactions in stars, one can develop a connection between their color and their luminosity. The blue stars are very luminous, but they also burn out quickly.

The Dutch astronomer Herman Visser has constructed a model (cf. fig. 1) for the galaxy M81 based on these concepts. In Visser's model, the shock essentially matches the observed dust lanes (one is shown in dotted line and one in solid line). He calculated the flow field of atomic hydrogen

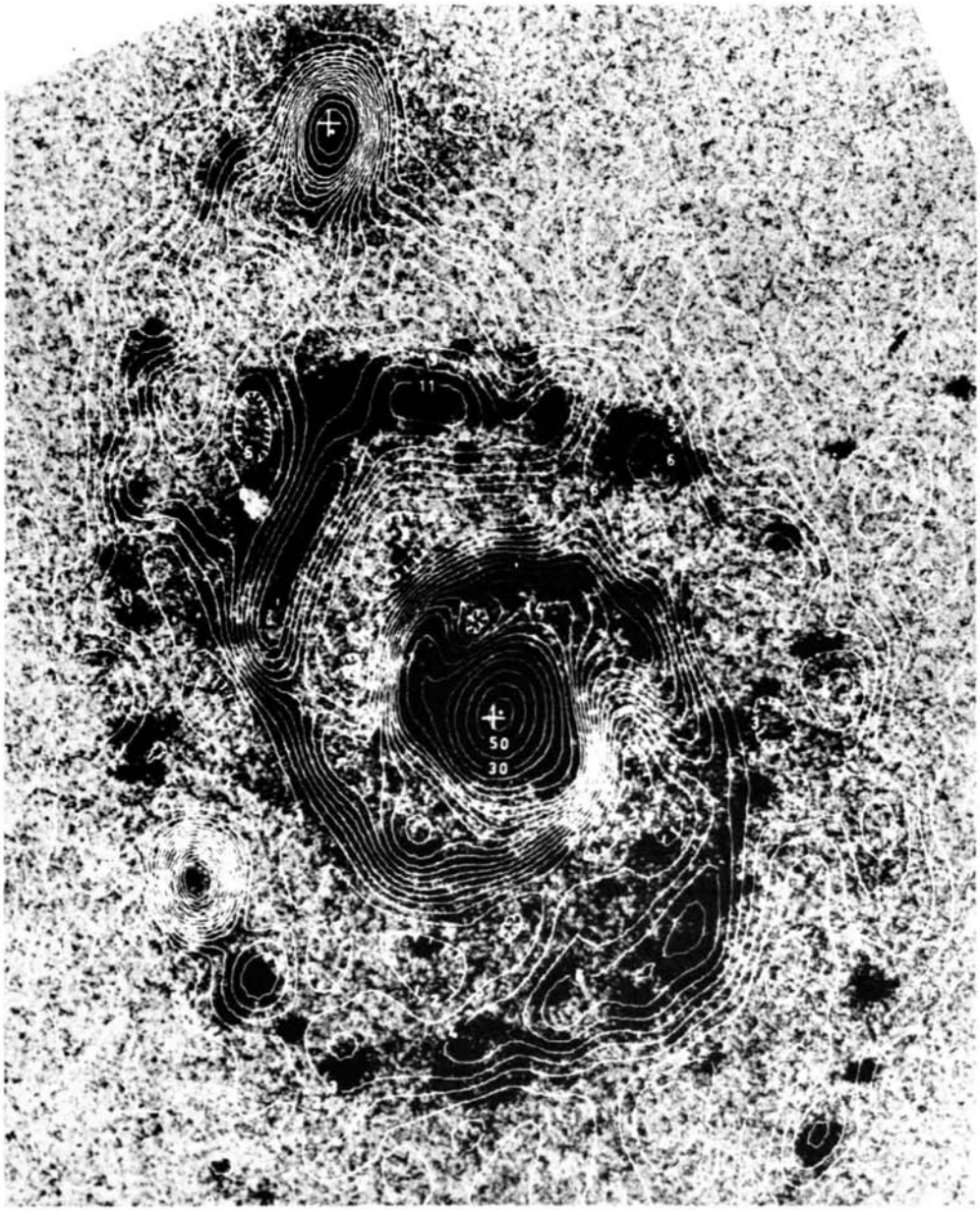

FIGURE 5. RIGHT PICTURE: The continuum radio map (at 20 cm) of the galaxy M51.

and its distribution in this galaxy, given such a gravitational field. The calculated motion of atomic hydrogen is shown in terms of iso-velocity lines; so are the data from observations (see fig. 2). Indeed, the quantitative agreement is very good.

Can we see the density variation postulated in the theory? It is not easy, but it has been done. Now, the bright young stars which we see on the spiral arms are not the ones which determine the gravitational field, because they are very few in number. We must look beyond those stars, i.e., we must filter out their light and look at the background stars which are more like the sun, a rather average, dim star. The bright stars are essentially those which are colored blue and the dim stars essentially red. The astronomer Schweitzer made the necessary observations with proper filters. When the blue color is filtered out and the color is essentially orange, one sees the fairly regular variations in the orange components from the dim stars. On the other hand, a rather chaotic variation is seen superposed when the blue components are put in. This work was done during just the past three years, so it could still be improved upon. But basically the results bear out the idea that there is a small density variation on the order of 10-20% (closer to 10%) in the actual density of the stellar mass.

There is another way to look at the existence of density waves. Roberts and Yuan made a calculation which predicted what is shown on the left hand side in the next figure (fig. 5). In this galaxy (M51), you can see very clearly the dust lane which is marked out by the dark strip side-by-side with the bright stars. The line drawn along this lane is not a physical object, but is drawn to show the location of the peak of synchrotron emission as explained below. Now we know that there is a shock, so there is a compression of gas. If there is a magnetic field, that compression would also strengthen the magnetic field because the latter is frozen into the material. So one would expect a strong magnetic field at the dust lane. This stronger magnetic field would manifest itself by the stronger synchrotron radiation from this region, because there are charged particles moving at relativistic speeds in the galaxy. Those particles would then emit at very high frequencies and one can detect them as a continuum emission. The right picture in figure 5 is an observed map of this emission by the radio telescope. The results indeed show a peak as indicated in the diagram on the left. The line was in fact drawn by the observers from the map on the right. So the results do show that there is a stonger radiation at the dust lane where the theory predicts a stronger radiation due to the strengthening of the magnetic field by a galactic shock.

We have thus seen two sets of data, one in M81 and another in M51, supporting the density wave theory. There are many other phenomena which have been observed to agree with the predictions based on the density wave theory.

3. Basic concepts and mechanisms

We record briefly some of the basic concepts and mechanisms visualized for the explanation of the observed phenomena.

(1) The above discussion places emphasis on the winding dilemma and on the existence of grand design. One should recall that the spiral structure in galaxies is indeed "often hopelessly irregular and broken-up" and hence there is *coexistence* of regular spiral patterns and spiral features in bits and pieces. Some of these may be material arms; others, waves. This situation is not very much different from that in a turbulent jet which shows both small scale chaos and large scale structures. There are only a few prominent large-scale modes, and hence at any instant the large-scale structure shows quite a deal of regularity. Hot-wire anenometer records of turbulence motions in a boundary layer (NBS) show similar behavior.

It is a matter for speculation how much regularity may be expected in the observed patterns of galaxies. In the above discussions, we assume a considerable amount of regularity and hence we conclude that it is indeed possible to have the Hubble classification in a *statistical* sense. Further detailed studies are desirable to clarify these issues.

(2) There are a number of similarities in mechanisms among the three subjects under discussion: galaxies, turbulence, and plasmas. We shall only record some of them without detailed explanation. [More details were given in the verbal presentation.]

(A) Both in hydrodynamic stability and in the study of spiral waves in galaxies, corotation resonance plays an important role in energy transfer.

(B) Analogous mechanisms may be found between the instability of the ballooning mode in contained plasmas and the instability of Couette flow with inner cyclinder rotating.

(C) The WASER mechanism (wave amplification by stimulation of emitted radiation) is important for spiral wave patterns in galaxies, as well as in plasma dynamics and in the instability of supersonic shear layers. It includes the interaction of wave of positive and negative energy densities.

(D) There is similarity between the density waves in galaxies and the Bernstein waves in magentically contained plasmas. This is due to the similarity between the Coriolis force in the former case and the Lorentz force in the latter case.

(3) *A unique feature.* The maintenance of density wave patterns must depend on waves propagating in opposite directions. A naive view would then require the existence of leading waves and trailing waves, and we may expect to find

only bar-like structures. Actually, there are *two* kinds of trailing waves propagating in opposite directions (see fig. 6). Thus, one can even form pure trailing spiral wave patterns without any leading component. Obviously, there are also barred spirals, which has contributions from leading components.

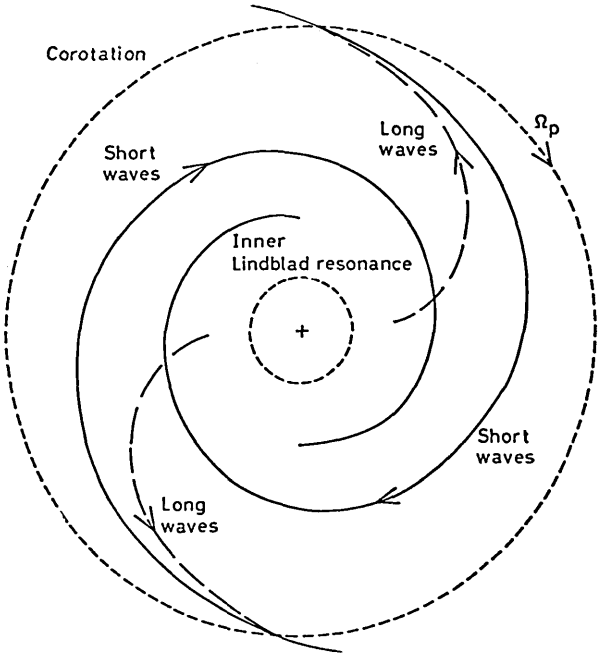

FIGURE 6. Schematic diagram showing composition of a spiral pattern by two trailing waves.

4. Concluding Remarks

Since this is an occasion to mark the contribution of Asian Americans, I should mention that a number of important contributors to the subjects under discussion are Asian-Americans. Contributors to the older subject of turbulence are too numerous to be named. However, I do wish at least to mention four persons who contributed both to plasma physics and to the study of the dynamics of stellar systems. They are James Mark, Y. Y. Lau, Linda Sugiyama, and C. S. Wu. If one examines the list of references in this subject one finds that the contribution of Asian-American scientists far outweighs the total percentage of Asian-Americans in the population as a whole. We have in this country, indeed, great opportunities for all ethnic groups, especially in science. By its very nature, science has a tendency to permeate international boundaries. Science and scientists do have a very important role to play in promoting mutual understanding among the countries in this world. American scientists with special ethnic backgrounds can contribute greatly to this effort. With this hopeful note, let me thank you again for inviting me here, and I wish you great success with the rest of your program.

JOURNAL OF RESEARCH of the National Bureau of Standards
Vol. 86, No. 6, November–December 1981

Highlights in Semiconductor Device Development

L. Esaki

IBM Thomas J. Watson Research Center, Yorktown Heights, NY 10598

August 4, 1981

Following a brief description of early semiconductor history, the invention of the transitor and subsequent important events are presented in perspective, with emphasis on the role of semiconductor physics in device development.

Key words: diode; field-effect transitor; IMPATT diode; integrated circuit; LASER; LED; photocell; solar cell; solid state; transitor; tunnel diode; III-V compounds.

I. Introduction

The agricultural civilization in the cultural history of man was said to be the result of two genetic accidents which gave birth to a new species of bread wheat some 10,000 years ago, involving wild wheat and goat grass. Large-scale agricultural activity in man's society followed. Great inventions or discoveries could be considered to be such genetic accidents—mutations. New knowledge, arising from these inventions, often leads to a large-scale engineering effort which eventually has far-reaching consequences in our society. The invention of the transistor by three solid state physicists, Shockley, Bardeen, and Brattain, is one such example. The development of the transistor began in 1947 through interdisciplinary cooperation with chemists, metallurgists, and electronic engineers, at Bell Laboratories. A large-scale development effort for a variety of semiconductor devices followed in a number of institutes throughout the world. Semiconductor know-how, thus established, has revolutionized the whole world of electronics—communications, control, data processing, and consumer electronics.

One of the major achievements of modern physics has been the success of solid-state physics in creating new technologies. Solid-state physics, which involves experimental investigation as well as theoretical understanding of the physical properties of solids, constitutes, by a substantial margin, the largest branch of physics; probably a quarter of the total number of physicists in the world belong to this branch. Semiconductor physics, one of the most important sub-fields of solid-state physics, covers electrical, optical, and thermal properties and interactions with all forms of radiation in semiconductors. Many of these have been of interest since the 19th century, partly because of their practical applications and partly because of the richness of intriguing phenomena that semiconductor materials present.

Point-contact rectifiers made of a variety of natural crystals found practical applications as detectors of high-frequency signals in radio telegraphy in the early part of this century. The natural crystals employed were lead sulphide (galena), ferrous sulphide, silicon carbide, etc. Plate rectifiers made of cuprous oxide or selenium were developed for handling large power [1].[1] The selenium photocell was also found useful in the measurement of light intensity because of its photo-sensitivity.

In the late 1920's and during the 1930's, the new technique of quantum mechanics was applied to develop electronic energy band structure [2] and a modern picture of the elementary excitations of semiconductors. Of course, this modern study has its roots in the discovery of x-ray diffraction by von Laue in 1912, which provided quantitative information on the arrangements of atoms in semiconductor crystals. Within this framework, attempts were made to obtain a better understanding of semiconductor materials and quantitative or semiquantitative interpretation of their transport and optical properties, such as rectification, photoconductivity, electrical breakdown, etc.

During this course of investigation on semiconductors, it was recognized in the 1930's that the phenomena of semiconductors should be analyzed in terms of two separate parts: surface phenomena and bulk effects. Rectification and photo-voltage appeared to be surface or interface phenomena, while ohmic electrical resistance with a negative temperature coefficient and ohmic photocurrent appeared to belong to bulk effects in homogeneous semiconductor materials. The depletion of carriers near the surface primarily arises from the existence of surface states which trap electrons and, also from relatively long screening lengths in semiconductors because of much lower carrier concentra-

[1] Figures in brackets indicate literature references at the end of this paper.

tions than in metals. Thus, it is possible to create potential barriers for carriers on the semiconductor surface or at the interface between a semiconductor and a metal contact, or between two semiconductors. The early recognition of the importance of surface physics was one of the significant aspects in semiconductor physics.

2. Transistors

Since the rectification in semiconductor diodes is analogous to that obtained in a vacuum diode tube, a number of attempts had been made to build a solid-state triode by inserting a "grid" into semiconductors or ironic crystals—a solid-state analog of the triode tube amplifier [3,4,5,]. Because of the relatively low density of carriers in semiconductors, Shockley thought that the control of the density of carriers near the semiconductor surface should be possible by means of an externally applied electric field between the surface and a metal electrode insulated from the surface—the field effect device. The observed effect, however, was much less than predicted [6]. In 1947, in the course of trying to make a good "field effect" device with two gold contacts less than fifty microns apart on the germanium surface, Bardeen and Brattain made the first point-contact transistor where they discovered a phenomenon—minority carrier injection into a semiconductor [7]. The importance of this phenomenon was soon recognized and led to the invention of the junction transistor by Shockley. The realization of this junction device, which did not occur until 1950 [8], was far more significant than its precursor.

The early version of the junction transistor was presented by Shockley as a post-deadline paper at the Reading Conference on "Semi-Conducting Materials," held July 10 to 15, 1950. This conference is now called "The First International Conference on the Physics of Semiconductors." Shockley's paper, however, was omitted from its Proceedings, apparently because a fabrication method used for the junction transistor was then proprietary at the Bell Laboratories [9].

The Foreword of the Proceedings of the Reading Conference [10] states: "During recent years physicists in many countries have made rapid and important advances in the field of solid state physics. Semiconducting materials, in particular, have become a subject of great interest by reason of their numerous practical application. . . ." Indeed, the development of transistors, as well as the progress in semiconductor physics of Ge and Si, would not have been accomplished without the key contribution of materials preparation techniques. Soon after Teal and Little prepared large Ge single crystals, Sparks successfully made a grown junction transistor at Bell Laboratories [11]. The subsequent development was Pfann's zone refining and then Theuerer's floating zone method for silicon processing. These developments made it possible to make Ge and Si of controlled purities and crystal perfection.

The early Ge junction transistors had poor frequency response and relatively low reliability. In fabricating these transistors, the grown-junction technique, or the alloying technique, was used to form p-n junctions; in other words, these techniques were used to control the spacial distribution of donors and acceptors in semiconductors. Then a procedure for forming p-n junctions by thermal diffusion of impurities was explored in order to obtain better reproducibility and tighter dimensional tolerances. This technique, indeed, enabled bringing forth the double diffused transistor with desirable impurity distribution, the prototype of the contemporary transistor [12]. Attention was also turned toward Si because of its expected high reliability and improved temperature capability.

In the 1940's, a team at the Bell Laboratories selected elemental semiconductors, Ge and Si, for their solid-state amplifier project, primarily because of the possible simplicity in understanding and material preparation, in comparison with oxide or compound semiconductors. This not only was a foresighted selection but also had important implications: Ge and Si single crystals exhibited long diffusion lengths of hundreds of microns at room temperature, which were prerequisites to the desirable operation of the transistor, because of both reasonably high mobilities of electrons and holes, and long trapless lifetimes of minority carriers. The latter fact may arise from the indirect energy-gap in these elemental semiconductors in contrast with the direct energy-gap in some III-V compound semiconductors which exhibit high rates of radiative combination of electrons and holes. The exploration of the III-V compound semiconductors was initiated through Welker's ingenuity and imagination, in the early 1950's, to produce semiconductor materials even more desirable for transistors than Ge or Si [13]. Although this initial expectation was not quite met, III-V compound semiconductors later found their most important applications in LED (light emitting diodes), injection lasers, Gunn microwave devices, etc.; these devices could not have been achieved through elemental semiconductors.

3. Important devices

Now, in order to reach a perspective in semiconductor device development, it may be worthwhile to comment on some selected semiconductor devices in chronological order:

1) Solar Cells. In 1940, Ohl observed a photovoltage as high as 0.5V by flashlight illumination in "naturally" grown Si p-n junctions [14]. The modern Si solar cell,

however, was created by bringing together seemingly unrelated activities, namely, large area p-n junctions by Fuller's diffusion method, Pearson's effort for power rectifiers, and Chapin's search for power sources for communication systems in remote locations. According to Smits' article [15], Pearson's diode showed "a conversion efficiency from solar energy to electrical energy of 4 percent. Low as this efficiency may seem today, in 1953, it was very exciting, improving on selenium by a factor of five." Development and production of solar cells were stimulated by the needs of the space program.

In 1972, heterojunction solar cells consisting of p $Ga_{1-x}Al_xAs$-p GaAs-n GaAs, exhibiting power conversion efficiency of 16-20 percent, were reported by Woodall and Hovel [16]. The improved efficiencies were attributed to the presence of the heavily-doped $Ga_{1-x}Al_xAs$ layer, which reduced both series resistance and surface recombination losses. The recent advent of the energy crisis has generated a renewed interest in research and development of solar cells which might be economically viable for terrestrial applications.

2) Tunnel Diodes. Interest in the tunneling effect goes back to the early years of quantum mechanics. Phenomena such as rectification, contact resistance, etc. in solids, were explained by tunneling in the early 1930's. However, since theories and experiments often gave conflicting results, not much progress was made at that time. Around 1950, semiconductor p-n junctions generated a renewed interest in the tunneling process. Experiments to observe this process in the reverse breakdown of the junctions, however, were again inconclusive.

In 1957, Esaki demonstrated convincing experimental evidence for tunneling in his heavily-doped (narrow) p-n junction—the tunnel diode [17, 18]. This diode found use in microwave applications because of its differential negative resistance being responsive to high frequencies. The discovery of the tunnel diode not only generated an interest in heavily-doped semiconductors but also helped to open a new research field on tunneling in semiconductors as well as in superconductors.

3) Integrated Circuits. In 1958, Kilby initiated the fabrication of a circuit which included a number of transistors, diodes, resistors, and capacitors, all residing on one semiconductor chip [19]. This structure is called the (monolithic) integrated circuit. Around the same time, Noyce and Moore introduced improved fabrication techniques called the "planar" process which enabled the birth of the first modern transistor—a landmark in semiconductor history. It was soon realized that this transistor with dished junctions (extending to the surface) and oxide passivation (protecting the junctions), was most suited for assembling integrated circuits, because metal stripes evaporated over the surface oxide layer could be readily used for interconnection [20].

Integrated circuits of digital as well as linear types have had one of the largest impacts on electronics; they are now the main building block in computers, instrumentation, control systems, and consumer products. According to a recent analysis by Moore [21], their complexity has almost doubled each year, now approaching one hundred thousand components on a single Si chip of, say, a quarter centimeter square, and yet the cost per function has decreased several thousandfold since their introduction at the beginning of the 1960's. Meanwhile system performance and reliability have been tremendously improved.

4) MOS FET (Metal Oxide Semiconductor Field Effect Transistor Devices. As mentioned earlier, the transistor was invented while searching for a field-effect device. The field-effect concept originated as early as the 1920's, but no successful device was made in spite of a number of attempts because of the lack of adequate technology.

Thermally-grown SiO_2 on Si single crystal surfaces, which was originally developed for oxide passivation of junctions in the later 1950's, was found to be a most suitable insulator for a field effect device by Kahng and Atalla [22]. This insulator, indeed, had relatively low loss and high dielectric strength, enabling the application of high gate field. More importantly, the density of surface states at the $Si\text{-}SiO_2$ interface was kept so low that the band bending in Si near the interface was readily controllable with externally applied gate fields. Thus, a simple, yet most practical, Si MOS transistor was created whereby the surface inversion layer conductance ("channel") was modulated by gate voltages. This transistor is called a unipolar device because of no minority carrier involvement; it requires fewer processes in fabrication than the bipolar transistor because of its structual two-dimensionality, and is especially adaptable for large-scale integrated circuits.

Presently, integrated circuits, consisting of MOS FET or MOS based components such as dynamic memory cells [23], charge-coupled devices [24], MNOS (Metal Nitride Oxide Semiconductor) memory cells, etc., are even more extensively used than bipolar transistors, in computer memories, microprocessors, calculators, digital watches, etc., while being challenged by advances in bipolar-based devices such as I^2L (Integrated Injection Logic). As the size of individual FETs has continued to decrease for large integrated circuits with the application of advanced processing techniques, the "channel" distance is shortened to one micron or even less and the oxide thickness is thinned to a few hundred angstroms. If one pushed this to the extreme, new physical problems arise from excessively high fields across thin oxide films as well as in the "channel" direction. There has been some discussion on physical limits in digital electronics [25, 26].

While taking measurements of Si surface transport properties at low temperatures, Fang and Howard discovered

that electrons in the "channel" were two-dimensional [27], which provided a unique opportunity for studying quantum effects [28].

5) Injection lasers. Since the early part of this century, the phenomenon of light emission from SiC diodes was recognized and studied, although a practical light emitting diode had not materialized until the development of efficient p-n junctions made of III-V compound semiconductors [29]. Apparently, reports of high-efficiency radiation in GaAs stimulated a few groups to engage in a serious experimental effort to find lasing action in semiconductors: These possibilities were previously discussed [30, 31]. In 1962, the announcement of the successful achievement of lasing action in GaAs came on the same date, independently, from two groups: Hall et al. at General Electric; and Nathan et al. at IBM; and a month later from Quist et al. at Lincoln Laboratory [32]. All of them observed a pulse coherent radiation of 8400Å from liquid nitrogen-cooled, forward-bias GaAs p-n junctions. This occurrence is not suprising in the present competitive environment of the technical community where new scientific information is rapidly disseminated and digested, and new ideas are quickly implemented. There was a two-year interval between the first reports of the Ruby and He-Ne lasers and the announcement of the injection laser.

The performance of the device was improved with incorporation of heterojunctions by Alferov et al [33, 34]. With double-heterostructure the threshold current density for lasing was substantially reduced by confinement of both carriers and photons between two heterojunctions [35]. Finally, in 1970, Hayashi et al. [36] succeeded in operating the device continuously at room temperature. Because of the compactness and the high efficiency of this laser, the achievement paved the way towards many practical applications such as optical (light-wave) communication, signal processing, display and printing. There is a development effort in integrated optics to mount miniaturized optical components, including injection lasers and waveguides, on a common substrate using heterojunction structures of III-V compound semiconductors, analogous to the integrated circuit, for improved signal processing.

6) Gunn and IMPATT (Impact Ionization Avalanche Transit Time) Microwave Devices—In 1962, Gunn discovered that, when the applied field across a short bar of reasonably pure n-type GaAs exceeded a threshold voltage of several thousand volts per cm, coherent microwave oscillations could be extracted by synchronizing the random current fluctuations with a resonator [37]. Furthermore, by his ingenious probe technique, he was able to show that the oscillations were related to the periodic formation and propagation of a narrow region of very high field—"domain." It took two years to confirm that Gunn's experimental discovery of oscillations was indeed due to the Ridley-Watkins-Hilsum transferred electron effect, proposed in 1961 and 1962 [38, 39].

As is true of any important discovery, Gunn's work triggered a wide spectrum of experimental and theoretical activity from device physics to microwave engineering. Apparently this achievement rejuvenated the work of microwave semiconductor devices in general, and, in 1964, IMPATT diodes finally started to oscillate—which was rather overdue since Read's proposal in 1958 [40]. The operation of the device was explained on the basis of dynamics of electrons involving the transit time and avalanche. IMPATT and Gunn devices are now widely used in many microwave gears: the former has high power capabilities (~50mW at 110 GHz), whereas the latter meets low noise requirements.

4. Summary

Figure 1 schematically illustrates the development path of a variety of semiconductor devices. It should be noted that the development path of each device appears to have had its own sequence of conception (theory) and observation (experiment): Typically, the theoretical prediction was later confirmed by the experiment, but, in may instances, the experimental discovery came first, followed by the theory and yet, in other instances, the initial idea which led to the discovery was irrelvant to its consequence. Obviously, this article cannot possibly cover all landmarks and indispensable innovations, not to mention a great number of wonderful, but nonworkable ideas. We will summarize some important items in semiconductor devices and processing techniques which have made remarkable progress since 1950: Si devices of new structures, such as controlled rectifiers, solar cells, photodetectors, I^2L, etc.; development of novel semiconductor devices, such as injection lasers, Gunn microwave oscillators, Schottky junction FETs, infrared detectors, etc., combined with the investigation of new materials, such as III-V compounds; and the introduction of new processing techniques for device fabrication, such as alloy contacts, etching, thermal diffusion of impurities, vapor and liquid-phase epitaxy, oxide formation, sputtering, photolithography and, more recently, ion etching, molecular beam epitaxy, etc.

Not all of this progress arises from engineering ingenuity and advanced material technology; pioneering research in semiconductor physics has also contributed to each significant development, exploring intriguing phenomena in semiconductors, for example, electron-hole multiplication (avalanche), tunneling, hot electrons, lasing by high carrier injection, two-dimensional electrons on the surface or in a semiconductor superlattice, etc. For a qualitative understanding, semiconductor materials, crystalline or amor-

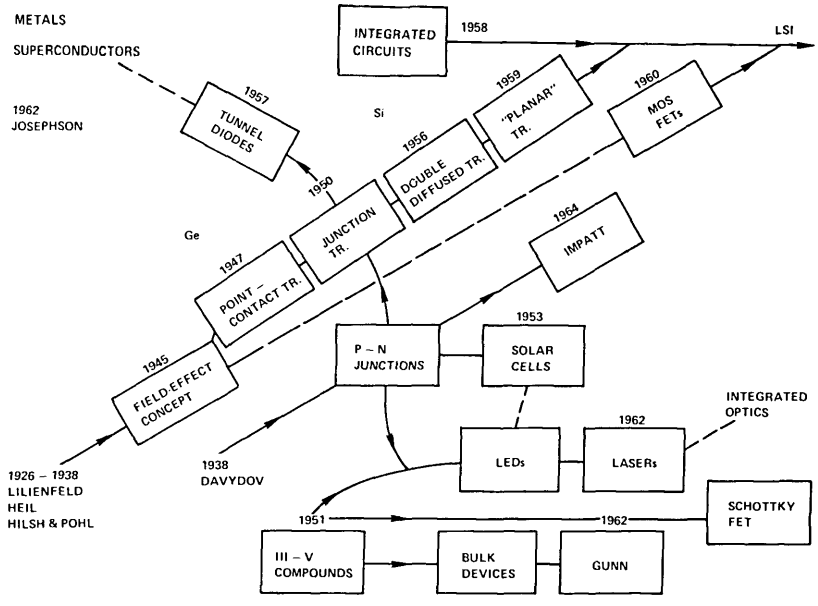

FIGURE 1. Schematic illustration of the development path of a variety of semiconductor devices.

phous, as well as surfaces, have been extensively investigated—often under extreme conditions with advanced instruments; measurements at high pressure or in ultrahigh vacuum, or under the synchrotron radiation fall into this category.

Semiconductor physics has a strong interaction with chemistry, metallurgy, and electrical engineering, and with the broader field of materials science. The separation between basic discoveries and applications in this field of physics is far less distinct than that in some of the other fields of physics. Semiconductor physics has a particularly effective interface with engineering.

"Science is the understanding of nature, whereas engineering is the control of nature." Following this notion, industrial laboratories appear to have played a dominant role as a junction between science and engineering in many technological developments, wherein there may possibly be a kind of gap between them. (Hopefully, this junction will always be forward-biased so that electrons and holes, carrying information, can flow easily from science to engineering and vice versa.) In the field of semiconductors, one may think that the coupling between science and engineering is strong, or that the gap between them is indeed narrow. After all, the semiconductor is a narrow-gap insulator!!

In the preparation of this manuscript, I am indebted to many authors who kindly sent me advance copies of papers which have appeared in the Special Issue of the IEEE Transactions on Electron Devices, July 1976.

5. References

Note: IEEE Trans. Electron Devices, Vol. ED-23 abbreviated herein by **ED-23.**

[1] Henisch, H. K. *Rectifying Semiconductor Contacts,* Clarendon Press, Oxford 1957.
[2] Wilson, A. H. Proc. Roy. Soc. A, **133,** 458 (1931).
[3] Lilienfeld, J.E. U.S. Patents 1,745,175 (1926); 1,877,140 (1928); 1,900,018 (1928).
[4] Heil, O. British Patent 439457 (1935).
[5] Hilsh, R. and Pohl, R.W., Zeits. f. Phys. **111,** 399 (1938).
[6] Shockley, W. and Pearson, G. L., Phys. Rev. **74,** 233 (1948).
[7] Bardeen, J. and Brattain, W. H., Phys. Rev. **74,** 230 (1948); Phys. Rev. **74,** 231 (1948); Phys. Rev. **75,** 1208 (1949).
[8] Shockley, **ED-23,** 597 (1976).
[9] Shockley, W., NBS Special Pub. 388, Proc. of Conf. on the Public Need and the Role of the Invention, Montery, CA, p. 47, June 1973.
[10] Proc. of Conf. Semi-Conducting Materials, Reading, 1950, published by Butterworths Scientific Pub. Ltd., London, 1951.
[11] Teal, G.K., **ED-23,** 621 (1976).
[12] Tanenbaum, M. and Thomas, D. E., B.S.T.J. **35,** 1 (1956).
[13] Welker, H.J., **ED-23,** 664 (1976).
[14] Ohl, R. S. U.S. Patent 2,402,662 (1941).
[15] Smits, F. M., **ED-23,** 640 (1976).
[16] Woodall, J.M. and Kovel, H.J., Appl. Phys. Lett. **21,** 379 (1972).
[17] Esaki, L. Nobel Lecture, Dec. 11, 1973, Pub. by Les Priz Nobel, p. 66 (1974).
[18] Esaki, L., **ED-23,** 644 (1976).
[19] Kilby, J. S., **ED-23,** 648 (1976); U.S. Patent 3,138,743 (1959).
[20] Noyce, R. N., U.S. Patent 2,981,877 (1959).
[21] Moore, G. E., Intn'l Electron Devices Meeting, Tech. Digest, Washington, DC, 1975, p. 11.
[22] Kahng, D., **ED-23,** 655 (1976).
[23] Dennard, R. H., U.S. Patent 3,387,286 (1968).

[24] Boyle W. S. and Smith, G. E., **ED-23,** 661 (1976).
[25] Keyes, R. W., Proc. IEEE **63,** 740 (1975).
[26] Wallmark, J.T., *Microelectronics,* E Keonjian, Ed., McGraw Hill, NY, p. 10 (1963).
[27] Fang F. F. and Howard W. E., Phys. Rev. Lett. **16,** 797 (1966).
[28] Fowler, A. B., Fang, F. F., Howard, W. E., and Stiles, P. J., Phys. Rev. Lett. **16,** 901 (1966).
[29] Loebner, E. E.,**ED-23,** 675 (1976).
[30] Bernard, M.G.A. and Duraffourg, G., Physica Status Solidi **1,** 699 (1961).
[31] Dumke. W.P., Phys. Rev. **127,** 1559 (1952).
[32] Hall, R. N., **ED-23,** 700 (1976).
[33] Alferov, Zh. I., Andreev, V. M., Korol'kov, V. I., Portnoi, E. L., and Tret'yakov, D. N., Fiz. Tekh. Poluprov. **2,** 1545 (1968).
[34] Alferov, Zh.I., Andreev, V. M., Portnoi. E. L., and Trukan, M. K., Fiz. Tekh. Poluprov. **3,** 1328 (1969).
[35] Kressel, H. and Hawrylo, F. Z., Appl. Phys. Lett. **17,** 169 (1970).
[36] Hayashi, I., Panish, M. B., Foy, P. W., and Sumski, S., Appl. Phys. Lett. **17,** 109 (1970).
[37] Gunn, J. B., **ED-23,** 705 (1976).
[38] Ridley, B. K. and Watkins, T. B., Proc Phys. Soc. (London) **74,** 293 (1961).
[39] Hilsum, C., Proc. IRE **50,** 185 (1962).
[40] DeLoach, Jr., B. C., **ED-23,** 657 (1976).

JOURNAL OF RESEARCH of the National Bureau of Standards
Vol. 86, No. 6, November–December 1981

Application of Light Scattering to Polymers, Liquid Crystals, and Biological Systems

Hyuk Yu

Department of Chemistry, University of Wisconsin, Madison, WI 53706

August 10, 1981

The applications of elastic and quasielastic light scattering techniques to polymers in dilute solution, thermotropic liquid crystals and biological membrane vesicles are presented. It is focused on how we extract specific structural features or dynamic processes of these condensed medium samples through the light scattering methods. The paper reviews the light scattering studies that were carried out at the author's laboratory in Wisconsin from 1973 until 1980.

Key words: amphoteric latex; dynamic light scattering; light scattering; nematic liquid crystal; photo-receptor membrane vesicles, random coil polymers.

1. Introduction

With the advent of the dynamic light scattering method and the attendant detection techniques, [1–5], we are now able to expand the application of light scattering methods to a variety of diverse condensed medium systems hitherto unexplored. In this paper, I will outline the kinds of light scattering methods that we use in my laboratory at Wisconsin to probe the structure and dynamics of polymers, nematic liquid crystals, and biological membranes. Four scattering techniques shall first be described with appropriate examples in each case, and then I will move on to the studies of (a) amphoteric latex system, (b) photo-receptor disk membrane vesicles, (c) binary nematic solution, and (d) intrachain dynamics of random coil polymers, in order to bring home the power and limitation of various light scattering techniques. At the outset I must emphasize that this paper is not intended as an exhaustive review of the state-of-the art of light scattering methods, but rather as a report of how one academic research laboratory uses these methods to explore diverse problems of interest.

2. Elastic Light Scattering

Extensive treatises have been written on the subject such that I need not dwell on the historic overview or lengthy explication of the technique. Instead, I will focus on a rather narrowly defined problem of how to determine the linear dimension of scattering particles with substantial symmetry in shape, particularly when the linear dimension R is comparable to the incident wavelength λ. The problem of this kind arises for example in trying to determine the large radius of gyration [9] of T even bacteriophage DNA whose molecular weights are on the order of 10^8 daltons. If one tries to effect the customary procedure of the Zimm plot [10] to extract the radius of gyration, the scattering intensity profile must be obtained at such small angles that one encounters substantial technical problems [9]. By small angle scattering, I mean that one must obtain the data in the Guinier region, [11] i.e., $QR \leq 1$ where Q is the momentum transfer. We propose a new scheme to determine the linear dimension R when the scattering particles are so large that $QR \leq 1$ is difficult to attain experimentally. The method is to focus on the structure of scattering profile at higher angles where the Bragg condition is fulfilled, i.e., $QR = m/\pi$ where m is an integral multiple constant. To be more specific, I quote some simple examples such as solid sphere, hollow sphere, spheroidal shape of either oblate or prolate axial ratio, and the corresponding shell structures. The isotropic parts of the particle form factor in the limit of Rayleigh-Gans-Debye scattering [12] of some of these are given below.

a. Solid sphere

$$P(\theta) = [j_0(x) + j_2(x)]^2 \tag{1}$$

[1] Figures in brackets indicate literature references at the end of this paper.

where $x \equiv QR$, R is the radius and $j_k(x)$ is the kth order spherical Bessel function.

b. Hollow sphere [13, 14]

$$P(\theta)=\left[\frac{3}{x^3(1-l^3)}(\sin x-\sin xl-x\cos x+xl\cos xl)\right]^2 \quad (2)$$

where $x \equiv QR$, $l \equiv a/R$, R and a are respectively the outer and inner radii.

c. Ellipsoids of revolution [15]

$$P(\theta) = \frac{9\pi}{2}\int_o^{2\pi}\frac{J_{3/2}^2(u)}{u^3}\cos\beta d\beta \quad (3)$$

where $u \equiv Qa(\cos^2\beta + \frac{b^2}{a^2}\sin^2\beta)^{1/2}$, a and b are semi-major and semi-minor axes, β is the angle between the semi-major axis and bisectrix, and $J_{3/2}$ is the 3/2th order Bessel function.

d. Circular cylinder

$$P(\theta)=\frac{\pi}{2v}\int_o^{\pi/2}\frac{1}{\cos\beta}\left[J_{1/2}(v\cos\beta)\cdot\frac{2J_1(u\sin\beta)}{u\sin\beta}\right]^2\sin\beta d\beta \quad (4)$$

where a and l are the radius and length of the cylinder, $u \equiv Qa$, $v \equiv Ql/2$, and β is the angle between the cylinder axis and bisectrix.

e. Spheroidal shells

$$P(\theta) = \int_o^1 \frac{\sin^2[x\sqrt{1-qt^2}]}{x^2(1-qt^2)}dt \quad (5)$$

$$= \int_o^1 \frac{\sin^2[y(\frac{1-qt^2}{1-q})^{1/2}]}{y^2(\frac{1-qt^2}{1-q})}dt \quad (6)$$

for oblate shell where $x \equiv Qb$, $y = Qa$, $q \equiv 1-(\frac{a}{b})^2$, and b and a are respectively the semi-major and semi-minor axes such that $0 \le q \le 1$.

$$P(\theta) = \int_o^1 \frac{\sin^2[x\sqrt{1+pt^2}]}{x^2(1+pt^2)}dt \quad (7)$$

$$= \int_o^1 \frac{\sin^2[y(\frac{1+pt^2}{1+p})^{1/2}]}{y^2(\frac{1+pt^2}{1+p})}dt \quad (8)$$

for prolate shell where x and y are the same as above, a and b are respectively the semi-major and semi-minor axes, and $p \equiv (a/b)^2 - 1$ such that $0 \le p \le \infty$.

As an illustration of the proposed method, we take the simplest structure, i.e., sphere, and show how the Bragg condition is extracted from which the radius of sphere is deduced. The isotropic particle form factor of sphere in the Rayleigh-Gans-Debye limit is given by the square of the sum of the zeroth and second order spherical Bessel function as in eq (1), and its structure is a monotonically decreasing function from unity at zero scattering angle to $x = \tan x$ where it gives the first minimum. This is illustrated in figure 1 where a semi-logarithmic plot of the particle form factor $P(\theta)$ versus sine of one-half of the scattering angle θ is given for spherical particles having the radii of 100, 110, 120, and 130 nm suspended in water and scattered by incident blue light of 436 nm in wavelength. It is clear from the plots that under these conditions the radius must exceed 120 nm for $P(\theta)$ to give the first minimum; $P(\theta)$ is fairly structureless for the radius less than 120 nm. If, on the other hand, we plot $(QR)^4P(\theta)$ against $\sin(\theta/2)$, the graphs as shown in figure 2 result. This arises because the damping profile of

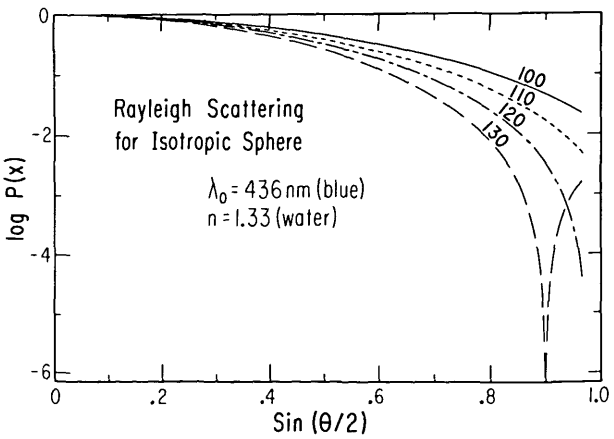

FIGURE 1. The isotropic part of the particle form factor $P(x)$ of Rayleigh-Gans-Debye scattering from solid, isotropic spheres against $\sin(\theta/2)$ for the radius of 100, 110, 120 and 130nm, with the incident wavelength of 436 nm (blue) in a medium with the refractive index n of 1.33 (water). Note that $x \equiv QR$ *hence* $P(x) = P(\theta)$.

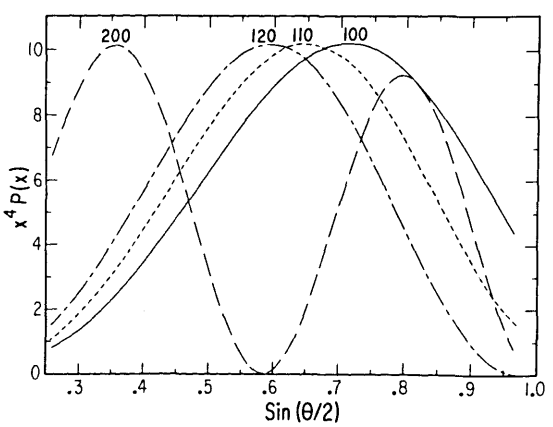

FIGURE 2. $x^4P(x)$ versus $\sin(\theta/2)$ of figure 1. In place of R = 130 nm, plot for 200 nm is shown.

$P(\theta)$ in eq (1) is compensated by the factor $(QR)^4$. Thus, the monotonic descrease of $P(\theta)$ for small particles is rendered to have a maximum by multiplying by $(QR)^4$. Algebraically this is easily seen from eq (1);

$$x^4 P(\theta) = 9\left(\frac{\sin x}{x} - \cos x\right)^2 \tag{9}$$

where $x \equiv QR = \frac{4\pi n}{\lambda_0} \sin(\theta/2) \cdot R$ and the extrema positions of $P(\theta)$ appear at

$$\tan x = \frac{x}{1-x^2} \text{ for maxima}$$

and

$$\tan x = x \text{ for minima}$$

The plots in figure 2 are drawn for the common experimental scattering conditions in mind, namely the scattering angle spans from 30° to 150°. Experimentally the ordinate scale is immaterial to the extent that one is interested in determining the extrema positions to extract the particle radius. For completeness sake, we show in figures 3 and 4 the analogous set of plots for spherical particles with longer radii as though they could be analyzed by the Rayleigh-Gans-Debye approximation, whereas its applicability is limited [8] in this size range, and $P(\theta)$ itself contains sufficient structure that $x^4P(\theta)$ plot affords at best sharper maxima and smoother minima. I shall later return to the limit of applicability of Rayleigh-Gans-Debye scattering relative to the particle size. We display in figure 5 why the factor x^4 is chosen as the multiplication factor to $P(\theta)$ in order to moderate its damping at higher angles. For a given radius of a particle, we show three profiles whereby it is made clear that a factor x^2 does not reduce the damping sufficiently, whereas a factor x^6 overcompensates the damping. The optimum is clearly the x^4 factor.

Turning to the experimental verification of the proposed method, [16], we show in figure 6 a plot of $I_{vv}(\theta) \cdot \sin^4(\theta/2)$ versus $\sin(\theta/2)$ for a polystyrene latex standard (Polysciences, Lot 2-1435), whose radius is given as 87 ± 4 nm determined by transmission electron microscope, suspended in distilled water. Here, the subscripts vv of the scattered intensity stand for the polarized scattering, namely the polarizer and analyzer are both oriented vertically relative to the scattering plane. We should note that the ordinate scale is arbitrary and $x^4P(\theta)$ is proportional to $I_{vv}(\theta) \cdot \sin^4(\theta/2)$, since $P(\theta)$ is the isotropic part of the particle form factor. The data points were taken at 1° increments and the solid curve was drawn according to eq (9) with $\lambda_0 = 436$, $n = 1.333$, $R = 80$ nm. The discrepancy of 10 percent between the radius of 87 nm by electron microscopy and that of 80 nm by this method may be ascribed to a number of artifacts arising from electron beam optics in the electron microscopy technique. In figure 7, we show a test of another

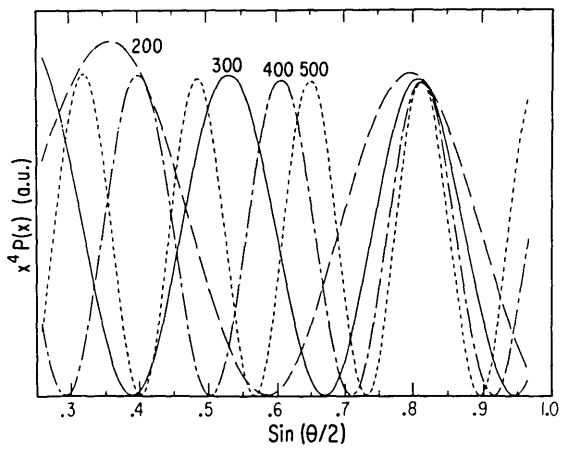

FIGURE 4. Similar to figure 2 with $R = 200, 300, 400$ and 500 nm.

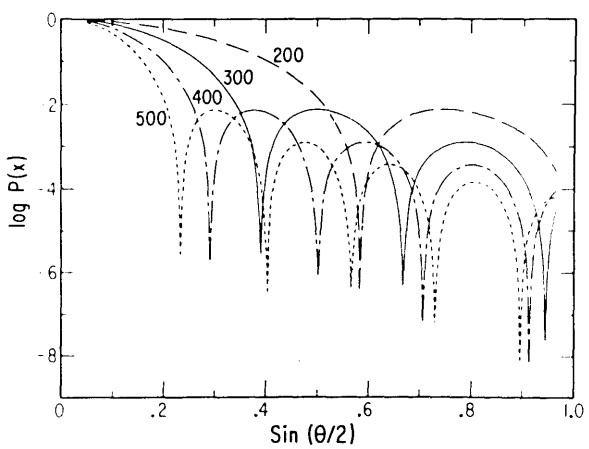

FIGURE 3. Similar to figure 1 with $R = 200, 300, 400$ and 500 nm.

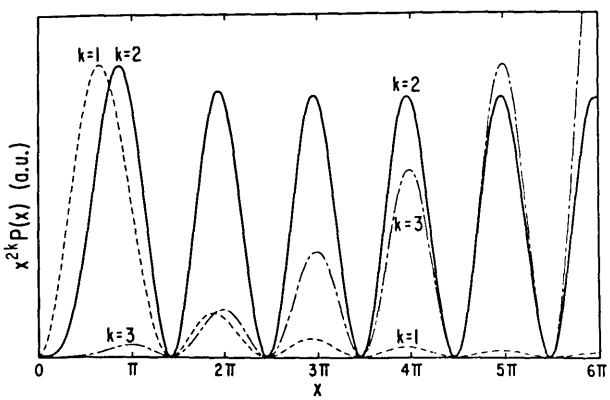

FIGURE 5. $x^2P(\theta)$ and $x^6P(\theta)$ versus x.

polystyrene latex standard (Polysciences, Lot 2380), having the radius of 139 nm again determined by electronic microscopy. Two curves are drawn for comparison. The first (solid curve) is that predicted by the Mie scattering function with R = 136 nm and the other (dashed curve) is that predicted by eq (9) with the same R. In the Mie function fitting, we use the refractive index ratio m of the particle to medium as 1.21 [17]. In the inset, the scattering profiles at different concentrations of the latex particles are shown where the concentration range of the most (a) to the least (d) concentrated is about one order of magnitude. It shows well that the scattering profiles are weakly dependent on the concentration, and we could have deduced the radius of 130 nm from the most concentrated case (a) shown in the inset. The least concentrated case (d) is expanded in the plot of figure 7. Ignoring the matching with the entire scattering profile but focusing on the maximum and minimum positions inferred from eq (9) for the Rayleigh-Gans-Debye scattering, we would have deduced the radius of 144 nm. Thus for this size particle, either scattering function would have sufficed if the radius determination within 4 percent is acceptable. It should however be noted that the discrepancy of the radius determinations by the two scattering functions exceeds the precision limit of extrema position determination in this size range.

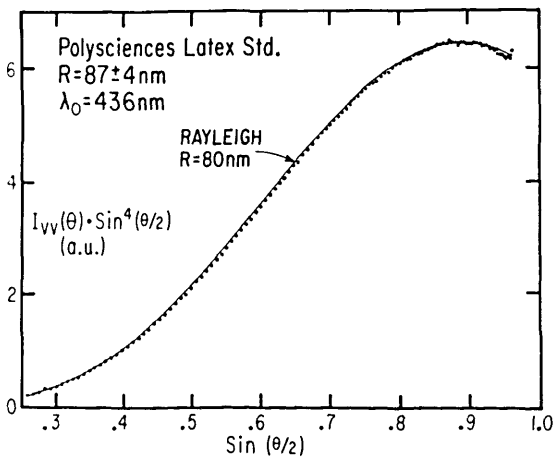

FIGURE 6. Calibration run of the light scattering method with Polysciences latex standard with R = 87±4 nm (mean ± s.d.). The scattering intensity here is observed with the incident and scattered beams vertically polarized relative to the scattering plane. The ordinate is scaled in arbitrary units, and the solid curve represents the Rayleigh-Gans-Debye scattering function for an isotropic solid sphere with 80 nm raduis.

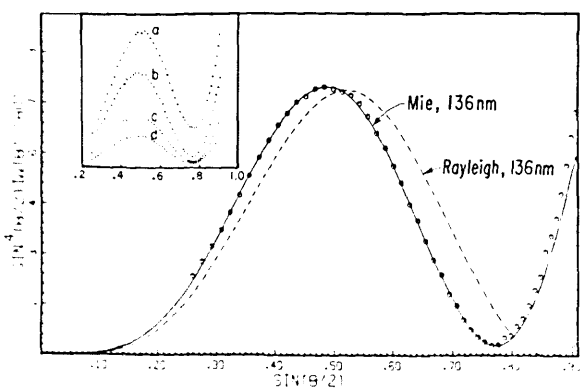

FIGURE 7. Calibration run with Polyscience latex standard with R = 135± 1 nm. Experimental conditions are identical with those in Figure 6. Dashed curve is drawn with the Rayleigh scattering function with R = 136 nm and solid curve with the Mie function with R = 136 nm. The inset shows the concentration dependence of scattering profile whereby a represents the most concentrated and d the least concentrated. The number density of latex particles in a is about one order of magnitude larger than in d.

Having thus established that our proposed method works for the radius determination of a spherical particle of $R \leq$ 140 nm suspended in aqueous media, we now turn to the applicability limit of Rayleigh-Gans-Debye scattering and when one must use the Mie scattering function. In order to stipulate the applicability limit, we compare the extrema positions predicted from eq (9) and those computed from the Mie functions. The latter computation was performed on a Harris/7 computer. The comparison is provided in figures 8(A) and 8(B) where the reduced size parameter α, defined as $2\pi R/\lambda$, is given in terms of the extrema positions in the scattering angle of $x^4P(\theta)$ profiles for the polarized and unpolarized scatterings respectively. When m = 1.0001, we recover the predictions of the Rayleigh-Gans-Debye scattering as given by eq (9); this particular value of m is not significant as long as m is very close but still larger than unity for the Mie function to be evaluated. These figures allow us to understand why the radius deduced from the Rayleigh function always overestimates. At any given extreme position, be it a maximum or minimum, α values for $m > 1$ invariably lie below that for $m = 1$ although the relative error committed by assuming $m \approx 1$ is not a monotonically increasing function of m for any size particles. This is particularly true with the maximum positions which show oscillation with respect to m. Hence, the relative error should also oscillate. In fact, we can evaluate the error. This is illustrated in figure 9(A) and 9(B) where the percent error of analyzing the scatterng profile extrema according to the Rayleigh-Gans-Debye scattering is plotted against the reduced size parameter α at different values of m. The polarized and unpolarized scattering cases are shown in (A) and (B), respectively, In either case, the error can be equal or less than 10 percent if $m \leq 1.15$ for $\alpha \leq 7$. The oscillation in the error estimate becomes progressively larger in amplitude as the m value increases. For the values of m close to unity, the error with respect to the particle size is sensibly constant though with a slight increase with α in each m. Hence, one should not approximate with impunity

the scattering of small particles by the Rayleigh scattering function regardless of the refractive index ratio m.

In closing this subject, let me emphasize that the spherical particle size analysis can be effected by determinations of the extrema positions of $\sin^4(\theta/2)I(\theta)$ profiles and these are provided by analytical solutions of

$$x = \tan x \qquad \text{(minima)}$$

$$\frac{x}{1 - x^2} = \tan x \qquad \text{(maxima)}$$

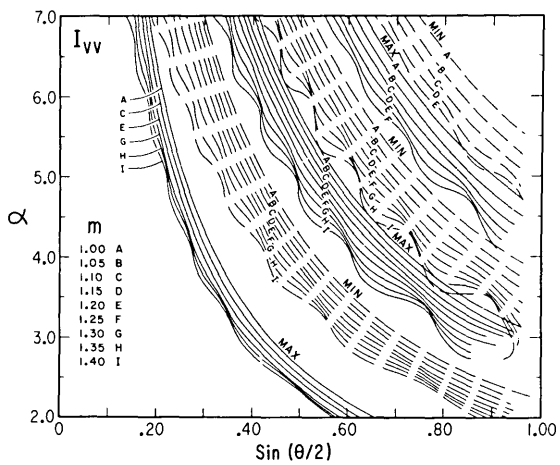

FIGURE 8A. Ratio of isotropic solid sphere's circumference to wavelength in scattering medium, $\alpha \equiv 2\pi R/\lambda$, versus sin $(\theta/2)$ at different extrema positions of the Mie function for $x^4P(\theta)$. Each set is drawn at different refractive index ratios m. The maxima and minima are distinguished by solid and dashed curves respectively. This is for the Mie function at the vertical/vertical optical configuration.

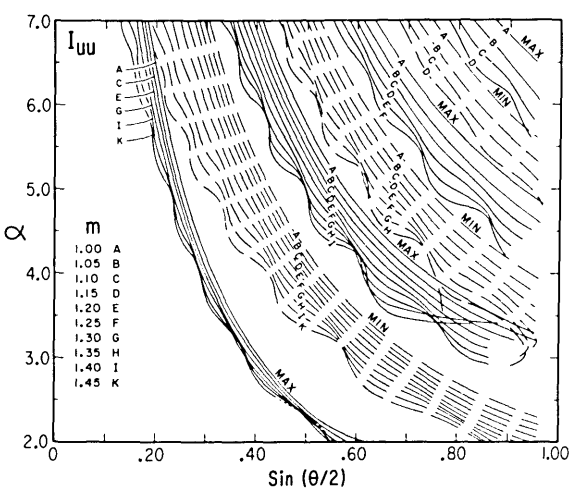

FIGURE 8B. Analogous to (8a) for the case of Mie function at unpolarized/unpolarized configuration.

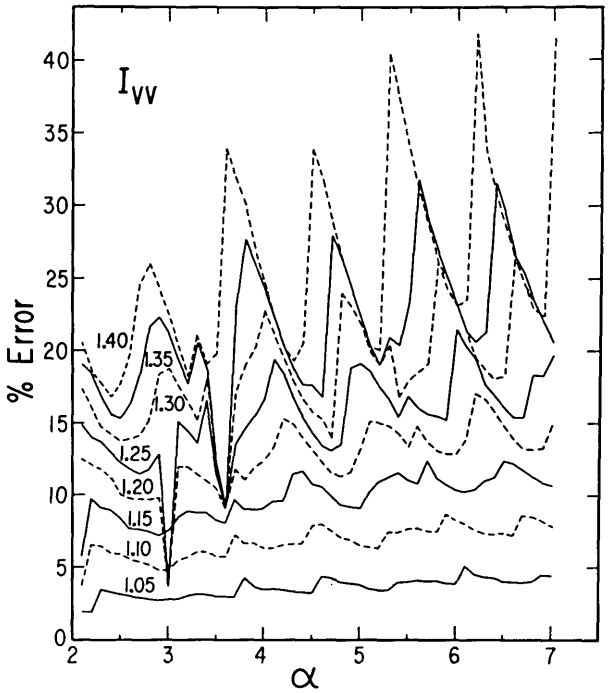

FIGURE 9A. Percent error of analyzing the profile extrema positions according to Rayleigh-Gans-Debye scattering as a function of the reduced size parameter α at different refractive index ratios m, for the polarized scattering.

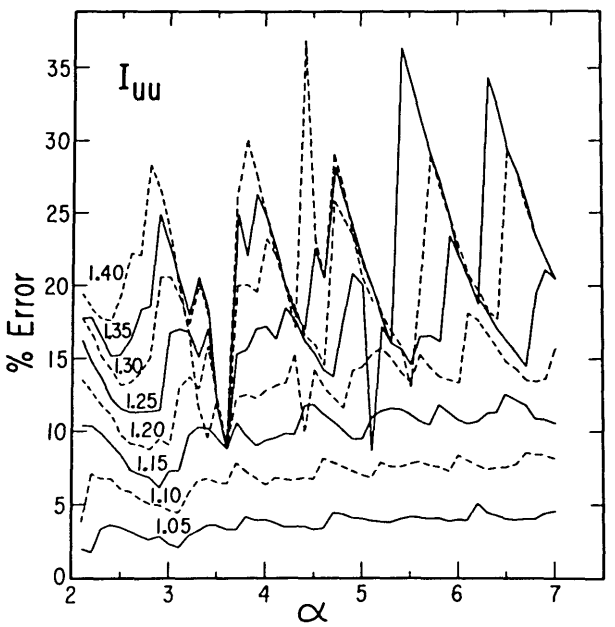

FIGURE 9B. Analogous to (9a) for the unpolarized scattering.

in the case of Rayleigh-Gans-Debye scattering whereas they must be evaluated numerically in the case of Mie scattering. Because the method depends on the structure of scattering function at high Q, it is restricted to monodisperse systems and extrapolation to infinite dilution is not an essential step in the procedure provided the scattering suspension is dilute enough.

3. Quasielastic Light Scattering

Here, we restrict our discussion to the thermally induced, spontaneous concentration fluctuations whereby the translational diffusion coefficient of the scattering particles at infinite dilution is deduced. The homodyne power spectrum [1] $S(\mathbf{Q},\nu)$ of the Doppler broadened scattering from a monodisperse system of particles is

$$S(\mathbf{Q},\nu) = A\frac{\Delta\nu_{1/2}}{\nu^2 + (\Delta\nu_{1/2})^2} + B \qquad (10)$$

where A is an optical constant which depends on the intensity factor of the spectrum, B is a constant, a measure of shot-noise level and the spectral half-width at half-height $\Delta\nu_{1/2}$ is related to the translational diffusion coefficient D by

$$\Delta\nu_{1/2} = DQ^2/\pi \qquad (11)$$

Our instrument [18] is schematically depicted in a block diagram in figure 10. A typical power spectrum obtained from a Dow Polystyrene Latex standard suspension (45.4 nm radius) is shown in figure 11 and the corresponding spectral halfwidth against Q^2/π is displayed in figure 12 where the scattering angle spans the range 10°–100°. The diffusion coefficient deduced via eq (11) is $(5.39\pm0.04)\times 10^{-8}$cm^2/s which is in turn converted to the Stokes radius of 45.5 ± 0.4 nm. Progression of the S/N ratio of the observed power spectrum with the number of accumulations is shown in figure 13.

4. Electrophoretic Light Scattering

The technique was first developed by Ware and Flygare in 1971 [19] and subsequently by Uzgiris in 1972, [20] and it has since undergone substantial refinements [21–29]. The

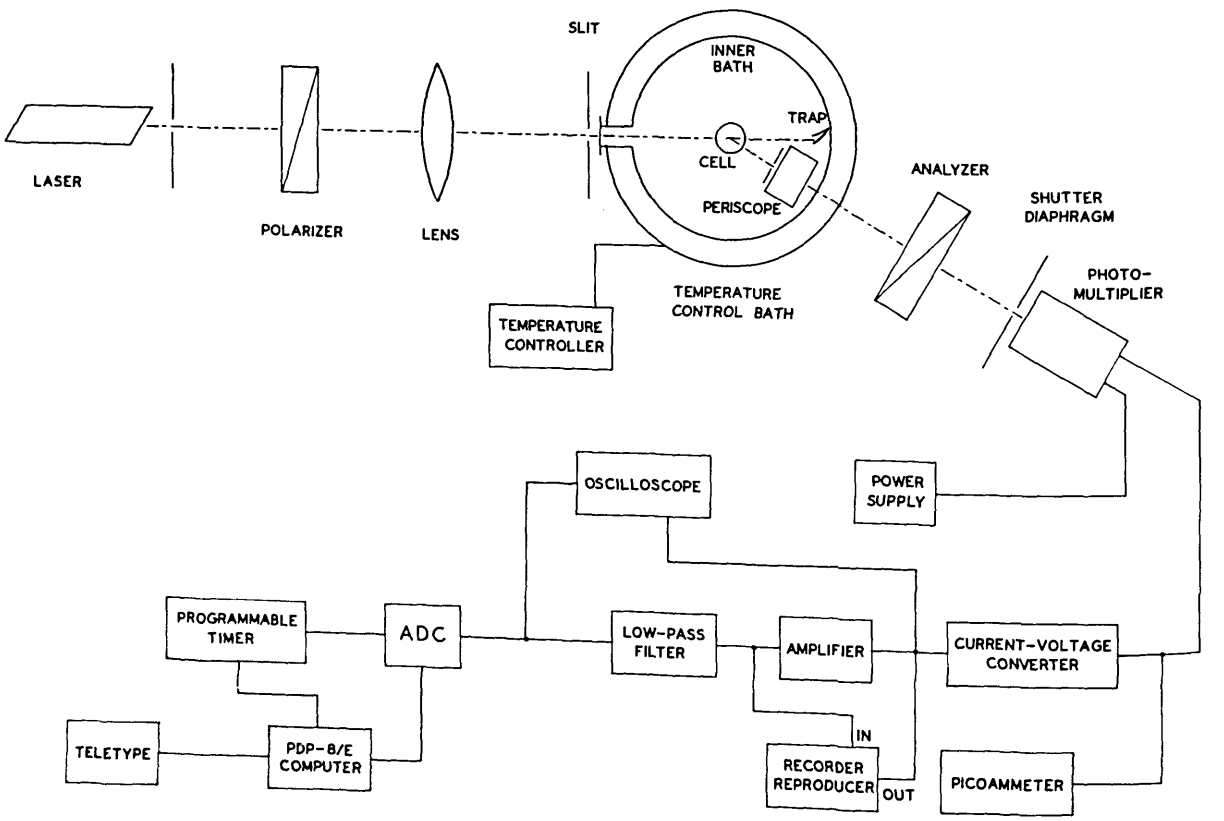

FIGURE 10. Block diagram of Rayleigh spectrometer.

advantages that it offers over the conventional electrophoresis methods have now been well-documented in the literature [25, 27]. As with any new technique, this one also had to first be calibrated against those of more conventional methods with the use of a test system. Ware and Flygare chose bovine serum albumin (BSA) for the purpose because it was one of the best characterized globular proteins and commercially available in a relatively pure form. Others have subsequently chosen BSA for the same reason to calibrate their instruments [28–32].

The method is no more than another application of laser velocimetry. A monodisperse system of charged particles in dilute solution under the influence of an applied electric field would drift uniformly to the oppositely charged electrode. The diffusion equation governing this situation [4] in terms of the self part of the space-time autocorrelation function $G_s(\mathbf{R},t)$ is

$$\frac{\partial}{\partial t} G_s(\mathbf{R},t) + \mathbf{V}_d \cdot \nabla G_s(\mathbf{R},t) = D\nabla^2 G_s(\mathbf{R},t) \qquad (12)$$

with the initial condition

$$G_s(\mathbf{R},0) = \delta(\mathbf{R}) \qquad (13)$$

where $\mathbf{V}_d$ is the uniform drift velocity, D the translational diffusion coefficient of particle and $\delta(\mathbf{R})$ is the Dirac delta function. Upon taking the space Fourier transforms of the above, we have

$$\frac{\partial}{\partial t} F_s(\mathbf{Q},t) + i\mathbf{Q} \cdot \mathbf{V}_d F_s(\mathbf{Q},t) = -Q^2 D F_s(\mathbf{Q},t) \qquad (14)$$

with

$$F_s(\mathbf{Q},0) = 1 \qquad (15)$$

The solution of eq (14) with the initial condition, eq (15), is

$$F_s(\mathbf{Q},t) = e^{-Q^2Dt}\, e^{i\mathbf{Q}\cdot\mathbf{V}_d t} \qquad (16)$$

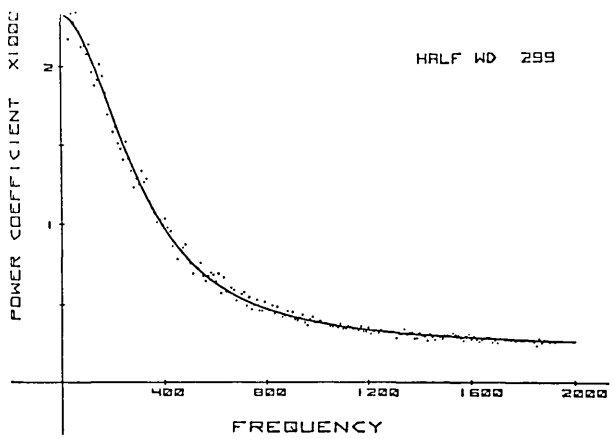

FIGURE 11. Homdyne power spectrum of a polystyrene latex standard at 2 kHz bandwidth with $\Delta\nu_{1/2}$ = 299 Hz.

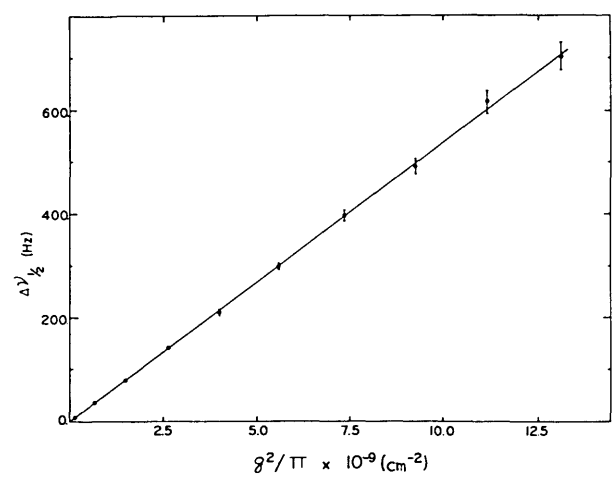

FIGURE 12. $\Delta\nu_0$ versus q^2/π whose slope yields $D = (5.39\pm0.04) \times 10^{-11}$m^2/s and the Stokes raduis of 45.6 ± 0.4 nm.

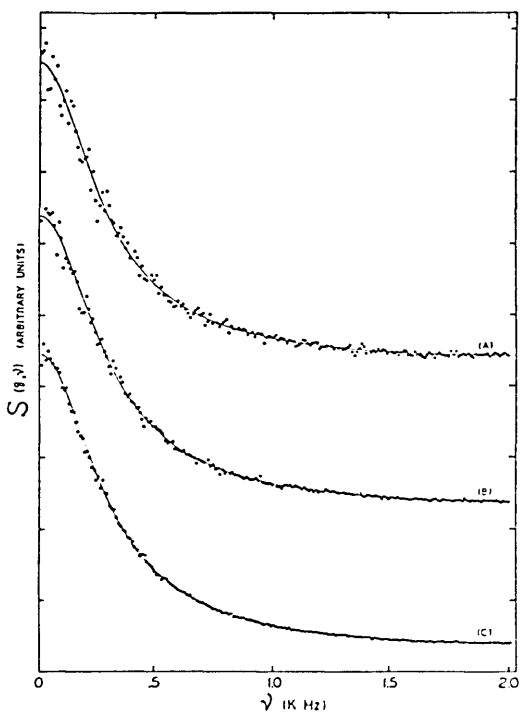

FIGURE 13. Power spectra of polystryene latex standard taken at 60° scattering angle. A, B, and C are 250, 1000 and 4000 scan averages, respectively.

The power spectrum of heterodyne beating from a system of charged particles governed by eq (16) is a Doppler shifted Lorentzian whose shifted angular frequency $\Delta\omega_s$ is given by

$$\Delta\omega_s = \mathbf{Q}\cdot\mathbf{V}_d \tag{17}$$

Our scattering geometry is represented in figure 14. In order to effect heterodyne beating, the scattering angle has to be fairly small (2°–8°) so as to make use of cell surface reflected light as the local oscillator component. Thus the shifted frequency

$$\Delta\nu_s = QV_d \cos(\theta/2)/2\pi \approx \pi n\mu(\theta V_{pp})/360d\lambda_o \tag{17}$$

where n is the refractive index of scattering medium, μ the electrophoretic mobility (the drift velocity per unit field strength), θ the scattering angle, V_{pp} the peak-to-peak applied voltage, d the electrode spacing (1.84 mm in our case) and λ_o the incident wavelength *in vacuo*. Hence, the shift frequency $\Delta\nu_s$ should be proportional to the product, θV_{pp}, and the electrophoretic mobility μ can be deduced by determining $\Delta\nu_s$ measured at different scattering angles and V_{pp}.

Since there were some discrepancies in the mobility values of BSA reported by Ware and Flygare [19, 21] and Mohan et al. [28] by electrophoretic light scattering and those by Schlessinger [30], Alberty [31], and Longsworth and Jacobsen [32] with the moving boundary method, we have set out to examine the discrepanices [33]. The purpose was to test the accuracy attainable by this technique *vis-a-vis* that of a more conventional method. In so doing, we have not only found the mobility by this technique to be in complete accord with those of the moving boundary method but also established that the BSA mobility depends on the ionic strength of the suspending medium according to Henry's formulation [34, 35]. The latter finding is neither without parallel nor unexpected [36–38], but the ease of the experiment to confirm it points to the utility and power of the technique. At the same time, our experiment, which covers a wide range of ionic strength, points to certain limitations and the complementary nature of the technique with more conventional methods.

The discrepancies referred to above were entirely due to the sample polydispersity and had little bearing on the veracity of the electrophoretic light scattering technique. This was confirmed by examining the two sets of samples. First is the so-called Fraction V of Armour (Lot A21505) which was used by Ware and Flygare as well as by all others with the moving boundary method, and the other is the BSA Monomer Standard of Pentex brand from Miles Laboratories. Polyacrylamide gel electrophoresis patterns of the two are compared in figure 15. In figure 16, we display how well the shifted frequency depends linearly on the product $(\theta\cdot V_{app})$ for the Fraction V sample. Finally we compare the deduced mobilities, corrected to 20 °C in water, of the two samples relative to their ionic strength dependence in figure 17. In the same figure, we plot all other available

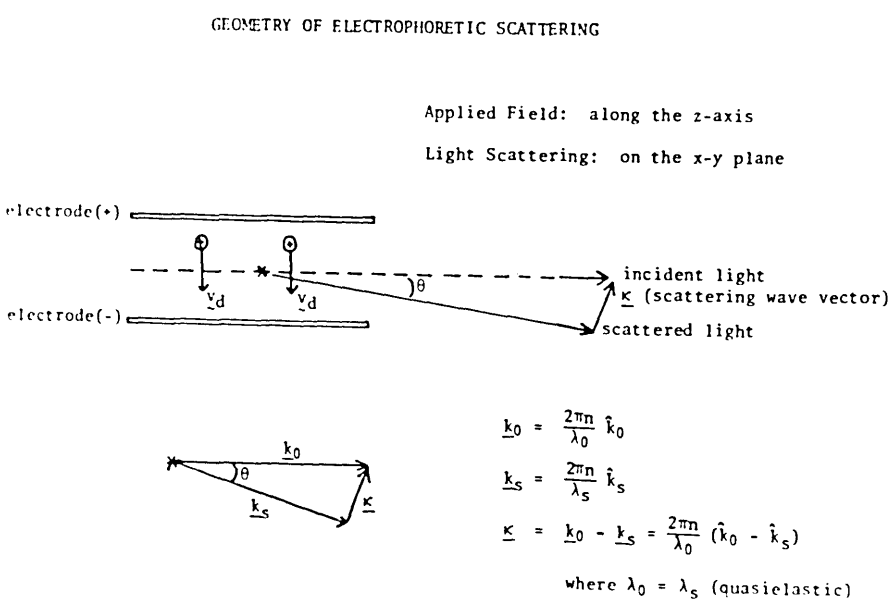

FIGURE 14. Scattering geometry of electrophoretic light scattering, where the symbol K is used in place of Q.

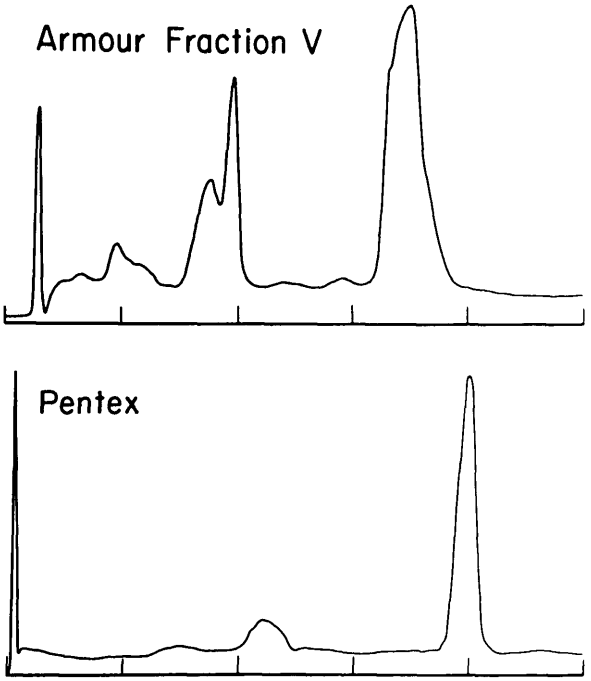

FIGURE 15. Polyacrylamide gel electrophoresis patterns of polydisperse BSA Fraction V of Armour and Pentex brand BSA monomer standard.

BSA data in the literature at pH 8.7–9.4 after making appropriate temperature correction. Two solid curves are drawn according to Henry's equation

$$\mu = \frac{Q_E}{6\pi\eta R} f(\varkappa R) \tag{18}$$

where Q_E is the net charge of the electrokinetic unit, η the viscosity of the medium, R the radius of the unit, $\varkappa^{-1}$ is the Debye screening length, and $f(\varkappa R)$, which accounts for the ionic strength dependent charge screening, is given by

$$f(\varkappa R)=(1+\varkappa R)^{-1}\{1+\frac{(\varkappa R)^2}{16}-\frac{5(\varkappa R)^3}{48}-\frac{(\varkappa R)^4}{96}+\frac{(\varkappa R)^5}{96} +\left[\frac{(\varkappa R)^4}{8}-\frac{(\varkappa R)^6}{96}\right] e^{\varkappa R}\int_{\varkappa R}^{\infty} t^{-1}e^{-t}dt\} \tag{19}$$

where the integral in the last term is the exponential integral $E_1(\varkappa R)$ [39]. With use of the Stokes radius of 36 Å deduced from the translational diffusion coefficient of BSA by Baldwin et al. [40] and with the dependence of $\varkappa^{-1}$ on ionic strength I at 20 °C as $\varkappa^{-1}=3.045/\sqrt{I(\text{Å})}$, the two curves are drawn with 20 and 26 electronic charges per BSA molecule for Q_E, respectively, for the lower (Fraction V) and upper (Pentex) sets. Since the data by the moving boundary method are all obtained with the Fraction V samples, it is

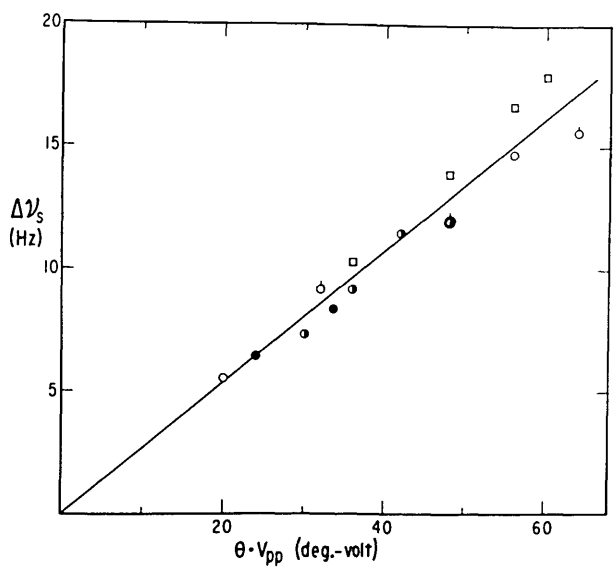

FIGURE 16. Electrophoresis Doppler shift frequency $\Delta\nu_s$ versus θV_{pp} for Fraction V samples at 5 mM ionic strength. Three independently prepared samples are examined. Scattering angles of two preparations are distinguished as (●) 2°, (◑) 3°, (○) 4°, (◌) 4° and third preparation is measured at (□) 6°.

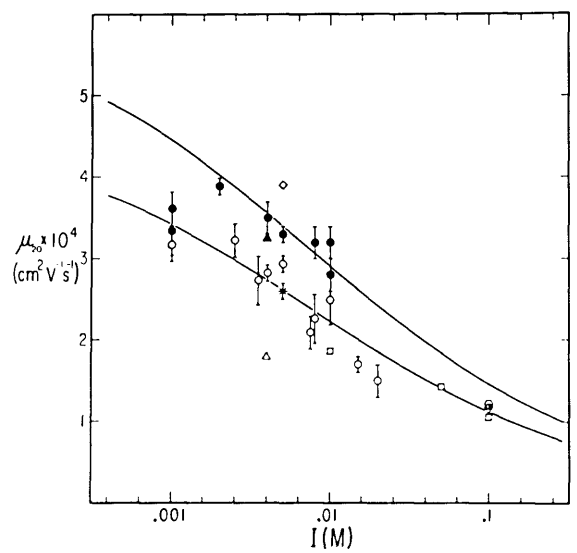

FIGURE 17. Electrophoretic mobility, corrected to 20 °C in water, versus ionic strength. Open circles with error bars are Fraction V sample, filled circles with error bars are Pentex sample. * is from the slope of figure 16. All others are from the literature; (□) Schlessinger, (◑) Alberty, (◇ and ▽) Longsworth and Jacobsen, (Δ) Ware and Flygare [20] and (▲) Ware and Flygare22 and (◇) Mohan et al. [29]

not surprising that they belong to the lower set and are consistent with ours. The results in figure 17 represent the first instance, to the best of our knowledge, of a systematic study of BSA mobility dependence on ionic strength at a given pH. It is clear that Henry's equation can well account for the ionic strength dependence of electrophoretic mobility.

5. Forward Depolarized Scattering (FDS)

The technique was first proposed and utilized by Wada and coworkers in 1969-70 [41, 42] for the determination of the rotatory diffusion coefficient of a rod-like molecule, i.e., tobacco mosaic virus. A further refinement was reported by Schurr and Schmitz in 1973 with the same system [43] and an extension to calf-thymus DNA followed [44]. I will illustrate the technique with use of an example, namely the intrachain dynamics of linear flexible macromolecules in dilute solution. A theoretical formulation of the spectral profile of a scattered optical field is provided by Ono and Okano. We have slightly generalized the scheme by concluding that the FDS spectrum is a superposition of uniformly weighted multiple Lorentzian as long as there exists the normal coordinate transformation for the intramolecular chain dynamic modes [45].

A model of dilute polymer solution is composed of optically isotropic solvent and linear flexible chains, each of which is constituted of n+1 anisotropic elements with cylindrical symmetry. The FDS spectral profile is formally given by

$$I_{V_h}(\omega)=B(N/V)\int_{-\infty}^{\infty}<\sum_{i=0}^{n}\sum_{j=0}^{n}\alpha_{xy}^{(i)}(\tau)\,\alpha_{xy}^{(j)}(0)>e^{-i\omega\tau}d\tau \quad (20)$$

where B is an optical constant, (N/V) is the number density of polymer molecules within the scattering volume, the subscripts V and h refer to the vertical and horizontal polarization directions of the incident and scattered optical fields, respectively, and $<\ >$ refer to the equilibrium ensemble average. If the normal coordinate transformation is possible, the long wavelength modes in hydrodynamic regime is

$$I_{V_h}(\omega)=B(N/V)(\Delta\alpha/3)^2\sum_{k=1}^{n}\frac{1/\tau_k}{\omega^2+(1/\tau_k)^2} \quad (21)$$

where $\Delta\alpha$ is the optical anisotropy of each element and τ_k is the kth normal mode relaxation time. In case of a monodisperse system of dilute rigid rod molecules, the heterodyne power spectrum corresponding to eq (21) is

$$S_{\perp}(0,\nu)=A\frac{(1/2\pi\tau)}{\nu^2+(1/2\pi\tau)^2} \quad (22)$$

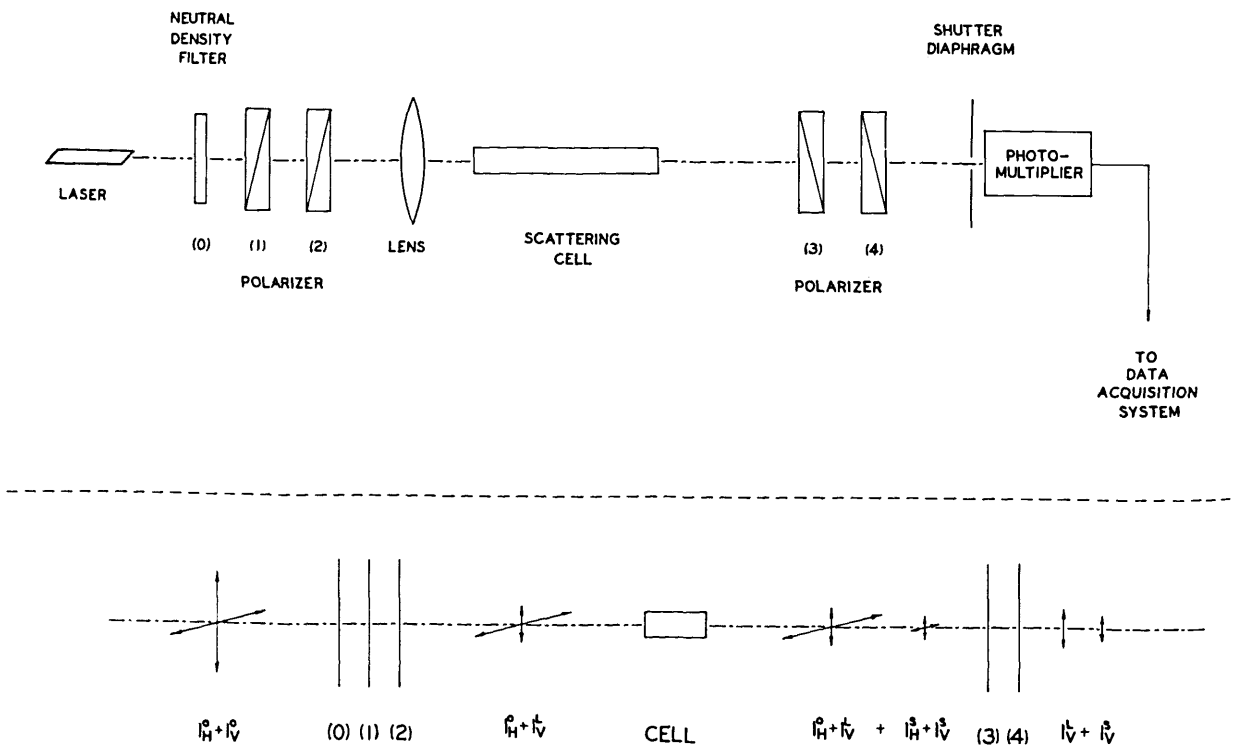

FIGURE 18. Block diagram of the Rayleigh spectrometer in the FDS configuration and the filter train. Here, I°, I^{L} and I^{S} stand for the incident, leakage and scattering intensities, respectively, and the subscripts V and H designate vertical and horizontal polarization directions.

where τ is the relaxation time of rotatory diffusion of the rod.

The optical train of our apparatus [46] is shown in figure 18, and an example of $S_{\perp}(0, \nu)$ for a dilute solution of poly(n-hexyl isocyanate), a rigid rod chain of 3500 Å in length, is given in figure 19.

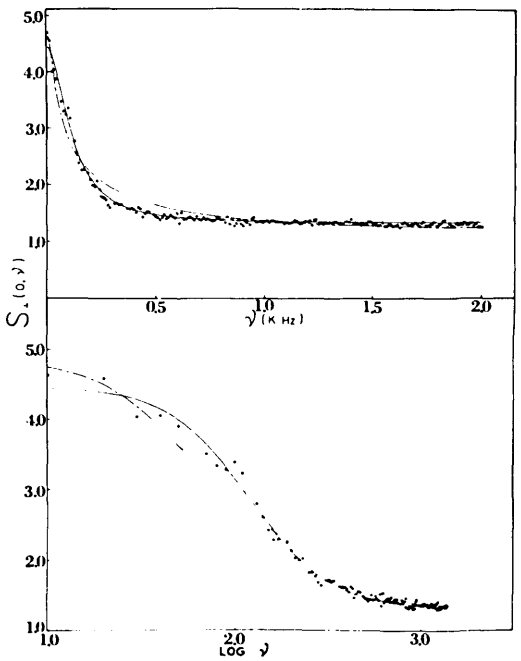

FIGURE 19 FDS power spectrum of PHIC (M.W. 3.2×20^5) in n-hexane at C = 2.16 mg/mL with single Lorentzian fit (—) and Zimm spacing fit (— · —). Upper and lower graphs are distinguished by linear and logarithmic frequency scales.

The four light scattering techniques that we employ to study a variety of scattering systems are summarized above. Before leaving this section, I note parenthetically that our data acquisition and analysis system makes use of a minicomputer (PDP8/e) and a set of two microprocessor computers (Apple II) interacting with a Harris/7 system. This is shown schematically in figure 20 where only the part dealing with computer controlled automatic goniometer on SOFICA light scattering photometer is yet to be implemented while all others are now in operation.

6. Systems

Turning to the four systems that were studied by one or more of the above techniques, table I summarizes what we were able to learn about these systems by the light scattering methods. For the sake of brevity, I will not discuss all of them in the same detail but rather highlight some selected aspects of some of them.

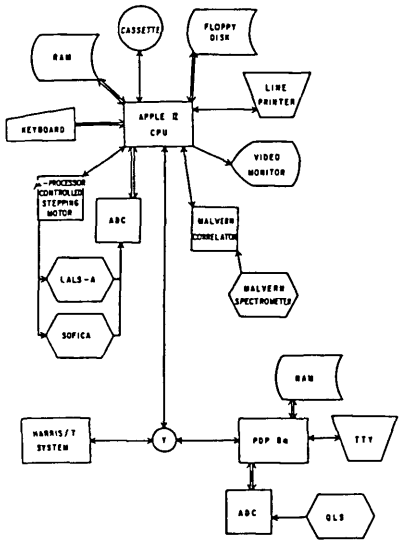

FIGURE 20. Data acquisition and analysis system of quasielastic light scattering in time domain (Malvern autocorrelator) and in frequency domain (PDP 8/e) and those of elastic light scattering.

a. Amphoteric Latex Particles

Monodisperse latex particles have been utilized in a wide variety of fields including immunochemical assays [47, 48] and biomembrane studies [49] in addition to their more conventional applications as the markers and calibration standards in microscopy and light scattering and as the model colloids [50]. Our interest coincides with the last instance where an amphoteric latex system with the well-defined number of charges can be invoked as a model for globular proteins and biomembrane vesicles relative to the ionization behavior of their surface groups. Recently, Homola and James [51] were able to prepare an amphoteric latex system without any added surfactants which now meets the requirement of a well-defined charge number. The latex particles consist of three monomers, styrene (S), methacrylic acid (MA), and N,N-diethylaminoethyl methacrylate (DEAM), emulsion polymerized with persulfate at 70 °C.

We were mainly interested in whether there exists any size change at different pH [52]. One of the transmission electron micrographs taken of the samples is shown in figure 21 which makes it evident that the sample has a relatively homogeneous size distribution. Results of the conductometric and potentiometric titrations, as shown in figure 22, give clear evidence that the latex particles are indeed amphoteric in nature and the titration valences at the extreme pH of 3 and 11 are fairly symmetric at about 6×10^5 electronic charges per particle. This was deduced from the titration results and the size determination, which was performed by elastic light scattering according to the method

TABLE 1. *List of the four systems studied by light scattering techniques*

SYSTEM	TECHNIQUES	STRUCTURE or PROPERTIES	VARIABLES
Amphoteric Latex Particles	ELS QLS EPLS	Surface Layer Dilation; electrostatic interactions	pH
Photoreceptor Retinal Disc Membranes	ELS QLS EPLS	1. osmotic deformation 2. membrane lateral stiffness 3. ion permeability 4. surface ion binding	1. photochemical states 2. chemical potential gradient 3. ion concentration
Nematic Liquid Crystals	Optical Birefringence NMR Line Splittings FDS	1. Orientation Distribution Function 2. order fluctuation dynamics	1. non-nematogen composition 2. temperature
Linear Macromolecules	FDS	internal normal modes	

ELS: elastic light scattering—total scattered intensity profile
QLS: quasielastic light scattering—angular dependent spectral shape
EPLS: electrophoretic light scattering—electrical field dependent QLS
FDS: forward depolarized scattering

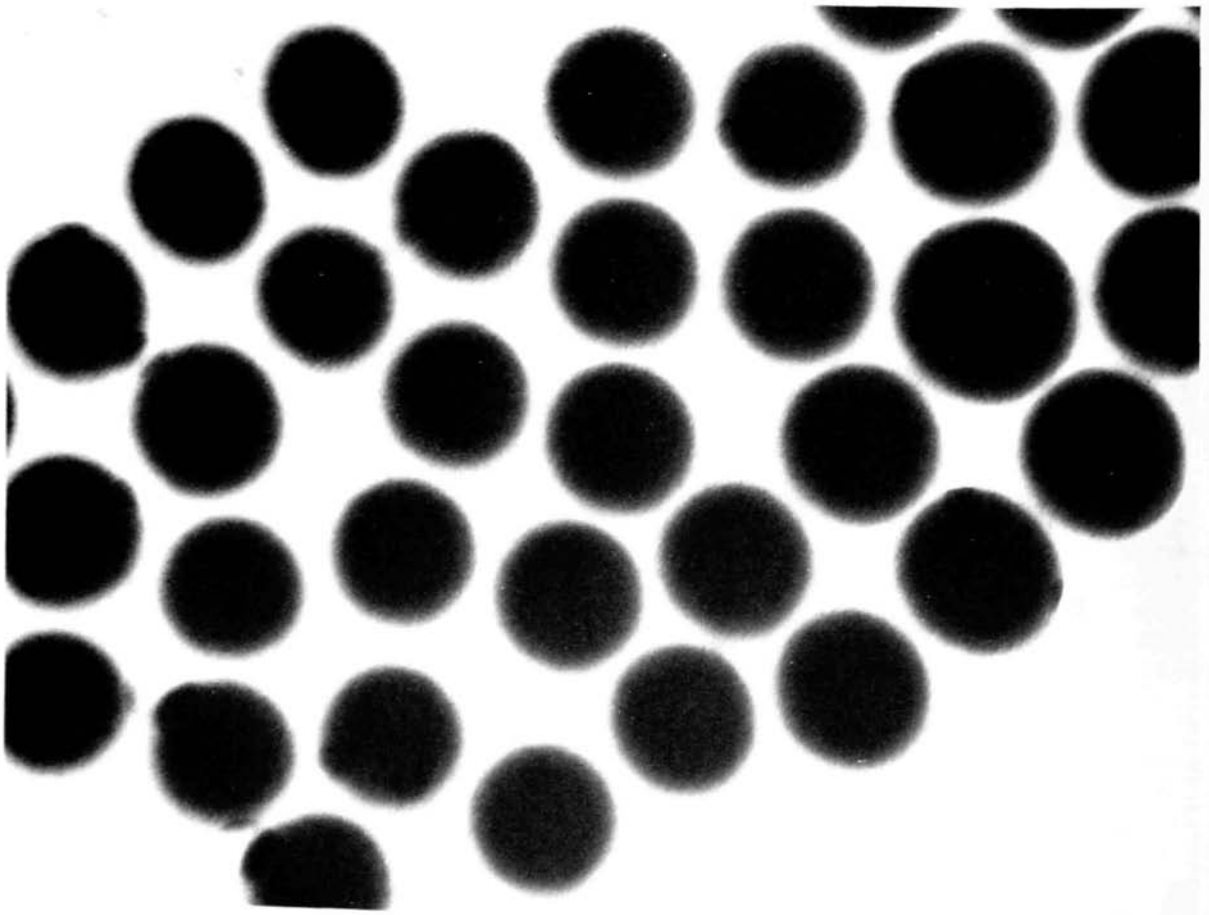

FIGURE 21. Transmission electron micrograph of amphoteric latex particles at X67,000.

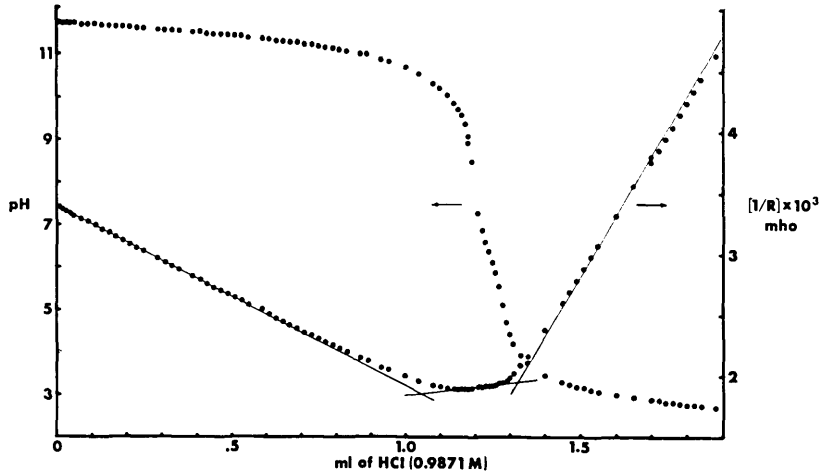

FIGURE 22. An example of potentiometric and conductometric titration. For the conductometry, the left intersection point of extrapolated lines is taken as the starting point of protonation of amino groups and the right intersection point as the termination point of protonation of carboxylate ions.

outlined earlier. In figures 23 through 25, we show the scattering profiles, plotted according to eq (9), at nominal pH of 3, 7 and 11, all at the same ionic strength of 1 mM. We display in figure 26 all the radius data so obtained at different pH from 3 to 11 at the same ionic strength. It is evident that there is a symmetric size change with respect to pH and the point of minimum radius at around pH 7 coincides with the isoelectric point determined by titration. The Stokes radii obtained by quasielastic light scattering agree with those in figures 23 and 25, 125 ± 3 nm and 123 ± 3 nm respectively at pH 3 and 11, while that of 118 ± 2 nm at pH 7 does not agree with the radius in figure 24, 112 ± 2 nm. Collecting all these results, we propose a model as depicted schematically in figure 27. It consists of hydrophobic core mainly constituted of styrene monomer and of hydrophilic shell made predominantly of ionic comonomers, MA and DEAM. The observed size change is then attributed to the chain expansion in the shell layer due to electrostatic repulsive interactions while the core remains relatively intact with respect to pH changes in the suspending medium. What remains uncertain however is the difference between the Stokes radius and that determined by elastic light scattering at pH 7. Whether the difference could be attributed to the thickening of the hydration layer at the isoelectric point must be examined by another technique such as NMR.

Before closing I must remark that one could raise the issue of whether our scheme of size determination is indeed probing the outer radius of swollen latex particles as contrasted to some ill-defined average of the inner and outer radii. After performing a set of simulation studies with concentric spheres having different segment densities in the shell volume relative to that in the core, we are convinced that our method is likely to underestimate the outer radius

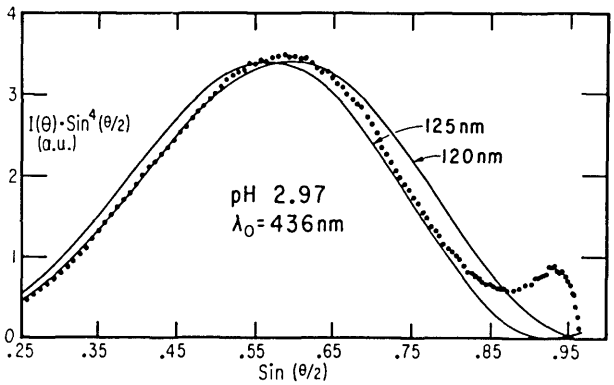

FIGURE 23. Light scattering profile of amphoteric latex at pH 2.97 where the polarization condition was unpolarized/unpolarized. Solid curves represent an isotropic solid sphere with the indicated radius in the Rayleigh-Gans-Debye scattering.

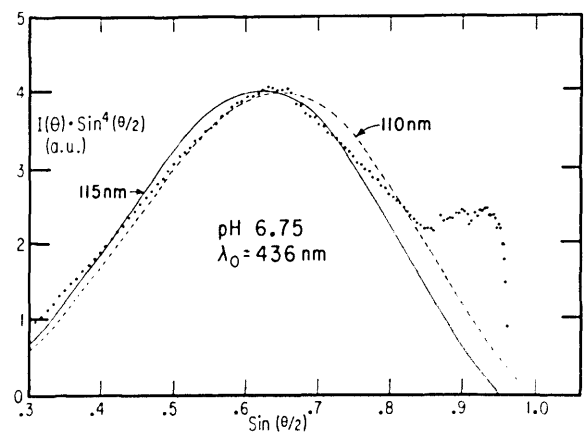

FIGURE 24. Same as figure 23 at pH 6.75.

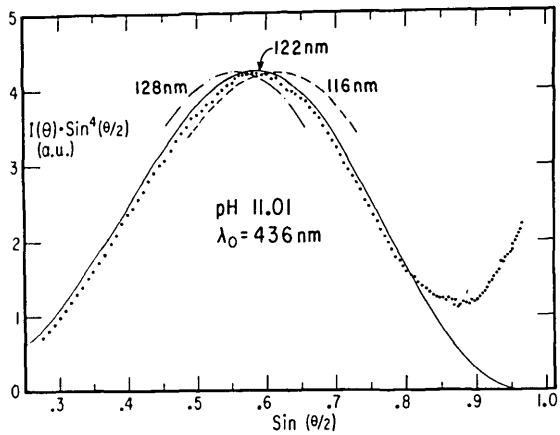

FIGURE 25. Same as figure 23 at pH 11.01.

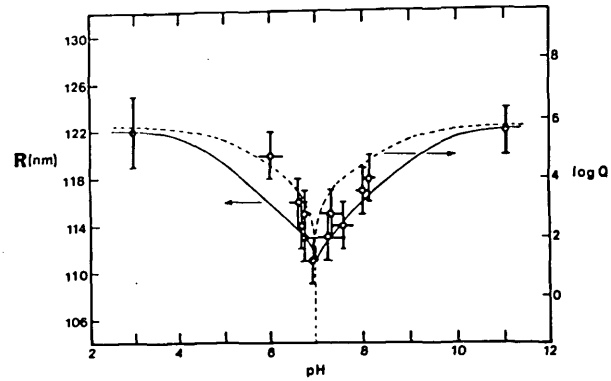

FIGURE 26. The particle radius versus pH. The dashed curve represents the degree of ionization and the solid curve a model of simple polyelectrolyte effect for the shell layer.

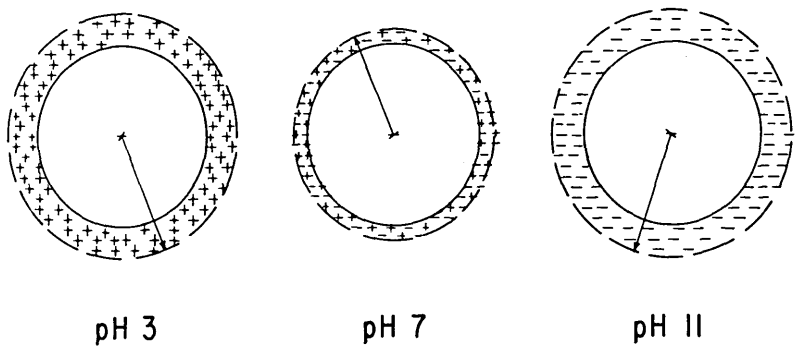

FIGURE 27. Schematic representation of pH induced swelling and deswelling of latex particles.

in the swollen state. Hence the latex particle dilation could easily be larger than what we report here. Unambiguous confirmation of the concentric sphere model is not possible with light scatterings alone. It might be possible to employ small angle neutron scattering [53] with perdeuterated core (with fully deuterated styrene monomer) and an appropriate D_2O/H_2O mixture to contrast match the core and solvent such that the scattering due to the shell volume can be accentuated, whereby we could indeed measure the shell thickness dilation with pH.

b. Photoreceptor Disk Membrane Vesicles

The vertebrate visual process involves complex sequences of events in transducing photochemical energy to electrical energy [54–56]. A vast literature exists concerning the role of the visual pigment membrane in this process [57, 58]. Our goal has been to isolate disk membranes from vertebrate rod outer segment (ROS) as intact as possible [59] and focus on their static and dynamic structure relative to the photoreceptor function. I shall now discuss what we have learned about these membranes by isolating the disk membranes from ROS, swelling them into vesicles in hypotonic media and examining them in dilute suspensions by quasielastic and elastic light scatterings.

A typical homodyne power spectrum is shown in figure 28 and the spectral halfwidths obtained at different scattering angles are displayed in figure 29. From these, we deduced the Stokes radius of 0.51 ± 0.05 μm. If the vesicles were spherical in shape, then modelling them as spherical shells was quite reasonable because the bilayer thickness [60] of about 75 nm was negligibly small compared to 500 nm for the Stokes radius. Analogous to eq (9), one obtains from Eqs (5) through (8) in the limit of $p=q=0$,

$$x^2P(\theta)=\sin^2 x \tag{23}$$

for spherical shell. The results of elastic light scattering plotted according to eq (23) are shown in figure 30. The equilibrium radius calculated from the Bragg condition of $QR=n\pi/2$, where the maxima are given by $n=$odd integers and the minima by $n=$even integers, is 0.48 ± 0.06 μm. In

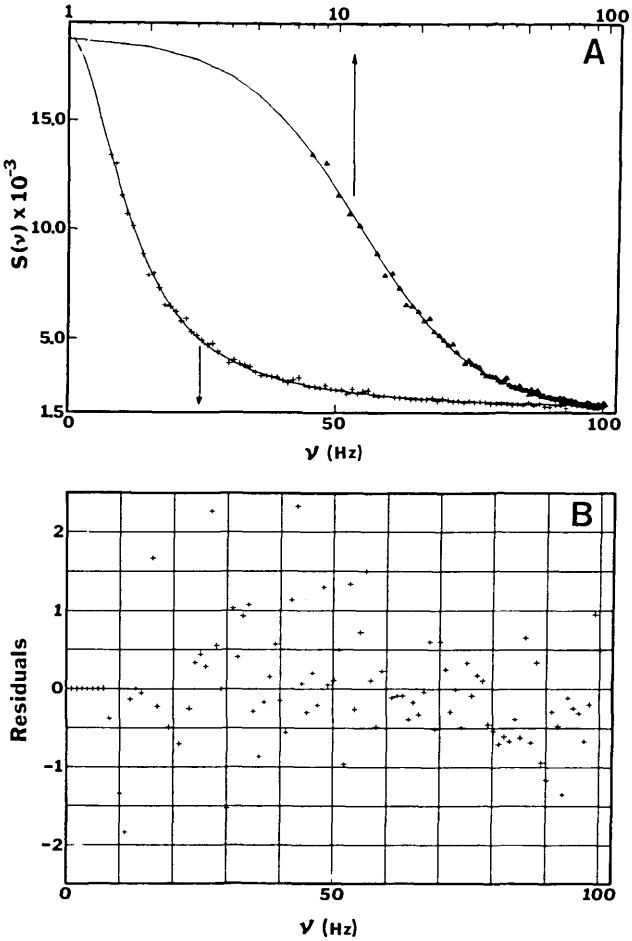

FIGURE 28. An example of homodyne power spectrum of the scattered light from photoreceptor disk membrane vesicles at 50° scattering angle. Each solid curve in the upper figure represents a single Lorentzian profile with a halfwidth $\Delta\nu_{1/2}$ of 16 Hz. In the lower figure, the normalized residuals of fitting to the single Lorentzian is plotted against frequency ν.

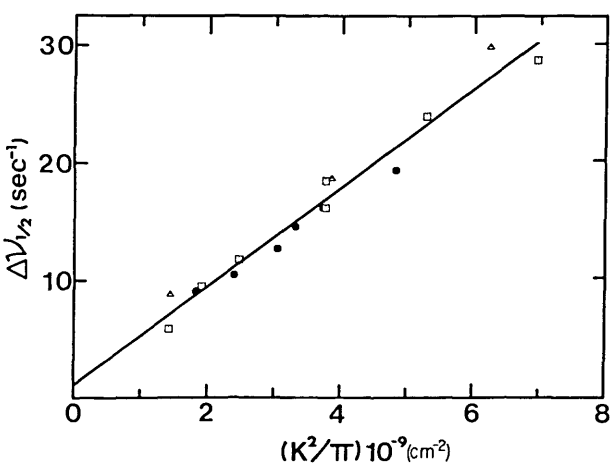

FIGURE 29. $\Delta\nu_{1/2}$ versus k^2/π. Three independently prepared samples are distinguished by different symbols.

view of the agreement between the results of quasielastic and elastic light scattering, we take the spherical shell model for the vesicles to be valid in this particular suspending medium [61, 62].

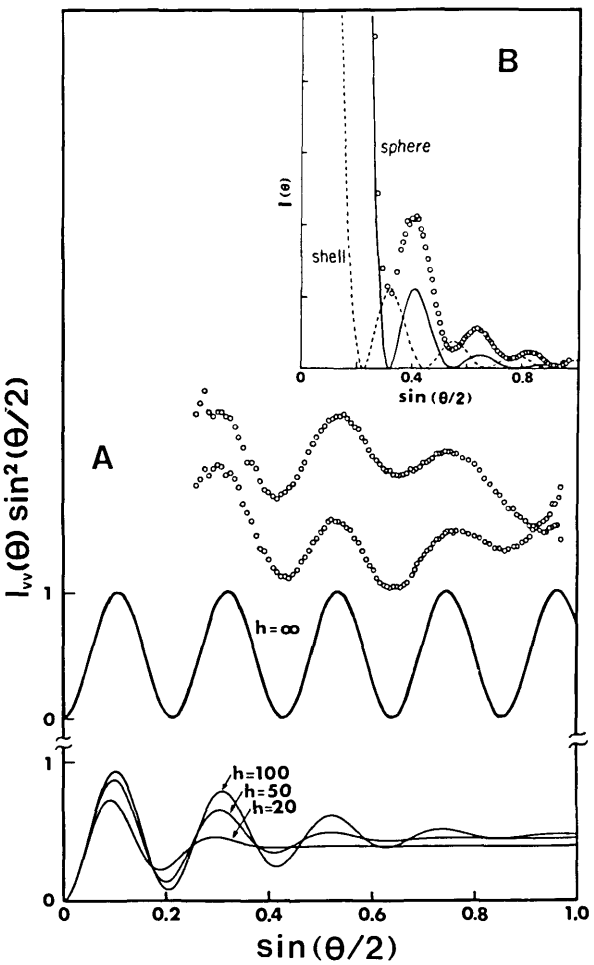

FIGURE 30A. The scattered intensity modulation profiles of two independently prepared vesicle suspensions of ROS membranes are displayed by plots of $I_{vv}(\theta)\sin^2(\theta/2)$ against $\sin(\theta/2)$. The two sets are vertically shifted to exhibit the reproducibility of the extrema positions. The solid curves $x^2P(x)$ or $(QR_w)^2<P(\theta)>$ is plotted against $\sin(\theta/2)$. The parameters used for the theoretical profiles are $R = 0.48\ \mu$m for monodisperse shells ($h = \infty$) and $R_w = 0.48\ \mu$m for polydisperse shells of the indicated distribution index h. Zimm-Schulz distribution function is used for the number fraction of shells with radius R as

$$f_w(R) = \frac{1}{h!}\left(\frac{h+1}{R_w}\right)^{h+1} R^h \exp\left[-\frac{(h+1)R}{R_w}\right]$$

where R_w is the weight average radius.

FIGURE 30B. Comparison of the intensity profiles of solid sphere (solid) and sperical shell (dashed) is given by two theoretical curves; the experimental data for polystyrene latex sphere (0.45 μm radius) are represented by the circles. Here, the plot is $I(\theta)$ versus $\sin(\theta/2)$ unlike those in (30a).

Upon changing the osmotic pressure of the suspending medium by an impermeable second solute, e.g., sucrose, we observe that the vesicles deform by deswelling, which is caused by the chemical potential gradient of the principal permeable component, namely H_2O. From the osmotic deformation behavior of the vesicles we were able to estimate the lateral compressive modulus of the membrane bilayer [63]. This turned out to be around 3×10^3Pa.

Since the membrane vesicles respond to the chemical potential gradient of water across the bilayer, their deformation behavior can be used to probe the permeability of ionic components including the hydrogen ion. Elastic light scattering studies of the vesicle shape have shown that the hydrogen ion is completely permeable within the pH range of 6–8 [64]. This is shown in figure 31 where the scattering profile of the spherical shell shape of the vesicles is hardly affected.

The binding of Ca^{+2} on vesicles was then studied by electrophoretic light scattering [65]. The Doppler shift spectra all at 7° scattering angle and 20 °C at a constant ionic strength of 1 mM are displayed in figure 32. The corresponding electrophoretic mobility profile at different Ca^{+2} concentrations is shown in figure 33 where the solid curve is drawn with a two-binding sites model. It can be represented by

$$r/C = K_1 C(n_1 - r) + n_2 K_2 \left(\frac{1 + K_1 C^2}{1 + K_2 C}\right) \qquad (24)$$

where r is the number average bound Ca^{+2} per vesicle, n_1 and K_1 are respectively the number of high affinity, a second order cooperative binding sites and the corresponding binding constant, and n_2 and K_2 are the other set of constants for low affinity, a first order non-cooperative binding. By replotting the data in figure 32, a Scatchard plot shown in figure 34 results, from which we estimate $n_1 = (1.4 \pm 0.1) \times 10^4$ and $K_1 = (7 \pm 2) \times 10^{10}\ M^{-2}$ while n_2 and K_2 are subject to a good deal of uncertainty.

c. Binary Nematic Solutions

Here, our interest was focused on examining how the phase behavior [66] and dynamic twist modes [67] were affected by mixing of non-nematogens (biphenyl and benzene) to a thermotropic nematic liquid crystal, methoxy benzylidene butyl-aniline (MBBA). The scattering technique is the FDS method where the director of the nematic system is oriented parallel to the polarization of incident light while that of scattered light is perpendicular to the director axis [68]. Two examples of the FDS power spectra are displayed in Fig 35. With use of the twist viscosity of Gahwiller [69], we were able to determine the twist elastic constant of pure MBBA as a function of the reduced temperature. This is shown in figure 36. Incorporating the concentration dependence of a non-nematogen to that of temperature, we could deduce the mapping of the twist diffusivity coefficient over the entire binary nematic phase region. In figure 37, such a mapping is displayed where the non-nematogen is biphenyl [68]. Fearing that this might have been unique to the biphenyl-MBBA system, benzene-MBBA nematic solution was also examined [70]. The result, as shown in figure 38, indicates that such a behavior is not restricted to the biphenyl-MBBA system.

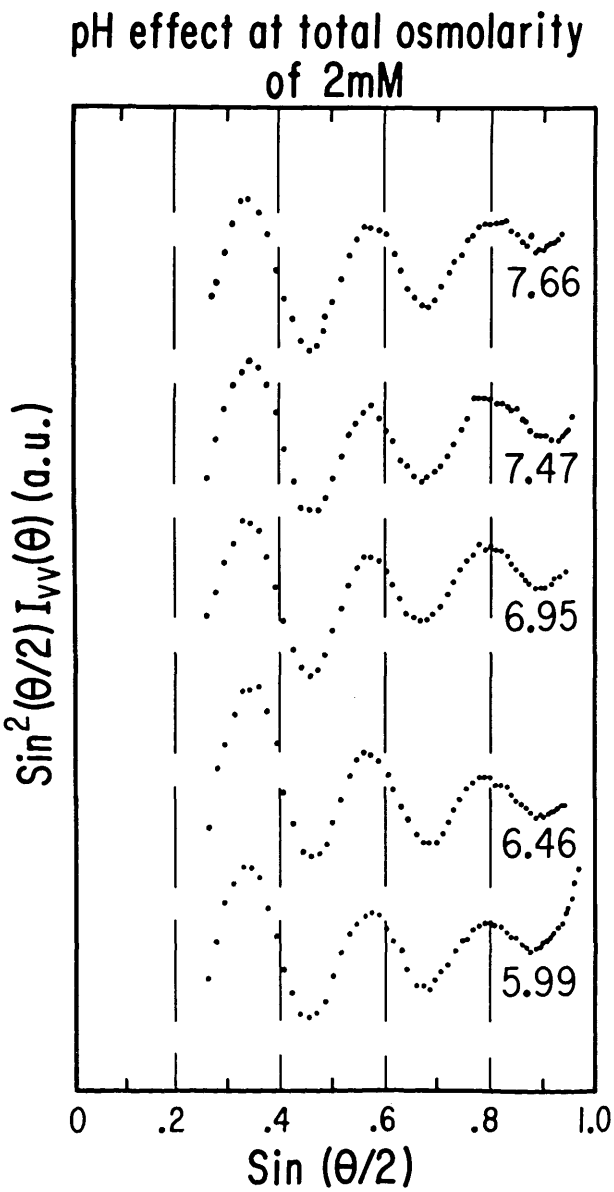

FIGURE 31. Light scattering intensity profiles of the vesicles at different pH to show that hydrogen ion is completely permeable to the membranes within the pH range studied. Profiles give no indication of the osmotic deformation which is clear evidence for shape invariability.

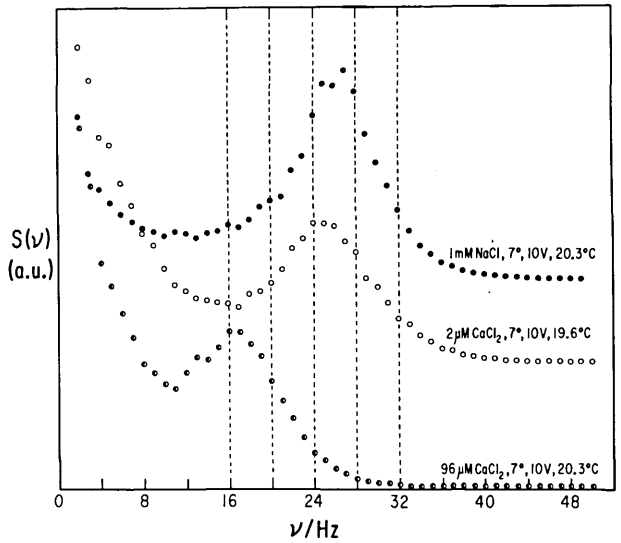

FIGURE 32. Three heterodyne spectra of electrophoretic light scattering, all at 7° scattering angle and 10V peak-to-peak (27V/cm) at three different Ca^{+2} concentrations at 1 mM ionic strength solution

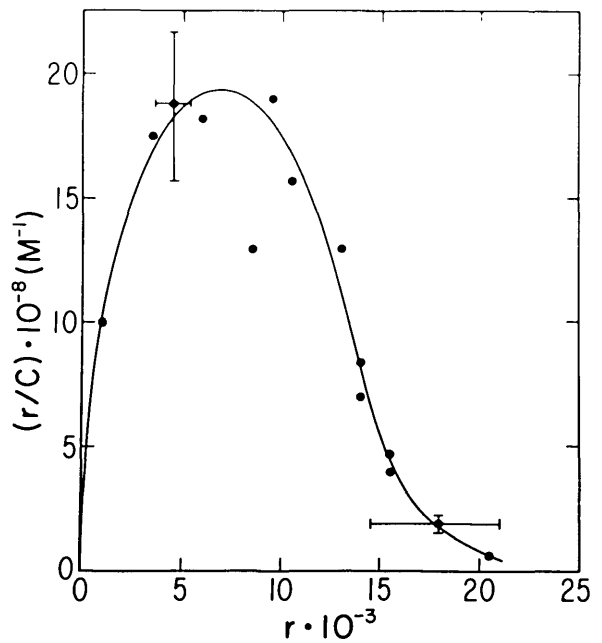

FIGURE 34. A Scatched plot where the number average degree of binding per unit ligand concentration r/C is plotted against the degree of binding r. Error bars apply to every data point although only two are shown. Solid curve is drawn according to the model discussed in the next while dashed line is drawn by ignoring lower five points in r. The intercept with the abscissa of the dashed line gives the apparent first order binding site number n_1 and its slope the apparent first order dissociation constant K_1^{-1}.

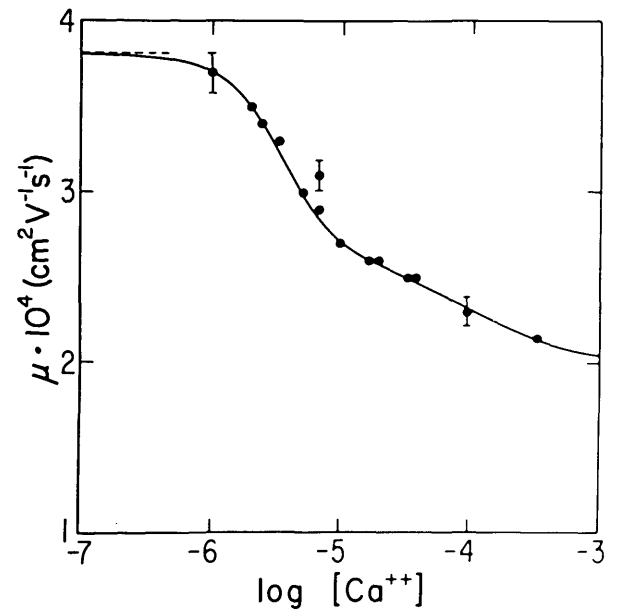

FIGURE 33. The electrophoretic mobility, corrected to 20 °C in water, is plotted against Ca^{+2} concentration in log scale. Error bars apply to every data point although only three are shown. The solid curve is drawn according to the model discussed in the text.

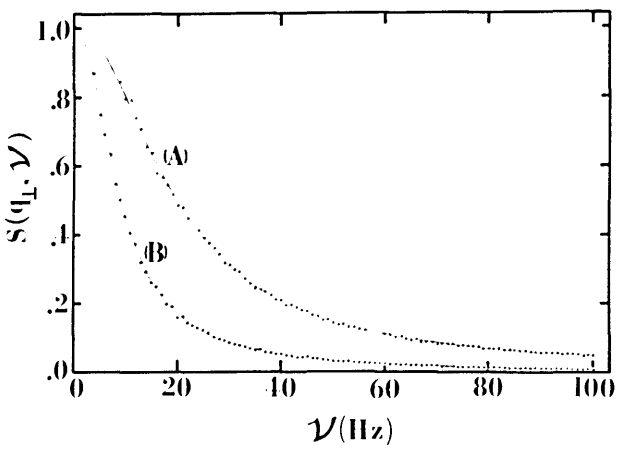

FIGURE 35. Heterodyne power spectra of pure MBBA at 36.90 °C, $\Delta\nu_{1/2}$ = 30.1±0.1 Hz (upper) and at 44.95 °C, $\Delta\nu_{1/2}$ = 6.9±0.6 Hz (lower).

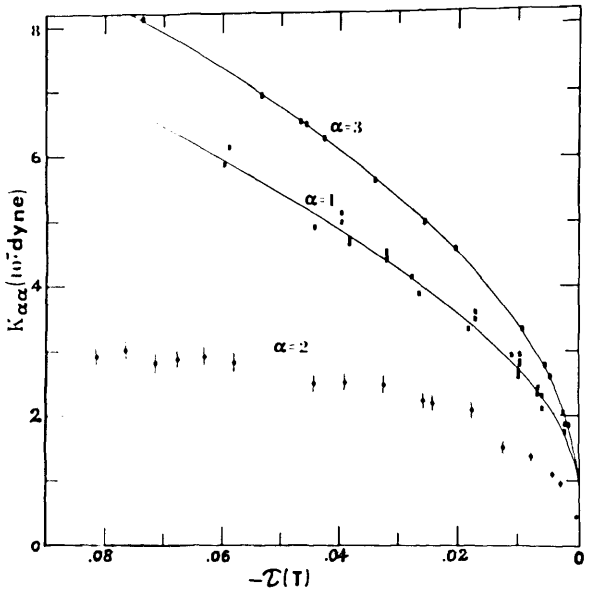

FIGURE 36. The elastic constants of pure MBBA versus the reduced temperature $\tau(T)$. The bend ($\alpha = 3$) and splay ($\alpha = 1$) elastic constants are from the work of Haller and the twist constant ($\alpha = 2$) is ours with use of the twist viscosity of Gahwiller.

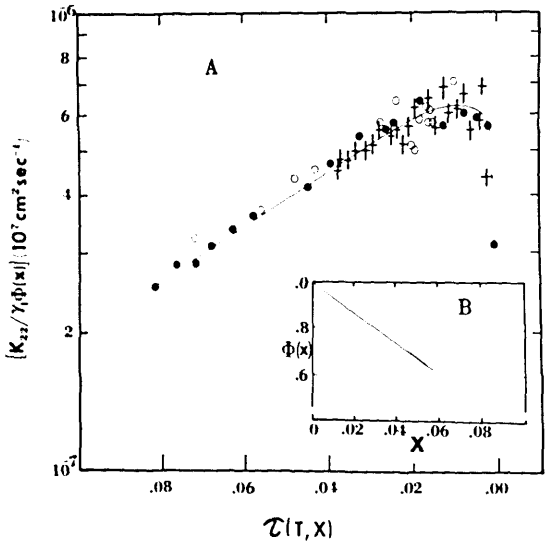

FIGURE 37A. Composition reduced twist diffusivity coefficient $K_{22}/\gamma_1\phi(X)$ versus the reduced temperature $\tau(T,X) \equiv T - T_{N1}(X)/T_{n1}(X)$, where $T_{n1}(X) = (0)(1\text{-}250X)$ as observed from the phase diagram. The filled circles are from temperature scan of pure MBBA, the open circles are from temperature scan of 0.081 mole fraction biphenyl solution and the crosses (+) are from composition scan at 23 °C.

FIGURE 37B. $\Phi(X)$, the composition dependent factor of the twist diffusivity coefficient at constant reduced temperature versus mole fraction of biphenyl.

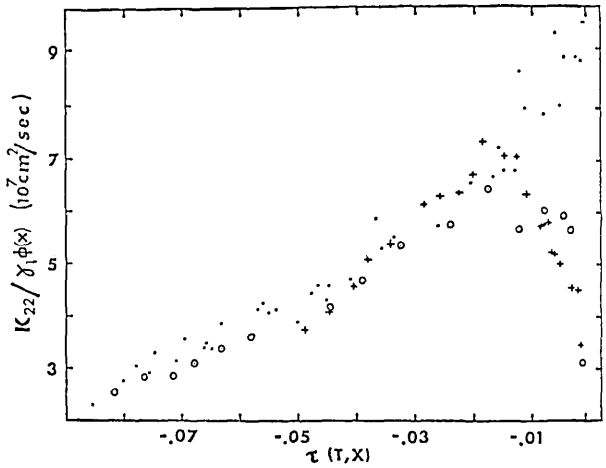

FIGURE 38. Same as figure 37 for the MBBA-benzene system.

d. Intramolecular Chain Dynamics of Isotactic Polystyrene

A typical FDS power spectrum [46] of an isotactic polystyrene sample ($Mw = 3.5 \times 10^6$, $<s^2>^{1/2} = 1270$ Å) in tetrahydrofuran at 4.0 mg/mL is shown in Fig 39. All spectra were analyzed according to eq (21) with the Zimm spacing [71] of relaxation times up to five relaxation modes. Truncation beyond the 6th mode was called for due to the chosen bandwidth of 2 kHz whereby the higher modes were obscured by the shot-noise level. Spectral analysis was effected by a 3-parameter fitting routine; the parameters were the spectral intensity, shot-noise level and the terminal relaxation time τ_1. By fixing the spacing to that of Zimm type, what we extract from the experiment is τ_1, the slowest relaxation time of internal normal modes. Because all measurements were performed at finite concentrations, we had to extrapolate the data to infinite dilution. This is effected by plotting τ_1 against relative viscosity η_r of polymer solution and extrapolating to $\eta_r = 1$. Such a plot is shown in figure 40 from which τ_1 at infinite dilution is determined as $(1.2\text{-}1.5) \times 10^{-4}$ sec with an experimental uncertainty of ±30%. The theoretical value of τ_1 for the polymer sample is 1.5×10^{-4} sec. Within the experimental error the two are in agreement.

7. Concluding Remarks

It is my hope that the readers of this report would be as excited as I have been about the potentials of light scattering techniques and have some appreciation for what kinds of problems can be tackled. I must again emphasize that this is intended only as a sketchy review of what my students and I have been able to do and not as an up-to-date review of the field. I have cited several excellent reviews in the text.

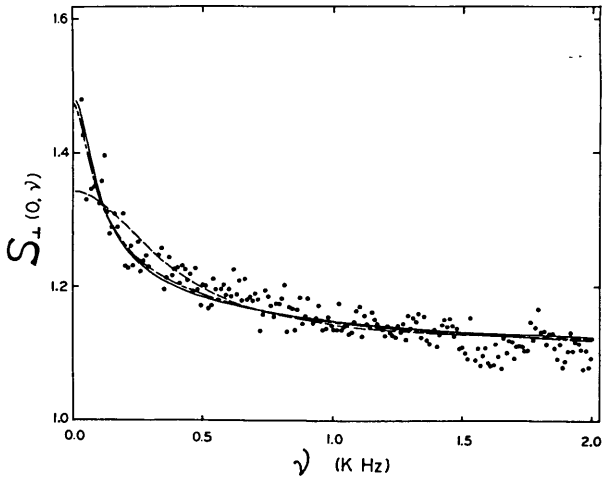

FIGURE 39. FDS power spectrum of isotactic polystyrene (M.W. 3.5×10^6) in THF at $C = 4.0$ mg/mL. The solid curve is for a single Lorentzian fit and the dashed curve is for Zimm fit with the first five relaxation times (Z5).

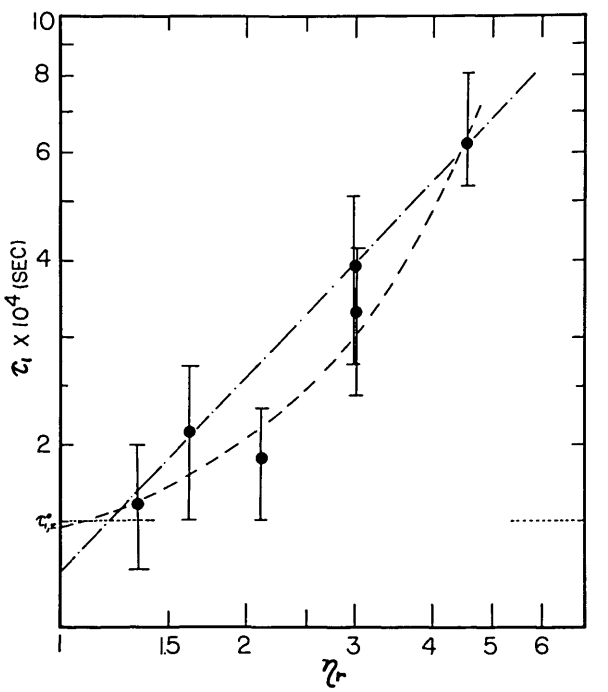

FIGURE 40. The terminal relaxation time deduced from the Z5 fit of the FDS power spectra of isotactic polystyrene in THF is plotted against relative viscosity at different concentrations (0.65 mg/mL – 4.0 mg/mL. Error bars define 95% confidence limit of the fit and the theoretical value of the Zimm model is designated as $\tau_{1\infty}^0$ in the ordinate.

The work presented here is the result of efforts by many former and current students and associates of mine with whom I have been fortunate enough to be associated in the past nine years, and I thank each and every one of them by name: Charles C. Han, Steven A. Shaya, Alex R. Sluzas, William F. Hoffman, Takashi Norisuye, George B. Caflisch, Eric J. Amis, David M. Piatt, Jeffrey A. Wesson, Taihyun Chang, Deborah A. Davenport, Jeffrey L. Nelson, Edward D. Erickson, Dong M. Pham, and Dan J. Wendt.

Support by the National Institutes of Health through EY 01483 and a Biomedical Research Support Grant administered through the Graduate School of the University of Wisconsin-Madison are gratefully acknowledged.

8. References

[1] Cummins, H. Z. and Swinney, H. L. (1970) Prog. Opt. **8**, 133.
[2] Pecora, R. (1972) Annu. Rev. Biophys. Bioeng. **1**, 257.
[3] Chu, B. (1974) *Laser Light Scattering* (Academic, New York).
[4] Berne, B. J. and Pecora, R. (1976) *Dynamic Light Scattering* (Wiley, New York).
[5] Cummins, H. Z. and Pike, E. R., ed. (1974) *Photon Correlation and Light Beating Spectroscopy* (Plenum Press, New York).
[6] Zimm, B. H., Stein, R. S. and Doty, P. (1945) Polym. Bull. **1**, 90.
[7] Stacey, K. A. (1956) *Light Scattering in Physical Chemistry* (Academic, New York).
[8] Kerker, M. (1969) *The Scattering of Light and Other Electromagnetic Radiation* (Academic, New York).
[9] Bloomfield, V. A., Crothers, D. M. and Tinoco, I., Jr. (1974) *Physical Chemistry of Nucleic Acids* (Harper and Row, New York), p. 187.
[10] Zimm, B. H. (1948) J. Chem. Phys. **16**, 1099.
[11] Debye, P. (1944) J. Appl. Phys. **15**, 338.
[12] Kerker, M. (1969) *The Scattering of Light and Other Electromagnetic Radiation* (Academic, New York), pp. 482-485.
[13] Oster, G. and Riley, D. P. (1952) Acta Crystallogr. **5**, 1.
[14] Pecora, R. and Aragon, S. R. (1974) Chem. Phys. Lipids **13**, 1.
[15] Saito, N. and Ikeda, Y. (1951) J. Phys. Soc. Japan **6**, 305.
[16] Chang, T., Pham, D. M., Piatt, D. M. and Yu, H., to be published.
[17] Heller, W. and Pugh, T. L. (1957) J. Colloid Sci. **12**, 294.
[18] Shaya, S.A., Han, C. C. and Yu, H. (1974) Rev. Sci. Instrum. **45**, 280.
[19] Ware, B. R. and Flygare, W. H. (1971) Chem. Phys. Lett. **12**, 81.
[20] Uzgiris, E. E. (1972) Opt. Commun. **6**, 55.
[21] Ware, B. R. and Flygare, W. H. (1972) J. Colloid Interface Sci. **39**, 670.
[22] Bennett, A. J. and Uzgiris, E. E. (1973) Phys. Rev. A **8**, 2662.
[23] Uzgiris, E. E. (1974) Rev. Sci. Instrum. **45**, 74.
[24] Uzgiris, E. E. and J. H. Kaplan (1974) Rev. Sci. Instrum. **45**, 120.
[25] Ware, B. R. (1974) Advan. Coll. Interface Sci. **4**,1.
[26] Haas, D. D. and Ware, B. R. (1976) Anal. Biochem. **74**,175.
[27] Flygare, W. H. and Ware, B. R. (1976) in *Molecular Electro-optics*, O'Konski, C. T., Ed. (Marcel Dekker, New York), p. 544.
[28] Mohan, R., Steiner, R. and Kaufman, R. (1976) Anal. Biochem. **79**, 506.
[29] Josefowicz, J. and Hallet, F. R. (1975) Appl. Opt. **14**, 740.
[30] Schlessinger, B. S. (1958) J. Phys. Chem. **62**, 916.
[31] Alberty, R. A. (1948) J. Chem. Edu. **25**, 426.

[32] Longsworth, L. G. and Jacobsen, C. F. (1949) J. Phys. Chem. **53**, 126.
[33] Caflisch, G. B., Norisuye, T. and Yu, Hyuk, (1980) J. Colloid Interface Sci. **76**, 174.
[34] Henry, D. C. (1931) Proc., Roy. Soc. (London) **A133**, 106.
[35] See for a recent survey, Shaw, D. J. (1969) *Electrophoresis* (Academic, New York).
[36] Tiselius, A. and Svensson, H. (1940) Trans. Faraday Soc. **36**, 16.
[37] Alexander, A. E. and Johndon, P. (1949) *Colloid Science* (Oxford University Press, London), p. 742.
[38] Cannan, R. K., Palmer, A. K. and Kibrick, A. (1942) J. Biol. Chem. **142**, 803.
[39] Abramowitz, M. and Stegun, I. A. (1964) *Handbook of Mathematical Functions*, NBS Applied Mathematics Series 55 (U.S. Government Printing Office, Washington, D.C.), p.555.
[40] Baldwin, R. L., Gosting, L. J., Williams, J. W. and Alberty, R.A. (1955) Discussions Faraday Soc. **20**, 13.
[41] Wada, A., Suda, N., Tsuda, T. and Soda, K. (1968) J. Chem. Phys. **50**, 31.
[42] Wada, A., Soda, K., Tanaka, T. and Suda, N. (1970) Rev. Sci. Instrum. **41**, 845.
[43] Schurr, J. M. and Schmitz, K. S. (1973) Biopolymers **12**, 1021.
[44] Schmitz, K. S. and Schurr, J. M. (1973) Biopolymers **12**, 1543.
[45] Norisuye, T. and Yu, H. (1978) J. Chem. Phys. **68**, 4038.
[46] Han, C. C. and Yu, H. (1974) J. Chem. Phys. **61**, 2650.
[47] Yen, S.P.S., Rembaum, A., Molday, R. S. and Dreyer, W. J. (1976) *Emulsion Polymerization*, Pirma, I. and Gordon, J. eds., ACS Symposium Series, Vol. 24 (American Chemical Society, Washington, DC), p. 236.
[48] Molday, R. S., Dreyer, W. J., Rembaum, A. and Yen, S.P.S. (1975) J. Cell. Biol. **64**, 75.
[49] Jacobson, B. S. and Branton, D. (1977) Science **195**, 302.
[50] Vanderhoff, J. W. and van den Hull, H. J. (1973) J. Macromol. Sci.-Chem. **A7**, 677.
[51] Homola, J. and James, R. O. (1977) J. Colloid Interface Sci. **59**, 123.
[52] Piatt, D. M., Wesson, J. A., Caflisch, G. B., Nelson, J. L. and Yu, H., to be published.
[53] See for a recent review, Maconnachie, A. and Richards, R. W. (1978) Polymer **19**, 739.
[54] Wald, G. (1968) Science **162**, 230.
[55] Rodieck, R. (1973) *The Vertebrate Retina* (Freeman, San Francisco).
[56] Kliger, D. S. and Menger, E. L. (1975) Acc. Chem. Res. **8**, 81.
[57] Hagins, W. A. (1972) Annu. Rev. Biophys. Bioeng. **1**, 131.
[58] Abrahamson, E. W. (1975) Acc. Chem. Res. **8**, 101.
[59] Amis, E. J., Davenport, D. A. and Yu, H., Anal. Biochem., in press.
[60] Worthington, C. R. (1973) Exp. Eye Res. **17**, 487.
[61] Norisuye, T., Hoffman, W. F. and Yu, H. (1976) Biochemistry **15**, 5678.
[62] Hoffman, W. F., Norisuye, T. and Yu, H. (1976) Biochemistry **16**, 1273.
[63] Norisuye, T. and Yu, H. (1977) Biochim. Biophys. Acta **471**, 436.
[64] Amis, E. J., Wendt, D. A., Erickson, E. D. and Yu, H., Biochim. Biophys. Acta, in press.
[65] Caflisch, G. B. (1979) Ph.D. Thesis, University of Wisconsin, Madison, Wisconsin; Piatt, D. M., Caflisch, G. B. and Yu, H., to be published.
[66] Shaya, S. A. and Yu, H. (1975) J. Phys. (Paris) **C1**(3), 59.
[67] deGennes, P. G. (1974) *The Physics of Liquid Crystals* (Oxford, New York).
[68] Shaya, S. A. and Yu, H. (1975) J. Chem. Phys. **63**, 221.
[69] Gahwiller, Ch. (1973) Mol. Cryst. Liquid Cryst. **20**, 301.
[70] Sluzas, A. R. (1975) Ph.D. Thesis, University of Wisconsin, Madison, WI.
[71] Zimm, B. H. (1956) J. Chem. Phys. **24**, 269.

JOURNAL OF RESEARCH of the National Bureau of Standards
Vol. 86, No. 6, November–December 1981

Computer Networks—The ALOHA System*

Franklin F. Kuo

University of Hawaii, Honolulu, HI 96822

August 11, 1981

The ALOHA System, an experimental UHF radio computer communication network, was developed at the University of Hawaii, 1970–76. In this survey paper, we give a general overview of packet communication techniques applied to computer networks. Then we discuss the concept of packet broadcasting and give a short description of the ALOHANET. Next, a discussion of the application of ALOHA techniques to satellite communications is presented. Finally, a short survey of present-day research and development efforts in packet broadcasting is presented.

Key words: ALOHA System; ALOHANET; compter network; packet broadcasting; radio computer communication network; satellite communication.

1. Introduction

Developments in remote access computing in the 1970's have resulted in greater and greater importance attached to computer-communication networks. In discussing computer-communications it is useful to distinguish between communications among computers, and communications using computers. For example, the ARPANET [1][1] is a computer-communications network that interconnects a collection of large or specialized research computers and uses both kinds of communications. Communications among the ARPANET computers is made possible through the use of message switching computers called IMP's (Interface Message Processor) and TIP's (Terminal Interface Processors).

In discussing the ALOHA broadcast packet communication network, we concentrate on communications using computers. The term *"broadcast"* implies radio. ALHOHA is one of the world's first time-sharing networks that uses packet radio as the communications medium. By the word *"packet"* we mean an allocated unit of transmitted information in terms of a specific number of bits. For example, in the mail system, a packet is a letter with a variable number of bits; in the ARPANET, a packet is a string of data of 1024 bits. Before we discuss the specifics of the ALOHANET, it is useful to examine what we mean by packet communications.

*The writing effort was supported by the Office of Naval Research under Contract No. N00014-C-78-0498.

[1] Figures in brackets indicate literature references at the end of this paper.

2. Packet Communications

In the early days of time-sharing, remote access to the central computer depended almost exclusively on the use of leased or dial-up facilities provided by the telephone company. Generally the terminal-to-computer access was by means of dial-up facilities which made use of telephone circuits on a *circuit-switched* basis. In circuit switching the telephone system's exchanges are switching nodes which piece together a continuous path or circuit from caller to receiver. The connection is maintained until either party hangs up. Usually the call is charged on an elapsed time and/or distance basis. Circuit switching is a technique that was developed at the turn of the century for voice communications. When applied to computer-communications, circuit switching is applicable but not totally satisfactory for one reason: cost effectiveness. Computer data is usually transmitted as bursts interspered between varying quiescent periods. When two people are conversing over a voice circuit, the circuit is used quite efficiently. However, for interactive computing on a time-sharing system, the circuit is utilized only a small percent of the total connect time for actual transmission of data [2].

Packet switching is a technique which has evolved in the late 1960's and early 1970's and is ideally suited for computer data communications. In a packet switching network, the topology takes the form of a highly connected (but not fully connected) set of nodes. At each node is a computer that acts as a message switch. In the case of the ARPANET this computer is the IMP or TIP.

Messages from Computer A to Computer B in the network are transmitted in the form of packets of a given number of bits. Each packet has a *"header"* which contains information giving a complete specification of the communication desired (e.g. destination, source size sequence number, priority, etc.). Each packet also has a given number of checksum bits for error detection purposes. A packet sent from A to B does not have a fixed route. It is sent to intermediate nodes in a store-and-forward manner. Each node examines the packet for its ultimate destination and makes a parity check to determine any error. If the packet is received with no errors, an acknowledgement is sent to the previous node traversed and the packet is successively forwarded to the next node down the line until it is received, error free at its ultimate destination. Route selection is dynamic in that each packet is directed along a path for which the total estimated transit time is minimum. This path is not predetermined but calculated at each intermediate node.

Since packet switching uses computers so heavily in the communications process, it has only become feasible in the past few years because of the increasing speed and lowered costs of digital computers. Roberts [3] makes clear this point in the introduction of his paper:

> "Packet switching (is) strongly dependent upon the cost of computing since it uses computers to correct transmission errors, to provide high reliability through alternate routing, and to allocate communication bandwidth on a demand basis rather than as a preassigned bandwidth."

Metcalfe [4] gives a good summary of the reasons why packet switching is too efficacious for computer communications.

> "In pure packet-switching, on the other hand, the communication system does not dedicate circuits to set up connections; rather, the messages which form a conversation are injected individually at the exact moment of their readiness. Because there is no connection setup to amortize over a conversation, short conversations are not seriously disadvantaged relative to long ones; because a packet-switching system allocates its resources to messages rather than conversations, the inactive periods in one conversation can be used to support other conversations. Packet-switching makes good use of communications facilities when the conversations being carried are either short or very bursty."

3. Packet Broadcasting

Packet broadcasting is a technique whereby data is sent from one node in a net to another by attaching address information to the data to form a packet typically from 30 to 100 bits in length. The packet is then *broadcast* over a communication channel which is shared by a large number of nodes in the net; as the packet is received by these nodes the address is scanned and the packet is accepted by the proper addressee (or addressees) and ignored by the others. The physical communication channel employed by a packet broadcasting net can be a ground based radio channel, a satellite transponder or a cable.

Packet broadcasting networks can achieve the same efficiencies as packet switched networks [1] but in addition they have special advantages for local distribution data networks, and for data networks using satellite channels [5]. In this paper we concentrate on those characteristics which are of interest for a local distribution data network. In particular, we discuss the design and implementation of the ALOHANET, a packet broadcasting radio network in operation at the University of Hawaii during 1970–76.

The ALOHANET was the first system which successfully utilized the packet broadcasting concept for on-line access of a central computer via radio. Although it has not been in operation since 1976, its design principles have been applied to a number of successfully operating present-day networks including ETHERNET [6], the Packet Radio Network (PRNET) [7], and the Packet Satellite Net (SATNET) [8]. In the next section we will briefly examine the operations of the ALOHANET [5].

4. Alohanet operations

In the ALOHANET, two 100 KHz channels were used in the UHF band—a *random access* channel for user-to-computer communication at 407.350 MHz and a *broadcast channel* at 413.375 MHz for computer-to-user messages. The original system was configured as a star network, allowing only a central node to receive transmissions in the random channel; all users received each transmission made by the central node in the broadcast channel. However, the subsequent addition of ALOHA repeaters generalized the network structure.

A block diagram of the ALOHANET is shown in figure 1. The central communications processor of the net is an HP 2100 minicomputer (32K of core, 16 bit words) called the MENEHUNE [5] (Hawaiian for IMP) which functioned as a multiplexor/concentrator in much the same way as an ARPANET IMP [1]. The MENEHUNE accepts messages from the UH central computer, and IBM System 370/158 running TSO or from ALOHA's own time-sharing computer, the BCC 500, or from any ARPANET computer linked to the MENEHUNE via the ALOHA TIP. Outgoing messages in the MENEHUNE are converted into packets, the packets are queued on a first-in, first-out basis, and are

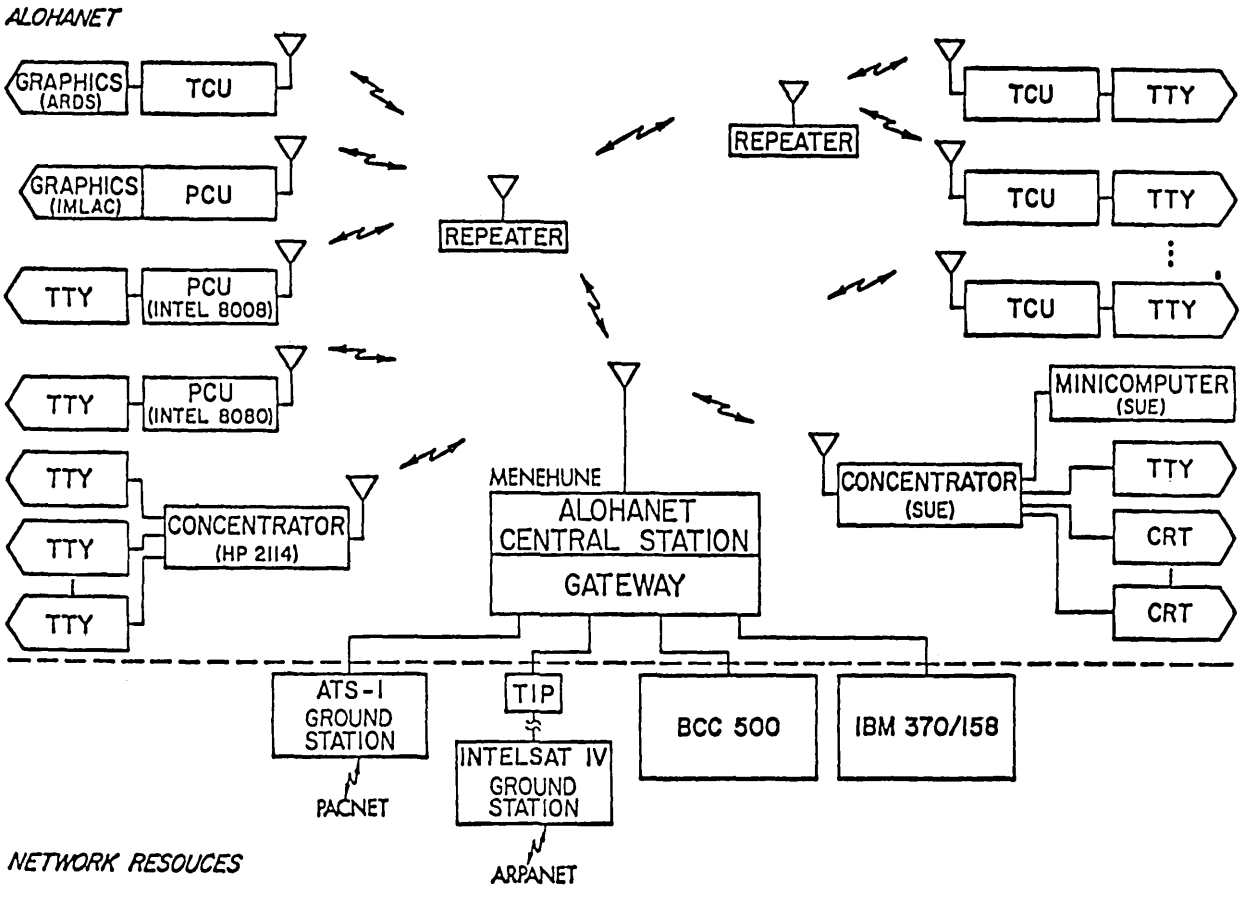

FIGURE 1.

then broadcast to remote users at a data rate of 9600 baud.

The packet consists of a header (32 bits) and a header parity check word (16 bits), followed by up to 80 bytes of data and a 16-bit data parity check word. The header contains information identifying the particular user so that when the MENEHUNE broadcasts a packet, only the intended user's node will accept it.

The random access channel (at 407.35 MHz) for communication between users and the MENEHUNE was designed specifically for the traffic characteristics of interactive computing. In a conventional communication system a user might be assigned a portion of the channel on either an FDMA or TDMA basis. Since it is well known that in time sharing systems, computer and user data streams are bursty [2] such fixed assignments are generally wasteful of bandwidth because of the high peak-to-average data rates that characterize the traffic. The multiplexing technique that was utilized by the ALOHANET was a purely random access packet switching method that has come to be known as the *pure ALOHA* technique [9]. Under a pure ALOHA mode of operation, packets were sent by the user nodes to the MENEHUNE in a completely unsynchronized manner—when a node was idle it used none of the channel. Each full packet of 704 bits required only 73 ms at a rate of 9600 baud to transmit (neglecting propagation time).

The random or multi-access channel can be regarded as a resource which is shared among a large number of users in much the same way as a multiprocessor's memory is "shared." Each active user node is in contention with all other active users for the use of the MENEHUNE receiver. If two nodes transmit packets at the same time, a collision occurs and both packets are rejected. In the ALOHANET, a positive acknowledgement protocol was used for packets sent on the random-access channel. Whenever a node sent a packet it had to receive an acknowledgement message (ACK) from the MENEHUNE within a certain time-out period. If the ACK was not received within this interval the node automatically retransmitted the packet after a randomized delay to

avoid further collisions. These collisions, however, limited the number of users and the amount of data which could be transmitted over the channel as loading was increased.

An analysis [9] of the random access method of transmitting packets in a pure ALOHA channel showed that the normalized theoretical capacity of such a channel was $\frac{1}{2e} = 0.184$. Thus, the average data rate which can be supported is about one sixth the data rate which could be supported if we were able to synchronize the packets from each user in order to fill up the channel completely. Put another way, this result shows the ALOHA 9600 bit/second random access channel could have supported between 100 and 500 active teletype users—depending upon the rate at which they generated packets and upon the packet lengths.

4.1. ALOHANET Remote Units

The original user interface developed for the system was an all-hardware unit called an ALOHANET Terminal Control Unit (TCU), and was the sole piece of equipment necessary to connect any terminal or minicomputer into the ALOHA channel. As such it took the place of two dedicated modems for each user, a dial-up connection and a multiplexor port usually used for computer networks. The TCU was composed of a UHF antenna, transceiver, modem, buffer and control unit.

The buffer and control unit functions of the TCU were also handled by minicomputers or microcomputers. In the ALOHA system several minicomputers were connected in this manner in order to act as multiplexors for terminal clusters or as computing stations with network access for resource sharing. A later version of the TCU, using an Intel 8080 microcomputer for buffer and control, was built. Since these programmable units allowed a high degree of flexibility for packet formats and system protocols, they were referred to as PCU's (Programmable Control Units).

Since the transmission scheme of the ALOHANET was by line-of-sight, the radio range of the transceivers was severely limited by the diversity of terrain (mountains, high rise buildings, heavy foliage) that exists in Hawaii. A late development allowed the system to expand its geographical coverage beyond the range of its central transmitting station. Because of the burst nature of the transmissions in the ALOHA channel it was possible to build a simple store-and-forward repeater which accepted a packet within a certain range of ID's and then repeated the packet on the same frequency. Each repeater performed identically and independently for packets directed either to or from the MENEHUNE. Two of the repeaters were built which extended coverage of the ALOHANET from the island of Oahu to other islands in the Hawaiian chain.

5. Satellite communications

Because of the geographic isolation, one of the original objectives of the ALOHA system was to study the feasibility of the computer-communications by means of satellite. With the development of digital communication systems by COMSAT in which data at the rate of 50K baud can be transmitted through a single voice channel data transmission by satellite has become both technologically and economically feasible [10].

There is a basic and important difference between the use of a satellite channel and a wire channel for data communications. The satellite channel is a broadcast channel as opposed to a point-to-point wire channel, so that a single voice channel, say between ground stations A and B can be used in broadcast mode among any set of ground stations, providing a full broadcast capability of two 50K baud channels. Thus a single commercial satellite voice channel could be employed with the following characteristics:

1. The single voice channel could provide two up-link and two down-link 50K baud data channels.
2. Each of these four channels could be simultaneously available to any COMSAT ground station in sight of the satellite.

In December 1972, the ALOHA system became the first operational satellite node on the ARPA network. The satellite used was the Pacific Ocean INTELSAT IV, and the mode of operation is the single-channel-per-carrier PCM voice link that is employed on the SPADE demand assignment system [11]. The PCM voice channel converts analog voice into 56 kilobit PCM. With 50 kilobit data transmission the conversion is unnecessary. The tariff for this service is charged on the basis of a single voice channel, which is a remarkable savings over land-line rates.

In addition to the operational satellite link on INTELSAT, we also worked on the NASA satellite ATA-1 doing experiments on packet broadcasting. In contrast to the standard 97 foot earth station of INTELSAT that costs several million dollars, the ATS-1 ground stations operating on a VHF channel used an antenna as small as ten feet and total ground station electronics costs were less than $5,000. In conjunction with NASA-Ames Research Center (ARC) and the University of Alaska we set up an experimental packet broadcasting network in which the ATS-1 VHF transponder was utilized as a

broadcast repeater and was operated in the ALOHA random access burst mode.

6. Present-Day Packet Broadcasting Networks

When funding ran out from the various U.S. Government sponsors, the ALOHANET stopped operations in the FALL of 1976. However, the spirit of ALOHA lives on in the following networks which are in operation today.

6.1 ETHERNET [6]

This network was one of the first cable-based local area networks ever developed. The basic concept of operation of ETHERNET is to use the cable transmission medium (The "ETHER") in an ALOHA mode with some embellishments such as reducing the probability of packet collisions by listening before and while transmitting. ETHERNET, developed by Metcalfe and Boggs at the Xerox Palo Alto Research Center in 1973-75, has spawned a number of imitators in the burgeoning field of local area networks. Thus, it appears that three generations of techology have evolved from the original ALOHA technology, developed only 10 years ago.

6.2 Packet Radio Network [7]

The PRNET is a direct descendent of the ALOHANET and was developed by a constortium, including the University of Hawaii, under the sponsorship of the Defense Advanced Research Projects Agency (DARPA). Although the original ALOHANET did use repeaters, it nevertheless represented a centralized system in that there existed only a centered computing facility to which the remote TCU's served as subscribers. The PRNET is a basic extension of ALOHANET and extends the domain of packet communications to permit mobile applications over a wide geographic area by the extensive use of repeaters and sophisticated protocols for addressing and routing. The PRNET is in prototype operation in the San Francisco Bay area, with its central station located at SRI International in Menlo Park, California.

6.3. Packet Satellite Network [8]

The Atlantic Packet Satellite System or SATNET, is another DARPA-sponsored effort that has led to a quasi-operational packet broadcasting system operating on a INTESAT IV satellite over the Atlantic. One of the most significant achievements of the SATNET experiment was the development of a very sophisticated demand-assignment protocol called PODA (Priority-Oriented Demand Assignment). Its design represents an integration of both circuit and packet-switched demand assignment and control techniques. For large populations of low duty-cycle stations, random access techniques (known as slotted ALOHA) are used in the system known as CPODA (Contention-PODA). Thus, it appears that the contention techniques, pioneered in the original ALOHANET, are being used in some of the most advanced packet communications systems of the 1980's.

7. References

[1] Roberts, Lawrence G., "The ARPA Network" in *Computer-Communication Networks*, edited by Norman Abramson and Franklin F. Kuo, Prentice-Hall, Inc., 1973, pp. 485-500.

[2] Jackson, P.E.; Stubbs, C. D., "A Study of Multi-access Computer Communications," *AFIPS Conference Proceedings, Spring Joint Computer Conference*, 1969, pp. 491-504.

[3] Roberts, Lawrence, G., "Data by the Packet," IEEE Spectrum, February 1974, pp. 46-51.

[4] Metcalfe, R. M. "Packet Communication," Ph.D. Thesis, Harvard University, 1973. Also available as Project MAC Report TR-114, MIT, Cambridge, MA 02139.

[5] Biner, Richard, et al., "Aloha Packet Broadcasting—A Retrospect," AFIPS Conference Proceedings, Vol. **44**, May 1975, pp. 203-215.

[6] Boggs, D. R.; Metcalfe, R. M., "Ethernet: Distributed Packet Switching for Local Computer Networks," Comm ACM, Vol. **19**, No. 7, July 1976, pp. 395-404.

[7] Kahn, R. E., et al., "Advances in Packet Radio Technology," Proc. IEEE, Vol. **66**, No. 11, November 1978, pp. 1468-1496.

[8] Jacobs, I. M., et al., "General Purpose Packet Satellite Networks," Proc. IEEE, Vol. **66**, No. 11, November 1978, pp. 1448-1467.

[9] Abramson, Norman, "The ALOHA System," in *Computer-Communication Networks*, edited by Norman Abramson and Franklin F. Kuo, Prentice-Hall, Inc., 1973, pp. 501-518.

[10] Cacciamani, Eugene R., Jr., "Data Services—American Satellite Corporation," *Proceedings of the Seventh Hawaii International Conference on System Sciences—Subconference on Computer Nets*, Western Periodicals Co., January 1974, pp. 66-69.

[11] Cacciamani, Eugene R., Jr., "The SPADE System as Applied to Data Communications and Small Earth Station Operation," COMSAT Technical Review, Vol. **1**, No. 1, Fall 1971, pp. 171-182.

JOURNAL OF RESEARCH of the National Bureau of Standards
Vol. 86, No. 6, November–December 1981

An Enskog Correction for Size and Mass Difference Effects in Mixture Viscosity Prediction*

James F. Ely†

National Bureau of Standards, Boulder, CO 80303

May 26, 1981

A method is presented which corrects the one-fluid conformal solution viscosity model for size and mass difference effects. This correction, which is based on the Enskog model for hard sphere mixtures, is empirical as applied to transport but has a rigorous basis in equilibrium theory. Comparisons of predictions and experimental viscosities for 24 binary mixtures are presented.

Key words: Corresponding states; Enskog theory; mass difference effects; mixture viscosity; size difference effects.

1. Introduction

In a series of recent reports [1, 2, 3],[1] Ely and Hanley have proposed a corresponding states method for the prediction of the viscosity and thermal conductivity of pure hydrocarbons and their mixtures. This work was an extension of the previous work of Hanley [4, 5], which dealt with the transport properties of liquefied natural gas mixtures, to molecular weight ranges corresponding to C_{20} and other chemical types (e.g., aromatics). The method is based on a one-fluid, conformal solution concept and requires only pure component, equilibrium parameters such as the critical parameters as input. No transport data are required.

Extensive comparisons of the predictions of the model with experimental data have been reported and are summarized in tables 1 and 2. In general the results are excellent with the average absolute error between experiment and prediction being less than 8 percent for both pure fluids and mixtures. It was noted, however, that when the size difference of two binary mixture species becomes large (e.g., $V_1^c/V_2^c \sim 6$), the predictions of the viscosity model become markedly worse. This failure of the one-fluid model for viscosity has been explained by the nonequilibrium molecular dynamics studies of Hanley and Evans [6, 7]. These studies have shown that for mixtures of molecules of substantially different size, the mean density approximation inherent in the one-fluid theory for the binary pair distribution function fails, even for a conformal mixture. A consequence of this failure is that the local or ambient concentration of the mixture components is not the same as the bulk concentration. This is shown in figure 1 for a 50/50 mixture of a conformal system whose size difference is two [7]. As one can see, the concentration of the larger component about a central large molecule (x_{22}) is greater than the bulk

TABLE 1. *Summary of One-Fluid Corresponding States Viscosity Results for Pure Fluids.*[a]

Fluid Type	N	AAD	BIAS
n-Paraffins	1301	4.89	−0.48
i-Paraffins	155	21.17	−21.17
Alkenes	58	11.29	7.85
Cycloalkanes	89	40.56	−40.56
Alkylbenzenes	155	8.45	−0.69
Carbon Dioxide	111	4.75	−4.53
Overall	1869	8.42	−4.10

[a] AAD = Average absolute percent deviation. BIAS = Average percent deviation.

TABLE 2. *Summary of One-Fluid Corresponding States Viscosity Results for Binary Mixtures.*[a]

Mixture Type	N	AAD	BIAS
Alkane/Alkane	303	5.89	−1.79
Alkane/Cycloalkane	24	17.31	−16.51
Alkane/Alkylbenzene	128	7.41	−0.01
Overall	455	6.95	−2.07

[a] AAD = Average absolute percent deviation. BIAS = Average percent deviation.

These results were obtained using the empirical size difference correction proposed by Ely and Hanley [1].

*Partially supported by the U.S. Department of Energy, Office of Basic Energy Sciences, Contract No. DE-A101-76PR06010.

†Thermophysical Properties Division, National Engineering Laboratory.

[1] Raised figures indicate literature references located at the end of this paper.

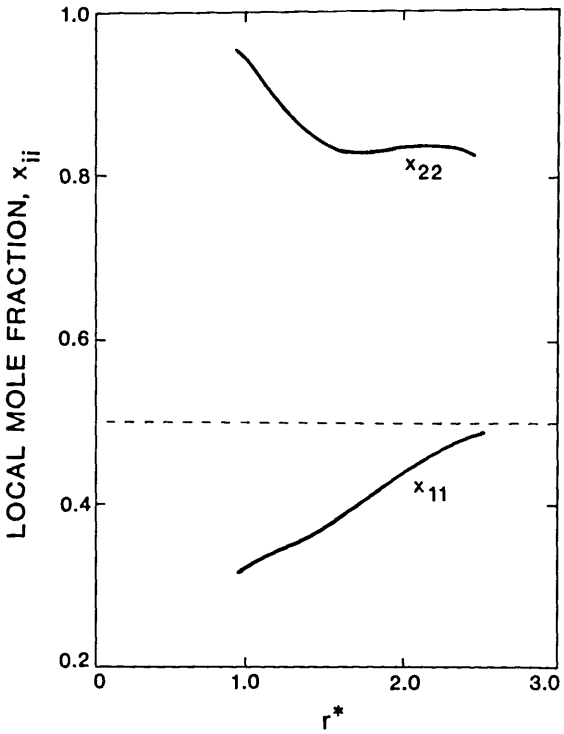

FIGURE 1. Local mole fractions for a conformal mixture of soft spheres with a mass ratio of 10 and size ratio of 2 plotted versus reduced intermolecular separation r^* [7].

concentration until one exceeds four or five molecular diameters. Since the viscosity (as well as other thermophysical properties) are determined from relatively short-range forces, the large component dominates the value of the mixture viscosity. Ely and Hanley [1] attempted to correct for this effect with an empirical relation based on the size ratios in the mixture. Although this function was somewhat successful (as is reflected in table 2), the size difference effects persist in the model predictions.

In this manuscript, a systematic correction to the one-fluid viscosity model is proposed for size and mass difference effects. This correction is based on the exact solution of the Enskog model for a multicomponent mixture of hard spheres [8]. This approach has a rigorous foundation in the perturbation expansion of an equilibrium property of a fluid [9], but is empirical as applied to transport phenomena. In spite of this empiricism, the proposed correction does improve the viscosity predictions for mixtures which exhibit large size and mass differences, for both the dense liquid and dilute gas states.

Section 2 of this article summarizes the assumptions and working equations of the one-fluid, conformal solution viscosity model (CSVM). Section 3 discusses the hard sphere expansion model and describes the Enskog solution for a multicomponent mixture of hard spheres which is the analytical formulation used to correct the CSVM. In section 4 the predictions of the corrected and uncorrected models are compared with experimental data for both the dilute gas and high density fluids. Unfortunately, for methane/n-decane like systems where the size and mass difference effects would be the most pronounced, no dilute gas experimental viscosities have been measured. For this reason, the model predictions are also compared to calculated Lennard-Jones viscosities.

2. One-Fluid Viscosity Model

In the one-fluid conformal solution viscosity model there are three basic assumptions: (1) the viscosity (η) of a mixture at a density ϱ, temperature T and composition $\{x_\alpha\}$ can be equated to the viscosity of a hypothetical pure fluid, i.e., $\eta_{mix}(\varrho, T, \{x_\alpha\}) = \eta_x(\varrho, T)$; (2) the viscosity of the hypothetical pure fluid may be evaluated via a corresponding states principle

$$\eta_x(\varrho, T) = \eta_o(\varrho_o, T_o)\, F_\eta \tag{1}$$

where F_η is a dimensional factor defined below and (3) the reference fluid density and temperature (ϱ_o and T_o) may be evaluated via an extended equilibrium corresponding states principle [10] viz.

$$\varrho_o = \varrho h_x \text{ and } T_o = T/f_x \tag{2}$$

where h_x and f_x are defined by the relations

$$A_x^R(\varrho, T) = f_x A_o^R(\varrho h_x,\ T/f_x)$$

and

$$Z_x(\varrho, T) = Z_o(\varrho h_x,\ T/f_x).$$

A^R denotes the residual Helmholtz free energy of the hypothetical or reference fluid (subscripts x or o, respectively) and Z is the compressibility factor, $p/\varrho RT$. In eq (1), F_η is given by

$$F_\eta = \left(\frac{M_x}{M_o}\right)^{1/2} f_x^{1/2}\, h_x^{-2/3} \tag{3}$$

where M denotes the mass.

In order to apply the model to pure fluids or mixtures, analytical expressions for f_x, h_x, and M_x as well as for the reference fluid equation of state and viscosity surface are required. In our previous work, methane was chosen as the reference fluid owing to the availability of pVT and viscosity data for that fluid. The appropriate correlations have been reported previously [1] and will not be repeated here.

For a mixture, f_x, h_x, and M_x must be obtained via mixing and combining rules for the corresponding mixture component parameters. We have adopted a set of one-fluid mixing rules given by the following

$$f_x = h_x^{-1} \sum_\alpha \sum_\beta x_\alpha x_\beta f_{\alpha\beta} h_{\alpha\beta} \tag{4}$$

$$h_x = \sum_\alpha \sum_\beta x_\alpha x_\beta h_{\alpha\beta} \tag{5}$$

and

$$M_x = \left[\sum_\alpha \sum_\beta x_\alpha x_\beta m_{\alpha\beta}^{1/2} f_{\alpha\beta}^{1/2} h_{\alpha\beta}^{4/3}\right]^2 f_x^{-1} h_x^{-8/3} \tag{6}$$

The combining rules for the binary pair parameters (as denoted by an "$\alpha\beta$" subscript) are given by

$$f_{\alpha\beta} = (f_\alpha f_\beta)^{1/2}(1-k_{\alpha\beta}) \tag{7}$$

$$h_{\alpha\beta} = \frac{1}{8}(h_\alpha^{1/3}+h_\beta^{1/3})^3(1-l_{\alpha\beta}) \tag{8}$$

and

$$m_{\alpha\beta} = 2m_\alpha m_\beta/[m_\beta+m_\beta]. \tag{9}$$

In eqs (7) and (8) $k_{\alpha\beta}$ and $l_{\alpha\beta}$ are the binary interaction parameters which can be set equal to zero in viscosity predictions. The parameters f_α and h_β are the equivalent substance reducing ratios for the energy and volume for component α in the mixture. They are given by

$$f_\alpha = (T_\alpha^c/T_o^c)\,\theta(V_\alpha^*, T_\alpha^*, \omega_\alpha) \tag{10}$$

$$h_\alpha = (V_\alpha^c/V_o^c)\,\phi(V_\alpha^*, T_\alpha^*, \omega_\alpha) \tag{11}$$

where the subscript "c" indicates a critical value, "$*$" denotes a value reduced by the critical point and ω is Pitzer's acentric factor. θ and ϕ are the shape factors of Leach and Leland [11, 12] whose detailed functional forms are given in reference [1]. T denotes the absolute temperature, V is the molar volume and m is the mass.

The mass mixing rule given by eq (6) was derived by Evans and Hanley [6] in their study of the viscosity of a mixture of conformal soft spheres. It arises by examining the potential contribution to the pressure tensor in terms of the nonequilibrium radial distribution function and thus is a mixing rule for the potential or in practice, high density contribution to the viscosity. This rule was adopted for all densities, however, since the emphasis of our previous work was on the dense fluid states. One might expect, therefore, that the CSVM might be somewhat less accurate for the dilute gas, kinetic regime where the mixture mass dependence is effectively proportional to $m^{1/2} f^{1/2} h^{-2/3}$ rather than $m^{1/2} f^{1/2} h^{4/3}$ as given in eq (6). This point will be discussed further in section 4.

3. The Enskog Correction

Mansoori and Leland and their co-workers [9, 13] have proposed a conformal solution model for equilibrium thermodynamic properties in which a dimensionless or reduced property of a mixture is expanded about the corresponding property of a hard sphere mixture. For example, if X_{mix} represents the value of the real mixture property, one obtains

$$X_{mix}(\varrho, T, \{x_\alpha\}) = X_{mix}^{HS}(\{\varrho\sigma_\alpha^3\}, \{x_\alpha\}) - X_x^{HS}(\varrho\sigma_x^3) + X_o(\varrho_o', T_o') \tag{12}$$

In this equation X_{mix}^{HS} denotes the value of the property in a mixture of hard spheres of diameters $\{\sigma_\alpha\}$, $\{x_\alpha\}$ denotes the mixture composition, X_x^{HS} is the property value in a pure hard sphere fluid of effective diameter σ_x (e.g., a one-fluid approximation) and X_o is the value obtained from a real, pure fluid reference substance, evaluated at the state point (ϱ_o, T_o) where $\varrho_o' = \varrho\sigma_x^3/\sigma_o^3$ and $T_o' = T\epsilon_o/\epsilon_x$. In terms of intermolecular potentials the parameters σ and ϵ correspond to the points where $u(\sigma)=0$ and $\min(u) = -\epsilon$. Both σ_x and ϵ_x are one-fluid parameters which must be evaluated via mixing rules. The difficulty in applying this approach lies in assigning values to σ and ϵ for the mixture components. One possible approach is to assume that $\sigma^3 \sim V_c$ and $\epsilon \sim T_c$ which leads to factors such as those given in eqs (10-11). The choice of parameters used in this work will be discussed in section 4.

Although transport properties cannot, in general, be expanded in a perturbation series [14], it is tempting to apply the hard sphere expansion (HSE) formalism to the conformal solution viscosity model presented in section 2. Formally this may be written as

$$\eta_{mix}(\varrho, T, \{x_\alpha\}, \{m_\alpha\}) = \eta_{mix}^{HS}(\{\varrho\sigma_\alpha^3\}, \{x_\alpha\}, \{m_\alpha\}) - \eta_x^{HS}(\varrho\sigma_x^3, m_x) + \eta_o(\varrho_o, T_o)\, F_\eta \tag{13}$$

where the notation is the same as defined previously. Note that in the case of transport we must also consider the masses of the particles $\{m_\alpha\}$.

In practice, we do not have an exact model for the viscosity of a hard sphere fluid (pure or mixed) at all densities. For this reason, the Enskog model [15], which has been solved for a multicomponent mixture of hard spheres by Tham and Gubbins [8], was selected to calculate η_{mix}^{HS} and η_x^{HS}. Their solution is given by

$$\eta_{mix}^{ENSKOG} = \sum_i \beta_i(T,\varrho)\, Y_i + \frac{48}{15\pi} \sum_i \sum_j x_i x_j u_{ij}^o y_{ij}$$

where

$$Y_i = x_i [1 + \tfrac{4}{5} \sum_j x_j M_{ji} y_{ij}]$$

and the β_i are the solutions to the set of linear equations defined by the following

$$\sum_j B_{ij} \beta_j = Y_i$$

where

$$B_{ij} = 2 \sum_t x_i x_t y_{it} M_{ti}^2 (u^o_{it})^{-1} \left[(1 + \tfrac{5}{3} \frac{m_i}{m_t}) \delta_{ij} - \tfrac{2}{3}(\frac{m_i}{m_t}) \delta_{jt}\right].$$

In these equations, $b_{ij} = 2\pi\sigma_{ij}^3/3$, $\sigma_{ij} = \frac{1}{2}(\sigma_i + \sigma_j)$, $M_{ji} = m_j/(m_i + m_j)$, $u^o_{ij} = b_{ij}\, n\, \eta^o_{ij}$, $\eta^o_{ij} = \frac{5}{16} (\frac{m_{ij}kT}{\pi})^{1/2}\sigma_{ij}^{-2}$, $m_{ij} = 2m_iM_{ji}$, $y_{ij} = n\, b_{ij} g_{ij}(\sigma_{ij})$, n = number density, g_{ij} is the hard sphere radial distribution function for the ij pair, and δ is the Kronecker delta function. Although these equations are somewhat complex, they may be readily solved on a digital computer.

The final model, which we shall call the hard sphere expansion-conformal solution viscosity model (HSE-CSVM), is given by

$$\eta_{mix}(\varrho, T, \{x_a\}, \{m_a\}) = \Delta\eta^{ENSKOG} + \eta_o(\varrho_o, T_o) F_\eta \quad (14)$$

with

$$\Delta\eta^{ENSKOG} = \eta^{ENSKOG}_{mix}(\{\varrho\sigma_a^3\}, \{x_a\}, \{m_a\}) - \eta^{ENSKOG}_x(\varrho\sigma_x^3, m_x) \quad (15)$$

4. Results

In order to apply eqs (14) and (15) values for the hard sphere diameters σ_a must be chosen and mixing rules for the one-fluid values σ_x and m_x in the hard sphere system must be selected. As was mentioned previously, considerable freedom exists for the choice of the molecular diameters. Unfortunately, the hard sphere contributions to the viscosity are rather sensitive to this choice, thus several possibilities were considered. The relationship which was selected is given by

$$\sigma_a = (V^c_o h_a/3.058\, N_o)^{1/3} \quad (18)$$

where h_a is the ratio defined in eq (11) and is obtained in the CSVM calculations and N_o is Avogadro's number. The factor 3.058 was chosen so that methane would have a diameter of 3.758 10^{-10} m which corresponds to the Lennard-Jones (12-6) intermolecular potential value given by Reid, et al. [16]. This choice, although resonable, is still somewhat arbitrary. The mixing rules for the one-fluid hard sphere system were chosen to be consistent with those used in the CVSM, eqs (5) and (6), viz.

$$\sigma_x^3 = \sum_a \sum_b x_a x_b \sigma_{ab}^3 \quad (16)$$

and

$$M_x = [\sum_a \sum_b x_a x_b m_{ab}^{1/2} \sigma_{ab}^4]^2 \sigma_x^{-8}$$

where $\sigma_{ab} = \frac{1}{2}(\sigma_a + \sigma_b)$ and m_{ab} is defined in eq (9).

4.1 Results for the Dilute Gas Limit

The correction was first tested on the dilute gas viscosity of a methane/propane mixture with the results being given in table 3. This table gives the experimental data [17], CSVM predictions and the HSE-CSVM predictions obtained using eqs (14–16). As one can see, the HSE-CSVM is consistently more accurate with average absolute percentage deviation being 3.6 percent as compared to 6.29 percent for the CSVM.

The size and mass difference in the methane/propane system is not very great—$\sigma_1/\sigma_2 \sim 1.4$ and $m_1/m_2 \sim 3$. One would expect that the effect of the correction would be more pronounced in a system like methane/n-decane where the size and mass ratios are 1.8 and 9, respectively. Unfortunately no experimental measurements for the dilute gas viscosity of this mixture have been reported. For this reason, the Lennard-Jones gas viscosities of this system were calculated using the standard kinetic theory formalism [15]. Although it is impossible to assess the absolute accuracy of these values, they do serve as a rational basis upon which the HSE-CSVM and CSVM may be compared.

In order to perform the dilute gas Lennard-Jones (LJ) calculations, values for the intermolecular potential minimum ϵ_a for the mixture components must be chosen as well as values for the σ_a. The σ_a were obtained from eq (18) and ϵ_a/k where k is Boltzmann's constant were calculated from the empirical relation

$$\epsilon_a/k = T^c_o f_a/1.282$$

where f_a is the CSVM reducing parameter given in eq (10). The factor 1.282 was chosen so that methane would have a value of ϵ/k of 148.6 which is the Lennard-Jones value reported by Reid, et al. [16].

Table 4 summarizes the results obtained with the LJ kinetic theory model and the HSE-CSVM and CSVM at three compositions and four temperatures. Comparing the

TABLE 3. *Comparison of Calculated and Experimental [17] Dilute Gas Viscosities of Methane/Propane Mixtures at 1 atm.*

Composition	Temperature	η_{exp}, 10^7 Pa•s	η_{calc}^{CSVM}		$\eta_{calc}^{HSE\text{-}CSVM}$	
mol %, methane	K		10^7 Pa•s	%	10^7 Pa•s	%
22.07	310.928	89.2	93.1	4.37	90.6	1.57
	344.261	98.8	103.2	4.45	100.7	1.92
	377.594	108.3	113.5	4.80	111.0	2.49
	410.928	118.0	123.8	4.92	121.3	2.80
38.78	310.928	93.0	99.2	6.67	95.6	2.80
	344.261	103.0	109.9	6.70	106.5	3.40
	377.594	113.0	120.6	6.73	117.0	3.54
	410.928	122.5	131.2	7.10	127.7	4.24
61.39	310.928	99.6	107.3	7.73	103.6	4.02
	344.261	109.6	118.4	8.03	114.9	4.84
	377.594	119.5	129.4	8.28	125.9	5.36
	410.928	129.2	140.1	8.44	136.7	5.80
79.10	310.928	107.2	112.6	5.04	110.2	2.80
	344.261	117.4	123.7	5.37	121.4	3.41
	377.594	126.8	134.5	6.07	132.3	4.34
	410.928	136.6	144.8	6.00	142.8	4.54
	Average absolute percent deviation			6.29		3.62

TABLE 4. *Comparison of Calculated and Lennard-Jones (12-6) Dilute Gas Viscosities of Methane/n-Decane Mixtures and CSVM Predictions*

Composition	Temperature	η_{exp}^{LJ} 10^7 Pa•s	η_{calc}^{CSVM}		$\eta_{calc}^{HSE\text{-}CSVM}$	
mol %, methane	K		10^7 Pa•s	%	10^7 Pa•s	%
25.0	300	46.5	54.9	18.06	43.4	−6.67
	400	65.4	76.2	16.51	62.8	−3.98
	500	86.4	99.2	14.81	84.1	−2.66
	600	108.8	124.2	14.15	107.6	−1.10
50.0	300	56.4	74.9	32.80	50.1	−11.17
	400	79.2	103.1	30.18	74.9	−5.43
	500	103.7	133.4	28.64	102.4	−1.25
	600	129.1	165.2	27.96	132.3	2.48
75.0	300	75.2	104.2	38.56	70.6	−6.12
	400	103.6	140.5	35.62	104.8	1.16
	500	132.2	177.0	33.89	140.5	6.28
	600	160.7	211.5	31.61	175.4	9.15
	Average absolute percent deviation			20.17		3.59
	Average percent deviation			20.17		−2.40

results we see a substantial difference in the CSVM predictions and the LJ calculations. In the case where the methane content is high, (75 percent) the HSE-CSVM is in better agreement with the LJ calculations by 20-30 percent. Also, the overall absolute percentage deviation for the HSE-CSVM is 3.6 percent as opposed to 20 percent for the CSVM version. Although the accuracy of the LJ calculations is uncertain, similar calculations on the methane/propane system where experimental data do exist yielded agreement between the LJ and experiment of better than 2 percent. One can postulate, therefore, that discrepancies similar to those shown in table 4 would exist between the CSVM and real experimental data for the methane/n-decane system.

Note that in both comparisons the CSVM predicts values which are too large in the dilute gas limit. We attribute this to the potential or high density mass mixing rule which is used in F_η in eq (3). Thus, we see that in the low density limit the HSE Enskog correction is negative and lowers the predicted viscosity.

4.2 High Density Results

The initial motivation for this work was to obtain a correction for the effect of size differences on the predicted high density viscosity of systems like methane/n-decane mixtures. Figure 2 compares the experimental [18] and CSVM predicted viscosities of methane/n-decane mixtures as a function of reduced density at three different compositions. Note that the predictions are worst for the high methane

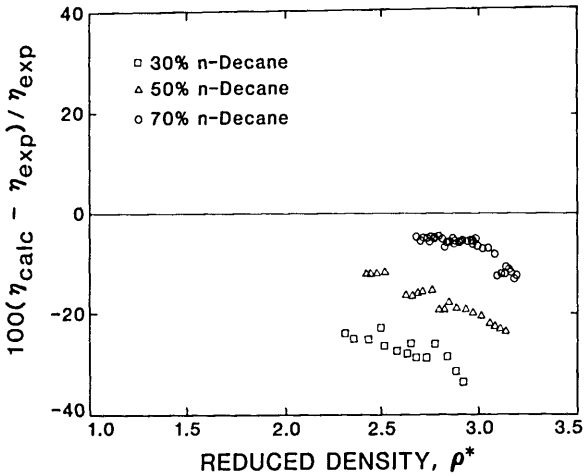

FIGURE 2. Comparison of calculated and experimental viscosities of methane/n-decane mixtures using the uncorrected model. Note that the predictions are worst (~ 30 percent error) for the highest methane concentration.

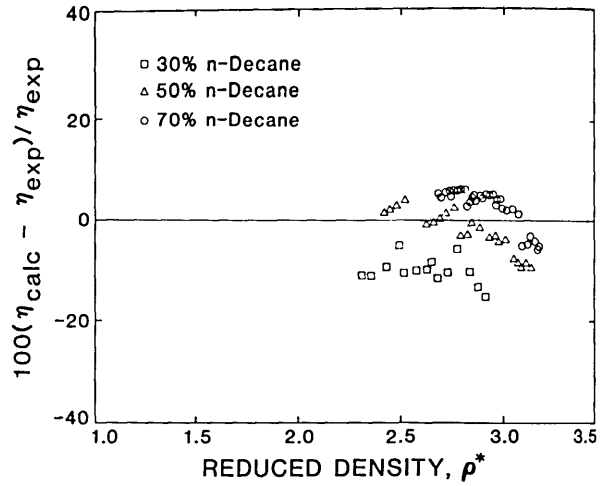

FIGURE 3. Comparison of calculated and experimental viscosities of methane/n-decane mixtures using the corrected model. Note that both the bias and average absolute deviations are improved.

composition and improve with increasing decane content. This is somewhat surprising since methane is the reference fluid in the CVSM calculations. This result was explained in the introduction and is attributable to a failure of the one-fluid theory to adequately represent the size difference effects in the high density region.

Figure 3 compares the experimental and calculated results for the HSE-CSVM. We see in this case that there is a marked improvement in both the bias and overall deviation. Note that in this case the HSE correction is positive. The density dependence of the HSE correction is illustrated in figure 4 which shows $\frac{\Delta\eta}{T^{1/2}} = (\eta_{mix}^{ENSKOG} - \eta_x^{ENSKOG})/T^{1/2}$ plotted against reduced density at a size ratio of $\sigma_1/\sigma_2 = 2.0$ and mass ratio of $m_1/m_2 = 8$ at three compositions. This corresponds approximately to a methane/decane like system. In figure 4 the density was reduced by an approximation to the critical density of the mixture given by $\rho_c^{-1} = 3.058\, N_o\, (x_1\sigma_1^3 + x_2\sigma_2^3)$. This figure demonstrates that the correction decreases in magnitude with increasing concentration of the larger component (x_1) and is small and negative below reduced densities of 1.5. Also the correction increases sharply above reduced densities of 1.5.

Table 5 compares the overall predictions for both the corrected and uncorrected model for 24 binary systems. The literature references for the experimental data are given in [1]. The systems where the size difference is large [$\sigma_2/\sigma_1 \approx (V_2^c/V_1^c)^{1/3}$] show substantial improvement while those of similar size are essentially unchanged. It may be possible to further improve the corrected model by a judicious choice of the σ_a. This possibility is currently being examined.

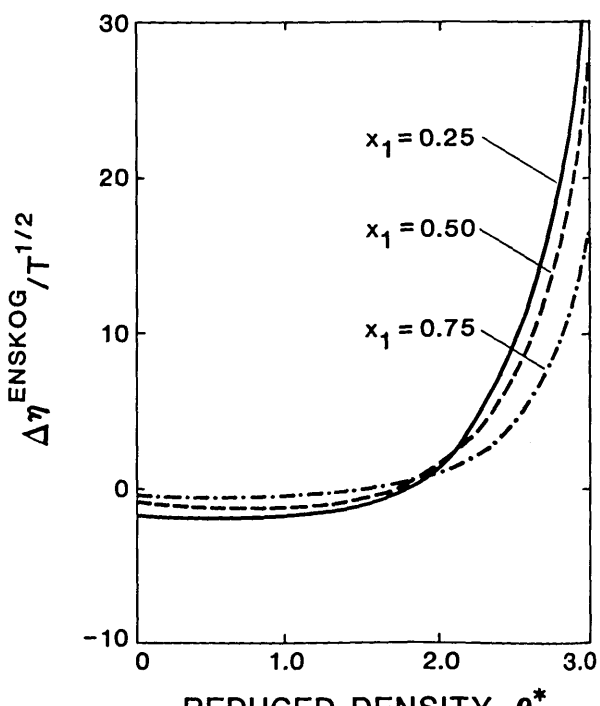

FIGURE 4. Plot of $\Delta\eta^{ENSKOG}/T^{1/2}$ versus reduced density at three compositions of the larger component (x_1). $\sigma_1/\sigma_2 = 2$ and $m_1/m_2 = 8$ which roughly corresponds to a methane/n-decane system.

TABLE 5. *Summary of Calculated and Experimental Dense Fluid Binary Mixture Viscosities.*[a]

Component 1	Component 2	σ_2/σ_1	N	AAD^{CSVM}	$BIAS^{CSVM}$	$AAD^{HSE\text{-}CSVM}$	$BIAS^{HSE\text{-}CSVM}$
Methane	Propane	1.273	134	5.91	−5.29	4.62	−3.45
	n-Nonane	1.778	32	6.37	−5.58	4.12	−2.61
	n-Decane	1.839	71	14.43	−14.43	5.35	−1.54
2,3-Dimethylbutane	n-Hexane	1.014	2	5.32	−5.32	5.31	−5.31
	n-Octane	1.110	2	6.03	−6.03	5.65	−5.65
n-Hexane	n-Tetradecane	1.304	10	2.15	−1.15	1.92	0.54
	n-Hexadecane	1.356	26	4.04	−3.85	2.59	−1.97
n-Heptane	n-Dodecane	1.185	3	2.47	2.47	3.44	3.44
	n-Tetradecane	1.242	3	1.19	0.10	1.82	1.51
	n-Hexadecane	1.291	3	3.03	−3.03	2.52	−1.32
	n-Octadecane	1.333	2	2.95	−2.95	1.92	−0.71
n-Octane	n-Decane	1.074	2	3.09	3.09	3.27	3.27
n-Tetradecane	n-Hexadecane	1.040	11	2.31	2.08	2.32	2.10
Benzene	n-Hexane	1.130	15	5.85	−2.70	5.74	−2.28
	n-Heptane	1.186	3	4.68	4.68	5.85	5.85
	2,2,4-Trimethylpentane	1.218	26	13.14	−13.14	12.46	−12.46
	n-Decane	1.329	3	4.45	0.73	5.47	3.46
	n-Dodecane	1.406	3	2.87	2.87	6.47	6.47
	n-Tetradecane	1.473	3	2.96	−1.47	3.63	2.55
	n-Hexadecane	1.531	3	3.75	−2.80	3.76	1.46
	n-Octadecane	1.581	3	2.99	−2.99	2.73	1.97
Toluene	n-Heptane	1.110	21	5.15	5.15	5.32	5.32
	n-Octane	1.157	20	9.03	9.03	9.50	9.50
	2,2,4-Trimethylpentane	1.140	28	6.61	−4.64	6.62	−4.37
	Overall		429	7.45	−5.23	5.31	−1.86

[a] The CSVM results were obtained without the empirical size difference correction give in [1].

5. Summary and Conclusions

We have shown that a relatively simple correction to the one-fluid conformal solution viscosity model may be obtained from the Enskog hard sphere theory. This function effectively corrects for errors in the mass mixing rules at low density and also for size difference effects at high density. Even though the effective correction is not substantial for systems of similar size and mass, it does systematically correct the model predictions as is reflected in the BIAS as given in table 4. In addition, when the size and mass difference is large, as in the methane/n-decane system, the improvement in the model predictions is substantial. Further work is in progress to extend this approach to other structural features such as branching and polarity which are not adequately handled by the one-fluid corresponding states model.

The author would like to acknowledge Dr. J. M. Kincaid of NBS and Professor G. Stell and Dr. John Karkheck of the State University of New York at Stony Brook for providing the original computer program which calculates the mixture Enskog viscosity. Further, the author would like to acknowledge many helpful discussions with Dr. H. J. M. Hanley. Ms. Karen Bowie assisted substantially in the preparation of the manuscript.

6. References

[1] Ely, J. F.; Hanley, H. J. M. Prediction of transport properties. I. Viscosity of fluids and fluid mixtures. Ind. Eng. Chem. Fundam., **20**(4): 323-332; 1981 November.

[2] Ely, J. F.; Hanley, H. J. M. Prediction of the viscosity and thermal conductivity in hydrocarbon mixtures—computer program TRAPP. Proceedings of the 60th annual GPA convention; 1981 March 23-25; San Antonio, TX.

[3] Ely, J. F.; Hanley, H. J. M. A computer program for the prediction of viscosity and thermal conductivity in hydrocarbon mixtures. Nat. Bur. Stand. (U.S.) Tech. Note 1039, 1981.

[4] Hanley, H. J. M. Prediction of the viscosity and thermal conductivity coefficients of mixtures. Cryogenics **16**(11): 643-651; 1976 November.

[5] Rainwater, J. C.; Hanley, H. J. M. Prediction of the transport properties of natural gas and similar mixtures. Advances in Cryogenic Engineering, Vol. **23**. K. D. Timmerhaus, ed. New York, NY: Plenum Press; 1978. 561-565.

[6] Evans, D. J.; Hanley, H. J. M. Viscosity of a mixture of soft spheres. Phys. Rev. A **20**(4): 1648-1654; 1979 October 1.

[7] Hanley, H. J. M.; Evans, D. J. Behavior of a nonconformal mixture via computer simulation. Int. J. Thermophys., **2**(1): 1-19; 1981 January.

[8] Tham, M. K.; Gubbins, K. E. Kinetic theory of multicomponent dense fluid mixtures of rigid spheres. J. Chem. Phys. **55**(1): 268-279; 1971 July 1.

[9] Mansoori, G. A.; Leland, T. W. Statistical thermodynamics of mixtures; a new version for the theory of conformal solution. J. Chem. Soc. Faraday Trans. II **6**(3): 320-344; 1972.

[10] Rowlinson, J. S.; Watson, I. D. The prediction of the thermodynamic properties of fluids and fluid mixtures—I. The principle of corresponding states and its extensions. Chem. Eng. Sci. **24**(8): 1565–1574; 1969 October 1.

[11] Leach, J. W.; Chappelear, P. S.; Leland, T. W. Use of molecular shape factors in vapor-liquid equilibrium calculations with the corresponding states principle. A.I.Ch.E. J. **14**(4): 568–576; 1968 July 1.

[12] Leach, J. W. Molecular structure corrections for application of the theory of corresponding states to non-spherical pure fluids and mixtures. Ph.D. Thesis, Rice University, Houston, TX; 1967.

[13] Chang, J. I. C.; Hwu, F. S. S.; Leland, T. W. Effective molecular dimaters for fluid mixtures. Chapter 2 in Equations of state in engineering research, Advances in chemistry series Vol. **182**, Chao, K. C.; Robinson, R. L., eds. Washington, DC: American Chemical Society; 1979. 31–48.

[14] Kincaid, J. M.; Kayser, R. F. Kinetic parturbation theory for dilute gases. Phys. Lett. **78A**(3): 215–216; 1980 August 4.

[15] Hirschfelder, J. O.; Curtiss, C. F.; Bird, R. B. *Molecular theory of gases and liquids.* New York, NY: John Wiley and Sons; 1954. 1217 p.

[16] Reid, R. C.; Prausnitz, J. M.; Sherwood, T. K. *The properties of gases and liquids,* 3rd edition. New York, NY: McGraw Hill; 1977. 688 p.

[17] Giddings, J. G.; Kao, J. T.; Kobayashi, R. Development of a high-pressure capillary tube viscometer and its application of methane, propane and their mixtures in the gaseous and liquid regions. J. Chem. Phys. **45**(2): 578–586; 1966 July 15.

[18] Lee, A. L.; Gonzalez, M. H.; Eakin, B. E. Viscosity of methane-decane mixtures. J. Chem. Eng. Data **11**(3): 281–287; 1966 July 1.

JOURNAL OF RESEARCH of the National Bureau of Standards
Vol. 86, No. 6, November-December 1981

Rate Constants for H-atom Transfer Reactions by the BEBO Method

R. L. Brown*

National Bureau of Standards, Washington, DC 20234

March 17, 1981

A detailed discussion of the calculation of rate constants for hydrogen atom transfer reactions based on the BEBO method is presented. Linear transition state models are used. A computer program using this method for determining rate constants is provided.

Key words: absolute chemical rate; BEBO activation energy; bond-order-bond-energy; chemical rate constants; computer program; hydrogen atom transfer.

CONTENTS

1. Introduction

The bond-energy-bond-order (BEBO) method is a procedure for calculating the activation energies of hydrogen transfer reactions from bond energies. When combined with absolute rate theory, it also yields values for the rate constants. It was formulated over 10 years ago by Johnston and Parr [1],[1] and has since been applied with considerable success to the calculation of a large number of activation energies. Less frequently, it has been used to evaluate rate constants. Although the details of the BEBO method itself have

[1] Figures in brackets indicate literature references at the end of this paper.

*Center for Thermodynamics and Molecular Science, National Measurement Laboratory.

been published by Johnston [2], this aspect represents only a relatively small part of a rate constant calculation. The purpose of this report is to give a detailed account, not only of the BEBO method and its theoretical background, but also of the absolute rate theory portion of the calculation. In addition, instructions are provided for the use of a computer program which calculates rate constants based on the BEBO method. The discussion is limited to linear transition state models.

2. Theory

2.1. Absolute Rate Theory & Transition State Model for BEBO Calculations

For a bimolecular reaction, $A + B \rightarrow [AB]^* \rightarrow$ products, absolute rate theory utilizes the concept of a molecular complex made up of the two reactants. This complex is assumed to be in equilibrium with these reactants. The resulting expression for the classical rate constant $\mathbf{k}_{cl}$ is

$$\mathbf{k}_{cl} = \frac{kT}{h} \frac{Q^*_{cl}\, e^{-V^*/kT}}{Q^A_{cl}\, Q^B_{cl}} \tag{1}$$

where k is the Boltzmann constant, T is the absolute temperature, h is Planck's constant, Q^A_{cl} and Q^B_{cl} are the classical partition functions per unit volume for reactants A and B, Q^*_{cl} is the classical partition function per unit volume for the complex, and V^* is the potential energy of the complex relative to that of the reactants. The complex contains one unstable vibrational mode whose evolution brings about its dissociation into product fragments. The partition function Q^*_{cl} is evaluated with this mode missing. A detailed derivation of eq (1) which explains all its inherent assumptions has been given by Mahan [3]. Quantum mechanical corrections to the partition functions at room temperature and above need be applied only to vibrational factors. For a particular vibration of frequency ν_i, the quantum correction Γ_i is given by the expression

$$\Gamma_i = \frac{u_i/2}{\sinh\,(u_i/2)}, \quad where\ u_i = h\nu_i/kT \tag{2}$$

We assume that all vibrational modes are independent so that the total quantum correction for a particular species is simply the product of terms given by eq (2), one for each vibrational mode. There is also a quantum correction to the unstable vibrational mode of the complex which we denote by Γ^*. This results from the effect of quantum mechanical tunneling through the potential barrier between reactants and products. It will be considered in detail in section 2.5. Applying these quantum corrections to eq (1) yields the rate expression

$$\mathbf{k} = \frac{kT}{h} \frac{Q^*_{cl} \left\{\prod_i \Gamma^*_i\right\} \Gamma^* e^{-V^*/kT}}{Q^A_{cl} \left\{\prod_i \Gamma^A_i\right\} Q^B_{cl} \left\{\prod_i \Gamma^B_i\right\}} \tag{3}$$

The general class of reactions we are considering has the form

$$A\text{-}H + B\bullet \rightarrow A\text{-}H\text{-}B \rightarrow A\bullet + H\text{-}B \tag{4}$$

Radical $B\bullet$ abstracts a hydrogen atom attached to A, the net result being the transfer of H from A to B. For this system, we take the most general transition state to be linear, having up to 5 mass points. Its structure and the notation which we shall use are shown in figure 1a. There can be up to four internuclear distances, R_a, R_b, R_c, and R_d. The bonds associated with R_a and R_d will be assumed to be rigid. (The two vibrational modes involving these bonds will have infinite frequencies and need not be formally included in the calculations.) Thus, there are only two vibrational stretching modes to be considered for this molecule, one of which will be unstable. These modes arise from the stretching of the two central bonds b and c which are shown by dotted lines to indicate their unstable character. Of the five possible masses, M_3 will normally be that of the hydrogen atom; the other masses will be assigned values in the manner described below. The three angles Ψ_2, Ψ_3, and Ψ_4 are defined by the bonds (a,b), (b,c), and (c,d) in the plane of the figure while the primed symbols denote the corresponding angles in the plane perpendicular to the figure. Changes in these angles from

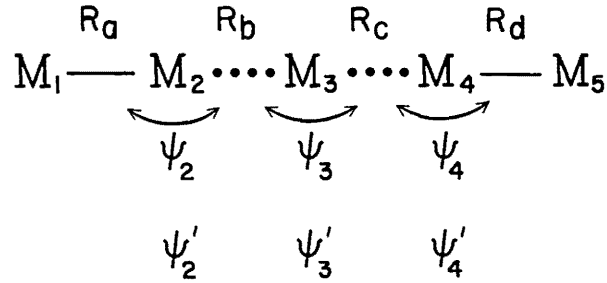

FIGURE 1a. Notation for five mass point linear transition state.

180° give rise to three doubly degenerate bending vibrations. To calculate the frequencies needed in eq (3), we require values for the two stretching force constants associated with bonds b and c, and three bending force constants arising from the three bond angles. As we shall see, these values can be generated by the BEBO process.

Within the framework of the transition state structure shown in figure 1a, it is possible to include all types of reactions implied by eq (4) by considering four cases; one having a 3 point transition state, two having 4 point states, and one having a 5 point state. These four cases are shown in figure 1b. In this figure, the subscript s appearing on the internuclear distances and force constants denote equilibrium values found in reactants or products. Because bonds a and d are assumed to be rigid, their bond distances will always be denoted by the single symbols R_{a_s} and R_{d_s}, respectively. The bond distance between M_2 and M_3 goes from R_{b_s} to R_b in the transition state, while that between M_3 and M_4 goes from ∞ to R_c in the transition state. In the transition state, the force constant F_{b_s} is modified and combined with that of the newly formed bond between M_3 and M_4 to produce two force constants F_ρ and F_σ. F_σ corresponds to the stable symmetric stretch and F_ρ to the unstable asymmetric stretch. In cases IVa and V, the bending force constant $F_{\psi 2_s}$ becomes $F_{\psi 2}$ in the complex. The newly formed bond angle made by M_2, M_3, and M_4 leads to the force constant $F_{\psi 3}$ in all cases. Finally, in cases IVb and V, we also have an additional bending force constant $F_{\psi 4}$ which goes to $F_{\psi 4_s}$ in the second product. The force constants associated with the out-of-plane bends are not shown since they are the same as the in-plane constants.

The way I have chosen to assign values to the mass points is somewhat arbitrary and is best explained by an example. Consider the reaction

$$\underset{\text{Species}}{\underset{\text{A}}{CH_3\text{-}CH_2\text{-}H} + \underset{\text{B}}{CH_3} \rightarrow CH_3\text{-}CH_2\text{··}H\text{··}CH_3 \rightarrow \underset{\text{C}}{CH_3\text{-}CH_2\bullet} + \underset{\text{D}}{H\text{-}CH_3}}$$

which is the abstraction of hydrogen from ethane by methyl radicals. The masses are assigned according to the following rules:

1) The mass of the transferred H is always assigned to M_3; therefore $M_3 = 1.008$ atomic mass units (a.m.u.).

2) The mass of the atom joined to the transferred H in reactant A is assigned to M_2; in this case $M_2 = 12.011$ a.m.u.

3) The masses of all the remaining atoms in A are added and assigned to M_1; thus in this example $M_1 = 17.051$ a.m.u.

4) The mass of the atom joined to the transferred H in the product D is assigned to M_4; here $M_4 = 12.011$ a.m.u.

5) The masses of all the remaining atoms in D are added and assigned to M_5; thus $M_5 = 3.024$ a.m.u. in this example.

Different models for the transition state, and different ways of arranging the masses in linear models have been explored in a limited way by Johnston [4] and by Sharp & Johnston [5]. They did find significant differences between various options. Presumably, complete vibrational analyses of the reactant and complex would yield more accurate rate constants than the linear models outlined above. Unfortunately, complete analyses are extremely complex even for fairly small molecules, and the ability to program the calculations

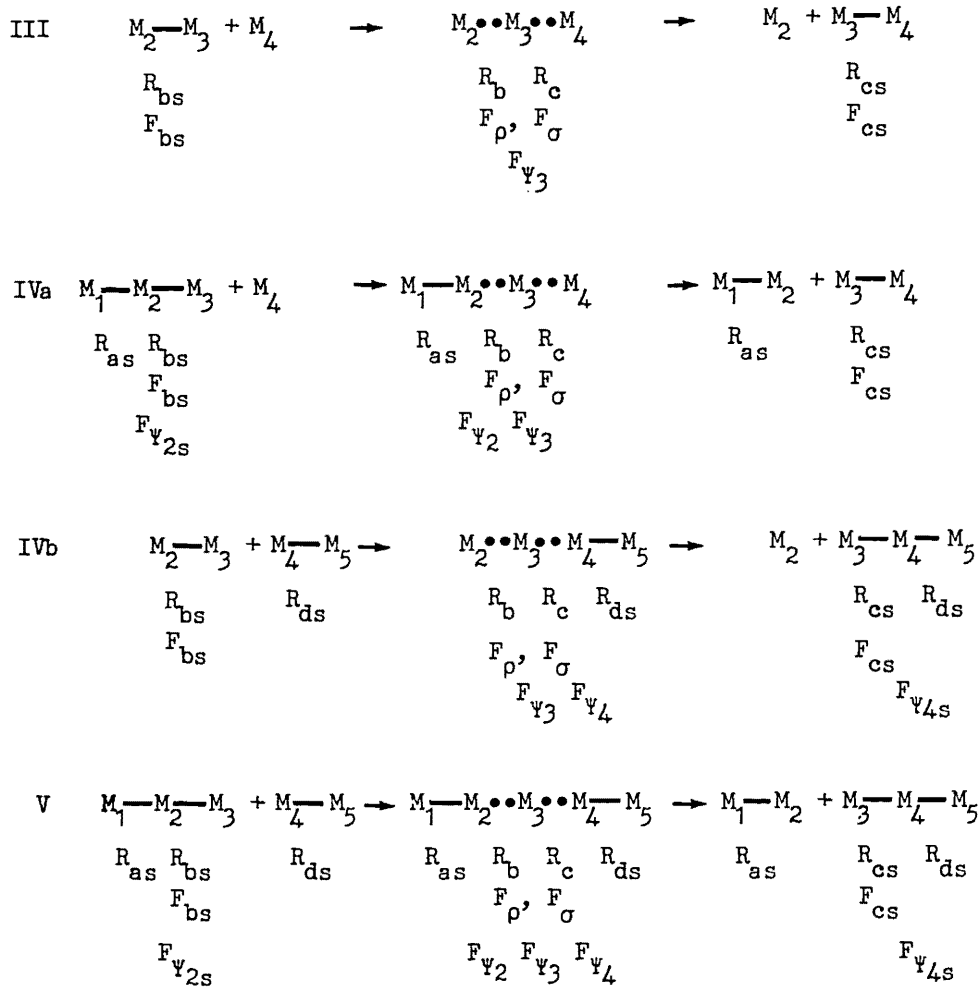

FIGURE 1b. Reaction cases to be used in BEBO calculations. All transition states shown here are linear. Masses are denoted by M, internuclear distances by R, and force constants by F. The subscript s denotes bond distances and force constants in the stable reactants and products.

in a general manner would be lost by such an approach. Also, it is unlikely that all of the force constant values required would be available for a complete analysis. In view of the crudity of the rest of the calculation, it is unnecessary to strive for high accuracy in the vibrational analysis. Intuitively, one expects that the major features of these reactions are controlled by the nature of the atoms adjacent to the H atom being transferred, with the effects from the remainder of the molecule appearing in the bond energy values. If this is the case, then the linear models should at least be able to match trends within homologous series.

So far, we have seen in this section that evaluation of rate constants by the use of eq (3), based on the linear models shown in figure 1b, requires a knowledge of the potential energy V* of the complex, two stretching force constants, and from one to three bending force constants. The potential energy of all of these linear models could, if it were known, be shown on a 2-dimensional contour diagram like that shown in figure 2 where the independent variables are the bond distances R_b and R_c. The required value of the potential energy V is that at the saddle point position shown by the asterisk. For a region close to the saddle point,

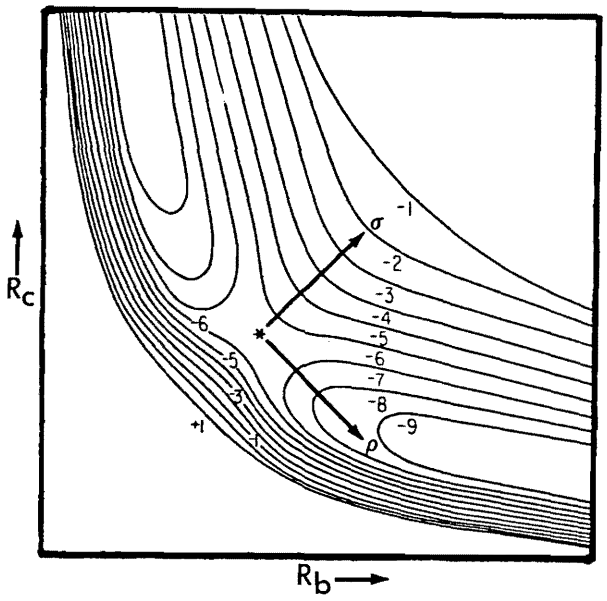

FIGURE 2. Typical potential energy diagram for H atom exchange reaction. The position of the saddle point is shown by the asterisk. The direction ϱ is that in which the potential energy decreases most rapidly. The direction σ is perpendicular to the ϱ direction.

it is customary to assume that the first derivatives of V with respect to R_b and R_c are negligible, and that the potential energy can be approximated by a power series containing only quadratic terms. Thus, for small displacements from the saddle point, we have

$$2\delta V \approx F_{11}(\delta R_b)^2 + 2F_{12}(\delta R_b)(\delta R_c) + F_{22}(\delta R_c)^2 \tag{5a}$$

where $F_{11} = \dfrac{\partial^2 V}{\partial R_b^2}$, $F_{12} = F_{21} = \dfrac{\partial^2 V}{\partial R_b \partial R_c}$, $F_{22} = \dfrac{\partial^2 V}{\partial R_c^2}$.

These derivatives are evaluated at the saddle point, and are, by definition, the stretching force constants of the complex. In matrix notation, this equation is

$$2\delta V \approx (\delta \mathbf{R})\dagger \mathbf{F}_r(\delta \mathbf{R}) \tag{5b}$$

where $\mathbf{F}_r = \begin{bmatrix} F_{11} & F_{12} \\ F_{21} & F_{22} \end{bmatrix}$ and $\delta\mathbf{R} = \begin{bmatrix} \delta R_b \\ \delta R_c \end{bmatrix}$.

This is the force constant matrix that will be used to calculate the vibrational stretching frequencies.

Starting at the saddle point, suppose we move in the direction in which V decreases most rapidly; call this the ϱ direction, and let σ denote the direction perpendicular to ϱ. These directions define a rotated set of cartesian coordinates which we assume makes an angle α with the R_b axis; (positive α is measured in the counter-clockwide direction). The transformation between the two sets of coordinates is given by the equation

$$\mathbf{R} = \begin{bmatrix} R_b \\ R_c \end{bmatrix} = \begin{bmatrix} \cos\alpha & -\sin\alpha \\ \sin\alpha & \cos\alpha \end{bmatrix} \begin{bmatrix} \varrho \\ \sigma \end{bmatrix} = \mathbf{UP} \tag{6}$$

the matrix $\mathbf{U}$ can now be used to express changes in V at the saddle point in terms of changes in ϱ and σ instead of R_b and R_c. Thus, eq (5b) becomes

$$2\delta V \approx (\delta \mathbf{R})\dagger \mathbf{F}_r(\delta \mathbf{R}) = (\mathbf{U}\delta\mathbf{P})\dagger \mathbf{F}_r(\mathbf{U}\delta\mathbf{P}) = (\delta\mathbf{P})\dagger(\mathbf{U}\dagger\mathbf{F}_r\mathbf{U})(\delta\mathbf{P}) \tag{7}$$

The matrix $\mathbf{U}\dagger\mathbf{F}_r\mathbf{U}$ has the elements

$$(\mathbf{U}\dagger\mathbf{F}_r\mathbf{U})_{11} = F_{11}\cos^2\alpha + 2F_{12}\cos\alpha\sin\alpha + F_{22}\sin^2\alpha$$

$$(\mathbf{U}\dagger\mathbf{F}_r\mathbf{U})_{12} = (\mathbf{U}\dagger\mathbf{F}_r\mathbf{U})_{21} = (F_{22} - F_{11})\cos\alpha\sin\alpha + F_{12}(\cos^2\alpha - \sin^2\alpha) \tag{8}$$

$$(\mathbf{U}\dagger\mathbf{F}_r\mathbf{U})_{22} = F_{11}\sin^2\alpha - 2F_{12}\cos\alpha\sin\alpha + F_{22}\cos^2\alpha$$

As we shall see in the next section, the BEBO method provides values for the second derivatives of V (i.e., the force constants) in the ϱ and σ directions. This will allow us to evaluate the matrix $\mathbf{U}\dagger\mathbf{F}_r\mathbf{U}$. The stretching force constant matrix $\mathbf{F}_r$, can then be obtained by inverting the transformation given by eq (6).

In this section I have presented a formula (eq (3)) for the rate constant and outlined the factors required to evaluate it. The details of the BEBO method will be given next. It will provide values for V^* and all of the necessary force constants, both the stretching and the bending ones.

2. BEBO Method

The BEBO method is based on the concept of bond order. In the reactants the bond b of figure 1a is said to have a bond order of unity, while in the products, its bond order is zero. The reverse of this situation holds for bond *c*. BEBO assumes that during the reaction, the total bond order of the two bonds is conserved; if n is the order of bond *b*, and m of bond *c*, then we have always $n + m = 1$. This is the basic assumption of the method. One bond is breaking at the same time that the other is forming. To apply this conservation condition it is necessary to relate the energies and lengths of bonds b and c to their bond orders n and m.

For the relationship between order and length, Pauling [6] proposed the formula

$$R_n = R_1 - \lambda ln(n) \tag{9}$$

where R_1 is the length of the bond which is considered to be representative of a single bond between the two elements of interest. The parameter λ is taken to have the same value for all element pairs. A plot of bond length versus the logarithm of the bond order is shown in figure 3 for certain element pairs. The data were

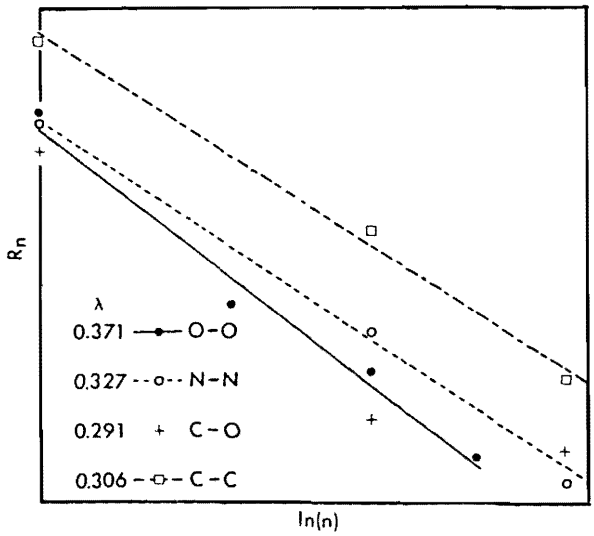

FIGURE 3. Plot of $R_n = R_1 - \lambda ln(n)$; bond distance versus the natural logarithm of the bond order for selected element pairs.

obtained from table 4–3 of Johnston's book [2]. Values of λ obtained from least squares fits are given in the figure for the different bonds. The constancy of λ does not seem particularly striking. Pauling chose a value of 0.26 for λ; he writes, "This equation, which is based upon the study of interatomic distances for non-resonating and resonating covalent bonds in simple non-metallic substances of known structure, is found to agree reasonably well with those data for metallic crystals which are suited to a check on its validity, and its use permits a penetrating analysis of the structure of metals and intermetallic compounds to be made. There is some evidence that the constant . . . varies with the kind of atom and with the type of bond; but the evidence is not sufficiently extensive to lead to the determination of the nature of this variation." Certainly Pauling's value doesn't appear to have been based very heavily on the data in figure 3 since none of these λ values are close to 0.26. Although 0.26 can hardly be construed as universal, it has nevertheless been the value used for most BEBO calculations. There appears to be no reason why a different value shouldn't be used if it gave better results.

Consider next the dependence of bond energy on bond order. Johnston [4] proposed the following relationship between the two quantities

$$E_n = E_s n^p \tag{10}$$

where E_s is the bond energy of a single bond and is analogous to R_s of eq (9). Note that this energy is the *electronic* dissociation energy of the bond in question; the zero point energy is *not* meant to be included in E_s. Plots of ln(E) versus $ln(n)$ are shown in figure 4 for the same bonds used in figure 3. The data are again from table 4–3 of Johnston [2]. We see that p depends on the kind of atoms in the bond. If more than one bond type occurs for a pair of atoms, then it is possible to extract values for p from plots like figure 4 provided we are not unduly bothered by a lack of linearity. When only a single bond type exists, then some other method must be devised. Actually, since we are interested in E_n and R_n for bond orders less than unity, even if multiple bonds were available for a plot like figure 4, some method of extrapolating to zero n would be necessary. Johnston [2], inspired by Badger's rule for force constants, has devised a way. Let us first eliminate n between eqs (9) and (10); this yields

$$ln(E_n/E_s) = (p/\lambda)(R_s - R_n) \tag{11}$$

This expression is analogous to Badger's rule (see Herschbach & Laurie [7]), which is a universal empirical

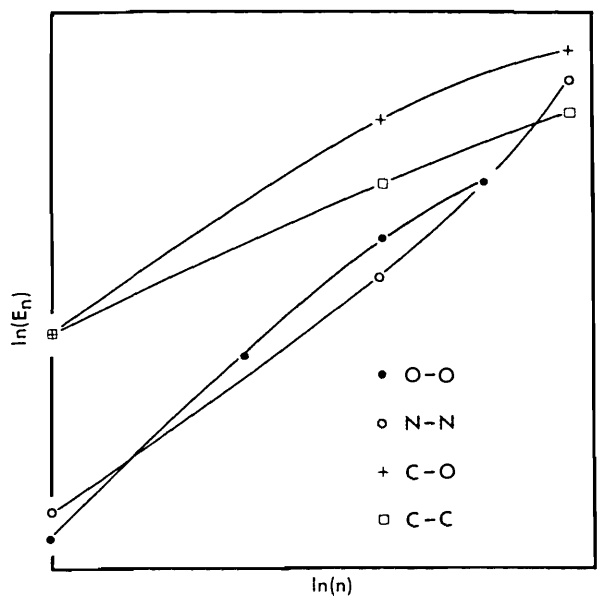

FIGURE 4. Plots of $ln(E_n)$ *versus* $ln(n)$ *for certain bonds.*

relation having the form $r = a_{ij} - b_{ij} \log(f)$, where r is the bond distance, f its force constant, a_{ij} and b_{ij} are constants, and i and j are the numbers of the rows in the periodic table in which the bound atoms are located. Johnston [8] found that plots of $\log(f)$ versus r extrapolated very nicely to two-atom Lennard-Jones noble gas clusters. For clusters having Lennard-Jones parameters σ and ϵ/k, the "bond" distance is $2^{\frac{1}{6}}\sigma$ and the "force" constant is $40.06(\epsilon/k)/\sigma^2$. He then examined plots of $ln(E_n)$ versus R_n to see if a comparable extrapolation would be possible. The results are shown in figure 5. The data are mostly from Johnston [2], tables 4–3 and 4–1. Values of E_n and R_n for the He-Ne cluster were taken from Gilliom [9]. The energies for the bonds examined in figures 3 and 4 are supposed to extrapolate to the Ne-Ne cluster. The lines shown were drawn to connect the corresponding single bonds with this cluster. Points corresponding to multiple bonds fall more or less in the general direction of these lines. The assumption made in BEBO is that such an extrapolation adequately represents the bond energies for $n < 1$. Therefore, if we have a bond A-H, where A is some atom in the first row of the periodic table connected to an H atom, and R_s and E_s are its bond length and energy, then if this bond were perturbed in some fashion so that its bond length were greater than R_s, then its bond energy would fall on the line drawn between the A-H and He-Ne points. Bonds involving atoms A from other rows of the periodic table will extrapolate to the appropriate rare gas-helium cluster. The slope of the line joining A-H to the cluster is, from eq (11), $-p/\lambda$. Since the value of λ has been chosen, we have a way of calculating p for the A-H bond of interest. Formally, in this case,

$$p = \frac{\lambda}{R_s - R_{He-Ne}} ln(E_{He-Ne}/F_s) \tag{12}$$

The parameter p thus depends on λ, the bond energy and internuclear distance of A-H, and the interaction parameters for the appropriate rare gas cluster.

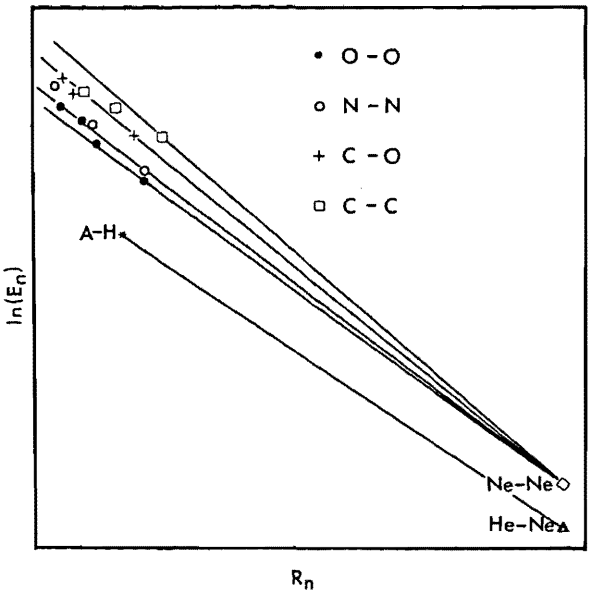

FIGURE 5. Extrapolation of bond energy to large bond distances. A of A-H is an atom in the first row of the periodic table in this case.

We have now almost all of the information needed for the BEBO calculations. Consider a triatomic complex A-H-B; there are three interactions; two between H and the atoms A and B considered above, and the interaction between A and B themselves. If H is to form stable bonds its electron spin must be opposite each of the spins of A and B. Consequently, A and B will have parallel spins and must repel each other. Johnston uses one half the value of the Sato [10] triplet function to represent this interaction. He uses the modified function because it more closely approximates the calculated H-H triplet interaction. This function has the form

$$V_t = E_{ts}\,E(1 + E) \tag{13}$$

where $E = \frac{1}{2}e^{-\beta\Delta R_t}$, $\Delta R_t = R_t - R_{ts} = R_b + R_c - R_{ts}$. E_{ts} is the electronic dissociation energy, R_{ts} the equilibrium internuclear distance, and β the Morse parameter (see Herzberg [11] p. 101) of the ground state of the diatomic molecule made up of A and B. Values of these paramaters for a number of such atom pairs are given in Table 11–1 of Johnston [2]. ΔR_t is the difference between the actual distance R_t between A and B in the complex and the equilibrium distance R_{ts} it would have in the diatomic molecule. It is worth pointing out that many people use E_{ts} as an adjustable parameter to fit the BEBO calculations to their experimental data. Other forms of the triplet function have been used and are discussed briefly in the Appendix. V_t can be expressed as a function of n, the bond order of the b bond, through the conservation condition $n + m = 1$, and through eq (9) which gives the distances R_b and R_c in terms of n and m.

We are now able to give the BEBO expression for the energy of the complex in terms of the bond order n. The energy is assumed to be given by

$$V(n) = E_{bs} - E_{bs}n^p - E_{cs}m^q + V_t(n) = E_{bs}(1 - n^p) - E_{cs}(1 - n)^q + V_t(n) \tag{14}$$

E_{bs} and E_{cs} are the single bond energies (electronic) for bonds b and c, and the parameters p and q are calculated from eq (12) for b and c, respectively. When $n \to 1$, then $m \to 0$, $V_t \to 0$, and $V \to 0$, so that the energy is measured relative to the energy of the reactants. When $n \to 0$, then $m \to 1$, $V_t \to 0$, and $V \to E_{bs} - E_{cs}$ which is the difference in the bond energies. BEBO assumes that the maximum value of V in the range $1 \geq n \geq 0$ is the desired potential energy of the saddle point. This value V^*, is obtained by substituting into eq (14) that value of n which makes $dV/dn = 0$. In what follows, all quantities are considered to be evaluated at the saddle point.

Next, we must determine the stretching force constants in the ϱ and σ directions shown in figure 3. Equation (14) does not give the complete potential surface, but only that portion lying along the line of constant total bond order. BEBO assumes that at the saddle point, this path of constant bond order lies in the ϱ direction. This assumption will enable us to calculate the force constant $F_\varrho \equiv \partial^2 V/\partial\varrho^2$ from the second derivative of V with respect to n, which we get by differentiating eq (14).

From eq (9), we can calculate the changes produced in R_b and R_c when n is changed. In vector notation these are

$$\delta\mathbf{R} = \begin{bmatrix} \delta R_b \\ \delta R_c \end{bmatrix} = -\lambda \begin{bmatrix} 1/n \\ -1/m \end{bmatrix} \delta n;\ m = 1 - n. \tag{15}$$

Because a change in n for constant total bond order is supposed to produce a move in the ϱ direction, the slope of a line in this direction can be gotten from eq (15). It is

$$\delta R_c/\delta R_b = -n/m = \tan\alpha \tag{16}$$

where α is the angle which ϱ makes with the R_b axis as discussed earlier. From eq (15) we can show that

$$\cos\alpha = m/\sqrt{(n^2 + m^2)};\ \sin\alpha = -n/\sqrt{(n^2 + m^2)} \tag{17}$$

The matrix $\mathbf{U}$ defined in eq (6) can now be written in terms of n and m.

$$\mathbf{U} = \frac{1}{\sqrt{(n^2 + m^2)}} \begin{bmatrix} m & n \\ -n & m \end{bmatrix} \tag{18}$$

By means of eq (6), $\delta\mathbf{R}$ can be expressed in terms of $\delta\mathbf{P}$; i.e., $\delta\varrho$ and $\delta\sigma$. Combining the differential form of eq (6) with eq (15), we get

$$\mathbf{U}\delta\mathbf{P} = -\lambda \begin{bmatrix} 1/n \\ -1/m \end{bmatrix} \delta n \tag{19}$$

Solving for $\delta\mathbf{P}$ gives

$$\delta\mathbf{P} = \begin{bmatrix}\delta\varrho\\ \delta\varrho\end{bmatrix} = -\lambda\mathbf{U}^{-1}\begin{bmatrix}1/n\\ -1/m\end{bmatrix}\delta n =$$

$$-\frac{\lambda}{\sqrt{(n^2+m^2)}}\begin{bmatrix}m & -n\\ n & m\end{bmatrix}\begin{bmatrix}1/n\\ -1/m\end{bmatrix}\delta n = -\lambda\sqrt{(n^2+m^2)}\begin{bmatrix}1/nm\\ 0\end{bmatrix}\delta n \tag{20}$$

As expected, σ does not change when n changes. From eq (20), we have for the derivative of n with respect to ϱ

$$\frac{\delta n}{\delta\varrho} \to \frac{dn}{d\varrho} = -\frac{1}{\lambda}\frac{nm}{\sqrt{(n^2+m^2)}} \tag{21}$$

The second derivative of V with respect to ϱ is obtained from the sequence

$$\frac{dV}{d\varrho} = \frac{dV}{dn}\frac{dn}{d\varrho}$$

$$\frac{d^2V}{d\varrho^2} = \frac{d^2V}{dn^2}\left(\frac{dn}{d\varrho}\right)^2 + \frac{dV}{dn}\frac{d^2n}{d\varrho^2}$$

Since $dV/dn = 0$ at the saddle point, we have

$$F_\rho = \frac{d^2V}{d\varrho^2} = \frac{d^2V}{dn^2}\frac{n^2m^2}{\lambda^2(n^2+m^2)} \tag{22}$$

This gives one of the stretching force constants.

In the σ direction, the stretching motion is assumed to be that of a normal molecule. Thus Badger's rule should be applicable. This says that the bond distance is proportional to the logarithm of the force constant, while eq (9) says that the bond distance is proportional to the logarithm of the bond order. Therefore, the force constant should be proportional to the bond order. We assume that

$$F_b = F_{bs}n, \text{ and } F_c = F_{cs}m \tag{23}$$

where F_{bs} and F_{cs} are single bond force constants. Consider the change in V when R_b and R_c are changed by motion in the σ direction. This is assumed to be given by

$$2(\delta V)_\sigma = F_{bs}n(\delta R_b)_\sigma^2 + F_{cs}m(\delta R_c)_\sigma^2 + \frac{\partial^2 V_t}{\partial R_t^2}(\delta R_t)_\sigma^2 = F_\sigma(\delta\sigma)^2 \tag{24}$$

To evaluate F_σ, we must express $(\delta R_b)_\sigma^2$, $(\delta R_c)_\sigma^2$, and $(\delta R_t)_\sigma^2$ in terms of $(\delta\sigma)^2$. From Eqs (6) and (18), we have

$$\delta\mathbf{R} = \begin{bmatrix}\delta R_b\\ \delta R_c\end{bmatrix} = \frac{1}{\sqrt{(n^2+m^2)}}\begin{bmatrix}m & n\\ -n & m\end{bmatrix}\begin{bmatrix}\delta_\rho\\ \delta_\sigma\end{bmatrix} \tag{25}$$

For $\delta\varrho = 0$,

$$(\delta R_b)_\sigma = n\delta\sigma/\sqrt{(n^2+m^2)}, \quad (\delta R_c)_\sigma = m\delta\sigma/\sqrt{(n^2+m^2)}$$

$$(\delta R_t)_\sigma = (\delta R_b)_\sigma + (\delta R_c)_\sigma = (n+m)\delta\sigma/\sqrt{(n^2+m^2)} = \delta\sigma/\sqrt{(n^2+m^2)}.$$

Therefore,

$$2(\delta V)_\sigma = \left(F_{bs}n^3 + F_{cs}m^3 + \frac{\partial^2 V_t}{\partial R_t^2}\right)(\delta\sigma)^2/(n^2+m^2).$$

Comparing this with eq (24) gives

$$F_\sigma = \frac{F_{bs}n^3 + F_{cs}m^3 + \partial^2 V_t/\partial R_t^2}{n^2 + m^2}. \tag{26}$$

The method assumes that if V is expanded at the saddle point in terms of ϱ and σ then there is no cross term; i.e., $\partial^2 V/\partial\varrho\,\partial\sigma$ is assumed to be zero. Thus, we have

$$2\delta V = (\delta\mathbf{P})\dagger\begin{bmatrix} F_\varrho & 0 \\ 0 & F_\sigma \end{bmatrix}(\delta\mathbf{P}) \tag{27}$$

The use of eq (7) shows that

$$\mathbf{U}\dagger\mathbf{F}_r\mathbf{U} = \begin{bmatrix} F_\varrho & 0 \\ 0 & F_\sigma \end{bmatrix} \tag{28}$$

Inverting this equation gives

$$\mathbf{F}_r = (\mathbf{U}\dagger)^{-1}\begin{bmatrix} F_\varrho & 0 \\ 0 & F_\sigma \end{bmatrix}\mathbf{U}^{-1} = \mathbf{U}\begin{bmatrix} F_\varrho & 0 \\ 0 & F_\sigma \end{bmatrix}\mathbf{U}\dagger \tag{29}$$

where use has been made of the fact that $\mathbf{U}^{-1} = \mathbf{U}\dagger$. Substituting eq (18) into (29) gives the desired stretching force constant matrix.

$$\mathbf{F}_r = \frac{1}{n^2 + m^2}\begin{bmatrix} m & n \\ -n & m \end{bmatrix}\begin{bmatrix} F_\varrho & 0 \\ 0 & F_\sigma \end{bmatrix}\begin{bmatrix} m & -n \\ n & m \end{bmatrix}$$

$$= \frac{1}{n^2 + m^2}\begin{bmatrix} F_\varrho m^2 + F_\sigma n^2, & -F_\varrho mn + F_\sigma mn \\ -F_\varrho mn + F_\sigma mn, & F_\varrho n^2 + F_\sigma m^2 \end{bmatrix} = \begin{bmatrix} F_{11} & F_{12} \\ F_{21} & F_{22} \end{bmatrix} \tag{30}$$

To complete the discussion of the BEBO method the bending force constants will now be evaluated. Consider first the one involving M_3 as the center mass. This will be F_{ψ_3} and appears in all of the transition states shown in figure 2. It is defined as the second partial derivative of V with respect to the angle made by the bonds b and c, with the bond lengths R_b and R_c held fixed. At equilibrium, this angle is 180° for our transition state models. The geometry, when the angle is less than 180° is shown in figure 6. To get F_{ψ_3}, we differentiate V twice,

$$\left(\frac{\partial V}{\partial\phi}\right)_{R_b,\,R_c} = \frac{\partial V_t}{\partial\phi} = \frac{\partial V_t}{\partial R_t}\frac{\partial R_t}{\partial\phi}$$

$$\left(\frac{\partial^2 V}{\partial\phi^2}\right)_{R_b,\,R_c} = \frac{\partial^2 V_t}{\partial\phi^2} = \frac{\partial^2 V_t}{\partial R_t^2}\left(\frac{\partial R_t}{\partial\phi}\right)^2 + \frac{\partial V_t}{\partial R_t}\frac{\partial^2 R_t}{\partial\phi^2} \tag{31}$$

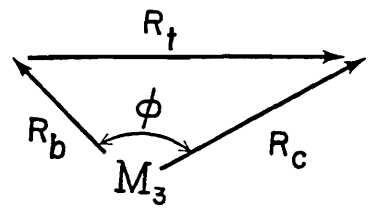

FIGURE 6. Definition of center bond angle.

The derivatives of V_t with respect to R_t can be gotten from eq (13). The dependence of R_t on ϕ can be determined from the following vector relationships,

$$\mathbf{R}_b \cdot \mathbf{R}_c = R_b R_c \cos\phi$$

$$\mathbf{R}_t = \mathbf{R}_c - \mathbf{R}_b$$

$$R_t^2 = \mathbf{R}_t \cdot \mathbf{R}_t = R_b^2 + R_c^2 - 2R_b R_c \cos\phi$$

$$\frac{\partial R_t}{\partial \phi} = \frac{R_b R_c}{R_t} \sin\phi \to 0 \quad \text{for } \phi = 180°$$

$$\frac{\partial^2 R_t}{\partial \phi^2} = \frac{R_b R_c \cos\phi}{R_t} - \frac{R_b^2 R_c^2}{R_t^2} \sin^2\phi \to -\frac{R_b R_c}{R_t} \text{ for } \phi = 180° \tag{32}$$

Thus,

$$F_{\psi_3} = -\frac{\partial V_t}{\partial R_t}\frac{R_b R_c}{R_t} = -\frac{\partial V_t}{\partial R_t}\frac{R_b R_c}{R_b + R_c} \tag{33}$$

The other two bending force constants F_{ψ_2} and F_{ψ_3} are assumed to obey Badger's rule. We assume

$$F_{\psi_2} = F_{\psi_{2,s}} n, \text{ and } F_{\psi_4} = F_{\psi_{4,s}} m \tag{34}$$

This concludes the BEBO part of the calculation. It has provided us with the potential energy V^* of the saddle point, the stretching force constants F_{11}, F_{22}, and F_{12} and the bending force constants F_{ψ_2}, F_{ψ_3}, and F_{ψ_4}. In the next section we shall use these force constants to carry out a frequency analysis for each of the transition state models shown in figure 2.

2.3. Vibrational Analysis

As we have seen in the force constant derivations, the potential energy V of the most general 5 mass point complex can be considered to depend on the variables R_a, R_b, R_c, R_d, Ψ_2, Ψ_3, Ψ_4, Ψ_2', Ψ_3', and Ψ_4'. These are called the internal coordinates. Because our model is linear, V increases when any of the angles departs from 180°. Since we assume a and d to be rigid, R_a and R_d need not be included in the list of variables. For the time being, however, they will be included in the analysis. Let $\mathbf{F}$ be the complete force constant matrix for the complex. We have

$$\mathbf{F} = \begin{bmatrix} \infty & & & & & & & & & \\ & F_{11} & F_{12} & & & & & 0 & & \\ & F_{21} & F_{22} & & & & & & & \\ & & & \infty & & & & & & \\ & & & & F_{\psi_2} & & & & & \\ & & & & & F_{\psi_3} & & & & \\ & & 0 & & & & F_{\psi_4} & & & \\ & & & & & & & F_{\psi_2}' & & \\ & & & & & & & & F_{\psi_3}' & \\ & & & & & & & & & F_{\psi_4}' \end{bmatrix} \tag{35}$$

The two infinite force constants come from the use of rigid bonds for a and d. Let $\mathbf{S}$ be the (column) vector which denotes small changes in the saddle point values of the variables.

$$\mathbf{S}\dagger = [\delta R_a, \delta R_b, \delta R_c, \delta R_d, \delta\Psi_2, \delta\Psi_3, \delta\Psi_4, \delta\Psi_2', \delta\Psi_3', \delta\Psi_4'] \tag{36}$$

The potential energy is assumed to be given by

$$V - V^* = \tfrac{1}{2}\dot{\mathbf{S}}\dagger\mathbf{F}\dot{\mathbf{S}} \tag{37}$$

Suppose there exists a matrix $\mathbf{G}$, such that the kinetic energy in terms of the internal coordinates is

$$T = \tfrac{1}{2}\dot{\mathbf{S}}\dagger\mathbf{G}^{-1}\dot{\mathbf{S}} \tag{38}$$

Consider a new set of coordinates $\mathbf{Q}$, the so-called normal coordinates, related to $\mathbf{S}$ by the linear transformation

$$\mathbf{S} = \mathbf{L}\mathbf{Q} \tag{39}$$

such that

$$V - V^* = \tfrac{1}{2}\mathbf{Q}\dagger\Lambda\mathbf{Q} = \Delta V \tag{40}$$

$$T = \tfrac{1}{2}\dot{\mathbf{Q}}\dagger\mathbf{E}\dot{\mathbf{Q}} \tag{41}$$

where Λ is a diagonal matrix having elements λ_i, and $\mathbf{E}$ is the identity matrix. In this coordinate system there are no cross terms in V and T.

Let Q_i denote the i'th normal coordinate. The Lagrangian equations of motion for the system are

$$\frac{d}{dt}\left(\frac{\partial L}{\partial \dot{Q}_i}\right) - \frac{\partial L}{\partial Q_i} = 0 \tag{42}$$

$$\text{where } L = T - \Delta V = \tfrac{1}{2}[\dot{\mathbf{Q}}\dagger\mathbf{E}\dot{\mathbf{Q}} - \mathbf{Q}\dagger\Lambda\mathbf{Q}] = \tfrac{1}{2}[\textstyle\sum_j \dot{Q}_j^2 - \sum_j \lambda_j Q_j^2]\,, \tag{43}$$

$$\frac{\partial L}{\partial \dot{Q}_i} = \dot{Q}_i, \tag{44}$$

$$\frac{\partial L}{\partial Q_i} = -\lambda_i Q_i. \tag{45}$$

Therefore

$$\ddot{Q}_i + \lambda_i Q_i = 0. \tag{46}$$

The solutions of this equation are

$$Q_i = Q_i^0 \cos(\lambda_i^{1/2} t + \epsilon_i). \tag{47}$$

Thus the $\lambda_i^{1/2} = 2\pi\nu_i$ are the frequencies of the vibrations of the Q_i coordinates. These are called the normal mode vibrations.

Solving eq (39) for $\mathbf{Q}$, and substituting into (40) and (41) yields

$$V - V^* = \tfrac{1}{2}(\mathbf{L}^{-1}\mathbf{S})\dagger\Lambda(\mathbf{L}^{-1}\mathbf{S}) = \tfrac{1}{2}\mathbf{S}\dagger(\mathbf{L}^{-1})\dagger\Lambda(\mathbf{L}^{-1})\mathbf{S} \tag{48}$$

$$T = \tfrac{1}{2}(\mathbf{L}^{-1}\dot{\mathbf{S}})\dagger\mathbf{E}(\mathbf{L}^{-1}\dot{\mathbf{S}}) = \tfrac{1}{2}\dot{\mathbf{S}}\dagger(\mathbf{L}^{-1})\dagger\mathbf{E}(\mathbf{L}^{-1})\dot{\mathbf{S}} \tag{49}$$

Comparison with eqs (37) and (38) yields

$$\mathbf{F} = (\mathbf{L}^{-1})\dagger\Lambda(\mathbf{L}^{-1}) \tag{50}$$

$$\mathbf{L}\dagger\mathbf{F}\mathbf{L} = \Lambda \tag{51}$$

$$\mathbf{G}^{-1} = (\mathbf{L}^{-1})\dagger\mathbf{E}(\mathbf{L}^{-1}) \tag{52}$$

$$\mathbf{L}\dagger\mathbf{G}^{-1}\mathbf{L} = \mathbf{E} \tag{53}$$

Next, solve eq (53) for $\mathbf{L}\dagger = \mathbf{L}^{-1}\mathbf{G}$, substitute this into eq (51) and multiply by $\mathbf{L}$ on the left. This gives

$$\mathbf{GFL} = \mathbf{HL} = \mathbf{L}\Lambda \tag{54}$$

as the set of equations which determine the transformation $\mathbf{L}$. Written out, eq (54) is

$$\Sigma_j[H_{ij} - \delta_{ij}\lambda_k]L_{jk} = 0 \tag{55}$$

This equation has solutions if the determinant

$$|\mathbf{H} - \mathbf{E}\lambda_k| = 0 \tag{56}$$

This is the so-called secular equation which must be solved to get the λ_k, the eigenvalues of $\mathbf{H}$ and thus the normal frequency values. Before doing this, it is first necessary to evaluate the matrix $\mathbf{G}$.

Equation (38) gives the kinetic energy in terms of the internal coordinates. As such, it does not include the kinetic energy of the center of mass or the rotational energy. We need to express the kinetic energy in terms of cartesian coordinates, transform the result to internal coordinates, and subtract out the center of mass and rotational energy. This will yield $\mathbf{G}^{-1}$. Let us begin by expressing the internal coordinates in terms of cartesian coordinates. Assume that the molecule lies along the x axis. A particular mass point M_i will have coordinates (x_i, y_i, z_i) where y_i and z_i are small and describe the departures of the molecule from linearity during bending vibrations. Because y_i and z_i are small, the bond distances can be expressed as functions of the x_i only. Thus,

$$\begin{aligned} R_a &= x_2 - x_1 \\ R_b &= x_3 - x_2 \\ R_c &= x_4 - x_3 \\ R_d &= x_5 - x_4 \end{aligned} \tag{57}$$

Since there are 5 cartesian x coordinates we need one more coordinate for the internal system. This is taken to be the x-component of the center of mass of the molecule multiplied by the total mass, and is defined by the equation,

$$Mx = \sum_{i=1}^{5} M_i x_i \tag{58}$$

$$\text{where } M = \sum_{i=1}^{5} M_i \tag{59}$$

In matrix form these equations are

$$\tilde{\mathbf{R}} = \begin{bmatrix} \mathbf{R} \\ Mx \end{bmatrix} = \begin{bmatrix} R_a \\ R_b \\ R_c \\ R_d \\ Mx \end{bmatrix} = \begin{bmatrix} -1 & 1 & 0 & 0 & 0 \\ 0 & -1 & 1 & 0 & 0 \\ 0 & 0 & -1 & 1 & 0 \\ 0 & 0 & 0 & -1 & 1 \\ M_1 & M_2 & M_3 & M_4 & M_5 \end{bmatrix} \begin{bmatrix} x_1 \\ x_2 \\ x_3 \\ x_4 \\ x_5 \end{bmatrix} = \mathbf{MX} \tag{60}$$

Note that the vector $\mathbf{R}$ is basically that defined by eq (15). Here we have included R_a and R_d.

We must next express the bond angles in terms of the cartesian coordinates. Consider Ψ_2, the angle formed by bonds a and b. The geometry and notation for this angle are shown in figure 7. The two vectors along the bonds a and b are given by

$$\mathbf{r}'_{21} = [x_1 - x_2, y_1 - y_2]$$
$$\mathbf{r}'_{23} = [x_3 - x_2, y_3 - y_2] \tag{70}$$

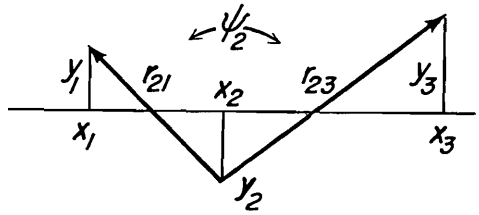

FIGURE 7. Geometry of the bond angle Ψ_2.

Ψ_2 is related to these by

$$\mathbf{r}_{21} \cdot \mathbf{r}_{23} = r_{21} r_{23} \cos\Psi_2. \tag{71}$$

Substituting eq (70) into (71) gives

$$-R_a R_b + (y_1 - y_2)(y_3 - y_2) = \{[R_a^2 + (y_1 - y_2)^2][R_b^2 + (y_3 - y_2)^2]\}^{1/2} \cos\Psi_2 \tag{72}$$

Because the y_i are small compared to R_a and R_b the radical can be expanded to give

$$-R_a R_b + (y_1 - y_2)(y_3 - y_2) \approx [R_a R_b + \tfrac{1}{2}(R_b/R_a)(y_1 - y_2)^2 + \tfrac{1}{2}(R_a/R_b)(y_3 - y_2)^2] \cdot \cos\Psi_2 \tag{73}$$

Let $\Psi_2 = 180° + \delta\Psi_2$ where $\delta\Psi_2$ is small. Then

$$\cos\Psi_2 = -\cos(\delta\Psi_2) \approx -1 + \tfrac{1}{2}(\delta\Psi_2)^2$$

Substituting this into eq (73) and keeping terms through second order gives

$$(\delta\Psi_2)^2 = (1/R_a^2)(y_1 - y_2)^2 + (2/R_a R_b)(y_1 - y_2)(y_3 - y_2) + (1/R_b^2)(y_3 - y_2)^2$$

$$\delta\Psi_2 = -[(y_1 - y_2)/R_a + (y_3 - y_2)/R_b] = -y_1/R_a + (1/R_a + 1/R_b)y_2 - y_3/R_b \tag{74}$$

To see why the minus sign is needed, let $y_1 = y_2 = 0$; then for $y_3 > 0$, $\Psi_2 < 180°$, so that $\delta\Psi_2$ must be < 0. There are analogous equations for the angles Ψ_3 and Ψ_4; there is also a set, identical in form, for the angles Ψ'_i in the x-z plane. These contain the z_i rather than the y_i coordinates. In these equations, the equilibrium values of $R_a, \ldots, R_d$ will be used.

The set of equations typified by eq (74) gives 3 equations in terms of the 5 y_i coordinates; two more are needed. We have one defining the y coordinate of the center of mass, like eq (58), and another defining a quantity η_z, which is given by the equation

$$\eta_z = \sum_{i=1}^{5} M_i x_i^* y_i \tag{75}$$

η_z is related to the z component of the angular momentum m_z by the relation

$$m_z = \dot{\eta}_z \tag{76}$$

The x_i^e are the equilibrium x_i values; these can be gotten relative to the center of mass component x, by inverting eq (60) and inserting equilibrium values for $R_a, \ldots, R_d$. In matrix form, these equations relating y_i to the bond angles in the x-y plane are,

$$\tilde{\Psi} = \begin{bmatrix} \Psi \\ \eta_z \\ My \end{bmatrix} = \begin{bmatrix} \delta\psi_2 \\ \delta\psi_3 \\ \delta\psi_4 \\ \eta_z \\ My \end{bmatrix} = \begin{bmatrix} -\varrho_a & \varrho_a+\varrho_b & -\varrho_b & 0 & 0 \\ 0 & -\varrho_b & \varrho_b+\varrho_c & -\varrho_c & 0 \\ 0 & 0 & -\varrho_c & \varrho_c+\varrho_d & -\varrho_d \\ M_1x_1^e & M_2x_2^e & M_3x_3^e & M_4x_4^e & M_5x_5^e \\ M_1 & M_2 & M_3 & M_4 & M_5 \end{bmatrix} \begin{bmatrix} y_1 \\ y_2 \\ y_3 \\ y_4 \\ y_5 \end{bmatrix} = \mathbf{AY} \quad (77)$$

where $\varrho_a, \ldots, \varrho_d$ are the reciprocals of the equilibrium values of $R_a, \ldots, R_d$. There is an analogous equation involving the z_i coordinates.

Having obtained expressions (60) and (77) for the internal coordinates in terms of the cartesian coordinates, we can now invert these equations and insert them into the expression for the total kinetic energy which we shall call $\tilde{T}$. Therefore

$$\begin{aligned} \tilde{T} &= \tfrac{1}{2}\,\dot{\mathbf{X}}\dagger\mathbf{D}_m\dot{\mathbf{X}} + \tfrac{1}{2}\,\dot{\mathbf{Y}}\dagger\mathbf{D}_m\dot{\mathbf{Y}} + \tfrac{1}{2}\dot{\mathbf{Z}}\dagger\mathbf{D}_m\dot{\mathbf{Z}} \\ &= \tfrac{1}{2}\,\dot{\tilde{\mathbf{R}}}\dagger(\mathbf{M}^{-1})\dagger\mathbf{D}_m(\mathbf{M}^{-1})\dot{\tilde{\mathbf{R}}} + \tfrac{1}{2}\,\dot{\tilde{\Psi}}\dagger(\mathbf{A}^{-1})\dagger\mathbf{D}_m(\mathbf{A}^{-1})\dot{\tilde{\Psi}} + z\text{-term} \\ &= \tfrac{1}{2}\dot{\tilde{\mathbf{R}}}\dagger\tilde{\mathbf{G}}_r^{-1}\dot{\tilde{\mathbf{R}}} + \tfrac{1}{2}\,\dot{\tilde{\Psi}}\dagger\tilde{\mathbf{G}}_\psi^{-1}\dot{\tilde{\Psi}} + z\text{-term} \\ &= \tfrac{1}{2}T + \tfrac{1}{2}M(\dot{x}^2 + \dot{y}^2 + \dot{z}^2) + \tfrac{1}{2}(m_y^2 + m_z^2)/I \\ &= \tfrac{1}{2}\dot{\mathbf{R}}\dagger\mathbf{G}_r^{-1}\dot{\mathbf{R}} + \tfrac{1}{2}\dot{\Psi}\dagger\mathbf{G}_\psi^{-1}\dot{\Psi} + z\text{-term} + \tfrac{1}{2}M(\dot{x}^2 + \dot{y}^2 + \dot{z}^2) + \tfrac{1}{2}(m_y^2 + m_z^2)/I \end{aligned} \quad (78)$$

where $I = \sum_{i=1}^{5} M_i x_i^{e2}$ is the moment of inertia, and

$$\mathbf{D}_m = \begin{bmatrix} M_1 & & & & \\ & M_2 & & \mathbf{0} & \\ & & M_3 & & \\ & \mathbf{0} & & M_4 & \\ & & & & M_5 \end{bmatrix} \quad (79)$$

We can satisfy eq (78) by writing $\tilde{\mathbf{G}}_r^{-1}$ and $\tilde{\mathbf{G}}_\psi^{-1}$ in the partitioned forms

$$\tilde{\mathbf{G}}_r^{-1} = \begin{bmatrix} \mathbf{G}_r^{-1} & 0 \\ 0 & M^{-1} \end{bmatrix} \quad (80)$$

$$\tilde{\mathbf{G}}_\psi^{-1} = \begin{bmatrix} \mathbf{G}_\psi^{-1} & 0 & 0 \\ 0 & I^{-1} & 0 \\ 0 & 0 & M^{-1} \end{bmatrix} = \tilde{\mathbf{G}}_\psi^{-1}$$

We can get $\mathbf{G}_r$ and $\mathbf{G}_\psi$ simply by inverting $\tilde{\mathbf{G}}_r^{-1}$ and $\tilde{\mathbf{G}}_\psi^{-1}$.

This gives

$$\tilde{\mathbf{G}}_r = \begin{bmatrix} \mathbf{G}_r & 0 \\ 0 & M \end{bmatrix} = \mathbf{M}\mathbf{D}_m^{-1}\mathbf{M}\dagger \quad (81)$$

$$\tilde{\mathbf{G}}_\psi = \begin{bmatrix} \mathbf{G}_\psi & 0 & 0 \\ 0 & \mathrm{I} & 0 \\ 0 & 0 & M \end{bmatrix} = \mathbf{A}\mathbf{D}_m^{-1}\mathbf{A}\dagger$$

Since $\mathbf{D}_m$ is diagonal its inverse is easily evaluated and we therefore require only matrix multiplications to get $\mathbf{G}_r$ and $\mathbf{G}_\psi$.

The complete $\mathbf{G}$ matrix for the internal coordinates in partitioned form is

$$\mathbf{G} = \begin{bmatrix} \mathbf{G}_r & 0 & 0 \\ 0 & \mathbf{G}_\psi & 0 \\ 0 & 0 & \mathbf{G}_{\psi'} \end{bmatrix} \tag{82}$$

In partitioned form, the complete force constant matrix, eq (35), is

$$\mathbf{F} = \begin{bmatrix} \mathbf{F}_r & 0 & 0 \\ 0 & \mathbf{F}_\psi & 0 \\ 0 & 0 & \mathbf{F}_{\psi'} \end{bmatrix} \tag{83}$$

Note that $\mathbf{F}_r$ here is like eq (30), but contains the two infinite force constants corresponding to the rigid a and d bonds. The matrix $\mathbf{H}$ in partitioned form is

$$\mathbf{H} = \begin{bmatrix} \mathbf{G}_r\mathbf{F}_r & 0 & 0 \\ 0 & \mathbf{G}_\psi\mathbf{F}_\psi & 0 \\ 0 & 0 & \mathbf{G}_\psi\mathbf{F}_{\psi'} \end{bmatrix} = \begin{bmatrix} \mathbf{H}_r & 0 & 0 \\ 0 & \mathbf{H}_\psi & 0 \\ 0 & 0 & \mathbf{H}_{\psi'} \end{bmatrix} \tag{84}$$

Because $\mathbf{H}$ factors in this way, we can set up separate secular equations for the stretching and bending modes. Note that $\mathbf{H}$ is normally unsymmetric.

Before solving the secular equations, let us write down explicit expressions for $\mathbf{G}_r$ and $\mathbf{G}_\psi$. The direct evaluation of $\widetilde{\mathbf{G}}_r$ from eq (81) yields

$$\widetilde{\mathbf{G}}_r = \begin{bmatrix} \mu_1+\mu_2 & -\mu_2 & 0 & 0 & 0 \\ -\mu_2 & \mu_2+\mu_3 & -\mu_3 & 0 & 0 \\ 0 & -\mu_3 & \mu_3+\mu_4 & -\mu_4 & 0 \\ 0 & 0 & -\mu_4 & \mu_4+\mu_5 & 0 \\ 0 & 0 & 0 & 0 & M \end{bmatrix} \tag{85}$$

where the μ_i are the reciprocals of the masses M_i. Comparison of this equation with eq (81) yields $\mathbf{G}_r$. Because we are treating the a and d bonds as rigid, the stretching part of the problems is equivalent to a 3 mass point system where the first mass is $M_1 + M_2$ and the third is $M_3 + M_4$. The resulting 2×2 matrix is the one actually used in the calculation. It is

$$\mathbf{G}_r(\text{rigid end bonds}) = \begin{bmatrix} \left(\dfrac{\mu_1}{\mu_1+\mu_2}\right)\mu_2+\mu_3 & -\mu_3 \\ -\mu_3 & \mu_3+\mu_4\left(\dfrac{\mu_4}{\mu_4+\mu_5}\right) \end{bmatrix} \tag{86}$$

The stretching force constant matrix to be used with eq (86) is that $\mathbf{F}_r$ as given by eq (30).

The $\mathbf{G}_\psi$ matrix elements for this 5 point case are

$$\begin{aligned} (\mathbf{G}_\psi)_{11} &= \varrho_a^2\mu_1 + \varrho_b^2\mu_3 + (\varrho_a + \varrho_b)^2\mu_2 \\ (\mathbf{G}_\psi)_{22} &= \varrho_b^2\mu_2 + \varrho_c^2\mu_4 + (\varrho_b + \varrho_c)^2\mu_3 \\ (\mathbf{G}_\psi)_{33} &= \varrho_c^2\mu_3 + \varrho_d^2\mu_5 + (\varrho_c + \varrho_d)^2\mu_4 \\ (\mathbf{G}_\psi)_{12} &= -\varrho_b[(\varrho_a + \varrho_b)\mu_2 + (\varrho_b + \varrho_c)\mu_3] \\ (\mathbf{G}_\psi)_{23} &= -\varrho_c[(\varrho_b + \varrho_c)\mu_3 + (\varrho_c + \varrho_d)\mu_4]; \quad (\mathbf{G}_\psi)_{13} = \varrho_b\varrho_c\mu_3 \end{aligned} \tag{87}$$

There are the expressions used in the calculation. Actually, they were not derived from eq (81) but were obtained from Wilson et. al. [12]. However, eq (81) was used for a numerical check of eq (87). To get the matrix elements for the two 4 mass point cases, simply delete from eq (87) those elements which contain either a missing ϱ or a missing μ or both. Do the same for the 3 point case, but delete also $(\mathbf{G}_\psi)_{13}$; (there is only one element, $(\mathbf{G}_\psi)_{22}$, in this case).

We are now ready to consider the secular equation. For the rate constant calculation only the λ_k are required, so that a solution of eq (54) for the transformation matrix $\mathbf{L}$ is not necessary. Nevertheless, $\mathbf{L}$ is easily obtained and is convenient to have for the purpose of illustrating the actual vibrational motions of the complex. Thus we shall solve eq (54) as well as eq (56). According to eq (84), there are two secular equations to be solved ($\mathbf{H}_\psi$ and $\mathbf{H}_{\psi'}$ are equal). Because we are using rigid a and d bonds, the dimension of $\mathbf{H}_r$ is 2×2. The maximum dimension of $\mathbf{H}_\psi$ is 3×3 and occurs for the 5 point model. Thus a solution of a 3×3 problem will suffice for our purpose and will also illustrate how an $n \times n$ problem is to be solved.

We begin by assuming that eq (56) has been solved. In the present work this was accomplished by expanding (56) and solving the resulting polynomial in λ. In our case, the maximum degree was cubic, so that this part of the calculation was easily performed. As eq (47) shows, the desired frequencies are $\nu_k = \lambda_k^{1/2}/2\pi$. For the stretching modes of the complex one of the two frequencies will be imaginary because its λ_k value will be negative. As mentioned earlier, this corresponds to the asymmetric stretch.

Consider now eq (55) for a general 3×3 $\mathbf{H}$ matrix. Written out in full, it is

$$\begin{aligned} (H_{11} - \lambda_k)L_{1k} + H_{12}L_{2k} + H_{13}L_{3k} &= 0 \\ H_{21}L_{1k} + (H_{22} - \lambda_k)L_{2k} + H_{23}L_{3k} &= 0 \\ H_{31}L_{1k} + H_{23}L_{2k} + (H_{33} - \lambda_k)L_{3k} &= 0 \end{aligned} \tag{88}$$

where λ_k is one of the three values of λ determined from the solution of the cubic (in this case) eq (56). Divide the first two of these equations by L_{3k}, and define the ratios $g_{ik} = L_{ik}/L_{3k}$. This yields two equations to be solved for the two unknowns g_{1k} and g_{2k}.

$$\begin{aligned} (H_{11} - \lambda_k)g_{1k} + H_{12}g_{2k} &= -H_{13} \\ H_{21}g_{1k} + (H_{22} - \lambda_k)g_{2k} &= -H_{23} \end{aligned} \tag{90}$$

We get two g_{ik} values for each value of λ_k substituted into eq (89), or six g_{ik} values in all. Using these values, we can express $\mathbf{L}$ in terms of the product of two matrices defined by

$$\mathbf{L} = \begin{bmatrix} g_{11} & g_{12} & g_{13} \\ g_{21} & g_{22} & g_{23} \\ 1 & 1 & 1 \end{bmatrix} \begin{bmatrix} L_{31} & 0 & 0 \\ 0 & L_{32} & 0 \\ 0 & 0 & L_{33} \end{bmatrix} = \Gamma\ell \tag{90}$$

To determine the components of ℓ, insert eq (90) into eq (51). We get

$$\ell\dagger\,\Gamma\dagger\mathbf{F}\Gamma\ell = \Lambda = \ell\dagger\ell\,\Gamma\dagger\mathbf{F}\Gamma \tag{91}$$

The final reordering is possible because ℓ and Λ are diagonal and therefore $\Gamma\dagger\mathbf{F}\Gamma$ is diagonal. This equation is easily solved for the elements $\ell\dagger\ell$ to give

$$(\ell\dagger\ell)_{kk} = L_{3k}^2 = \lambda_k/(\Gamma\dagger\mathbf{F}\Gamma)_{kk} \tag{92}$$

The other elements of $\mathbf{L}$ are gotten from these values and the ratios g_{ik} already determined.

The actual motions in the cartesian system can now be obtained by combining eq (39) with the inverse of eq (60) or eq (77). For the stretching motions we have

$$\mathbf{X}=\mathbf{M}^{-1}\tilde{\mathbf{R}}=\mathbf{M}^{-1}\begin{bmatrix}\mathbf{L}_r\mathbf{Q}_r\\0\end{bmatrix} \tag{93}$$

where $\mathbf{L}_r$ arises from the secular equation containing $\mathbf{H}_r$. $\mathbf{Q}_r$ is the normal coordinate vector and the x-component of the center of mass has been set to zero. A similar equation results for the bending modes. This is

$$\mathbf{Y}=\mathbf{A}^{-1}\tilde{\Psi}=\mathbf{A}^{-1}\begin{bmatrix}\mathbf{L}_\psi\mathbf{Q}_\psi\\0\\0\end{bmatrix} \tag{94}$$

where the z-component of the angular momentum and the y-component of the center of mass have been set to zero.

This completes the frequency analysis. In the next section we will consider the partition functions.

2.4. Partition Functions.

Herschbach et. al. [13] have shown how to express the classical partition function for polyatomic molecules in terms of local properties. We shall use their method because it allows for cancellations of considerable portions of the partition functions of the complex and reactants when their ratios are evaluated in the rate constant expression, eq (3). We begin the discussion with the classical partition function for a *linear* polyatomic molecule. This is (see Herzberg [14], pp. 502–509),

$$q_{cl}=q_e V(2\pi MkT/h^2)^{3/2}\,(kT/(\sigma hcB))\prod_i^{3N-5}(kT/(\omega_i hc)) \tag{95}$$

where q_e is the electronic partition function, V is the volume, M is the total mass of the molecule, c is the velocity of light, ω_i is the frequency of the i'th vibrational mode in cm^{-1} ($\omega_i=\nu_i/c$), N is the number of atoms in the molecule, B is the rotational constant; $B=h/(8\pi^2 cI)$, where I is the moment of inertia of the molecule; σ is the symmetry number which is the number of indistinguishable positions into which the molecule can be turned by simple rigid rotations. For linear molecules $\sigma=1$ or 2. Equation (95) neglects nuclear spins, anharmonicity, and non-rigidity of the molecule. Let us rewrite eq (95) in terms of I and $u_i=h\nu_i/kT$. It becomes

$$q_{cl}=q_e V4\pi\sigma^{-1}(2\pi kTh^{-2})^{5/2}M^{3/2}\,I\prod_i^{3N-5}u_i^{-1} \tag{96}$$

q_{cl} can also be written in the form

$$q_{cl}=q_e\sigma^{-1}Z\prod_\alpha^N\Lambda_\alpha^{-3} \tag{97}$$

where

$$Z=\int\ldots\ldots\int e^{-V/kT}dx_1\ldots\ldots dz_n \tag{98a}$$

$$\Lambda_\alpha=h(2\pi M_\alpha kT)^{-1/2} \tag{98b}$$

Z is the so-called configuration integral, V is the potential energy, and $x_1, y_1, z_1, \ldots\ldots x_N, y_N, z_N$ are the cartesian coordinates of each of the N atoms. Eliminating q_{cl} between eqs (96) and (97) gives

$$Z = V4\pi(2\pi kTh^{-2})^{-1/2(3N-5)}M^{3/2}\,I\prod_\alpha^N M_\alpha^{-3/2}\prod_i^{3N-5}u_i^{-1} \tag{99}$$

Consider now the matrix $\mathbf{H}=\mathbf{GF}$ defined by eq (84). A theorem of matrix algebra states that the determinant of $\mathbf{H}$ equals the product of its eigenvalues (see Hohn [15], p. 283). There is also a theorem (Hohn, p. 65),

stating that the determinant of product of two matrices equals the products of the determinants of the matrices in the product. Consequently,

$$|\mathbf{H}|^{1/2} = |\mathbf{G}|^{1/2}|\mathbf{F}|^{1/2} = \prod_{i}^{3N-5} \lambda_i^{1/2} = (2\pi kT/h)^{3N-5} \prod_{i}^{3N-5} u_i \tag{100}$$

Solving for the product over u_i gives

$$\prod_{i}^{3N-5} u_i^{-1} = (2\pi kT/h)^{3N-5} |\mathbf{G}|^{-1/2}|\mathbf{F}|^{-1/2} \tag{101}$$

Inserting eq (101) into (99) yields

$$Z = V4\pi(2\pi kT)^{1/2(3N-5)} M^{3/2} I \prod_{\alpha}^{N} M_\alpha^{-3/2} |\mathbf{G}|^{-1/2}|\mathbf{F}|^{-1/2} \tag{102}$$

This can be rearranged to give

$$|\mathbf{F}|^{1/2} (2\pi kT)^{-1/2(3N-5)} Z = V4\pi M^{3/2} I \prod_{\alpha}^{N} M_\alpha^{-3/2} |\mathbf{G}|^{-1/2} = \mathbf{J}_N \tag{103}$$

The left side of eq (103) does not involve the masses, while the right side does not contain force constants. Therefore, the quantity denoted by J_N does not depend on either the force constants or the masses, but must depend only on geometrical parameters. Herschbach et. al. [13] have shown that for linear molecules

$$J_N = V4\pi \prod_{i=1}^{N-1} R_{i+1,i}^2 \tag{104}$$

where $R_{i+1,i}$ is the equilibrium distance between mass M_i and M_{i+1}. For a general linear molecule, the classical partition function per unit volume can now be written

$$Q_{cl} = q_{cl}/V = V^{-1} q_e \sigma^{-1} J_N (2\pi kT)^{1/2(3N-5)} |\mathbf{F}|^{-1/2} \prod_{\alpha}^{N} \Lambda_\alpha^{-3} \tag{105}$$

This form of the partition function is suitable for the reactant molecules.

Let us now consider the partition function for the complex. Using eq (96), we have

$$kTh^{-1} q^* = kTh^{-1} q_e \sigma^{-1} V4\pi(2\pi kTh^{-2})^{5/2} M^{3/2} I \prod_{i}^{3N-6} u_i^{-1} \tag{106}$$

Note that the product is over $3N-6$; i.e., one less vibration than in a stable linear molecule. Consider next the quantity

$$\left(\prod_{i}^{3N-6} u_i^{-1}\right) kTh^{-1} = (kT/h)^{3N-5} \prod_{i}^{3N-6} \nu_i^{-1} = (kT/h)^{3N-5} \prod_{i}^{3N-6} 2\pi\lambda_i^{-1/2}$$

$$= (kT/h)^{3N-5} (2\pi)^{3N-6} \lambda^{*1/2} \prod_{i}^{3N-6} \lambda_i^{-1/2}\lambda^{*-1/2}$$

$$= (2\pi kT/h)^{3N-5} \nu^* |\mathbf{F}|^{-1/2}|\mathbf{G}|^{-1/2} \tag{107}$$

where λ^* is the negative eigenvalue and ν^* is the associated imaginary frequency; eq (100) has been used. Using eq (107) in (106) gives

$$kTh^{-1} Q^* = kTh^{-1} q^* V^{-1} = V^{-1} q_e \sigma^{-1} \{V4\pi M^{3/2} I \prod_{\alpha}^{N} M_\alpha^{-3/2} |\mathbf{G}|^{-1/2}\} \nu^* |\mathbf{F}|^{-1/2} (2\pi kT)^{3N-5/2}$$

$$\cdot h^{-3N} \prod_{\alpha}^{N} M_\alpha^{3/2}$$

$$= V^{-1} q_e \sigma^{-1} J_N \nu^* |\mathbf{F}|^{-1/2} (2\pi kT)^{1/2(3N-5)} \prod_{\alpha}^{N} \Lambda_\alpha^{-3} \tag{108}$$

This equation is very similar to eq (105), the partition function of a stable molecule. Note that $|\mathbf{F}|^{-1/2}$ will be imaginary for the complex.

We can now write down the specific partition functions per unit volume for the four reaction cases shown in figure 1b.

Case III.

Species $A = M_2 - M_3$
Species $B = M_4$
Species $C = M_2 \ldots M_3 \ldots M_4$
$Q_A = q_{eA}\sigma_A^{-1}\, 4\pi R_{bs}^2 (2\pi kT)^{1/2} F_{bs}^{-1/2} (\Lambda_2\Lambda_3)^{-3}$
$Q_B = q_{eB}\Lambda_4^{-3}$
$Q_C kT/h = q_{eC}\sigma_C^{-1}\, 4\pi R_b^2 R_c^2 \nu^* |\mathbf{F}_r|^{-1/2} F_{\psi_3}^{-1} (2\pi kT)^2 (\Lambda_2\Lambda_3\Lambda_4)^{-3}$
The matrix $\mathbf{F}_r$ is the 2×2 one given by eq. (5b), and not the 4×4 used in eq (83).

Case IVa.

Species $A = M_1 - M_2 - M_3$
Species $B = M_4$
Species $C = M_1 - M_2 \ldots M_3 \ldots M_4$
$Q_A = q_{eA}\sigma_A^{-1}\, 4\pi R_{as}^2 R_{bs}^2 (2\pi kT)^2 (F_{as}F_{bs})^{-1/2} F_{\psi_{2s}}^{-1} (\Lambda_1\Lambda_2\Lambda_3)^{-3}$
$Q_B = q_{eB}\Lambda_4^{-3}$
$Q_C kT/h = q_{eC}\sigma_C^{-1}\, 4\pi R_{as}^2 R_b^2 R_c^2 \nu^* F_{as}^{-1/2} |\mathbf{F}_r|^{-1/2} F_{\psi_2}^{-1} F_{\psi_3}^{-1} (2\pi kT)^{7/2} (\Lambda_1\Lambda_2\Lambda_3\Lambda_4)^{-3}$
Note that I have included F_{as} in Q_A and Q_C even though it is supposed to be infinite; it will cancel out when the ratio Q_C/Q_A is taken. Also note that the bending force constants appear with twice the power of the stretching force constants. This is because of the degeneracy.

Case IVb.

Species $A = M_2 - M_3$
Species $B = M_4 - M_5$
Species $C = M_2 \ldots M_3 \ldots M_4 - M_5$
$Q_A = q_{eA}\sigma_A^{-1}\, 4\pi R_{bs}^2 (2\pi kT)^{1/2} F_{bs}^{-1/2} (\Lambda_2\Lambda_3)^{-3}$
$Q_B = q_{eB}\sigma_B^{-1}\, 4\pi R_{ds}^2 (2\pi kT)^{1/2} F_{ds}^{-1/2} (\Lambda_4\Lambda_5)^{-3}$
$Q_C kT/h = q_{eC}\sigma_C^{-1}\, 4\pi R_b^2 R_c^2 R_{ds}^2 \nu^* |\mathbf{F}_r|^{-1/2} F_{\psi_3}^{-1} F_{\psi_4}^{-1} (2\pi kT)^{7/2} (\Lambda_2\Lambda_3\Lambda_4\Lambda_5)^{-3} F_{ds}^{-1/2}$

Case V.

Species $A = M_1 - M_2 - M_3$
Species $B = M_4 - M_5$
Species $C = M_1 - M_2 \ldots M_3 \ldots M_4 - M_5$
$Q_A = q_{eA}\sigma_A^{-1}\, 4\pi R_{as}^2 R_{bs}^2 (2\pi kT)^2 (F_{as}F_{bs})^{-1/2} F_{\psi_{2s}}^{-1} (\Lambda_1\Lambda_2\Lambda_3)^{-3}$
$Q_B = q_{eB}\sigma_B^{-1}\, 4\pi R_{ds}^2 (2\pi kT)^{1/2} F_{ds}^{-1/2} (\Lambda_4\Lambda_5)^{-3}$
$Q_C kT/h = q_{eC}\sigma_C^{-1}\, 4\pi R_{as}^2 R_b^2 R_c^2 R_{ds}^2\, \nu^* F_{as}^{-1/2} |\mathbf{F}_r|^{-1/2} F_{ds}^{-1/2} F_{\psi_2}^{-1} F_{\psi_3}^{-1} F_{\psi_4}^{-1} (2\pi kT)^5 (\Lambda_1\Lambda_2\Lambda_3\Lambda_4\Lambda_5)^{-3}$

We now have everything for eq (3) except the tunneling correction. This will be taken up in the next section.

2.5. Tunneling Correction

The one-dimensional Eckart potential function was used to approximate the barrier to quantum mechanical tunneling from reactants to products. Three parameters are required for its definition; these are shown in figure 8. Its functional form is

$$V(x) = \frac{Ay}{1-y} - \frac{By}{(1-y)^2} \tag{109}$$

where

$$\begin{aligned} y &= -e^{2\pi x/L} \\ A &= V_1 - V_2 \\ B &= (V_1^{1/2} + V_2^{1/2})^2 \\ L &= 2\pi(-2/F)^{1/2}\,(V_1^{-1/2} + V_2^{-1/2})^{-1}, \text{ and} \\ F &= \frac{\partial^2 V}{\partial x^2} \end{aligned}$$

evaluated at the maximum in the curve. F is a force constant. Using this potential function, Eckart [16] solved the wave equation and obtained the transmission coefficient for a particle with mass m approaching the barrier from the left with an energy E. His result is

$$\mathbf{K}(E,V_1,V_2,F) = 1 - \frac{\cosh[2\pi(\alpha_1-\alpha_2)]+\Delta}{\cosh[2\pi(\alpha_1+\alpha_2)]+\Delta} \tag{110}$$

where $\Delta = \cosh[2\pi\delta]$ if δ is real, and $\Delta = \cos[2\pi|\delta|]$ if δ is imaginary. The relationships of α_1, α_2, and δ to the parameters of figure 8, are

$$\begin{aligned} \alpha_1 &= \tfrac{1}{2}(E/C)^{1/2} \\ \alpha_2 &= \tfrac{1}{2}[(E-A)/C]^{1/2} \\ \delta &= \tfrac{1}{2}[(B-C)/C]^{1/2} \\ C &= h^2/(8mL^2) \end{aligned} \tag{111}$$

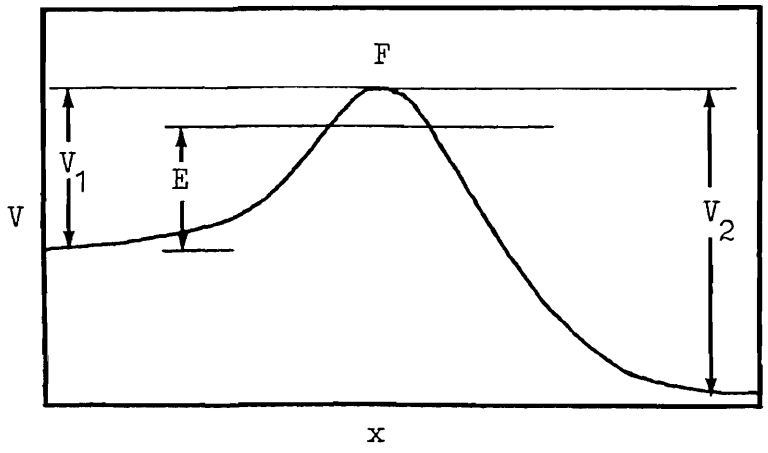

FIGURE 8. Eckart potential function.

Given the transmission coefficient, Johnston [2], pp. 42 and 43, has derived the correction factor Γ^* which is the ratio of the quantum barrier crossing rate to the classical crossing rate. His result is

$$\Gamma^* = e^{V_1/kT} \int_{E_o}^{\infty} \mathbf{K}(E) e^{-E/kT}\, dE/kT \tag{112}$$

where $E_o = 0$ when $V_1 \leq V_2$ and $E_o = V_1 - V_2$ when $V_1 > V_2$

Let us rewrite this in a more symmetrical form. We define a new variable $\epsilon = (E - V_1)/kT$, $E = kT\epsilon + V_1$. Equation (112) becomes

$$\Gamma^* = \int_{\epsilon_o}^{\infty} \mathbf{K}(\epsilon) e^{-\epsilon} d\epsilon \tag{113}$$

where $\epsilon_o = -V_1/kT$ when $V_1 \leq V_2$ and $\epsilon_o = -V_2/kT$ when $V_1 > V_2$.

With this substitution, the parameters α_1 and α_2 become

$$\alpha_i = \tfrac{1}{2}(kT\epsilon/C + V_i/C)^{1/2}, \quad i = 1 \,\&\, 2 \tag{114}$$

From eq (110) we have

$$\mathbf{K} = \mathbf{K}(\alpha_1,\alpha_2,\delta) = \mathbf{K}(kT\epsilon/C, V_1/C, V_2/C, B/C)$$

But

$$B/C = V_1/C + 2[(V_1/C)(V_2/C)]^{1/2} + V_2/C \tag{115}$$

is a function of V_1/C and V_2/C. Therefore

$$\mathbf{K} = \mathbf{K}(\epsilon, p, p_1, p_2) \tag{116}$$

where

$$p = kT/C,\ p_1 = V_1/C \text{ and } p_2 = V_2/C.$$

Γ^* thus depends on three parameters. Furthermore, it is invariant when p_1 and p_2 are interchanged; i.e., $\Gamma^*(p,p_1,p_2) = \Gamma^*(p,p_2,p_1)$. To see this let $p_1' = p_2$ and $p_2' = p_1$. From eq (115) we see that

$$(B/C)' = p_1' + 2(p_1'p_2')^{1/2} + p_2' = p_2 + 2(p_2p_1)^{1/2} + p_1 = B/C$$

Thus, $\delta' = \delta$. From eq (114) we have

$$\alpha_1' = \tfrac{1}{2}(p\epsilon + p_1')^{1/2} = \tfrac{1}{2}(p\epsilon + p_2)^{1/2} = \alpha_2$$
$$\alpha_2' = \alpha_1$$

Using these results in eq (110), we get

$$\mathbf{K}(\epsilon,p,p_1',p_2') = \mathbf{K}(\epsilon,p,p_2,p_1) = \mathbf{K}(\epsilon,p,p_1,p_2) \tag{117}$$

Suppose that $p_1' > p_2'$; i.e., $V_1' > V_2'$. Using eq (117), eq (113) becomes

$$\Gamma^*(p,p_1',p_2') = \int_{-p_1'/p}^{\infty} \mathbf{K}(\epsilon,p,p_1',p_2') e^{-\epsilon} d\epsilon = \int_{-p_1/p}^{\infty} \mathbf{K}(\epsilon,p,p_1,p_2) e^{-\epsilon} d\epsilon = \Gamma^*(p,p_1,p_2)$$

The way Eq (113) was integrated to get Γ^* will be considered later when the computer program is discussed.

In applying this correction, it is assumed that the x coordinate of Eckart's potential lies in the ϱ direction discussed earlier. This is that direction at the saddle point in which the potential energy decreases most rapidly. It is also the direction of the path of constant total bond order. We therefore use the force constant F_ρ given by eq (22) for the second derivative of the Eckart potential at its maximum. The effective mass for tunneling, M_t, is the proportionality factor between the kinetic energy and $\frac{1}{2}\dot{\varrho}^2$. We can calculate M_t in the following way: As far as tunneling is concerned, in the 4 and 5 mass point cases there are effectively 3

masses, since the end bonds are supposed to be rigid. Thus, there are only the two variables, R_b and R_c, involved. (Bending modes are not considered.) The kinetic energy T_r for changes in these two bonds is given by

$$T_r = \tfrac{1}{2}\dot{\mathbf{R}}\dagger\mathbf{G}_r^{-1}\dot{\mathbf{R}} \tag{118}$$

where $\mathbf{R}$ is the 2-dimensional vector defined by eq (6), and $\mathbf{G}_r$ is the 2 × 2 matrix given by eq (86). The inverse of this matrix is easily calculated and found to be

$$\mathbf{G}_r^{-1} = \begin{bmatrix} M_2'(M_3+M_4') & M_2'M_4' \\ M_2'M_4' & (M_2'+M_3)M_4' \end{bmatrix} \mathbf{M}^{-1} \tag{119}$$

where $M_2' = M_1 + M_2$ and $M_4' = M_4 + M_5$ in the 5 point case. The transformation between R_b, R_c and ϱ, σ is given by the matrix $\mathbf{U}$ whose value, determined by the BEBO calculation, is given by eq (18). $\mathbf{U}$ can be used to express T_r in terms of ϱ and σ. Thus

$$T_r = \tfrac{1}{2}\dot{\mathbf{R}}\dagger\mathbf{G}_r^{-1}\dot{\mathbf{R}} = \tfrac{1}{2}\dot{\mathbf{P}}\dagger\mathbf{U}\dagger\mathbf{G}_r^{-1}\mathbf{U}\dot{\mathbf{P}}$$

The desired quantity M_r is simply the matrix element $(\mathbf{U}\dagger\mathbf{G}_r^{-1}\mathbf{U})_{\dot{\varrho}\dot{\varrho}}$. This is

$$M_r = \frac{M_2'(M_3+M_4')m^2 - 2M_2'M_4'nm + (M_2'+M_3)M_4'n^2}{(n^2+m^2)M} \tag{120}$$

where n and m are the bond orders from the BEBO calculation, and M is the total mass of the molecule.

The bases from which the tunneling parameters V_1 and V_2 are measured are taken to be the zero point energies of the reactants and products, respectively, and not the potential minimums as might be expected. The maximum of the potential, on the other hand, is placed at the potential minimum of the complex; i.e., at the saddle point. Johnston [2], pp. 190–196, gives reasons for this particular method of using the Eckart function for tunneling corrections.

We finally have everything needed for eq (3). In the next section explicit rate constant expressions will be given for the four reaction cases of figure 2.

2.6. Rate Constant Expressions

The rate constant expression eq (3) is not quite complete. It should be multiplied by the number of equivalent H atoms on the molecule being attacked. Let us call this factor the chemical multiplicity, σ_{ch}. For example, there are 6 identical reaction paths for H abstraction of the 6 terminal H atoms on propane, and 2 paths for abstraction of the 2 central H atoms. Thus $\sigma_{ch} = 6$ in the first case, and 2 in the second. With this factor added, the rate constants for the four cases shown in figure 2 are

Case III. $M_2 - M_3 + M_4 \rightarrow M_2 \ldots M_3 \ldots M_4$

$$\mathbf{k} = SF_{\nu_3}^{-1}(2\pi kT)^{3/2}(\Gamma_3^{\ddagger})^2$$

Case IVa. $M_1 - M_2 - M_3 + M_4 \rightarrow M_1 - M_2 \ldots M_3 \ldots M_4$

$$\mathbf{k} = SF_{\nu_{2'}}(F_{\nu_2}F_{\nu_3})^{-1}(2\pi kT)^{3/2}(\Gamma_2^{\ddagger}\Gamma_3^{\ddagger})^2(\Gamma_2^{A})^{-2} \tag{121}$$

Case IVb. $M_2 - M_3 + M_4 - M_5 \rightarrow M_2 \ldots M_3 \ldots M_4 - M_5$

$$\mathbf{k} = S(F_{\nu_3}F_{\nu_4})^{-1}(2\pi kT)^{5/2}(\Gamma_3^{\ddagger}\Gamma_3^{\ddagger})^2(4\pi)^{-1}$$

Case V. $M_1 - M_2 - M_3 + M_4 - M_5 \rightarrow M_1 - M_2 \ldots M_3 \ldots M_4 - M_5$

$$\mathbf{k} = SF_{\psi_2} (F_{\psi_2} F_{\psi_3} F_{\psi_4})^{-1} (2\pi kT)^{5/2} (\Gamma_2^* \Gamma_3^* \Gamma_4^*)^2 (\Gamma_2^A)^{-2} (4\pi)^{-1}$$

The common factor in all these expressions is

$$S = \sigma_{ch} \frac{q_{eC}\, \sigma_A \sigma_B\, R_b^2 R_c^2}{q_{eA} q_{eB}\, \sigma_C\, R_{bs}^2}\, \nu^* \frac{F_{bs}^{1/2}\, \Gamma_s^*}{|\mathbf{F}_r|^{1/2}\, \Gamma_s^A}\, \Gamma^*\, e^{-V^*/kT}.$$

The calculated factors in S are:

1) R_b and R_c; these are calculated from n and m through Pauling's relation, eq (9).
2) ν^* is the imaginary frequency obtained from the vibration analysis for the asymmetric stretch.
3) $|\mathbf{F}_r|$ is the determinant of the matrix given by eq (30). It is negative.
4) Γ_s^* is the quantum correction factor for the symmetric stretching frequency obtained from the vibrational analysis.
5) Γ^* is the tunneling correction factor obtained in section 2.5.
6) V^* is the saddle point potential energy given by the BEBO calculation.

Other calculated factors are:

1) F_{ψ_3} is the bending force constant given by eq (33).
2) F_{ψ_2} and F_{ψ_4} are the bending force constants given by eq (34).
3) The quantum correction factors Γ_2^*, Γ_3^*, Γ_4^* for the bending modes come from the frequency analysis via eq (2).

This concludes the theoretical part of this discussion. The next section contains a brief discussion of the computer program which was written to implement the rate constant calculations. This will be followed by instructions on how to use it.

3. Computer Implementation of BEBO

The computer program consists of a main section and six subroutines. It is written in an enhanced form of BASIC for use on a Hewlett-Packard 9845A computer.

3.1. Description of the Main Program

The main program begins by reading the following data:

1) Runid$

This is a string variable having up to 79 alphanumeric characters to be used for the run identification.

2) Opt(M), M = 1,7

These are flags which provide a series of available options. These will be described in detail in the instruction section.

3) Ntemp

This is the number of temperature values at which the rate constant is to be evaluated. A maximum of 16 values will be allowed.

4) Tmin,Tmax

The minimum and maximum temperature values desired. The reciprocal temperature scale is divided into Ntemp − 1 equal intervals and the temperature evaluated from the reciprocal values. This gives a better distribution on an Arrhenius plot than if the temperature scale were divided into equal intervals.

5) M1,M2,M3,M4,M5

These are the five mass point values determined according to the rules given in section 2.1.

6) Ras,Rbs,Rcs,Rds

These are the equilibrium bond distances for single bonds.

7) Ebs,Ecs,P,Q

The first two parameters are the electronic energies for single bonds b and c; the last two are the BEBO parameters obtained from eq (12).

8) Rts,Ets,Beta

These are the bond distance, bond energy, and Morse parameter β for the triplet interaction.

9) Fbs,Fcs,Fpsi2s,Fpsi4s

These are the stretching force constants for single b and c bonds, and the bending force constants about the M2 and M4 masses.

10) Sa,Sb,Sc

These are the partition function symmetries σ_A, σ_B, and σ_O.

11) Schem

This is the chemical multiplicity σ_{ch}.

12) Sea,Seb,Sec

These are the electronic degeneracies q_{eA}, q_{eB}, and q_{eC}.

The program next prints out this input data to provide an easily read record and a check of the numbers.

After these preliminaries, the program then determines the saddle point position. This is done by an iterative procedure; n is initially set to 0.5; then the potential energy V is calculated according to eq (14) along with its first and second derivatives, Vn and Vnn, with respect to n. The subroutine Trpl is used to calculate the triplet part of V. A new n is estimated by the Newton, Raphson method from the formula $n' = n - Vn/Vnn$. The process is repeated using n' and continued until covergence is obtained. This yields a value of n which makes Vn zero; this will correspond to the desired maximum in V. (I have not investigated the conditions for which a maximum is expected or if there could be more than one maximum.)

Having obtained the value of n for the saddle point, the program calculates the stretching force constant matrix Fr given by eq (30), its determinant, and the saddle values of Rb and Rc from Pauling's relation eq (9). It then evaluates the mass to be used for tunneling from a somewhat rearranged eq (120). Next, the 2×2 matrix Gr is calculated from eq (86). This is then combined with Fr to form Hr, and the stretching frequencies obtained by solving the resulting quadratic secular equation. The bending frequencies are next determined through the matrices F (eq (35)) and G (eq (87)). The sizes of these matrices will depend on the type of reaction. For the three mass point model there is only one element and thus a linear secular equation with one bending frequency. The two four point models require solving a quadratic secular equation for two frequencies. The five point model uses the subroutine Cubic to solve the cubic secular equation for three frequencies. The subroutine Normod then calculates the matrix for the normal coordinate transformation of the stretching modes.

At this point, the program prints out a number of properties of the complex. This will be discussed in detail in the instruction section.

The rate constants are then evaluated from eqs (121) at the different temperatures. The activation energy is gotten by numerically differentiating the logarithm of the rate constant by means of suitable finite difference formulas. Subroutine Fit is a least-squares routine which is used to fit Arrhenius equations through the calculated points. The program concludes with subroutine Pltk which draws an Arrhenius plot of the results.

3.2. Discussion of Subroutine Tun

The only subroutine worth discussing is Tunl, the routine for evaluating the integral of eq (112) for the tunneling correction factor Γ^*. Johnston and Heicklen [17] calculated this integral numerically by an unspecified method for a range of input parameter values. The three input parameters which they used were $h\nu^*/kT$, where $\nu^* = (-F/m)^{1/2}/(2\pi)$, $2\pi V_1/(h\nu^*)$, and $2\pi V_2/(h\nu^*)$. Their results are in the form of a table. The method used in the present program is a modified 6-point Gaussain quadrature formula based on Legendre polynomials (see Abramowitz and Stegun [18]). This was used even though the nature of the integral suggests using a formula based on Laguerre polynomials. Neither of these formulas was satisfactory for the whole range of parameter values given by Johnston and Heicklen, so a modification of the first method was developed. It was based on the following ideas: When ϵ gets large, the transmission approaches unity. The

idea is to use the Gaussian formula for that part of the integral where $\mathbf{K}(\epsilon) < 1$. After $\mathbf{K}(\epsilon)$ has gotten sufficiently close to unity, the remainder of the integral can be evaluated analytically; i.e., if $\mathbf{K}(\epsilon) \approx 1$ for $\epsilon > \epsilon_b$, then

$$\int_{\epsilon_b}^{\infty} \mathbf{K}(\epsilon) e^{-\epsilon} d\epsilon \approx \int_{\epsilon_b}^{\infty} e^{-\epsilon} d\epsilon = e^{-\epsilon_b}$$

The problem is to estimate ϵ_b. Let us examine eqs (114) as $\epsilon \to \infty$. We get $\alpha_i \to \frac{1}{2}\xi^{\frac{1}{2}}$, where $\xi = kT\epsilon/C$. From eq (110), we have

$$\mathbf{K} \to 1 - (1 + \Delta)(\tfrac{1}{2}\exp(2\pi\xi^{\frac{1}{2}}) + \Delta)^{-1} = \mathbf{K}_B$$

We can set $\mathbf{K}_b$ to some arbitrary value close to unity and solve this equation for ϵ and then ξ and then ϵ_b which will be our cutoff point. The result is

$$\epsilon_b = C\,\{(2\pi)^{-1} ln\,[2(1 + \Delta)/(1 - \mathbf{K}_b)]\}^{2}(kT)^{-1}$$

It turns out that this value is not entirely satisfactory and subtracting from this the average value of V_1 and V_2 works better. Also it can happen that ϵ_b as calculated from this formula can be very large when $\mathbf{K}$ is close to unity. Thus, $\exp(-\epsilon_b)$ will be very small. There is no point in using a value for ϵ as the upper bound to the Gaussian formula if the integrand at this point is negligible because of the exponential factor. Thus ϵ_b was kept below a certain fixed value ϵ_{max}. This yielded two parameters, $\mathbf{K}_b$ and ϵ_{max} which were adjusted to minimize the squares of the differences between the results of this method and the results of Johnston and Heicklen. The differences averaged 1.3 percent with only two value differing by as much as 6 percent. Such accurancy should be quite adequate for the rate constant calculations.

4. INSTRUCTIONS FOR USING BEBO

4.1. Input

It will be assumed that the reader is familiar with the general operation and command system of the HP9845A. The program lines 5000 to 5240 contain a series of DATA statements which hold the input data. As an example, data for the ethane plus methyl radical reaction is contained in these statements. The general nature of the input has been discussed briefly in the last section; here this is considered in more detail.

1) Runid$ is a string variable containing identifying information; 79 characters can be used.
2) Opt(M),M=1,7 are flags for the following options:

Opt(0): This picks out the version of the triplet function V_i; these different forms of V_i will be discussed in the Appendix.

Opt(1): As mentioned earlier, the activation energy Eact at any temperature is obtained by numerically differentiating the logarithm of the rate constants. This is done in either of two ways. The more accurate method evaluates the rate constant three times at each temperature; at the particular point and slightly above and below the point. The derivative is then estimated from a 3 point finite difference formula. This is automatically the method used when only a single temperature point is requested. The second, less accurate, but faster method uses the rate constants calculated at Ntemp (see last section or below) points and uses a 5 point difference formula for the derivative. The more points requested and the narrower the temperature range, the more accurate is this method. The value of Opt(1) determines which of these methods will be used. Thus, when

Opt(1)=1, 5 point difference formula used to get Eact (fastest method).
Opt(1)=2, 3 point difference formula used to get Eact (most accurate method).

Opt(2): When
Opt(2)=1, the lnatural logarithm of the rate constant is calculated.
Opt(2)=2, the logarithm, base 10 of the rate constant is calculated.

Opt(3): When
Opt(3)=1, the cathode ray tube is used for the printout. In this mode, execution of the program pauses before the Arrhenius plot is produced, and before the caption to the plot is generated. In each case execution can be resumed by pressing the "cont" key.
Opt(3)=0, the internal printer is used for the output.

Opt(4): When
Opt(4)=1, the rate constant is in cm^3/mole-s.
Opt(4)=2, the rate constant is in cm^3/molecule-s.
Opt(4)=3, the rate constant is in liters/mole-s.
Opt(4)=4, the rate constant is in liters/molecule-s.

Opt(5): Not used.

Opt(6): When
Opt(6)=0, the Eckart tunneling correction is not applied. It will automatically not be applied if the zero point energy of the reactants is greater than the potential energy V^* of the saddle point.
Opt(6)=1, the tunneling correction is applied.

Opt(7): When
Opt(7)=3, the three parameter Arrhenius type equation, $AT^{n}_{c-Exact \to RT}$ is fit to the calculated rate constant values.
Opt(7)=2, the standard two parameter Arrhenius equation $Ae^{-Eact \to RT}$ is fit to the calculated rate constant values.
3) Ntemp is the number of temperature values (up to 16) at which the rate constant is to be evaluated. Use the absolute temperature scale.

4) Tmin, Tmax are the minimum and maximum temperature values to be used. If Ntemp=1, then only one temperature value should be entered on this line.
5) *M*1,*M*2,*M*3,*M*4,*M*5 are the five mass point values determined by the rules on page 5. For 3 point models set *M*1 and *M*5 to zero. The 4 point models will have either *M*1 or *M*5 equal to zero. Atomic mass units are to be used.

6) *Ras,Rbs, Rcs, Rds* are the single bond distances in Å. For 3 point models set *Ras* and *Rds* to zero. For 4 point models, set either *Ras* or *Rds* to zero.

7) *Ebs,Ecs,P,Q;* the first two parameters are the electronic energies for single bonds in kcal/mole. The quantity normally available is the bond dissociation energy DH° which is defined as the enthalpy change in the process in which one mole of the bond of interest is broken, with reactants and products being in their standard states as ideal gases at 1 atm and 25 °C. This is not the energy we want. The desired energy E is shown in figure 9, which illustrates the energy relationships involved in the removal of an H atom from some group A. Z_{A-H} and $Z_{A\cdot}$ are the zero point energies for the reactant and molecular product, and H^T_{A-H}, $H^T_{A\cdot}$, and $H^T_{H\cdot}$ are enthalpies of the speices *A-H*, A·, and H·, respectively. In general, a particular enthalpy is the sum of the translational, rotational, vibrational, and PV contributions. We have

$$H^T = H^T(\text{trans}) + H^T(\text{rot}) + H^T(\text{vib}) + PV$$

By examing figure 9 it is easy to derive the relationship between E and DH°. It is

$$E = DH^\circ + (H^T_{A-H} - H^T_{A\cdot}) + (Z_{A-H} - Z_{A\cdot}) - H^T_{H\cdot} \qquad (122)$$

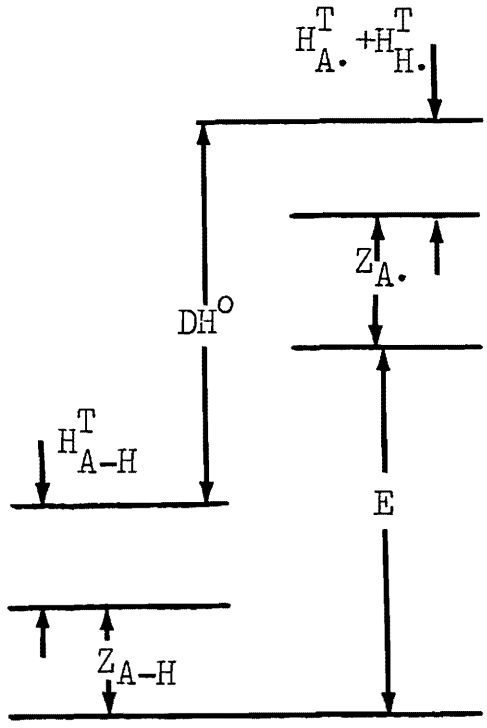

FIGURE 9. Bond energy relationships.

The second term is

$$H^T_{A-H} - H^T_{A\cdot} = H^T_{A-H}(\text{trans}) - H^T_{A\cdot}(\text{trans}) + H^T_{A-H}(\text{rot}) - H^T_{A\cdot}(\text{rot}) + H^T_{A-H}(\text{vib})$$

$$H^T_{A-H} - H^T_{A\cdot} = H^T_{A-H}(\text{trans}) - H^T_{A\cdot}$$

Assuming equipartition of energy, the translational and rotational enthalpies will be the same and the difference in vibrational enthalpies will normally be negligible. Thus, the second term in eq (122) can be neglected. The last term $H^T_{H\cdot} = E^T_{H\cdot} + PV = 3RT/2 + RT$, where $3RT/2$ is the translational energy of the H atom and RT is PV for an ideal gas. Thus, eq (122) becomes

$$E = DH^\circ = (Z_{A-H} - Z_{A\cdot}) - 5RT/2$$

As an example, consider the process $CH_3{-}H \rightarrow CH_3\cdot + H\cdot$. To estimate the difference in zero point energies between $CH_3{-}H$ and $CH_3\cdot$, I have assumed that one C-H stretch of 3100 cm^{-1} and two H-C-H bends of 1450 cm^{-1} have been lost in going from A-H to A· and H·.This corresponds to a zero point energy difference of 8.575 kcal. For cases like this, the bond energy will be

$$Ecs = DH^\circ + 8.575 - 5RT_{298}/2 = DH^\circ + 7.095 \text{ kcal}$$

The zero point energy difference for other types of bonds can probably be satisfactorily estimated in a similar manner. Having obtainedf Ebs and Ecs in this manner we can calculate P and Q from eq (12).

8) *Rts,Ets,Beta* are the triplet interaction parameters in Å kcal and $Å^{-1}$, respectively. I have been using the values given in Johnston [1966], table 11-1.

9) *Fbs,Fcs,Fpsi2s, Fpsi4s* are the single bond force constants. The first two are the stretching constants in dynes/cm; the second two are bending force constants in dyne-cm. In the 3 mass point case, both the bending force constants are set to zero. For 4 point models, only one of the bending force constants will have a value of zero.

10) *Sa,Sb,Sc* are the partition function symmetries for A-H, B·, and A··H··B, respectively.

11) Schem is the chemical multiplicity.

12) *Sea,Seb,Sec* are the electronic degeneracies for A-H, B·, and A··H··B. Sea will normally have the value one. Since B· and A··H··B each have an unpaired electron, Seb and Sec will normally have the value two.

4.2. Output

BEBO first prints out the input data. It then the following properties of the complex:
1) The potential energy of activation V^* in kcal/mole.
2) The bond orders n and m of the b and c bonds.
3) The bond distances *Rb* and *Rc* in Å.
4) The force constant in the ϱ direction in dynes/cm and the angle ϱ makes with the Rb axis on a contour plot like figure 3.
5) The force constant in the σ in dynes/cm, and the angle to the Rb axis.
6) The force constant in the unstable normal mode direction in dynes/cm, and the angle to the *Rb* axis.
7) The force constant in the stable normal mode direction in dynes/cm, and the angle to the *Rb* axis. Note that the normal mode directions are usually not orthogonal.
8) The stretching force constant matrix *Fr* in dynes/cm.
9) The equations for transforming back and forth between the normal mode and valence bond coordinates.
10) The bending force constants in dyne-cm.
11) The two stretching frequencies in cm^{-1}.
12) The one to three bending frequencies in cm^{-1}.
13) The zero point energy of the complex in kcal/mole.
14) The zero point energy of the reactants in kcal/mole.
15) The zero point energy of the products in kcal/mole.
16) The Eckart potential function parameters *V*1 and *V*2 in kcal/mole.
17) The reduced mass for tunneling M_t = Mrho.
18) The second two of Johnston and Heicklen's tunneling parameters (see section 2.5).
The program then prints out the rate constants as a function of temperature. Also given at each temperature is the logarithm of the rate constant, the logarithm of the Arrhenius preexponential factor, the activation energy, the tunneling correction factor, and the first of Johnston and Heicklen's tunneling parameters. Since the tunneling algorithm has not been checked outside the parameter ranges used by Johnston and Heicklen, their parameters values are listed to make sure that they are within the proper ranges. The limits are *A*1 and *A*2 = 0 to 20, and U^* = 0 to 16.

Finally, there are listed the differences between the calculated values of the logarithm of the rate constant and the values predicted by the least squares fitted Arrhenius equation. This fitted curve is shown by the dotted line on the Arrhenius plot. The fitted Arrhenius parameters are given in the caption ot the plot. On the next two pages there is a sample output for the ethane and methyl radical reaction.

5. References

[1] Johnston, Harold S. and Parr, Christopher. Activation energies from bond energies. I. Hydrogen transfer reactions. J. Am. Chem. Soc. 85(17):2544–2551; September 5, 1963.

[2] Johnston, Harold S. *Gas phase reaction rate theory.* New York: The Ronald Press; 1966. 362 p.

[3] Mahan, Bruce, H. Activated complex theory of bimolecular reactions. J. Chem. Ed. 51(11):709–711; November 1974.

[4] Johnston, Harold S. Large tunnelling corrections in chemical reaction rates. Advances in Chemical Physics **3**:131-170; 1961.
[5] Sharp, Terry E. and Johnston, Harold S. Hydrogen-deuterium kinetic isotope effect, an experimental and theoretical study over a wide range of temperature. J. Chem. Phys. **37**(7):1541-1553; October 1, 1962.
[6] Pauling, Linus. Atomic radii and interatomic distances in metals. J. Am. Chem. Soc. **69**(3):542-553; 1947 March.
[7] Herschbach, Dudley R. and Laurie, Victor W. Anharmonic potential constants and their dependence upon bond length. J. Chem. Phys. **35**(2):458-463; August 1961.
[8] Johnston, Harold S. Continuity of bond force constants between normal molecules and Lennard-Jones pairs. J. Am. Chem. Soc. **86**(8):1643-1645; April 20, 1964.
[9] Gilliom, Richard D. Activation energies from bond energies. A modification. J. Am. Chem. Soc. **99**(26):8399-8405; December 21, 1977.
[10] Sato, Shin. On a new method of drawing the potential energy surface. J. Chem. Phys. **23**(3):592-593; March 1955.
[11] Herzberg, Gerhard. *Molecular spectra and molecular structure I. Spectra of Diatomic Molecules.* New York: D. Can Nostrand Company; 1950. 658 p.
[12] Wilson, E. Bright, Jr., Decius, J. C., and Cross, Paul C. *Molecular Vibrations.* New York:McGraw-Hill Book Company; 1955. 388 p.
[13] Herschbach, Dudley R., Johnston, Harold S., and Rapp, Donald. Molecular parlition functions in terms of local properties. J. Chem. Phys. **31**(6):1652-1661; December 1959.
[14] Herzberg, Gerhard. *Molecular spectra and molecular structure II. Infrared and raman spectra of polyatomic molecules.* Princeton, New Jersey: D. Van Nonstrand Company; 1945. 632 p.
[15] Hohn, Franz E. *Elementary matrix algebra.* New York: MacMillan Company; 1964. 395 p.
[16] Eckart, Carl. The penetration of a potential barrier by electrons. Phys. Rev. **35**(11):1303-1309; June 1, 1930.
[17] Johnston, Harold S. and Heicklen, Julian. Tunnelling corrections for unsymmetrical Eckart potential energy barriers. J. Phys. Chem. **66**(3):532-533; March 1962.
[18] Abramowitz, Milton and Stegun, Irene A. Handbook of mathematical functions with formulas, graphs, and mathematical tables. Nat. Bur. Stand. (U.S.) Appl. Math. Ser. 55; June 1964. 1046 p.
[19] Arthur, N. L., Donchi, K. F., and McDonnell, J. A. BEBO calculations. III. A new triplet repulsion energy term. J. Chem. Phys. **62**(4):1585-1586; February 15, 1975.
[20] Hirschfelder, J. O. and Linnett, J. W. The energy of interaction between two hydrogen atoms. J. Chem. Phys. **18**(1):130-142; January 1950.

6. APPENDIX: Various Triplet Functions

The subroutine Trpl is able to provide three different triplet functions which are selected according to the value of flag Opt(0). They are as follows:

Opt(0)= 0: This is the modified Sato triplet function with a small portion neglected. Instead of Eq. (13), $V_t = E_{ts}$ is used. This simpler formula seems to have been used in the days of mechanical desk calculators. This option is useful when attempts are being made to reproduce the results of earlier workers.

Opt(0)= 1: Eq. (13) is used.

Opt(0)= 2: Arthur et. al. [19] have developed a triplet energy formula by fitting a function to the H-H triplet potential energy values given by Hirschfelder and Linnett [20]. Their formula is

$$V_t = 5.873 E_{ts} e^{-1.747\beta(R_b+R_c)}(\beta(R_b+R_c))^{1.525}$$

They claim better results in certain cases when this function is used.

```
*******************************************************************************
Run Identification:
CH3CH2-H + CH3 = CH3CH2 + H-CH3
*******************************************************************************
Options Used in Calculations:
Modified Sato triplet function.
Five-point difference formulas used to get activation energy.
Base 10 logarithm of the rate constant.
Rate constant units in liters/mole-s.
*******************************************************************************
Masses, in Atomic Mass Units.
  M1= 17.0510,  M2= 12.0110,  M3=  1.0080,  M4= 12.0110,  M5=  3.0240
Single Bond Distances, in Angstroms.
  Ras=1.52600,  Rbs=1.09000,  Rcs=1.09000,  Rds=1.09000
Single Bond Energies of Center Bonds, in kcal; also p & q Parameters.
  Ebs=105.100, Ecs=111.100,  p=1.085,  q=1.093
Single Bond Energy, Distance, & Morse Parameter for Triplet Interaction.
  Ets= 84.400,  Rts=1.54000,  Beta=1.4250
Single Bond Stretching Force Constants in dynes/cm for Center Bonds.
  Fbs=4.79000E+05,  Fcs=4.79000E+05
Single Bond Bending Force Constants in dyne-cm for Outer Masses.
  Fpsi2s=9.14837E-12,  Fpsi4s=5.46530E-12
Partition Function Symmetry Numbers for Species A, B, & C.
  SA=1,  SB=1,  SC=1
Chemical Multiplicity.
  Schem=6
Electronic Degeneracy for Species A, B, & C.
  SeA=1,  SeB=2,  SeC=2
Pauling's Bond-Order Parameter.
  Lamda=0.2800
*******************************************************************************
Properties of Complex.
Potential Energy of Activation: V=14.596 kcal
Bond Order Parameters: N=0.5804, M=0.4196
Bond Distances for Center Bonds: Rb=1.24235, Rc=1.33313 Angstroms
Force Const. in Rho Direction:   Frho= -8.25841E+04 dynes/cm: Angle= -54.13 deg
Force Const. in Sigma Direction: Fsigma=2.90227E+05 dynes/cm: Angle=  35.87 deg
Force Const. in Qr n.m. direction: Fqr=-7.58801E+04 dynes/cm: Angle= -46.42 deg
Force Const. in Qs n.m. direction: Fqs= 2.21465E+05 dynes/cm: Angle=  10.44 deg
F Matrix for Stretches in dynes/cm
   1.62224E+05     1.77020E+05
   1.77020E+05     4.54188E+04
Normal Coordinate Transformations
  Qs=  3.2115 Rb +   3.0558 Rc          Rb=  0.2649 Qs +  -0.9779 Qr
  Qr= -0.1525 Rb +   0.8279 Rc          Rc=  0.0488 Qs +   1.0277 Qr
F Matrix Elements for Bends; (these equal the bending force constants)
  Fpsi2=5.30936E-12, Fpsi3=7.54613E-13, Fpsi4=2.29351E-12 dyne-cm
Stretching Frequencies: 1610.40i,  522.47 wave nos.
Bending Frequencies: 1132.37,  148.99,  440.72 wave nos.
Zero Point Energy of Complex=  5.669 kcal
*******************************************************************************
Zero Point Energy of Reactants= 7.906 kcal
Zero Point Energy of Products=  7.478 kcal
Energy Bases for Eckart Tunneling: V1= 6.690, V2=13.117 kcal
Reduced Mass for Tunneling: Mrho=  .9314
Johnston's tunneling parameters: A1= 8.812, A2=17.279
*******************************************************************************
```

Temp., 1000/T	T	Rate Const., K	Log(K)	A factor, Log(A)	Act. Energy, Eact	Eckart U* Factor, Gam	U*	Deviation from Fit
0.50	2000	1.796E+09	9.254	11.724	22.597	1.041	1.200	-0.018
0.78	1286	1.030E+08	8.013	11.179	18.626	1.091	1.867	0.019
1.06	947	9.106E+06	6.959	10.718	16.294	1.166	2.534	0.017
1.33	750	1.036E+06	6.015	10.347	14.866	1.273	3.200	0.006
1.61	621	1.396E+05	5.145	10.022	13.850	1.422	3.867	-0.006
1.89	529	2.129E+04	4.328	9.727	13.079	1.627	4.534	-0.013
2.17	462	3.577E+03	3.553	9.454	12.462	1.909	5.201	-0.016
2.44	409	6.501E+02	2.813	9.193	11.943	2.300	5.867	-0.011
2.72	367	1.264E+02	2.102	8.944	11.502	2.851	6.534	0.001
3.00	333	2.599E+01	1.415	8.716	11.135	3.627	7.201	0.020

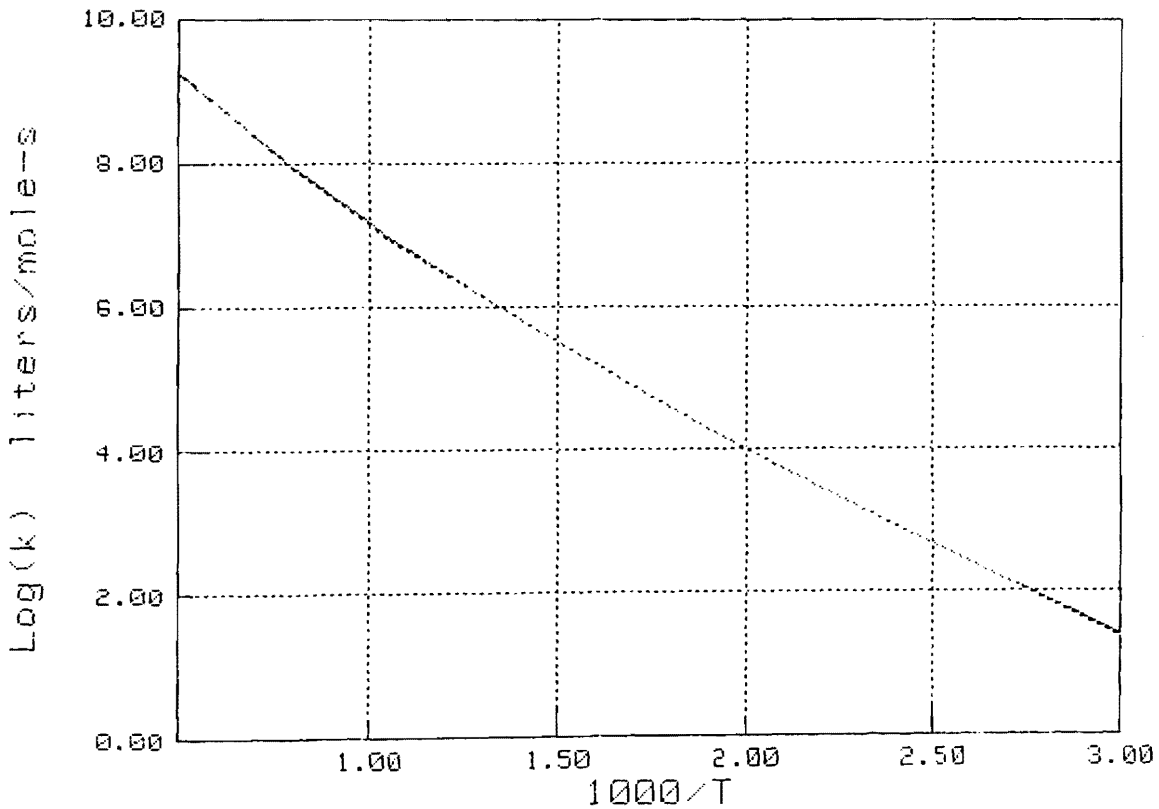

Figure 1. Plot of logarithm of rate constant as a function of the reciprocal of the temperature.
A least squares fit of the calculated rate constant to the Arrhenius expression, k=A*(T^n)*EXP(-Earr/RT), yields the following values for the parameters:
Log(A)=-2.362E+00, n= 3.821, Earr= 8.374

```
      This is a listing of the computer program for calculating the rate
      constants of hydrogen atom transfer reactions according to the
      bond-energy-bond-order method (customarily referred to as BEBO).
      It is written in an enhanced form of the BASIC language for use
      on a Hewlett-Packard 9845A computer.
   10 OVERLAP
   20 READ H,K,Lam,Pmass,Econv,Prec1,Imax,C,Null
   30 DATA 6.6234E-27,1.38033E-16,.28,1.65972E-24,6.94612E-14,1E-9,15,2.99776E10,0
   40 Tpfac=2*PI*K*1.439651E13
   50 DIM Runid$[79]
   60 DIM Opt[7],Temp[1:16],Tpktkcal[1:16],Ktkcal[1:16],Kqpr[1:16],Eactpr[1:16]
   70 DIM Gampr[1:16],Lkqpr[1:16],Lapr[1:16],Ustr[1:16],Error[1:16],Par[1:3]
   80 COM Delta,Lam,Nbebo,Rbs,Rcs,Rts,Betab,Betac,Beta,Ebs,Ecs,Ets
   90 READ Runid$              !Run identification.
  100 READ Opt[0],Opt[1],Opt[2],Opt[3],Opt[4],Opt[5],Opt[6],Opt[7]
  110 READ Ntemp               !Number of temperature values.
  120 IF Ntemp<=16 THEN L62
  130 PRINT "Error-03"
  140 BEEP
  150 STOP
  160 L62:  IF Ntemp<5 THEN Opt[1]=2
  170 REDIM Temp[1:Ntemp],Tpktkcal[1:Ntemp],Ktkcal[1:Ntemp],Kqpr[1:Ntemp]
  180 REDIM Eactpr[1:Ntemp],Gampr[1:Ntemp],Lkqpr[1:Ntemp],Lapr[1:Ntemp],Error[1:Ntemp]
  190 IF Ntemp=1 THEN READ Tmax       !A single temperature entered.
  200 IF Ntemp=1 THEN Tmin=1
  210 IF Ntemp=1 THEN Opt[1]=2
  220 IF Ntemp>1 THEN READ Tmin,Tmax  !The minimum and maximum temperatures.
  230 Rtmin=1000/Tmax
  240 Rtmax=1000/Tmin
  250 IF Ntemp>1 THEN Delrt=(Rtmax-Rtmin)/(Ntemp-1)
  260 FOR L=1 TO Ntemp
  270 Temp[L]=1000/(Rtmin+(L-1)*Delrt)
  280 Tpktkcal[L]=Tpfac*Temp[L]
  290 Ktkcal[L]=Tpktkcal[L]/(2*PI)
  300 NEXT L
  310 Delrt=Delrt/1000
  320 READ M1,M2,M3,M4,M5          !Atomic mass units.
  330 IF M1>0 THEN Mu1=1/M1
  340 IF M5>0 THEN Mu5=1/M5
  350 READ Ras,Rbs,Rcs,Rds         !Angstroms.
  360 IF Ras>0 THEN Rhoa=1/Ras
  370 IF Rds>0 THEN Rhod=1/Rds
  380 READ Ebs,Ecs,P,Q             !Energies in kcal/mole.
  390 READ Rts,Ets,Beta
  400 READ Fbs,Fcs,Fpsi2s,Fpsi4s !Stretching constants in dynes/cm.
  410                              ! Bending constants in dynes-cm.
  420 READ Sa,Sb,Sc                !Partition function symmetries.
  430 READ Schem                   !Chemical multiplicity.
  440 READ Sea,Seb,Sec             !Electronic degeneracy.
  460 PRINTER IS 16
```

```
470 L72:  IF Opt(3)=0 THEN PRINTER IS 0
480  PRINT "                                        BEBO  Calculations."
490  PRINT "*****************************************************************************"
500  PRINT "Run Identification:"
510  PRINT Runid$
520  PRINT "*****************************************************************************"
530  PRINT "Options Used in Calculations:"
540  IF Opt(0)=0 THEN PRINT "Simplified, modified Sato triplet function."
550  IF Opt(0)=1 THEN PRINT "Modified Sato triplet function."
560  IF Opt(0)=2 THEN PRINT "Two-parameter Arthur et.al., triplet function."
570  IF Opt(0)=3 THEN PRINT "Three-parameter Arthur et.al., style triplet function."
580 L64:  IF Opt(1)=1 THEN PRINT "Five-point difference formulas used to get activation energ
    y."
590  IF Opt(1)=2 THEN PRINT "Three-point difference formulas used to get the activation energ
    y."
600  IF Opt(2)=1 THEN PRINT "Natural logarithm of the rate constant."
610  IF Opt(2)=2 THEN PRINT "Base 10 logarithm of the rate constant."
620  IF Opt(4)=1 THEN PRINT "Rate constant units in cc/mole-s."
630  IF Opt(4)=2 THEN PRINT "Rate constant units in cc/molecule-s."
640  IF Opt(4)=3 THEN PRINT "Rate constant units in liters/mole-s."
650  IF Opt(4)=4 THEN PRINT "Rate constant units in liters/molecule-s."
660  IF Opt(6)=0 THEN PRINT "Tunneling correction not applied."
670  PRINT "*****************************************************************************"
680  PRINT "Masses, in Atomic Mass Units."
690  PRINT USING Format31;M1,M2,M3,M4,M5
700 Format31:  IMAGE "  M1=",3D.4D,",  M2=",3D.4D,",  M3=",3D.4D,",  M4=",3D.4D,",  M5=",3D.4
    D
710  PRINT "Single Bond Distances, in Angstroms."
720  PRINT USING Format32;Ras,Rbs,Rcs,Rds
730 Format32:  IMAGE "  Ras=",Z.5D,",  Rbs=",Z.5D,",  Rcs=",Z.5D,",  Rds=",Z.5D
740  PRINT "Single Bond Energies of Center Bonds, in kcal; also p & q Parameters."
750  PRINT USING Format33;Ebs,Ecs,P,Q
760 Format33:  IMAGE "  Ebs=",3D.3D,", Ecs=",3D.3D,",  p=",Z.3D,",  q=",Z.3D
770  PRINT "Single Bond Energy, Distance, & Morse Parameter for Triplet Interaction."
780  PRINT USING Format34;Ets,Rts,Beta
790 Format34:  IMAGE "  Ets=",3D.3D,",  Rts=",Z.5D,",  Beta=",Z.4D
800  PRINT "Single Bond Stretching Force Constants in dynes/cm for Center Bonds."
810  PRINT USING Format35;Fbs,Fcs
820 Format35:  IMAGE "  Fbs=",Z.5DE,",  Fcs=",Z.5DE
830  PRINT "Single Bond Bending Force Constants in dyne-cm for Outer Masses."
840  PRINT USING Format36;Fpsi2s,Fpsi4s
850 Format36:  IMAGE "  Fpsi2s=",Z.5DE,",  Fpsi4s=",Z.5DE
860  PRINT "Partition Function Symmetry Numbers for Species A, B, & C."
870  PRINT USING Format37;Sa,Sb,Sc
880 Format37:  IMAGE "  SA=",Z,",  SB=",Z,",  SC=",Z
890  PRINT "Chemical Multiplicity."
900  PRINT USING Format38;Schem
910 Format38:  IMAGE "  Schem=",Z
920  PRINT "Electronic Degeneracy for Species A, B, & C."
930  PRINT USING Format39;Sea,Seb,Sec
```

```
940 Format39:  IMAGE "  SeA=",Z,",  SeB=",Z,",  SeC=",Z
950  PRINT "Pauling's Bond-Order Parameter."
960  PRINT USING Format41;Lam
970 Format41:  IMAGE "  Lamda=",Z.4D
980  PRINT "*****************************************************************************"
990  Sym=Schem*Sec*Sa*Sb/(Sea*Seb*Sc)
1000 Fbs=1E-16*Fbs/Econv     !Force constants are converted to kcal energy units.
1010 Fcs=1E-16*Fcs/Econv
1020 Fpsi2s=Fpsi2s/Econv
1030 Fpsi4s=Fpsi4s/Econv
1040 ! ***********************************************************************
1050 ! The saddle point position is calculated.
1060 N=.5
1070 Icount=0
1090 L11: IF N<0 THEN N=.5*Nold
1100 IF N>1 THEN N=.5*(Nold+1)
1101 Nold=N
1110 CALL Trpl(Rbs,Rcs,Rts,Ets,Beta,Lam,N,Vt,Vtn,Vtnn,Vtr,Vtrr,Opt(0))
1120 M=1-N
1130 V=Ebs*(1-N^P)-Ecs*M^Q+Vt
1140 Vn=-Ebs*P*N^(P-1)+Ecs*Q*M^(Q-1)+Vtn
1150 Vnn=-Ebs*P*(P-1)*N^(P-2)-Ecs*Q*(Q-1)*M^(Q-2)+Vtnn
1160 N=Nold-Vn/Vnn
1170 IF ABS((N-Nold)/Nold)<Prec1 THEN L10
1180 Icount=Icount+1
1190 IF Icount>Imax THEN L12
1200 GOTO L11
1210 L12: PRINT "Error-01"
1220 STOP
1230 L10: N=Nbebo=Nold
1240 ! ***********************************************************************
1250 ! Next, the stretching part of the force constant matrix is calculated.
1260 Nsq=N^2
1270 Msq=M^2
1280 N2m2=Nsq+Msq
1290 Nm=N*M
1300 Frho=Vnn*Nm^2/(N2m2*Lam^2)
1310 Fsigma=(Fbs*N^3+Fcs*M^3+Vtrr)/N2m2
1320 DIM Fr(1:2,1:2)
1330 Fr(1,1)=(Frho*Msq+Fsigma*Nsq)/N2m2
1340 Fr(1,2)=Fr(2,1)=(-Frho+Fsigma)*Nm/N2m2
1350 Fr(2,2)=(Frho*Nsq+Fsigma*Msq)/N2m2
1360 Rb=Rbs-Lam*LOG(N)
1370 Rc=Rcs-Lam*LOG(M)
1380 Dfr=DET(Fr)
1390 Dfr=SGN(Dfr)*SQR(ABS(Dfr))
1400 Jfac=(Rb*Rc/Rbs)^2
1410 Rhob=1/Rb
1420 Rhoc=1/Rc
1430 Cc=-Nbebo/(1-Nbebo)
```

```
1440 Ma=M1+M2
1450 Mx=M3
1460 Mb=M4+M5
1461 Maxb=Ma+Mx+Mb
1470 Mrho=(Ma*Mb*(1+Cc)^2+Mb*Mx*Cc^2+Ma*Mx)/(Maxb*(1+Cc^2))
1471 DIM Azr(1:3,1:2),Alq(1:3,1:2)
1472 Azr(1,1)=-(Mb+Mx)/Maxb
1473 Azr(1,2)=Azr(2,2)=-Mb/Maxb
1474 Azr(2,1)=Azr(3,1)=Ma/Maxb
1475 Azr(3,2)=(Ma+Mx)/Maxb
1480 ! Mrho=1
1490 ! ************************************************************************
1500 ! Next, the Gr matrix is calculated. This will hold for 3,4,&5 atom models
1510 ! with rigid bonds on the ends.
1520 ! First, the type of model being used is determined. (Note, all are linear)
1530 DIM Gr(1:2,1:2)
1540 Model=5
1550 IF (M1=0) OR (M5=0) THEN Model=4
1560 IF (M1=0) AND (M5=0) THEN Model=3
1570 Model2=Model-2
1580 Mu2=1/M2
1590 Mu3=1/M3
1600 Mu4=1/M4
1610 Gr(1,1)=Mu2/(1+M1/M2)+Mu3
1620 Gr(1,2)=Gr(2,1)=-Mu3
1630 Gr(2,2)=Mu3+Mu4/(1+M5/M4)
1640 ! Stretching frequencies evaluated.
1650 DIM Hr(1:2,1:2)
1660 MAT Hr=Gr*Fr
1670 Bh=Hr(1,1)+Hr(2,2)
1680 Ch=Hr(1,1)*Hr(2,2)-Hr(1,2)*Hr(2,1)
1690 Dh=SQR(Bh^2-4*Ch)
1700 DIM Evs(1:2),Frqs(1:2),Ls(1:2)
1710 Evs(1)=.5*(Bh+Dh)
1720 Evs(2)=.5*(Bh-Dh)
1730 FOR I=1 TO 2
1740 Frqs(I)=SGN(Evs(I))*682.427*SQR(ABS(Evs(I)))/(2*PI)  !In 1/cm.
1750 NEXT I
1760 ! ************************************************************************
1770 ! Bending frequencies now calculated.
1780 Fpsi3=-Rb*Rc*Vtr/(Rb+Rc)
1790 DIM G(1:3,1:3),F(1:3,1:3),H(1:3,1:3),Evb(1:3),Frqb(1:3),Lb(1:3)
1800 REDIM G(1:Model2,1:Model2),F(1:Model2,1:Model2),H(1:Model2,1:Model2)
1810 REDIM Evb(1:Model2),Frqb(1:Model2),Lb(1:Model2)
1820 ON Model2 GOTO La3,La4,La5
1830 ! ..........................................................................
1840 ! Three atom model.
1850 La3: G(1,1)=Mu2*Rhob^2+Mu4*Rhoc^2+Mu3*(Rhob+Rhoc)^2
1860 F(1,1)=Fpsi3
1870 MAT H=G*F
```

```
1880 Evb(1)=H(1,1)
1890 GOTO L20
1900 ! ..........................................................................
1910 ! Four atom models.
1920 La4: IF M1=0 THEN La4sub
1930 G(1,1)=Mu1*Rhoa^2+Mu3*Rhob^2+Mu2*(Rhoa+Rhob)^2
1940 G(1,2)=G(2,1)=-Rhob*((Rhoa+Rhob)*Mu2+(Rhob+Rhoc)*Mu3)
1950 G(2,2)=Mu2*Rhob^2+Mu4*Rhoc^2+Mu3*(Rhob+Rhoc)^2
1960 F(1,1)=Fpsi2=Fpsi2s*N
1970 F(1,2)=F(2,1)=0
1980 F(2,2)=Fpsi3
1990 MAT H=G*F
2000 GOTO La4end
2010 La4sub: G(1,1)=Mu2*Rhob^2+Mu4*Rhoc^2+Mu3*(Rhob+Rhoc)^2
2020 G(1,2)=G(2,1)=-Rhoc*((Rhob+Rhoc)*Mu3+(Rhoc+Rhod)*Mu4)
2030 G(2,2)=Mu3*Rhoc^2+Mu5*Rhod^2+Mu4*(Rhoc+Rhod)^2
2040 F(1,1)=Fpsi3
2050 F(1,2)=F(2,1)=0
2060 F(2,2)=Fpsi4=Fpsi4s*M
2070 MAT H=G*F
2080 La4end: Bh=H(1,1)+H(2,2)
2090 Ch=H(1,1)*H(2,2)-H(1,2)*H(2,1)
2100 Dh=SQR(Bh^2-4*Ch)
2110 Evb(1)=.5*(Bh+Dh)
2120 Evb(2)=.5*(Bh-Dh)
2130 GOTO L20
2140 ! ..........................................................................
2150 ! Five atom model.
2160 La5: G(1,1)=Mu1*Rhoa^2+Mu3*Rhob^2+Mu2*(Rhoa+Rhob)^2
2170 G(2,2)=Mu2*Rhob^2+Mu4*Rhoc^2+Mu3*(Rhob+Rhoc)^2
2180 G(3,3)=Mu3*Rhoc^2+Mu5*Rhod^2+Mu4*(Rhoc+Rhod)^2
2190 G(1,2)=G(2,1)=-Rhob*((Rhoa+Rhob)*Mu2+(Rhob+Rhoc)*Mu3)
2200 G(2,3)=G(3,2)=-Rhoc*((Rhob+Rhoc)*Mu3+(Rhoc+Rhod)*Mu4)
2210 G(1,3)=G(3,1)=Mu3*Rhob*Rhoc
2220 MAT F=ZER
2230 F(1,1)=Fpsi2=Fpsi2s*N
2240 F(2,2)=Fpsi3
2250 F(3,3)=Fpsi4=Fpsi4s*M
2260 MAT H=G*F
2270 DIM Rz(0:2)
2280 Rz(0)=H(1,1)*H(2,2)*H(3,3)+H(2,1)*H(3,2)*H(1,3)+H(3,1)*H(1,2)*H(2,3)
2290 Rz(0)=Rz(0)-H(2,2)*H(3,1)*H(1,3)-H(1,1)*H(3,2)*H(2,3)-H(3,3)*H(2,1)*H(1,2)
2300 Rz(1)=H(3,1)*H(1,3)+H(3,2)*H(2,3)+H(2,1)*H(1,2)
2310 Rz(1)=Rz(1)-H(1,1)*H(2,2)-H(1,1)*H(3,3)-H(2,2)*H(3,3)
2320 Rz(2)=H(1,1)+H(2,2)+H(3,3)
2330 CALL Cubic(Rz(*),Evb(*))
2340 ! ..........................
2350 ! Bending frequencies.
2360 L20: FOR I=1 TO Model2
2370 Frqb(I)=682.427*SQR(Evb(I))/(2*PI)
```

```
2380 NEXT I
2390 PRINT "Properties of Complex."
2400 PRINT USING Format1;V
2410 Format1: IMAGE "Potential Energy of Activation: V=",DD.3D," kcal"
2420 PRINT USING Format2;N,M
2430 Format2: IMAGE "Bond Order Parameters: N=",Z.4D,", M=",Z.4D
2440 PRINT USING Format3;Rb,Rc
2450 Format3: IMAGE "Bond Distances for Center Bonds: Rb=",Z.5D,", Rc=",Z.5D," Angstroms"
2460 PRINT USING Format4;Frho*Econv*1E16,ATN(Cc)*180/PI
2470 Format4: IMAGE "Force Const. in Rho Direction:   Frho= ",MZ.5DE," dynes/cm:"," Angle=",M
       DDZ.DD," deg"
2480 PRINT USING Format5;Fsigma*Econv*1E16,ATN(-1/Cc)*180/PI
2490 Format5: IMAGE "Force Const. in Sigma Direction: Fsigma=",Z.5DE," dynes/cm:"," Angle=",M
       DDZ.DD," deg"
2491 DIM Lqi(1:2,1:2),Lq(1:2,1:2)
2492 CALL Normod(Hr(*),Evs(*),Fr(*),Lqi(*))
2493 MAT Lq=INV(Lqi)
2494 DEF FNGg(Z)=Fr(1,1)*COS(Z)^2+2*Fr(1,2)*SIN(Z)*COS(Z)+Fr(2,2)*SIN(Z)^2
2495 Z=Lq(2,2)/Lq(1,2)
2496 Zr=ATN(Z)
2500 PRINT USING Format4a;FNGg(Zr)*Econv*1E16,Zr*180/PI
2510 Format4a: IMAGE "Force Const. in Qr n.m. direction: Fqr=",MZ.5DE," dynes/cm:"," Angle=",
       MDDZ.DD," deg"
2511 Z=Lq(2,1)/Lq(1,1)
2512 Zs=ATN(Z)
2520 PRINT USING Format4b;FNGg(Zs)*Econv*1E16,Zs*180/PI
2530 Format4b: IMAGE "Force Const. in Qs n.m. direction: Fqs=",MZ.5DE," dynes/cm:"," Angle=",
       MDDZ.DD," deg"
2531 MAT Alq=Azr*Lq
2532 ! MAT PRINT Alq;
2533 DIM Rcomplex(1:2),Zeq(1:3)
2534 Rcomplex(1)=Rb
2535 Rcomplex(2)=Rc
2536 MAT Zeq=Azr*Rcomplex
2537 ! MAT PRINT Zeq
2540 PRINT "F Matrix for Stretches in dynes/cm"
2550 PRINT USING "2X,MZ.5DE,2X";Fr(1,1)*Econv*1E16,Fr(1,2)*Econv*1E16
2560 PRINT USING "2X,MZ.5DE,2X";Fr(2,1)*Econv*1E16,Fr(2,2)*Econv*1E16
2600 PRINT "Normal Coordinate Transformations"
2610 PRINT USING Format45;Lqi(1,1),Lqi(1,2),Lq(1,1),Lq(1,2)
2620 Format45: IMAGE "   Qs= ",MZ.4D," Rb + ",MZ.4D," Rc","          Rb= ",MZ.4D," Qs +  ",MZ.
       4D," Qr"
2630 PRINT USING Format46;Lqi(2,1),Lqi(2,2),Lq(2,1),Lq(2,2)
2640 Format46: IMAGE "   Qr= ",MZ.4D," Rb + ",MZ.4D," Rc","          Rc= ",MZ.4D," Qs +  ",MZ.
       4D," Qr"
2650 PRINT "F Matrix Elements for Bends; (these equal the bending force constants)"
2660 PRINT USING Format6;Fpsi2*Econv,Fpsi3*Econv,Fpsi4*Econv
2670 Format6: IMAGE "   Fpsi2=",Z.5DE,",  Fpsi3=",Z.5DE,", Fpsi4=",Z.5DE," dyne-cm"
2680 PRINT USING Format7;-Frqs(2),Frqs(1)
2690 Format7: IMAGE "Stretching Frequencies: ",4D.DD,"i, ",4D.DD," wave nos."
```

```
2700 IF Model=3 THEN PRINT USING Format8;Frqb(1),Null,Null
2710 IF Model=4 THEN PRINT USING Format8;Frqb(1),Frqb(2),Null
2720 IF Model=5 THEN PRINT USING Format8;Frqb(1),Frqb(2),Frqb(3)
2730 Format8: IMAGE "Bending Frequencies: ",4D.DD,", ",4D.DD,", ",4D.DD," wave nos."
2740 Zcmplx=Frqs(1)
2750 FOR I=1 TO Model2
2760 Zcmplx=Zcmplx+2*Frqb(I)
2770 NEXT I
2780 Zcmplx=.5*Zcmplx*2.8585E-3
2790 PRINT USING Format9;Zcmplx
2800 Format9: IMAGE "Zero Point Energy of Complex=",3D.3D," kcal"
2810 PRINT "*************************************************************"
2820 ! *************************************************************
2830 ! The rate constants are now evaluated at the different temperatures.
2840 Unit=1
2850 ON Opt(4) GOTO Lunit1,Lunit2,Lunit3,Lunit4
2860 Lunit2: Unit=6.02E23
2870 GOTO Lunit1
2880 Lunit3: Unit=1000
2890 GOTO Lunit1
2900 Lunit4: Unit=6.02E26
2910 Lunit1: ! Continue
2920 DEF FNG(Z)=Z*EXP(-.5*Z)/(1-EXP(-Z))
2930 DIM Lograte(-1:1)
2940 Npt=0
2950 IF Opt(1)=1 THEN L61
2960 Delrt=1.987E-3*.05/V
2970 Npt=1
2980 L61: Evbs=Fbs*(Mu2+Mu3)
2990 Frqbs=682.427*SQR(Evbs)/(2*PI)
3000 Zreact=Frqbs/2
3010 Evcs=Fcs*(Mu3+Mu4)
3020 Frqcs=682.427*SQR(Evcs)/(2*PI)
3030 Zprod=Frqcs/2
3040 IF Model=3 THEN L40
3050 IF (Model=4) AND (M1<>0) THEN L46
3060 Rhocs=1/Rcs
3070 Rhods=1/Rds
3080 Evpsi4s=Fpsi4s*(Mu3*Rhocs^2+Mu5*Rhods^2+Mu4*(Rhocs+Rhods)^2)
3090 Frqpsi4s=682.427*SQR(Evpsi4s)/(2*PI)
3100 Zprod=Zprod+Frqpsi4s
3110 L46: IF (Model=4) AND (M1=0) THEN L40
3120 Rhoas=1/Ras
3130 Rhobs=1/Rbs
3140 Evpsi2s=Fpsi2s*(Mu1*Rhoas^2+Mu3*Rhobs^2+Mu2*(Rhoas+Rhobs)^2)
3150 Frqpsi2s=682.427*SQR(Evpsi2s)/(2*PI)
3160 Zreact=Zreact+Frqpsi2s
3170 IF Opt(6)=0 THEN Tunnel=0
3180 L40: IF Opt(6)=0 THEN L85
3190 Zreact=Zreact*2.8585E-3
```

```
3200 Zprod=Zprod*2.8585E-3
3210 PRINT USING Format10;Zreact
3220 Format10: IMAGE "Zero Point Energy of Reactants=",DD.3D," kcal"
3230 PRINT USING Format11;Zprod
3240 Format11: IMAGE "Zero Point Energy of Products=",3D.3D," kcal"
3250 V1=V-Zreact
3260 Tunnel=1
3270 IF V1>0 THEN L84
3280 Tunnel=0
3290 PRINT "Eckart tunneling factor not applied because zero point energy of reactants is"
3300 PRINT "greater than the barrier height."
3310 GOTO L85
3320 L84: V2=V-Ebs+Ecs-Zprod
3330 PRINT USING Format12;V1,V2
3340 Format12: IMAGE "Energy Bases for Eckart Tunneling: V1=",DD.3D,", V2=",DD.3D," kcal"
3350 PRINT USING Format13;Mrho
3360 Format13: IMAGE "Reduced Mass for Tunneling: Mrho=",DD.4D
3370 ! Johnston's tunneling factors calculated.
3380 Nu=SQR(-Evs(2)*Econv*1E16/(Mrho*Pmass))/(2*PI)
3390 A1=V1*Econv*2*PI/(H*Nu)
3398 A2=V2*Econv*2*PI/(H*Nu)
3400 IF (A1<20) AND (A2<20) THEN L300
3401 Tunnel=0
3402 PRINT "Eckart tunneling factor not calculated because A1 or A2 is greater then 20."
3403 GOTO L85
3410 L300: PRINT USING Format16;A1,A2
3420 Format16: IMAGE "Johnston's tunneling parameters: A1=",DZ.3D,", A2=",DZ.3D
     ****"
3430 L85: PRINT "**********************************************************************
3440 IF Opt(3)=0 THEN PRINTER IS 16
3450 FOR L=1 TO Ntemp
3460 PRINT USING Format20;L,Ntemp
3470 Format20: IMAGE "Calculating rate const. at ",DD,"'th temperature value out of ",DD," va
     lues."
3480 Rtemp=1/Temp(L)
3490 FOR Nt=-Npt TO Npt
3500 Rt=Rtemp+Nt*Delrt
3510 T=1/Rt
3520 Tpktkcalsub=Tpfac*T
3530 Ktkcalsub=Tpktkcalsub/(2*PI)
3540 Kfac=EXP(-V/Ktkcalsub)*Sym*Jfac*C*Frqs(2)*SQR(Fbs)/(Dfr*Unit)
3550 Tf=1.439/T
3560 ON Model2 GOTO Lb3,Lb4,Lb5
3570 Lb3: Kcl=Kfac*Tpktkcalsub^1.5/Fpsi3
3580 G3=FNG(Tf*Frqs(1))*FNG(Tf*Frqb(1))^2/FNG(Tf*Frqbs)
3590 Kg=G3*Kcl
3600 GOTO L30
3610 Lb4: IF M1=0 THEN Lb4sub
3620 Kcl=Kfac*Tpktkcalsub^1.5*Fpsi2s/(Fpsi2*Fpsi3)
3630 G4a=FNG(Tf*Frqs(1))*(FNG(Tf*Frqb(1))*FNG(Tf*Frqb(2)))^2
```

```
3640 G4a=G4a/(FNG(Tf*Frqbs)*FNG(Tf*Frqpsi2s)^2)
3650 Kq=G4a*Kcl
3660 GOTO L30
3670 Lb4sub: Kcl=Kfac*Tpktkcalsub^2.5/(4*PI*Fpsi3*Fpsi4)
3680 G4b=FNG(Tf*Frqs(1))*(FNG(Tf*Frqb(1))*FNG(Tf*Frqb(2)))^2
3690 G4b=G4b/FNG(Tf*Frqbs)
3700 Kq=G4b*Kcl
3710 GOTO L30
3720 Lb5: Kcl=Kfac*Tpktkcalsub^2.5*Fpsi2s/(4*PI*Fpsi2*Fpsi3*Fpsi4)
3730 G5=FNG(Tf*Frqs(1))*(FNG(Tf*Frqb(1))*FNG(Tf*Frqb(2))*FNG(Tf*Frqb(3)))^2
3740 G5=G5/(FNG(Tf*Frqbs)*FNG(Tf*Frqpsi2s)^2)
3750 Kq=G5*Kcl
3760 L30: Gam=1
3770 IF Tunnel=0 THEN L87
3781 CALL Tunl(V1*Econv,V2*Econv,Frho*Econv*1E16,Mrho*Pmass,T,Gam)
3790 L87: Kcl=6.025E23*1E-24*Kcl
3800 Kq=6.025E23*1E-24*Kq*Gam
3810 IF Nt=0 THEN Kqtab=Kq
3820 IF Nt=0 THEN Gamtab=Gam
3830 Lograte(Nt)=LOG(Kq)
3840 NEXT Nt
3850 IF Npt=0 THEN L59
3860 Eactpr(L)=-1.987E-3*(-Lograte(-1)+Lograte(1))/(2*Delrt)
3870 IF Opt(2)=1 THEN Lapr(L)=LOG(Kqtab*EXP(Eactpr(L)/Ktkcal(L)))
3880 IF Opt(2)=2 THEN Lapr(L)=LGT(Kqtab*EXP(Eactpr(L)/Ktkcal(L)))
3890 L59: Kqpr(L)=Kqtab
3900 IF Opt(2)=1 THEN Lkqpr(L)=Lograte(0)
3910 IF Opt(2)=2 THEN Lkqpr(L)=LGT(Kqtab)
3920 Ustr(L)=Nu*H/(K*Temp(L))
3930 Gampr(L)=Gamtab
3940 NEXT L
3950 IF Opt(3)=0 THEN PRINTER IS 0
3960 IF Npt=1 THEN L60
3970 DIM D0(1:5),D1(1:5),Di(1:5)
3980 D0(1)=-2.08333333333
3990 D0(2)=4
4000 D0(3)=-3
4010 D0(4)=1.33333333333
4020 D0(5)=-.25
4030 D1(1)=-.25
4040 D1(2)=-.833333333333
4050 D1(3)=1.5
4060 D1(4)=-.5
4070 D1(5)=8.33333333333E-2
4080 Di(1)=8.33333333333E-2
4090 Di(2)=-.666666666667
4100 Di(3)=0
4110 Di(4)=.666666666667
4120 Di(5)=-8.33333333333E-2
4130 MAT Eactpr=ZER
```

```
4140 FOR J=1 TO 5
4150 Eactpr(1)=Eactpr(1)+D0(J)*Lkqpr(J)
4160 Eactpr(2)=Eactpr(2)+D1(J)*Lkqpr(J)
4170 Eactpr(Ntemp-1)=Eactpr(Ntemp-1)-D1(J)*Lkqpr(Ntemp-J+1)
4180 Eactpr(Ntemp)=Eactpr(Ntemp)-D0(J)*Lkqpr(Ntemp-J+1)
4190 FOR Na=3 TO Ntemp-2
4200 Eactpr(Na)=Eactpr(Na)+Di(J)*Lkqpr(Na+J-3)
4210 NEXT Na
4220 NEXT J
4230 IF Opt(2)=1 THEN MAT Eactpr=Eactpr*(-1.987E-3/Delrt)
4240 IF Opt(2)=2 THEN MAT Eactpr=Eactpr*(-1.987E-3*LOG(10)/Delrt)
4250 L60: FOR L=1 TO Ntemp
4260 Afac=Kqpr(L)*EXP(Eactpr(L)/Ktkcal(L))
4270 IF Opt(2)=1 THEN Lapr(L)=LOG(Afac)
4280 IF Opt(2)=2 THEN Lapr(L)=LGT(Afac)
4290 NEXT L
4300 IF (Opt(3)=0) AND (Ntemp>1) THEN PRINT PAGE
4301 IF Ntemp>1 THEN CALL Fit(Opt(2),Ntemp,Temp(*),Lkqpr(*),Error(*),Par(*),Variance,Opt(7))
4310 PRINT "*****************************************************************************"
4320 PRINT "Temp., Rate Const., A factor, Act. Energy, Eckart U* Factor, Deviation from Fit"
4330 IF Opt(2)=1 THEN PRINT "1000/T   T        K        Ln(K)   Ln(A)   Eact     Gam      U*
       Fit"
4340 IF Opt(2)=2 THEN PRINT "1000/T   T        K       Log(K)  Log(A)   Eact     Gam      U*
       Fit"
4350 FOR L=1 TO Ntemp
4360 PRINT USING Format14;1000/Temp(L),Temp(L),Kqpr(L),Lkqpr(L),Lapr(L),Eactpr(L),Gampr(L),Us
       tr(L),Error(L)
4370 NEXT L
4380 Format14: IMAGE 1X,Z.DD,2X,4D,2X,Z.3DE,6(1X,MDZ.3D)
4390 PRINT "*****************************************************************************"
4400 IF Ntemp=1 THEN L63
4401 IF Opt(3)=1 THEN PAUSE
4410 CALL Pltk(Opt(*),Ntemp,Temp(*),Lkqpr(*),Error(*))
4411 IF Opt(3)=1 THEN PAUSE
4420 IF Opt(3)=0 THEN DUMP GRAPHICS
4430 EXIT GRAPHICS
4440 PRINT "Figure 1.  Plot of logarithm of rate constant as a function of the reciprocal of"
4441 PRINT "the temperature."
4442 PRINT "A least squares fit of the calculated rate constant to the Arrhenius expression,"
4443 IF Opt(7)=2 THEN PRINT "k=A*EXP(-Earr/RT), yields the following values for the parameter
       s:"
4444 IF Opt(7)=3 THEN PRINT "k=A*(T^n)*EXP(-Earr/RT), yields the following values for the par
       ameters:"
4445 IF (Opt(7)=2) AND (Opt(2)=1) THEN PRINT USING Arrhenius1a;Par(1),Par(3)/1000
4446 IF (Opt(7)=2) AND (Opt(2)=2) THEN PRINT USING Arrhenius2a;Par(1),Par(3)/1000
4448 Arrhenius1a: IMAGE "  Ln(A)=",MZ.3DE,",   Earr=",MDZ.3D
4449 Arrhenius2a: IMAGE "  LOG(A)=",MZ.3DE,",   Earr=",MDZ.3D
4453 IF (Opt(7)=3) AND (Opt(2)=1) THEN PRINT USING Arrhenius1b;Par(1),Par(2),Par(3)/1000
4454 IF (Opt(7)=3) AND (Opt(2)=2) THEN PRINT USING Arrhenius2b;Par(1),Par(2),Par(3)/1000
4457 Arrhenius1b: IMAGE "  Ln(A)=",MZ.3DE,",   n=",MZ.3D,",   Earr=",MDZ.3D
4458 Arrhenius2b: IMAGE "  Log(A)=",MZ.3DE,",   n=",MZ.3D,",   Earr=",MDZ.3D
4460 L63: PRINTER IS 16
4470 IF Opt(5)=0 THEN L82
4480 ! Position of normal coordinate plot.
4490 L82: PRINTER IS 16
4500 SERIAL
4510 END
```

```
5000 ! Run Identification
5010 DATA CH3CH2-H + CH3 = CH3CH2 + H-CH3
5020 ! Options:
5021 !     0,1,2,3,4,5,6,7
5030 DATA 1,1,2,1,3,0,1,3
5040 ! Number of temperature values.
5050 DATA 10
5060 ! Minimum and maximum temperatures, (or a single temperature if Ntemp=1).
5070 DATA 333.3333333,2000
5080 ! Masses: M1, M2, M3, M4, M5
5090 DATA 17.051,12.011,1.008,12.011,3.024
5100 ! Single bond distances: Ra, Rb, Rc, Rd
5110 DATA 1.526,1.09,1.09,1.09
5120 ! Bond energies: Ebs and Ecs;  BEBO parameters: p and q
5130 DATA 105.1,111.1,1.0852,1.0925
5140 ! Triplet single bond distance, bond energy, and Morse parameter:
5150 ! Rts, Ets, and Beta
5160 DATA 1.54,84.4,1.425
5170 ! Stretching constants Fbs, Fcs and bending constants Fpsi2s, Fpsi4s
5180 DATA 4.79E5,4.79E5,9.14837E-12,5.4653E-12
5190 ! Partition function symmetries for species A, B, and C
5200 DATA 1,1,1
5210 ! Chemical multiplicity
5220 DATA 6
5230 ! Electronic degeneracies for species A, B, and C
5240 DATA 1,2,2
```

```
5400 SUB Trpl(Rbs,Rcs,Rts,Ets,Beta,Lam,N,Vt,Vtn,Vtnn,Vtr,Vtrr,Version)
5402 ! Version=0; Simplified, modified Sato function.
5404 ! Version=1; Modified Sato function.
5406 ! Version=2; Arthur et.al., function (2 parameter form).
5410 Delrs=Rbs+Rcs-Rts
5412 IF Version=2 THEN Delrs=Delrs+Rts
5414 M=1-N
5416 R=Delrs-Lam*LOG(N*M)
5418 Rn=Lam*(1/M-1/N)
5420 Rnn=Lam*(1/N^2+1/M^2)
5422 IF (Version=1) OR (Version=0) THEN L10
5426 P1=5.873
5428 P2=1.747
5430 P3=1.525
5440 D=Ets*P1*Beta^P3
5442 E=EXP(-P2*Beta*R)
5444 Er=-P2*Beta*E
5446 En=Er*Rn
5448 Enn=-P2*Beta*(Rnn*E+Rn*En)
5450 Err=-P2*Beta*Er
5452 Rp3=R^P3
5454 Vt=D*E*Rp3
5456 Vtn=D*Rp3*(En+E*P3*Rn/R)
5458 Vtnn=D*Rp3*(Enn+P3*((2*En+E*(P3-1)*Rn/R)*Rn+E*Rnn)/R)
5460 Vtr=D*Rp3*(Er+P3*E/R)
5462 Vtrr=D*Rp3*(Err+2*P3*Er/R+P3*(P3-1)*E/R^2)
5464 SUBEXIT
5466 L10: E=.5*EXP(-Beta*R)
5468 Er=-Beta*E
5470 En=Er*Rn
5472 Enn=-Beta*(Rnn*E+Rn*En)
5474 Err=-Beta*Er
5476 IF Version=0 THEN L15
5478 Vt=Ets*E*(1+E)
5480 Efac=1+2*E
5482 Vtn=Ets*En*Efac
5484 Vtr=Ets*Er*Efac
5486 Vtnn=Ets*(Enn*Efac+2*En^2)
5488 Vtrr=Ets*(Err*Efac+2*Er^2)
5490 SUBEXIT
5492 L15: Vt=Ets*E
5494 Vtn=Ets*En
5496 Vtnn=Ets*Enn
5498 Vtr=Ets*Er
5500 Vtrr=Ets*Err
5502 SUBEND
```

```
5600 SUB Cubic(Cf(*),Rt(*))
5602 R=-Cf(0)
5604 Q=-Cf(1)
5606 P=-Cf(2)
5608 A=(3*Q-P^2)/3
5610 B=(2*P^3-9*P*Q+27*R)/27
5612 Fc1=A^3/27
5614 Fc=B^2/4+Fc1
5616 IF Fc<0 THEN L89
5618 PRINT "Error-005"
5620 STOP
5622 L89: Psi=-B/(2*SQR(-Fc1))
5624 DEG
5626 Psi=ACS(Psi)/3
5628 Fc=2*SQR(-A/3)
5630 Rt(1)=Fc*COS(Psi)-P/3
5632 Rt(2)=Fc*COS(Psi+120)-P/3
5634 Rt(3)=Fc*COS(Psi+240)-P/3
5636 RAD
5638 SUBEND
5700 SUB Normod(H(*),Ev(*),F(*),Li(*))
5710 DIM G(1:2,1:2),Gt(1:2,1:2),Fg(1:2,1:2),Gfg(1:2,1:2),L(1:2,1:2)
5720 FOR I=1 TO 2
5730 G(1,I)=-H(1,2)/(H(1,1)-Ev(I))
5740 G(2,I)=1
5750 NEXT I
5760 MAT Fg=F*G
5770 MAT Gt=TRN(G)
5780 MAT Gfg=Gt*Fg
5790 FOR I=1 TO 2
5800 L(2,I)=SQR(Ev(I)/Gfg(I,I))
5810 L(1,I)=G(1,I)*L(2,I)
5820 NEXT I
5830 MAT Li=INV(L)
5840 SUBEND
```

```
6000 SUB Tunl(V1,V2,F,M,T,Gam)     ! 6 point Gaussian Lengendre
6005 OPTION BASE 1
6010 DIM X(6),W(6)
6015 DATA .238619186083,.661209386466,.932469514203
6020 FOR N=4 TO 6
6025 READ X(N)
6030 X(7-N)=-X(N)
6035 NEXT N
6040 DATA .467913934573,.360761573048,.171324492379
6045 FOR N=4 TO 6
6050 READ W(N)
6055 W(7-N)=W(N)
6060 NEXT N
6065 H=6.6234E-27
6070 K=1.38033E-16
6075 Kt=K*T
6080 A=V1-V2
6085 V1h=SQR(V1)
6090 V2h=SQR(V2)
6095 B=(V1h+V2h)^2
6100 Pi2=2*PI
6105 L=Pi2*SQR(-2/F)/(1/V1h+1/V2h)
6110 C=H^2/(8*M*L^2)
6115 DEF FNCosh(Z)=.5*(EXP(Z)+EXP(-Z))
6120 Delta=(B-C)/C
6125 IF Delta<0 THEN L10
6130 Dfac=FNCosh(PI*SQR(Delta))
6135 GOTO L11
6140 L10: Dfac=COS(PI*SQR(-Delta))
6145 L11: IF V2>=V1 THEN E0=-V1/Kt
6150 IF V1>V2 THEN E0=-V2/Kt
6155 Vav=.5*(V1+V2)
6160 Eb1=(C*(LOG(2*(1+Dfac)/.014)/Pi2)^2-Vav)/Kt
6165 Eb2=3.2
6170 Eb=MIN(Eb1,Eb2)
6175 Em=.5*(Eb-E0)
6180 Ep=.5*(Eb+E0)
6185 Gam=0
6190 FOR N=1 TO 6
6195 E=Em*X(N)+Ep
6200 Kte=Kt*E
6205 Alph1=PI*SQR((Kte+V1)/C)
6210 Alph2=PI*SQR((Kte+V2)/C)
6215 Facp=FNCosh(Alph1+Alph2)
6220 Facm=FNCosh(Alph1-Alph2)
6225 Ke=(Facp-Facm)/(Facp+Dfac)
6230 Y=Ke*EXP(-E)
6235 Gam=Gam+W(N)*Y
6240 NEXT N
6245 L50: Gamfac=EXP(-Eb)
6250 Gam=Em*Gam+Gamfac
6255 SUBEND
```

```
6500 SUB Pltk(Opt(*),Nm,T(*),Lk(*),E(*))
6502 DEG
6504 PLOTTER IS 13,"GRAPHICS"
6506 GRAPHICS
6508 LOCATE 19,119,18,95
6510 DIM Xtics(1:11),Ytics(1:11)
6512 DATA .01,.02,.025,.05,.1,.2,.25,.5,1,2,2.5
6514 MAT READ Xtics
6516 Xmin=1000/T(1)
6518 Xmax=1000/T(Nm)
6520 Xspan=Xmax-Xmin
6522 FOR I=1 TO 11
6524 Itab=I
6526 IF INT(Xspan/Xtics(I))<=6 THEN L30
6528 NEXT I
6530 L30: Xtic=Xtics(Itab)
6532 Xstart=INT(Xmin/Xtic)*Xtic
6534 Xstop=INT(Xmax/Xtic)*Xtic
6535 IF (Xstop>Xmax) AND (Xstop-Xmax>1E-2*Xtic) THEN Xstop=(INT(Xmax/Xtic)+1)*Xtic
6536 Ymin=Ymax=Lk(1)
6538 FOR N=2 TO Nm
6540 IF Ymin>Lk(N) THEN Ymin=Lk(N)
6542 IF Ymax<Lk(N) THEN Ymax=Lk(N)
6544 NEXT N
6546 Yspan=Ymax-Ymin
6548 MAT Ytics=Xtics
6550 FOR I=1 TO 11
6552 Itab=I
6554 IF INT(Yspan/Ytics(I))<=6 THEN L40
6556 NEXT I
6558 L40: Ytic=Ytics(Itab)
6560 Ystart=INT(Ymin/Ytic)*Ytic
6562 Ystop=(INT(Ymax/Ytic)+1)*Ytic
6564 SCALE Xstart,Xstop,Ystart,Ystop
6566 LINE TYPE 3
6568 GRID Xtic,Ytic,Xstart,Ystart
6570 LINE TYPE 1
6572 AXES Xtic,Ytic,Xstart,Ystart,2,2,6
6574 FRAME
6576 CSIZE 3
6578 LORG 8
6580 FOR Ypos=Ystart TO Ystop STEP Ytic
6582 MOVE Xstart,Ypos
6584 LABEL USING "MDD.DDX";Ypos
6586 NEXT Ypos
6588 LORG 6
6590 FOR Xpos=Xstart+Xtic TO Xstop STEP Xtic
6592 MOVE Xpos,Ystart-Ytic/10
6594 LABEL USING "Z.DD";Xpos
6596 NEXT Xpos
```

```
6598 LDIR 90
6600 CSIZE 4.5
6602 LORG 1
6604 ON Opt(2) GOTO L1,L2
6606 L1: ON Opt(4) GOTO La1,La2,La3,La4
6608 La1: MOVE Xstart-Xspan*.15,Ystart+Yspan*.27
6610 LABEL USING "K";"Ln(k)  cc/mole-s"
6612 GOTO Lout
6614 La2: MOVE Xstart-Xspan*.15,Ystart+Yspan*.18
6616 LABEL USING "K";"Ln(k)  cc/molecule-s"
6618 GOTO Lout
6620 La3: MOVE Xstart-Xspan*.15,Ystart+Yspan*.18
6622 LABEL USING "K";"Ln(k)  liters/mole-s"
6624 GOTO Lout
6626 La4: MOVE Xstart-Xspan*.15,Ystart+Yspan*.12
6628 LABEL USING "K";"Ln(k)  liters/molecule-s"
6630 GOTO Lout
6632 L2: ON Opt(4) GOTO Lb1,Lb2,Lb3,Lb4
6634 Lb1: MOVE Xstart-Xspan*.15,Ystart+Yspan*.25
6636 LABEL USING "K";"Log(k)  cc/mole-s"
6638 GOTO Lout
6640 Lb2: MOVE Xstart-Xspan*.15,Ystart+Yspan*.16
6642 LABEL USING "K";"Log(k)  cc/molecule-s"
6644 GOTO Lout
6646 Lb3: MOVE Xstart-Xspan*.15,Ystart+Yspan*.16
6648 LABEL USING "K";"Log(k)  liters/mole-s"
6650 GOTO Lout
6652 Lb4: MOVE Xstart-Xspan*.15,Ystart+Yspan*.08
6654 LABEL USING "K";"Log(k)  liters/molecule-s"
6656 Lout: LDIR 0
6658 MOVE Xstart+.43*Xspan,Ystart-Yspan*.12
6660 LABEL USING "K";"1000/T"
6662 MOVE T(1),Lk(1)
6664 FOR N=1 TO Nm
6666 PLOT 1000/T(N),Lk(N)
6668 NEXT N
6669 LINE TYPE 3
6670 MOVE 1000/T(1),Lk(1)-E(1)
6674 FOR N=1 TO Nm
6676 PLOT 1000/T(N),Lk(N)-E(N)
6680 NEXT N
6682 RAD
6684 SUBEND
```

```
   6800 SUB Fit(Opt2,N,T(*),Xob(*),E(*),P(*),E2,Opt7)
   6801 OPTION BASE 1
   6810 DIM A(N,3),At(3,N),Ata(3,3),Atai(3,3),Atx(3),X(N)
   6820 FOR I=1 TO N
   6830 A(I,1)=1
   6831 A(I,2)=0
   6850 IF Opt2=2 THEN L10
   6860 IF Opt7=3 THEN A(I,2)=LOG(T(I))
   6870 A(I,3)=-1/(1.987*T(I))
   6880 GOTO L11
   6890 L10:  IF Opt7=3 THEN A(I,2)=LGT(T(I))
   6900 A(I,3)=-.43429/(1.987*T(I))
   6910 L11: NEXT I
   6920 MAT At=TRN(A)
   6930 MAT Ata=At*A
   6940 MAT Atai=INV(Ata)
   6950 MAT Atx=At*Xob
   6960 MAT P=Atai*Atx
   6970 MAT X=A*P
   6980 MAT E=Xob-X
   6990 E2=DOT(E,E)
   7000 SUBEND
EOF
/
```

JOURNAL OF RESEARCH of the National Bureau of Standards
Vol. 86, No. 6, November-December 1981

Enthalpy of Combustion of Microcrystalline Cellulose

J.C. Colbert*, He Xiheng†, and D.R. Kirklin*

National Bureau of Standards, Washington, DC
20234

August 14, 1981

A test substance with characteristics and properties similar to those of cellulose-based solid waste products is needed to calibrate calorimeters and combustors which will be routinely burning these materials to determine their calorific values precisely for use in commerce. Microcrystalline cellulose was found to be a good calibrant for this purpose. The enthalpy of combustion of microcrystalline cellulose ΔH_c° at (25 °C), and its estimated uncertainty, was determined to be −2812.401±1.725 kJ/mol based upon the sample mass.

A calculated heat of wetting correction of 1.514 kJ/mol was applied to the combustion data.

Keywords: alternative fuel, bomb calorimetry, cellulose, enthalpy of combustion, refuse-derived-fuel, test substance.

1. Introduction

The enthalpies of combustion of heterogeneous feedstocks such as refuse-derived-fuel (RDF) and wood wastes, are important thermochemical data because of the potential application of these materials in commerce as supplemental or alternative fuels. When determining the enthalpy of combustion of RDF in a conventional bomb calorimeter or a newly designed multi-kilogram flow calorimeter, it is desirable to have a "test substance"[1][1] which can be used for their calibration which is as close to RDF in character as possible. This test substance will permit the intercomparison of the thermochemical results of different investigators in the new field of fuels from cellulose-based solid wastes and will essentially serve to control the chemical part of the investigation. Since there is a large fraction of cellulosic materials (i.e., paper products) in municipal solid waste (MSW), we decided to investigate the possibility of using a pure cellulose as a test substance. Cellulose not only has a close compositional relationship to the major components of MSW, but also possesses a similar kinship to wood species, wood wastes from the manufacture of paper, bagasse from the sugar refining industry, agricultural wastes, and some forms of peat. These materials have a potential as supplemental or alternative fuels just like RDF.

A search was carried out to find a suitable cellulosic test substance. We needed a cellulose which was high in purity, homogeneous, inexpensive, easy to pelletize, and one which could be obtained in large quantities. Avicel,[2] a readily available commercial cellulose, was chosen because it possesses most of the requirements for use as a calibrant in a bomb calorimeter. This cellulose is very homogeneous, 99.81 percent pure, and presses into a pellet very easily.

Calibration of the oxygen bomb calorimeter was performed using SRM benzoic acid, standard sample, 39i, which is the accepted primary standard substance for calibrating bomb calorimeters. Comparative calorimetric measurements were conducted on the cellulose sample. These measurements for benzoic acid and cellulose, along with the heat of wetting correction for cellulose, are presented in this paper.

2. Experimental

2.1 Sample Characterization

Avicel, pH-101, lot 1018-152, is a microcrystalline cellulose, which is an acid hydrolyzed derivative of a dissolving grade of wood pulp. It has an average particle size of 50 micrometers and a pH of 5.5 to 7.

The sample was not subjected to any further purification but these additional analyses were made to further

†Guest worker from July 1980-February 1981, Chemistry Laboratory, National Institute of Metrology, P.O. Box 2112, Peking, People's Republic of China.

*Center for Chemical Physics, Chemical Thermodynamics Division

[1]Numbers in brackets indicate literature references at the end of this paper.

[2]The commercial sources cited in this paper are included to adequately describe the experimental procedure. Such identification does not imply recommendation or endorsement by the National Bureau of Standards.

characterize the cellulose. The percent moisture of seven cellulose samples was 4.910 ± 0.060 (sd.) at a relative humidity of 36 percent, as determined by drying in a 105 °C oven until a constant weight was reached.

The water soluble impurities of fluoride, chloride, nitrate, and sulfate were analyzed for by the method of ion-chromatography.[3] Two cellulose samples of different masses, 0.51 g and 1.62 g were diluted in a solution containing the buffer: 0.003M $NaHCO_3$/0.0018M Na_2CO_3. The diluted sample was mixed, allowed to settle, and filtered through a 0.2 micrometer syringe filter. The average concentration of water soluble impurities for the two samples was 62.46 ppm. This level of anions is negligible when looking at the overall sample purity.

The amount of ash was found to be negligible when determined according to the American Society for Testing and Materials (ASTM) Standard Test Method D-3174-73 for Coal and Coke. The samples were fired for two hours in a furnace operating at 575-600 °C.

The purity of the Avicel was determined in duplicate CO_2 analyses of the bomb combustion products. The gaseous products of combustion were released from the bomb and passed through absorption tubes containing Ascarite and magenesium perchlorate for removal of CO_2 and H_20, respectively, and phosphorus pentoxide [2] to prevent the back-flow of moist room air into the absorption system. The amount of CO_2 was then determined gravimetrically. The purity of the cellulose was found to be 99.809 ± 0.103 (sd.) percent.

2.2. Description of Calorimeter

The combustion measurements were made in an isoperibol oxygen bomb calorimeter. This is an isothermal-jacket calorimeter with the calorimeter reaction vessel submerged in a water bath at 301 K and controlled to ±0.003K. This prevents any thermal leakage between the laboratory environment and calorimeter. The heat generated when a measured amount of sample is burned is compared to the heat evolved when a measured amount of standard substance is burned in the same calorimetric system. Benzoic acid, the primary calibrant, is burned and produces a three degree temperature rise in the calorimeter. The energy equivalent of the calorimeter is determined from the amount of energy produced by the benzoic acid and divided by the temperature rise. The temperature rise is corrected for the stirring energy produced in the stirred water of the calorimeter vessel and any thermal leakage between the environment and calorimeter.

In a cellulose experiment, the corrected temperature rise is multiplied by the energy equivalent of the calorimeter. This calulation gives the total energy produced in a cellulose combustion experiment. This total energy is finally corrected for any side reactions, or thermal corrections, and is divided by the mass of the cellulose sample to produce the internal energy of combustion at constant volume, ΔU_c°. Conversion to the enthalpy of combustion at constant pressure, ΔH_c°, carried out by applying a correction term for pressure-volume expansion (ΔnRT). The ΔnRT term for this reaction is 0, therefore $\Delta U_c^\circ = \Delta H_c^\circ$.

All of the cellulose samples for combustion are pressed into pellets under an approximate force of 44.4 kN. A sample weight of 2.3 g was pre-determined in a trail experiment as the necessary amount of sample required to produce a three degree temperature rise.

2.3 Sample Preparation

A dried sample weight is necessary for the combustion experiments. Since cellulose is very hygroscopic, this was very difficult. The samples were placed into pre-weighed ground glass neck weighing bottles, dried at 105 °C until a constant weight of ± 0.3 mg was obtained, and stored in a desiccator over P_2O_5 until ready for testing.

2.4 Example of Calorimetric Procedure

A dried pellet was transferred from the weighing bottle to a preweighed platinum crucible. The empty weighing bottle was again weighed to account for any cellulose remaining in the bottle. The platinum crucible with pellet was placed on the crucible support of the bomb head. The fuse leads had been previously connected with a 2 cm length of 0.075 mm platinum wire which is placed in contact with the top of the pellet. Normally, 1 ml of water is added to the bottom of the bomb to provide a saturated atmosphere and ensure that water formed as a combustion product is present in the liquid state. For this series of cellulose combustions, 0.2 ml of water was added directly to the pellet in the crucible and 0.8 ml added to the bottom of the bomb. The sample was wetted before burning because it was found in the previous study by Jessup and Prosen [3][4] that a more complete combustion results with a wetted sample rather than a dry one.

The sealed bomb is charged with 3.10 MPa (30.62 atm) of high purity oxygen and placed on the bench for approximately 1 hour for the sample to equilibrate with the moist environment inside the bomb. The calorimeter vessel is filled with a known amount of water, the bomb is lowered into the vessel, and the covered calorimeter is submerged in the constant temperature water bath. The rate of tempera-

[3]The analyses were performed by the Inorganic Analytical Research Division of the National Bureau of Standards.

[4] In a private consultation with E.J. Prosen, who had done a similar study in 1950, we were advised to wet the cellulose sample before placing it in the bomb.

ture rise is measured during the period before the sample is ignited, during the reaction period immediately after the sample is ignited, (main reaction period), and during the period after the reaction is completed. The difference between the temperature at which the final drift rate begins, and the temperature at which the sample is ignited, gives the observed temperature rise. The slope of the fore- and after-periods allows one to calculate that portion of the temperature rise due to stirring energy and thermal leakage [4].

3. Results and Discussion

3.1 Correction for Heat of Wetting of Cellulose

Since the samples were wet when they were ignited in the bomb, the heat produced in the combustion reaction is lower than for a dry sample. This amount of heat is equal to the heat of wetting and has to be corrected for in the calculation for the enthalpy of combustion. These heat of wetting determinations were not experimentally performed in the laboratory because of time constraints, and after searching the literature, it was felt an adequate amount of data already existed so that a calculated correction could be made.

The literature search extended back to 1948 or to about the time period when Jessup and Prosen's calorimetric work on cellulose was carried out at NBS [3]. Table I gives a summary of the heat of wetting data on cellulose in the literature. Rees' result of 46.02 [12] was in the same range as the other data listed, but his heat of wetting data also included the actual data points at different moisture contents of the sample. It was also presented in such a way as to easily select which sample was the closest counterpart to our Avicel sample.

TABLE I. *Published Data on ΔH Wetting of Cellulose*

Researcher	Type of cellulose	T °C	ΔH wet. cal/g(J/g)
Jessup, et al, 1950[3]	wood pulp	30	14.1 (58.95)
Jessup, et al. 1950[3]	cotton linters	30	11.2 (46.80)
Wahba, et al, 1952[5]	standard cellulose	20	11.0 (46.02)
Wahba, 1948[6]	raw cotton	30	12.2 (51.04)
Wahba, 1950[7]	standard cellulose	30	10.72 (44.85)
Wahba, 1959[8]	stabilized cellulose[a]	30	10.52 (44.02)
Wahba, 1959[8]	unstabilized cellulose	29.8	10.70 (44.77)
Wahba, 1975[9]	stabilized cellulose	15	11.48 (48.03)
Argue, et al, 1935[10]	standard cellulose[b]	—	10.16 (42.51)
Morrison, et al, 1959[11]	cotton cellulose[c]	—	12.33 (51.59)
Rees 1948[12]	American cotton	25	11.0 (46.02)

[a] Cellulose treated by repeated wetting and drying.
[b] Heated samples in air at 100 °C.
[c] Dried at room temperature.

Using his data for cotton we were able to fit it to a least squares program and generate a polynomial expression for the data. Using that curve we selected hypothetical moisture contents for the cellulose sample that gave a calculated heat of wetting that reached a minimum value. The equation which was generated is given below:

$$Y = 10.8719 - 2.16135X + 0.13516X^2$$

where Y is the resulting calculated heat of wetting correction, 2.23134 cal/g (9.33592 J/g), and where X is the mass fraction of the moisture present in the cellulose sample before absorption begins. The value for the heat of wetting of cellulose was multiplied by the mass of cellulose burned in each experiment and the resulting numbers used as the correction for each heat of combustion measurement.

3.2 Bomb Calorimetric Measurements

Standard Reference Material, benzoic acid (SRM 39i), was used as the calibrant for the calibration experiments and has an energy of combustion of 26 434 ± 3 J/g at 25°C and standard bomb conditions. The average energy equivalent of the calorimeter (Esi) was determined from nine benzoic acid combustions and was found to be 14 347.75 ± 0.82 J/K (sdm) at 301 K. Table II contains the detailed presentation of the nine calibration experiments, numbered from 1000–1013. The headings, in the order in which they appear in the table, are defined as follows:

Expt. No., the number of the experiment, which can easily be traced back to our records.

ΔU_c° *(28* °C), the internal energy evolved by the combustion of benzoic acid at the selected final temperature in J/g.

m-BA(vac), the mass of the benzoic acid sample, in g, reduced to mass in vacuum.

q-BA, the energy evolved by the combustion of benzoic acid, in J.

q-ign, the electrical energy added to the system to ignite the sample, in J.

q-HNO_3, the energy evolved by the formation of nitric acid in the combustion process, in J. (usually due to nitrogen impurities in the oxygen).

q-WC, The Washburn Correction [13, 14, 15] applied to correct the combustion data from bomb conditions to conditions in which the reactants and products are in their pure standard states at one atmosphere pressure, in J.

Q-total, the total energy delivered to the calorimeter after corrections for ignition energy, formation of nitric acid, and Washburn correction, in J.

ΔT*-corr,* the observed temperature rise of the calorimeter corrected for stirring energy and thermal leakage, in K.

E-cal, the energy equivalent of the actual calorimeter system at the final temperature, (28 °C) in J/K.

TABLE II. *Benzoic Acid Calibration Results.*

Expt. No.	ΔU_c°(28 °C) J/g	m-BA(vac) g	*q*-BA J	*q*-ign J	*q*-HNO_3 J	*q*-WC J	*Q*-total J	ΔT-corr K	E-cal J/K	Ei-cont J/K	E,si-empty J/K
1000	−26410.68	1.636294	−43215.64	1.16	6.24	34.646	−43257.62	3.010633	14368.28	18.92	14349.36
1001	−26410.68	1.629256	−43029.76	1.16	5.72	34.415	−43070.99	2.997890	14367.10	18.89	14348.21
1002	−26410.68	1.632134	−43105.76	1.21	5.07	34.461	−43146.44	3.002835	14368.57	18.88	14349.69
1004	−26410.68	1.630985	−43075.41	0.94	3.44	34.463	−43114.21	3.001051	14366.37	18.89	14347.48
1008	−26410.68	1.629405	−43033.69	1.16	5.66	34.503	−43074.97	2.998000	14367.90	18.93	14348.97
1010	−26410.68	1.630515	−43063.02	0.94	4.55	34.580	−43103.42	3.001390	14361.15	18.95	14342.20
1011	−26410.68	1.630601	−43065.29	0.94	2.99	34.500	−43103.98	3.000125	14367.39	18.91	14348.48
1012	−26410.68	1.630203	−43054.76	1.06	6.04	34.625	−43096.67	2.999317	14368.83	18.97	14349.86
1013	−26410.68	1.630414	−43060.33	1.16	5.33	34.567	−43101.69	3.000575	14364.48	18.95	14345.53

E,si-mean	J/K	14347.75
Std. Dev.	J/K	2.47(0.017%)
Std. Dev. Mean	J/K	0.82(0.006%)

Ei-cont, the heat capacity of the initial bomb contents, including the sample, crucible, water, and oxygen, in J/K.

E,si-empty, the energy equivalent of the empty calorimeter at 28 °C, in J/K.

E,si-mean, the mean value of the measured energy equivalent, in J/K.

Std. Dev., the standard deviation of a measurement, (sd), in J/K (and the percent standard deviation, % sd).

Std. Dev. Mean, the standard deviation of the mean, (sdm) in J/K (and the percent standard deviation of the mean, % sdm).

The combustion data for Avicel are presented in table III. These are additional headings used in the table that were not described previously and are identified as follows:

q-wetting, a correction to the overall energy due to the combustion of the wetted sample, in J. When the sample is wetted, heat is evolved. During the burning process, that amount of water used in pre-wetting the sample is dried during the combustion. Therefore, the amount of heat generated in the combustion reaction is less than would be expected due to the amount of heat required to dry the sample. The number of joules due to the combustion of the compound initially is smaller and the amount of heat due to the wetting must be put back in to produce the correct enthalpy of combustion.

q-corr to t_f, A correction applied for the deviation of the actual final temperature from the selected standard final temperature (ussually 28 °C), in J.

Q-cellulose, total energy delivered to the calorimeter after corrections for ignition energy, formation of nitric acid, sulfuric acid, heat of wetting and the like, in J.

m-cellulose, mass of the Avicel (cellulose) sample, in g, reduced to mass in vacuum.

ΔU_c° *(28 °C),* the internal energy of combustion of the cellulose sample at constant volume in J/g.

ΔnRT, the correction term needed to change ΔU_c° to ΔH_c° at a given temperature.

ΔH_c°*(28 °C),* the enthalpy of combustion of the sample in pure oxygen at the final temperature, in kJ/mole.

$\Delta C_p \Delta T$, a correction which includes the calculated change of heat capacity of the calorimeter system with temperature (25–28 °C), in kJ/mole. The following values for C_p/Jmol^{-1} at 298 K were used: α-cellulose $C_6H_{10}O_5$(c), 188.554 [16]: O_2(g), 29.355: CO_2(g), 37.112: H_2O(liq), 75.291.

ΔH_c°*(25 °C),* the enthalpy of combustion of the sample at the standard temperature, in kJ/mole.

A mean value of −17 340.76 ± 3.44 J/g (2 sdm) was obtained for the internal energy of combustion, ΔU_c°, of the Avicel sample at 28 °C, according to eq. (1).

$$C_6H_{10}O_5(c) + 6O_2(g) \rightarrow 6CO_2(g) + 5H_2O(liq) \qquad (1)$$

The formula weight of cellulose used in this study is 162.1439 g/mole.

The results of this study and the values derived from the results are summarized in table IV. The uncertainties assigned to ΔU_c° and ΔH_c° were obtained by combining (square root of the sum of the squares) 2 sdm (in %) for the calibration experiments, 2 sdm (in %) for the combustion experiments, 0.01 percent for the possible effect of organic impurities in the sample, 0.01 percent for the uncertainty in the certified value for benzoic acid and reasonable estimates of all other sources of error, 0.01 percent.

Our values are calculated at 30 °C for purposes of comparison with work that was carried out by Jessup and Prosen [3]. Their ΔU_c° (30 °C) for wood pulp is −17 385.9 ± 18.9 J/g (sdm) which is a mean of three experiments. Our results are ΔU_c°(30 °C) = −17 337.86 ± 3.44 J/g (2 sdm). Both of these values are calculated based upon the mass of sample burned. A 0.276 percent difference exists between the two

TABLE III. *Combustion Data on Cellulose*

Expt. No.		1014	1015	1016	1018	1020	1021	1023	1024	1032
E,*si*-empty	J/K	14347.75	14347.75	14347.75	14347.75	14347.75	14347.75	14347.75	14347.75	14347.75
Ei-cont	J/K	28.04	28.62	28.79	28.47	28.24	28.28	28.15	28.46	28.29
E-cal	J/K	14375.79	14376.37	14376.55	14376.23	14375.99	14376.03	14375.90	14376.22	14376.04
ΔT-corr	K	2.755973	2.894679	2.941978	2.858541	2.801024	2.811611	2.779214	2.851034	2.816332
Q-total	J	−39619.30	−41614.99	−42295.48	−41095.04	−40267.49	−40419.82	−39953.71	−40987.08	−40487.71
q-ign	J	1.16	1.16	1.49	1.22	1.49	1.18	1.24	0.92	0.84
q-HNO_3	J	−44.5308	−45.3003	−23.7486	−45.0477	−45.9112	−44.7364	−45.6938	−43.9845	−29.0646
q-wetting	J	−21.2809	−22.3577	−22.7384	−22.0796	−21.6333	−21.7140	−21.4625	−22.0711	−21.7420
q-WC	J	34.6815	36.8266	37.5677	36.2776	35.3811	35.5512	35.0807	36.2219	35.6218
q-corr to t_f	J	−2.0237	−1.4655	−1.2200	−1.5837	−1.7402	−1.8014	−1.9352	−1.6774	−1.7742
*Q*cellulose	J	−39562.23	−41555.25	−42256.64	−41036.15	−40208.08	−40361.86	−39895.09	−40929.65	−40445.70
m-cellulose	g	2.281250	2.396698	2.437510	2.366881	2.319141	2.327693	2.300729	2.360262	2.330697
ΔU_c°(28 °C)	J/g	−17352.35	−17338.66	−17355.98	−17337.65	−17337.49	−17339.86	−17340.20	−17341.15	−17353.48
$^a\Delta nRT$[a]	kJ/mol	0	0	0	0	0	0	0	0	0
ΔH_c°(28 °C)	kJ/mol	−2811.956	−2811.358	−2810.923	−2811.194	−2811.168	−2811.553	−2811.608	−2811.762	−2813.761
$\Delta C_p(\Delta T)$	kJ/mol	−0.703	−0.703	−0.703	−0.703	−0.703	−0.703	−0.703	−0.703	−0.703
ΔH_c°(25 °C)	kJ/mol	−2812.659	−2812.061	−2811.626	−2811.897	−2811.871	−2812.256	−2812.311	−2812.465	−2814.464

[a]The values of atomic weights used in this work are:
O = 15.9994, C = 12.0112, H = 1.00797

Mean, ΔH_c°(28 °C)	kJ/mol	−2811.698
Std. Dev.	kJ/mol	0.84 (.030%)
Std. Dev. Mean	kJ/mol	0.28 (.010%)

TABLE IV. *Data Summary with Estimated Uncertainty.*

ΔU_c°(28 °C)	−17 340.76 ± 10.64 J/g
ΔH_c°(28 °C)	−2 811.698 ± 1.725 kJ/mol
ΔH_c°(25 °C)	−2 812.401 ± 1.725 kJ/mol

values, but considering that Jessup and Prosen's sample was not well characterized and its purity uncertain, the values are in very good agreement. Our precision indicates that the Avicel can be burned very reproducibly.

4. Summary and Conclusions

A test substance with characteristics and properties similar to those of cellulose-based solid waste products is needed to calibrate calorimeters and combustors which will be routinely burning these materials to determine their calorific values precisely for use in commerce.

Microcrystalline cellulose is a good calibrant for this purpose because it is ashless, of high purity, homongeneous, inexpensive, and easy to pelletize. For hygroscopic cellulose materials a heat of wetting correction is neccessary. Extremely dry cellulose does not produce a complete burn in a combustion calorimeter. Our heat of wetting correction of 1.514 kJ/mol was calculated based upon previous data in the literature. The enthalpy of combustion of microcrystalline cellulose, ΔH_c° at (25 °C), and its estimated uncertainty, was determined to be −2812.401 ± 1.725 kJ/mol based upon the sample mass. Microcrystalline cellulose appears to have good potential for serving as a test substance in the combustion calorimetry of cellulose-based solid waste products.

5. References

[1] Waddington, Guy. Physicochemical Standards for Thermochemistry, chap. 13 in *Experimental Thermochemistry*, Vol. **1**. F.D. Rossini, ed. NY: Interscience Publishers, Inc.; 1956. 287-295.

[2] Prosen, Edward J.; Rossini, Frederick D. "Heats of Izomerization of the Five Hexanes." J. Res. Nat. Bur. Stand. (U.S.) **27**: 289-310; September 1941.

[3] Jessup, Ralph S.; Prosen, Edward J.; "Heats of Combustion and Formation of Cellulose and Nitrocellulose." J. Res. Nat. Bur. Stand. (U.S.) **44**: 387-393; April 1950.

[4] Coops, J.; Jessup, R.S.; van Nes, K. Calibration of Calorimeters for Reactions in a Bomb at Constant Volume, chapter 3 in *Experimental Thermochemistry*, Vol. **1**. F.D. Rossini, ed. NY: Interscience Publishers, Inc.; 1956. 27-58.

[5] Wahba, M.; Nashed, S. The effect of hysteresis on the heat of wetting of partially saturated cellulose in water and its bearing on the physical structure of cellulose. Proceedings of the Egyptain Academy of Sciences. **8**: 128-139; December 1952.

[6] Wahba, M.; Moisture relationships of cellulose. I. J. Physical & Colloidal Chem. **52**: 1197-1208; 1948.

[7] Wahba, M.; Moisture relationships of cellulose. II. J. Physical & Colloidal Chem. **54**: 1148-1160; 1950.

[8] Wahba, M.; Aziz, K.; Moisture relations of cellulose, J. Textile Institute **50**: T558-T568; 1959.

[9] Wahba, M.; Aziz, K.; Hysteresis and the heats of sorption of water on cotton cellulose below and above its second-order transition of about 25 °C. Chemica. Scripta. **7**: 233-238; 1975.

[10] Argue, G.H.; Maas, O.; Measurement of the heats of wetting of cellulose and wood pulp. Can. J. Chem. **12**: 564-574; 1935.

[11] Morrison, J.L.; Dzieciuch, M.A. The thermodynamic properties of the system cellulose-water vapor. Can. J. Chem. **37**(9): 1379–1390; September 1959.

[12] Rees, Howard W. The heat of absorption of water by cellulose. Journal of the Textile Institute, Transactions. **39**: T351–T367; November 1948.

[13] Sunner, S. and Mansson, M.; Combustion Calorimetry, *Experimental Chemical Thermodynamics*, Volume **1**, Pergamon Press; 1979.

[14] Rossini, F.D., *Experimental Thermochemistry*, Interscience Publishers, Inc., New York, N.Y. 1956.

[15] Washburn, E.W.; J. Res. Nat. Bur. Stand. (U.S.) **10**: 525; 1933.

[16] Domalski, Eugene S.; Evans, William H.; Jobe, Thomas L. Jr., Thermodynamic Data for Waste Incineration. Nat. Bur. Stand. (U.S.) NBSIR 78–1479; August 1978. 158 p.

JOURNAL OF RESEARCH of the National Bureau of Standards
Vol. 86, No. 6, November–December 1981

Automatic Computing Methods for Special Functions. Part IV. Complex Error Function, Fresnel Integrals, and Other Related Functions

Irene A. Stegun* and Ruth Zucker*

National Bureau of Standards, Washington, DC 20234

July 15, 1981

Accurate, efficient, automatic methods for computing the complex error function to any precision are detailed and implemented in an American Standard FORTRAN subroutine. A six significant figure table of erfc z, e^{z^2} erfc z, and e^{z^2} erfc$(-z)$ is included for z in polar coordinate form with the modulus of z ranging from 0 to 9. The argand diagram is given for erf z.

Key words: Argand diagram; complex error function; continued fraction; Dawson's function; FORTRAN subroutine; Fresnel integrals; key values; line broadening function; plasma dispersion function; Voigt function.

1. Introduction

In computing many of the functions of mathematical physics, for example, Fresnel integrals, Dawson's integral, Voigt function, plasma dispersion function, etc., difficulties are frequently encountered. Since these functions may be expressed in terms of the error function of complex argument, we have chosen this function for Part IV.[1] The major part of the coding of the power series, continued fraction and asymptotic expansion computations for complex arguments will carry over equally well for other functions.

As Part I was devoted to the error function of a real variable, the probability function and other related functions, Part IV will only emphasize those functions and pitfalls due to complex arguments.

While accuracy over the entire domain of definition remains our main concern, the methods employed ensure efficiency, portability and ease of programming and modification.

If one supplies approximate values for the maximum machine value, minimum machine value, the upper bound of the sine, cosine routine, and the upper bound to the acceptable relative error and gives the square root of π to the required number of significant figures, the detailed methods will work for computations ranging from very low precision to multi-precision.

The argand diagram of erf z is included as well as the implementing ANS FORTRAN program and a six significant figure table of erfc z, e^{z^2} erfc z and e^{z^2} erfc$(-z)$ for z in polar coordinate form with the modulus of z ranging from 0 to 9.

2. Mathematical properties

Relevant formulas are collected here for completeness and ease of reference. In keeping with the convention of the Handbook [1],[2] $z = x + iy$ is a complex variable.

---

*Mathematical Analysis Division, Center for Applied Mathematics.

[1] Part I. Error, Probability, and Related Functions. J. Res. Nat. Bur. Stand. (U.S.). 74(3): 211-224; 1970. Part II. The Exponential Integral $E_n(x)$. J. Res. Nat. Bur. Stand. (U.S.). 78(4): 199-216; 1974. Part III. The Sine, Cosine, Exponential Integrals, and Related Functions. J. Res. Nat. Bur. Stand. (U.S.). 80(2): 291-311; 1976.

[2] Figures in brackets indicate literature references at the end of this paper.

A. Definitions

$$\operatorname{erf} z = \frac{2}{\sqrt{\pi}} \int_0^z e^{-t^2}\, dt$$

$$\operatorname{erfc} z = \frac{2}{\sqrt{\pi}} \int_z^\infty e^{-t^2}\, dt = 1 - \operatorname{erf} z$$

(The path of integration is subject to the restriction $\arg t \to \alpha$ with $|\alpha| < \frac{\pi}{4}$ as $t \to \infty$ along the path. If Rt^2 remains bounded to the left, $\alpha = \frac{\pi}{4}$ is permissible.)

$$w(z) = e^{-z^2}\left(1 + \frac{2i}{\sqrt{\pi}} \int_0^z e^{t^2}\, dt\right) = e^{-z^2} \operatorname{erfc}(-iz) = e^{\xi^2} \operatorname{erfc} \xi \quad (\xi = -iz)$$

$$= \frac{i}{\pi} \int_{-\infty}^{\infty} \frac{e^{-t^2}\, dt}{z - t} = \frac{2iz}{\pi} \int_0^\infty \frac{e^{-t^2}\, dt}{z^2 - t^2} \quad (I\, z > 0)$$

with $F(z) = e^{-z^2} \int_0^z e^{t^2}\, dt$ (Dawson's Function)

and $Z(z) = \frac{1}{\sqrt{\pi}} \int_{-\infty}^{\infty} \frac{e^{-t^2}\, dt}{t - z}$ (Plasma Dispersion Function)

$$E(z) = C(z) + i\, S(z) = \int_0^z e^{i\pi t^2/2}\, dt = \int_0^z \cos\left(\frac{\pi t^2}{2}\right) dt + i \int_0^z \sin\left(\frac{\pi t^2}{2}\right) dt$$

$$= \frac{1+i}{2} \operatorname{erf}\left[\frac{\sqrt{\pi}}{2}(1-i)\, z\right] \qquad \text{(Fresnel Functions)}$$

$$W(x,t) = \frac{\omega}{(4\pi t)^{1/2}} \int_{-\infty}^{\infty} \frac{e^{-u^2}\, du}{u^2 + \omega^2} = \left(\frac{\pi}{4t}\right)^{1/2} e^{\omega^2} \operatorname{erfc} \omega$$

where

$$\omega = (1 - ix)/2\, t^{1/2}$$

$$= U(x,t) + i\, V(x,t) \qquad \text{(Voigt Function)}$$

$$= \frac{1}{(4\pi t)^{1/2}} \int_{-\infty}^{\infty} \frac{e^{-(x-y)^2/4t}}{1+y^2}\, dy + \frac{i}{(4\pi t)^{1/2}} \int_{-\infty}^{\infty} \frac{y e^{-(x-y)^2/4t}}{1+y^2}\, dy$$

$$\mathrm{H}(a,u) = \frac{a}{\pi} \int_{-\infty}^{\infty} \frac{e^{-t^2}\, dt}{(u-t)^2 + a^2} = \frac{1}{a\sqrt{\pi}}\, U(u/a,\ 1/4a^2) \qquad \text{(Line Broadening Function)}$$

B. Series Expansions

$$\operatorname{erf} z = \frac{2}{\sqrt{\pi}} \sum_{n=0}^{\infty} \frac{(-1)^n z^{2n+1}}{n!\,(2n+1)}$$

$$= \frac{2}{\sqrt{\pi}}\, e^{-z^2} \sum_{n=0}^{\infty} \frac{2^n\, z^{2n+1}}{1 \cdot 3 \cdots (2n+1)}$$

C. Continued Fraction ($Rz > 0$)

$$e^{z^2} \operatorname{erfc} z = \frac{1}{\sqrt{\pi}}\left[\frac{1}{z+} \frac{1/2}{z+} \frac{1}{z+} \frac{3/2}{z+} \frac{2}{z+} \cdots\right]$$

$$= \frac{2z}{\sqrt{\pi}}\left[\frac{1}{2z^2+1} - \frac{1 \cdot 2}{2z^2+5} - \frac{3 \cdot 4}{2z^2+9} - \cdots\right] \quad \text{("Even" Form)}$$

D. Asymptotic Expansion

$$e^{z^2}\operatorname{erfc} z \sim \frac{1}{\sqrt{\pi}}\left[\frac{1}{z} + \sum_{n=1}^{\infty} \frac{(-1)^n 1 \cdot 3 \cdots (2n-1)}{z(2z^2)^n}\right] \left(z \to \infty, \left|\arg z\right| < \frac{3\pi}{4}\right)$$

E. Symmetry Relations

$$\operatorname{erf}(-z) = -\operatorname{erf} z$$

$$\operatorname{erf} \bar{z} = \overline{\operatorname{erf} z}$$

$$w(-z) = 2e^{-z^2} - w(z)$$

$$w(\bar{z}) = \overline{w(-z)}$$

$$C(-z) = -C(z),\ S(-z) = -S(z)$$

$$C(iz) = i\,C(z),\ S(iz) = -i\,S(z)$$

$$C(\bar{z}) = \overline{C(z)},\ S(\bar{z}) = \overline{S(z)}$$

3. Method

The main functions under consideration are the error function ERFZ, the complementary error function ERFCZ, and the exponential of z^2 times the complementary error function EZ2CZ. All other functions may be obtained from these three. To simplify testing, computations are performed for z in the first quadrant AZ and symmetry relations are then employed to make adjustments for other quadrants. For the special case $z = 0$, no computations are performed and the following function values are returned: ERFZ = 0, ERFCZ = 1 and EZ2CZ = 1.

Real type variables are used throughout to readily allow for double precision computation if greater accuracy is needed. The machine dependent constants are placed in a labeled section at the beginning of the subroutine. Function references are likewise grouped together when possible and attention called to the statement labels of the remaining function references. Real and imaginary parts of complex variables have R and I as final characters.

Since EZ2CZ for z in the first quadrant is machine representable even with the real and imaginary parts of z equal to the maximum machine value CMAX (provided its reciprocal is larger than the minimum machine value CMIN), checking for the range of the argument z has been omitted. However, the extensive range necessitates a fair amount of testing for overflows. Underflows are assumed to be set to zero. Overflows are set equal to the maximum machine value and an error indicator IERR set for the number of functions affected. If only EZ2CZ lies outside the machine range, IERR = 1, otherwise IERR = 3. As often as possible, computations are arranged so as to give the correct results for the three functions if they lie within the range of the machine.

In computing the modulus RHO = $\sqrt{(AZR)^2 + (AZI)^2}$ of a complex quantity AZ = AZR + i AZI in the first quadrant, RHO may lie in the machine range but $(AZR)^2$, $(AZI)^2$ or their sum may be outside the range. We select the larger ARIMX and smaller ARIMN of either AZR or AZI, and compute the ratio RMNMX = ARIMN/ARIMX. A factor of RHO called PRHO is computed as the square root of (RMNMX*RMNMX + ONE). This factor, which is greater than or equal to one and less than or equal to the square root of 2, can then be used to check for overflow. The quantity ARIMX must be less than CMAX divided by PRHO for RHO to lie in the machine range. A similar procedure is followed in computing the real and imaginary parts of $(AZ)^2$ = Z2R + i AZ2I = $(AZR)^2 - (AZI)^2 + i\,2AZR*AZI$ with first checking to ensure ARIMX is greater than or equal to 1.

Analysis has indicated and testing confirmed that the power series PS is most useful from the standpoint of accuracy and efficiency for RHO less than RHOLS(=1.5) and when AZR is less than or equal to 1 provid-

ed RHO is less than AELL ($=\sqrt{-1n(TOLER)}$) where TOLER is the upper limit for the relative error. The continued fraction expansion CF is most useful for AZR greater than 1 and RHO greater than or equal to RHOLS. The asymptotic expansion AE is most useful for AZR less than or equal to 1 for RHO greater than or equal to AELL. For RHO greater than or equal to RHOLC ($=\sqrt{0.5/TOLER}$) a rearrangement of arithmetic operations for the first term of the asymptotic expansion is necessary to maintain the accuracy of EZ2CZ. In the continued fraction and asymptotic expansion regions only, EZ2CZ is first computed; it tends to zero for large $|z|$ and the exponential of $-z^2$ tends to infinity for small AZR. To maintain accuracy here, we compute the exponential of $-Z2R/6$ and do continuous multiplication and testing with appropriate factors to obtain ERFC. The imaginary part of $(AZ)^2$ is tested against ULSC, the upper limit of the sine, cosine routine.

Figure 1 below maps the regions for the various methods.

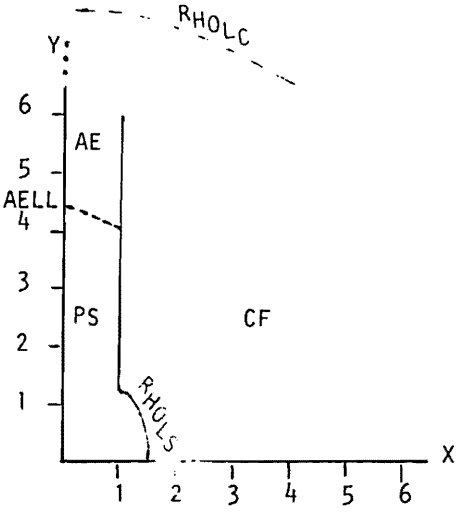

FIGURE 1. Parameter plane.

The dividing line RHO = AELL between the use of the power series and the asymptotic expansion and RHO = RHOLC are the only boundaries subject to the required precision. Single and double precision results, for example on the Univac 1108, are the results of two different methods in the region where RHO roughly lies between 4.3 and 6.4.

This mapping of the region ensures for the required precision that the least number of terms are computed and the loss of significance is kept to a minimum. While the second form of the power series is preferable for real positive z, since all terms are positive, the first form ensures greater accuracy for complex z since the real and imaginary parts of the terms may be positive, negative or zero for any RN($=n$). The power series is there more rapidly convergent; the relative error may then be approximated by the ratio of the term to the sum of terms; comparison of this approximant with the tolerance for the relative error controls the number of terms needed. Since the terms tend to zero through underflow, there will always be convergence even if the tolerance is made considerably smaller than the precision of the machine. The power series is evaluated using recurrence relations in the following form:

$$ERFZ = \frac{TWO}{SQRT(PI)} \sum_{RN=0}^{RNF} SGN(RN)*TM(RN) = \frac{TWO}{RTPI} * SUM$$

where

SGN(0) = 1, SGN(RN + 1) = −SGN(RN)
TM(RN) = ((AZ**(2*RN + 1))/1*2* . . . RN)/(2*RN + 1)
TM(RN) = PTM(RN)/DN(RN)
PTM(0) = AZ, PTM(RN + 1) = (AZ**2)*PTM(RN)/(RN + 1)
DN(0) = 1, DN(RN + 1) = DN(RN) + 2

In determining the terminal value of RN, normalization is necessary to avoid overflows and underflows. The normalization factor TMAX is the maximum of the absolute value of the real and imaginary parts of TM and SUM. If TMAX equals zero or $|TM/TMAX|^2$ underflows, RNF = RN.

If $|SUM/TMAX|^2$ underflows, additional terms are obtained. Otherwise, if $|TM/TMAX|^2/|SUM/TMAX|^2$ is less than $TOLER^2$, then RNF = RN.

The continued fraction expansion starts to converge more slowly as z tends to zero. The "even" form is used since the required number of terms is halved at the expense of very little extra computation for successive numerators and denominators. The continued fraction is evaluated by using the recurrence relations in the "forward" direction. The number of terms needed is determined by checking to see if the relative error of two successive convergents is less than the tolerance. On the other hand, if the relative error remains constant or starts to increase, the recurrence is terminated and the prior convergent taken as the value of the continued fraction. In this way, the process is always terminated when maximum precision is attained.

The "even" form of the continued fraction takes on the following implementation:

$$EZ2CZ = \frac{2*AZ}{RTPI} \prod_{RN=1}^{RNF} \frac{AM(RN)}{BM(RN)}$$

with $AM(1) = 1,\ AM(RN + 1) = -WM(RN + 1)*(WM(RN + 1) + 1)$

$BM(1) = 2*(AZ**2) + 1,\ BM(RN + 1) = BM(RN) + 4$

where $WM(1) = -1,\ WM(RN + 1) = WM(RN) + 2$

$EZ2CZ = (AZ*(FM/GM))*2/RTPI = (AZ*F(RN))*2/RTPI$

where $FM(-1) = 1,\ FM(0) = 0$

$GM(-1) = 0,\ GM(0) = 1$

and $FM(RN) = BM(RN)*FM(RN - 1) + AM(RN)*FM(RN - 2)$

$GM(RN) = BM(RN)*GM(RN - 1) + AM(RN)*GM(RN - 2)$

The relative error may be approximated by $[F(RN) - F(RN - 1)]/F(RN) = RE(RN)$. If the modulus squared of the relative error REM2(RN) is less than the square of the tolerance divided by 8, RNF = RN. If REM2(RN) is greater than or equal to REM2(RN − 1), then RNF = RN − 1. Normalization is likewise necessary here to avoid overflows in computing the relative error and its modulus squared and also in the generation of the successive convergents.

The asymptotic expansion is likewise evaluated using recurrence relations in the following form:

$$EZ2CZ = \frac{1}{SQRT(PI)} \sum_{RN=0}^{RNF} SGN(RN)*TM(RN) = SUM/RTPI$$

where $SGN(0) = 1,\ SGN(RN + 1) = -SGN(RN)$

$TM(RN) = (1/AZ)*(1*3* \ldots (2*RN - 1))/(2*(AZ**2))**RN$

$TM(0) = 1/AZ,\ TM(RN + 1) = DN(RN + 1)*\ TM(RN)*(1/(2*(AZ**2)))$

with $DN(1) = 1,\ DN(RN + 1) = DN(RN) + 2.$

The relative error may be approximated here by the ratio TM/SUM. The convergence test precedes the divergence test and is implemented as REM2 less than (TOLER**2)/8 to attain greater accuracy in both the real and imaginary parts. If the modulus squared of the term remains the same or increases, the prior sum is taken as the final sum.

For z along the imaginary axis, the error function is purely imaginary; the real part of erfc z = 1 and of e^{z^2} erfc $z = e^{-(AZI)^2}$. No difficulties arise in the use of the power series. However, since the asymptotic expansion is given for $|z| \to \infty$, the correction must be applied for AZR $\to$ 0.

The following table gives an indication of the number of terms needed to obtain maximum machine accuracy on the Univac 1108 with the various methods of computation.

Method	Number of Terms	
	Single Precision TOLER = .745E-8	Double Precision TOLER = .867D-18
Power Series	50	112
Continued Fraction	25	99
Asymptotic Expansion	22	45

4. Range

If the real part of z is zero or positive, e^{z^2} erfc z is valid for z throughout the entire machine range. Otherwise, the real part of z^2 is essentially limited by the range of the exponential library subroutine with the imaginary part of z^2 limited by the range of the sine, cosine library subroutine.

5. Accuracy and Precision

The maximum relative error, generally in erfc z, except for regions in the immediate neighborhood of zeros of the real and/or imaginary parts of the functions is 8E-6 for single precision computation on the Univac 1108.

The precision may be varied by changing the value of TOLER.

6. Timing (Univac 1108 Time/Sharing Executive System)

The time estimates given below are highly dependent on the operating system environment and consequently should not be relied on for critical timing measurements.

	Time (Seconds)	
Region	Single Precision TOLER = .745E-8	Double Precision TOLER = .867D-18
ZR = 0(.1)4, ZI = 0(.2)8 (1681 values)	5.94	22.5
Method	Maximum Time/Evaluation	
Power Series	.0101	.038
Continued Fraction	.0088	.052
Asymptotic Expansion	.0035	.0093

7. Testing

The language of the subroutine was checked for conformity with the PFORT VERIFIER.[3] Test arguments were devised and used in the analysis of the subroutine with the PROFILER.[4]

[3] The PFORT Verifier, A. D. Hall and B. G. Ryder, Bell Laboratories, Murray Hill, N.J. Proceedings of the Computer Science and Statistics Eighth Annual Symposium on the Interface, University of California, Los Angeles, February 13-14, 1975.

[4] Program Execution Profiles, G. Sande, World Bank, Washington, D.C. Proceedings of the Computer Science and Statistics Eighth Annual Symposium on the Interface, University of California, Los Angeles, February 13-14, 1975.

The subroutine was used to obtain related functions which were checked against available published tables ([1]-[5], [7]-[9], [13], [15]). Single precision results covering the 9 × 9 grid were compared against double precision results. This precision test particularly verified that the scaling operations were valid and undetected overflows had not occurred.

Where applicable, results were obtained by independent methods, for example, the power series and continued fraction, the power series and asymptotic expansion or all three methods. Otherwise, both forms of the power series or continued fraction were used. In addition, numerical integration of various forms of the integral representation was employed.

8. Test Values

Six-significant figure tables of erfc z, e^{z^2} erfc z and e^{z^2} erfc$(-z)$ are included in the appendix. The computations were performed with double precision arithmetic to provide more accurate values for checking purposes. The arguments are in polar coordinate form $z = \varrho e^{i\theta}$ for $\varrho = 0(.02).2(.1)3(.5)9$, $\Theta = 0°(15°)30°$, 37.5°, 45°, 50°(10°)90°. Values of the functions for z in other quadrants are readily obtainable with symmetry relations.

9. Argand Diagram of erf z $= \frac{2}{\sqrt{\pi}} \int_0^{z=\rho e^{i\theta}} e^{-t^2}\, dt$

Since erf z and erfc z are complementary functions, erf z is not tabulated but the argand diagram of the function is included to illustrate divergent and convergent spirals.

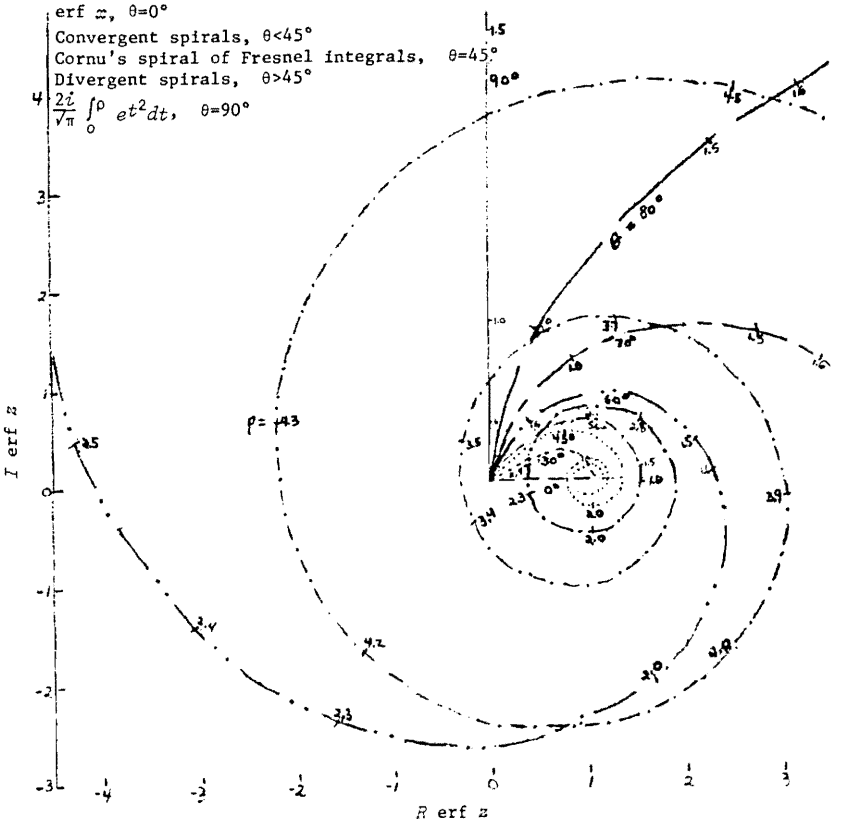

10. Special Values

Relevant values are collected here for completeness and ease of modification and checking of the program.

Zeros

	$\operatorname{erf} z_s = 0$
s	z_s
1	1.45061616 + i 1.88094300
2	2.24465927 + i 2.61657514
3	2.83974105 + i 3.17562810

	$w(z_s) = 0$
s	z_s
1	1.99146684 − i 1.35481013
2	2.69114902 − i 2.17704491
3	3.23533087 − i 2.78438761

	$C(z_s) = 0$	$S(z_s) = 0$
s	z_s	z_s
1	1.7437 + i .3057	2.0093 + i .2885
2	2.6515 + i .2529	2.8335 + i .2443
3	3.3204 + i .2240	3.4675 + i .2185

Maxima and Minima of Fresnel Integrals

s	$M_s = C(\sqrt{4s+1})$	$m_s = C(\sqrt{4s+3})$	$M_s^* = S(\sqrt{4s+2})$	$m_s^* = S(\sqrt{4s+4})$
0	.779893	.321056	.713972	.343416
1	.640807	.380391	.628940	.387969
2	.605721	.404261	.600362	.408301
3	.588128	.417922	.584942	.420516

Radius of Univalence ϱ

$\int_0^z e^{-t^2}\,dt \qquad e^{z^2}\int_0^z e^{-t^2}\,dt$

ϱ = 1.5748376 .92413887

Maximum and Inflection Point for Dawson's Integral

$F(.92413\ 88730) = .54104\ 42246$

$F(1.50197\ 52682) = .42768\ 66160$

Related Constants

1° = 1.74532 92519 94329 57692 36907 68488 61271 $(-2)r$
π = 3.14159 26535 89793 23846 26433 83279 50288
$\pi/2$ = 1.57079 63267 94896 61923 13216 91639 75144
$\sqrt{\pi}$ = 1.77245 38509 05516 02729 81674 83341 14518
$\sqrt{\pi}/2$ = .88622 69254 52758 01364 90837 41670 57259
2π = 6.28318 53071 79586 47692 52867 66559 00576
$2\sqrt{\pi}$ = 3.54490 77018 11032 05459 63349 66682 29036
e = 2.71828 18284 59045 23536 02874 71352 66249
$1/\pi$ = .31830 98861 83790 67153 77675 26745 02872
$2/\pi$ = .63661 97723 67581 34307 55350 53490 05744
$1/\sqrt{\pi}$ = .56418 95835 47756 28694 80794 51560 77258
$2/\sqrt{\pi}$ = 1.12837 91670 95512 57389 61589 03121 54517
$1/2\pi$ = .15915 49430 91895 33576 88837 63372 51436
$1/2\sqrt{\pi}$ = .28209 47917 73878 14347 40397 25780 38629
1/e = .36787 94411 71442 32159 55237 70161 46086
erf 1 = .84270 07929 49714 86934 12206 35082 60926

$$\int_0^1 e^{-t^2}dt = (\sqrt{\pi}/2)\,\mathrm{erf}\,1 = \sum_{n=0}^{\infty}\frac{(-1)^n}{n!(2n+1)} = .74682\ 41328\ 12427\ 02539\ 94674\ 36131\ 85300$$

$$(\sqrt{\pi}/2)e^1\mathrm{erf}\,1 = \sum_{n=0}^{\infty}\frac{2^n}{1\cdot 3\ldots(2n+1)} = 2.03007\ 84692\ 78704\ 97553\ 90899\ 25665\ 95044$$

$$\int_0^1 e^{t^2}dt = \sum_{n=0}^{\infty}\frac{1}{n!(2n+1)} = 1.46265\ 17459\ 07181\ 60880\ 40485\ 86856\ 98815$$

$$\sum_{n=0}^{\infty}\frac{1}{(2n)!(4n+1)} = 1.10473\ 79393\ 59804\ 31710\ 17580\ 11494\ 42058$$

$$\sum_{n=0}^{\infty}\frac{1}{(2n+1)!(4n+3)} = .35791\ 38065\ 47377\ 29170\ 22905\ 75362\ 56757$$

$$\sum_{n=0}^{\infty}\frac{2^{2n}}{1\cdot 3\ldots(4n+1)} = 1.28407\ 89880\ 95736\ 69733\ 77386\ 73036\ 75360$$

$$\sum_{n=0}^{\infty}\frac{2^{2n+1}}{1\cdot 3\ldots(4n+3)} = .74599\ 94811\ 82968\ 27820\ 13512\ 52629\ 19684$$

$$e^{-1}\int_0^1 e^{t^2}dt = \sum_{n=0}^{\infty}\frac{(-1)^n 2^n}{1\cdot 3\ldots(2n+1)} = .53807\ 95069\ 12768\ 41913\ 63874\ 20407\ 55675$$

Typical Tolerances and Their Natural Logarithms

2^{-16} = 0.15258 78906 25(−4)
2^{-24} = .59604 64477 53906 25(−7)
2^{-27} = .74505 80596 92382 8125(−8)
2^{-36} = .14551 91522 83668 51806 64062 5(−10)
2^{-48} = .35527 13678 80050 09293 55621 33789 0625(−14)
2^{-56} = .13877 78780 78144 56755 29539 58511 35253 90625(−16)
2^{-60} = .86736 17379 88403 54720 59622 40695 95336 91406 25(−18)
2^{-108} = .30814 87911 01957 73648 89564 70813 58837 09660 96263 71446 21112 38390 20729 06494 14062 5(−32)

$\log_e(2^{-16})$ = −11.09035 48889 59124 95067 57139 43330 82508
$\log_e(2^{-24})$ = −16.63553 23334 38687 42601 35709 14996 23763
$\log_e(2^{-27})$ = −18.71497 38751 18523 35426 52672 79370 76733

$\log_e(2^{-36}) = -24.95329\ 85001\ 58031\ 13902\ 03563\ 72494\ 35645$
$\log_e(2^{-48}) = -33.27106\ 46668\ 77374\ 85202\ 71418\ 29992\ 47526$
$\log_e(2^{-56}) = -38.81624\ 21113\ 56937\ 32736\ 49988\ 01657\ 88781$
$\log_e(2^{-60}) = -41.58883\ 08335\ 96718\ 56503\ 39272\ 87490\ 59408$
$\log_e(2^{-108}) = -74.85989\ 55004\ 74093\ 41706\ 10691\ 17483\ 06935$

Maximum and Minimum Machine Values and Their Natural Logarithms
(Univac 1108 Single and Double Precision Limits)

NBC = Number of binary digits in the (biased) characteristic of a floating point number

$$2^{-(2^{NBC-1}+1)} \leq x < 2^{2^{NBC-1}-1}$$

NBC = 8

$2^{127} = 0.17014\ 11834\ 60469\ 23173\ 16873\ 03715\ 88410(39)$
$2^{-129} = .14693\ 67938\ 52785\ 93849\ 60920\ 67152\ 78070(-38)$
$\log_e(2^{127}) = 88.02969\ 19311\ 13054\ 29598\ 84794\ 25188\ 42414$
$\log_e(2^{-129}) = -89.41598\ 62922\ 32944\ 91482\ 29436\ 68104\ 77728$

NBC = 11

$2^{1023} = 0.89884\ 65674\ 31157\ 95386\ 46525\ 95394\ 51236(308)$
$2^{-1025} = .27813\ 42323\ 13400\ 17288\ 62790\ 89666\ 55050(-308)$
$\log_e(2^{1023}) = 709.08956\ 57128\ 24051\ 53382\ 84602\ 51714\ 62914$
$\log_e(2^{-1025}) = -710.47586\ 00739\ 43942\ 15266\ 29244\ 94630\ 98227$

11. References

[1] Abramowitz, M. and Stegun, I. A. Handbook of Mathematical Functions. Nat. Bur. Stand. (U.S.) Appl. Math. Ser. 55; 1964.

[2] Faddeeva, V. N. and Terent'ev, N. M. *Tables of Values of the Function* $w(z)=e^{-z^2}[1+(2i/\sqrt{\pi})\int_0^z e^{t^2}\,dt]$ *for Complex Arguments.* New York: English Trans., Pergamon Press; 1961.

[3] Fettis, H. E., Caslin J. C. and Cramer, K. R. Complex Zeros of the Error Function and of the Complementary Error Function. Math. Comp. **27**, 122: 401-407; 1973.

[4] Finn, G. D. and Mugglestone, D. Tables of the Line Broadening Function H(a,v). Mon. Not. R. Astr. Soc. **129**: 221-235; 1965.

[5] Fried, B. D. and Conte, S. D. *The Plasma Dispersion Function, The Hilbert Transform of the Gaussian.* New York: Academic Press; 1961.

[6] Gautschi, W. Efficient Computation of the Complex Error Function. SIAM J. Numer. Anal. 7, **1**: 187-198; 1970.

[7] Hummer, D. G. The Voigt Function: An Eight-Significant Figure Table and Generating Procedure. Mem. Roy. Astronom, Soc. **70**: 1-31, 1965.

[8] Karpov, K. A. Tablitsy Funktsii $w(z) = e^{-z^2}\int_0^z e^{z^2}\,dx$ v Kompleksnoi Oblasti. Moscow, U.S.S.R.: Izdat. Akad. Nauk S.S.S.R.; 1954.

[9] Karpov, K. A. Tablitsy Funktsii $F(z) = \int_0^z e^{z^2}dx$ v Kompleksnoi Oblasti. Moscow, U.S.S.R.: Izdat. Akad. Nauk S.S.S.R.; 1958.

[10] Kreyszig, E. and Todd, J. The Radius of Univalence of the Error Function. Numerische Mathematik **1**: 78-89; 1959.

[11] Kreyszig, E. and Todd, J. On the Radius of Univalence of the Function $exp\ z^2\int_0^z exp(-t^2)dt$. Pacific Journal of Mathematics 9, **1**: 123-127; 1959.

[12] Lohmander, B. and Rittsten, S. Table of the Function $y = e^{-x^2}\int_0^x e^{t^2}\,dt$. Kungl. Fysiogr. Sallsk. i Lund Forh. **28**: 45-52; 1958.

[13] Martz, C. W. Tables of the Complex Fresnel Integral. NASA Report SP-3010; Washington; 1964.

[14] Pearcey, T. Table of the Fresnel Integral. London, England: Cambridge University Press; 1956.

[15] Rosser, J. B. *Theory and Application of* $\int_0^x e^{-x^2}\,dx$ *and* $\int_0^x e^{-p^2y^2}\,dy\int_0^x e^{-x^2}dx$. Brooklyn, NY: Mapleton House; 1948.

[16] Tablitsy Integralov Frenelya. Moscow, U.S.S.R.: Izdat. Akad. Nauk S.S.S.R.; 1953.

[17] Van Wijngaarden, A. and Scheen, W. L., Table of Fresnel Integrals. Verh. Nederl. Akad. Wetensch. Afd. Natuurk. Sec. I, 19, **4**: 1-26; 1949.

```
C****                          APPENDIX
C                        IMPLEMENTING PROGRAM
C LANGUAGE. AMERICAN NATIONAL STANDARD FORTRAN
C (SUBROUTINE SUBJECTED TO PFORT VERIFIER*)
C DEFINITIONS. Z. A COMPLEX VARIABLE=ZR+I ZI
C     ERF(Z)=(2/SQRT(PI))*INTEGRAL(EXP(-T**2))DT FROM 0 TO Z
C            =ERFZR+I ERFZI
C     ERFC(Z)=(2/SQRT(PI))*INTEGRAL(EXP(-T**2))DT FROM Z TO
C                                                      INFINITY
C            =1-ERF(Z)
C            =ERFCZR+I ERFCZI
C     EXP(Z**2)*ERFC(Z)=EZ2CZR+I EZ2CZI
C   SYMMETRY RELATIONS
C     ERF(-Z)=-ERF(Z)
C     ERF(Z CONJG)=CONJG(ERF(Z))
C     ERFC(-Z)=2-ERFC(Z)
C     ERFC(Z CONJG)=CONJG(ERFC(Z))
C     EXP(Z**2)*ERFC(-Z)=2*EXP(Z**2)-EXP(Z**2)*ERFC(Z)
C     EXP(Z CONJG**2)*ERFC(Z CONJG)=CONJG(EXP(Z**2)*ERFC(Z))
C   SPECIAL CASE, Z=0
C       ERF(Z)=0
C       ERFC(Z)=1
C       EXP(Z**2)*ERFC(Z)=1
C USAGE. CALL ERRZ (ZR,ZI,ERFZR,ERFZI,ERFCZR,ERFCZI,EZ2CZR,
C                                                 EZ2CZI,IERR)
C       ARGUMENTS
C       (REAL TYPE VARIABLES ARE USED THROUGHOUT TO READILY
C       ALLOW FOR DOUBLE PRECISION COMPUTATION. REAL AND
C       IMAGINARY PARTS OF COMPLEX VARIABLES HAVE R AND
C       I AS FINAL CHARACTERS.)
C         ZR,ZI          REAL(OR DOUBLE PRECISION) TYPE INPUT
C         ERFZR,ERFZI          (SAME TYPE AS Z)         OUTPUT
C         ERFCZR,ERFCZI                "                 OUTPUT
C         EZ2CZR,EZ2CZI                "                 OUTPUT
C         IERR                    INTEGER TYPE           OUTPUT
C               IERR
C                0                                  NORMAL RETURN
C                1 EXP(Z**2)*ERFC(Z)                    INVALID
C                2 ERF(Z),ERFC(Z)                       INVALID
C                3 ERF(Z),ERFC(Z),EXP(Z**2)*ERFC(Z)     INVALID
C                  (Z IN 2ND OR 3RD QUADRANTS(ZR .LT. 0))
C           COMMONLY USED INTERNAL VARIABLES
C             AELL      LOWER LIMIT OF |ZI FOR ASYMPTOTIC
C                        EXPANSION(A.E.) ABS(ZR) .LE. 1
C             AZI       ABS(ZI)
C             AZR       ABS(ZR)
C             AZ2I      ABS(IMAG(Z**2))
C             CMAX      MAXIMUM MACHINE VALUE
C             CMIN      MINIMUM MACHINE VALUE
C             REM2      MODULUS SQUARED OF RELATIVE
C                        ERROR(R.E.)
C                        |R.E.|**2=REM2(N)
C             REPM2     REM2(N-1)
C             RHO       |ZI=SQRT(ZR**2+ZI**2)
C             RHOLC     LOWER LIMIT OF RHO FOR USING ONLY
C                         1ST TERM OF A.E.
C             RHOLS     UPPER LIMIT OF RHO, UNRESTRICTED
```

```
58      C                          ABS(ZR), FOR POWER SERIES
59      C             RTPI         SQRT(PI=3.14...)
60      C             SUMM2        !SUMI**2=SUMR**2+SUMI**2
61      C                          OR !SUM/TMAX!**2
62      C             TMAX         NORMALIZATION FACTOR
63      C             TMM2         !TMI**2=TMR**2+TMI**2
64      C                          OR !TM/TMAX!**2
65      C             TOLER        UPPER LIMIT FOR RELATIVE ERRORS
66      C             TOLER2       TOLER**2
67      C             TOL2         TOLER2/8
68      C             ULSC         MAXIMUM ARGUMENT FOR SIN/COS ROUTINE
69      C MODIFICATIONS.
70      C    THE CODE IS SET UP FOR SINGLE PRECISION COMPUTATION
71      C    WITH SINGLE PRECISION FUNCTION REFERENCES AND SINGLE
72      C    PRECISION MACHINE DEPENDENT CONSTANTS. FOR THE UNIVAC
73      C    1108, CMAX APPROX. 2**127,CMIN=2**(-129),ULSC=2**20 AND
74      C    TOLER=.745E-8. RTPI IS GIVEN IN DOUBLE
75      C    PRECISION FORMAT TO 19 SIGNIFICANT FIGURES.
76      C  DOUBLE PRECISION RESULTS ARE OBTAINED BY INSERTING
77      C    (1) THE DOUBLE PRECISION TYPE STATEMENT
78      C    (2) DOUBLE PRECISION INTRINSIC FUNCTION REFERENCES -
79      C        DABS,DMAX1 AND DMIN1
80      C    (3) DOUBLE PRECISION EXTERNAL FUNCTION REFERENCES -
81      C        DCOS,DEXP,DLOG,DSIN AND DSQRT AND
82      C    (4) FOR THE UNIVAC 1108 ADJUSTING THE CONSTANTS
83      C        CMAX APPROX. 2**1023,CMIN=2**(-1025),ULSC=2**56 AND
84      C        TOLER=.667D-18.
85      C   THE DETAILED METHODS SHOULD WORK FOR ANY PRECISION
86      C   IF THE MACHINE DEPENDENT CONSTANTS ARE CHANGED
87      C   WITH RTPI GIVEN TO THE REQUIRED NUMBER OF SIGNIFICANT
88      C   FIGURES.
89      C METHOD.    Z=ZR+I ZI =RHO*EXP(I*ARCTAN(ZI/ZR))
90      C              ALL METHODS APPLY TO AZ=ABS(ZR)+I ABS(ZI)=AZR+
91      C              I AZI. USE IS THEN MADE OF SYMMETRY RELATIONS.
92      C     POWER SERIES
93      C              RHO .LT. RHOLS(=1.5)
94      C              AZR .LE. 1. RHOLS .LE. RHO .LT. AELL
95      C                                      AELL=SQRT(-LOG(TOLER))
96      C         ERF(AZ)=(2/SQRT(PI))*SUM(SGN(RN)*TM(RN))
97      C                                              RN=0,1,....,RNF
98      C                    SGN(0)=1
99      C                    SGN(RN+1)=-SGN(RN)
100     C                    TM(RN)=((AZ**(2*RN+1))/1*2...RN)/(2*RN+1)
101     C                    TM(RN)=PTM(RN)/DN(RN)
102     C                         PTM(0)=AZ
103     C                         PTM(RN+1)=(AZ**2)*PTM(RN)/(RN+1)
104     C                         DN(0)=1
105     C                         DN(RN+1)=DN(RN)+2
106     C            RNF=RN IF TM=0 AND SUM=0, IF !TM/TMAX!**2(=TMM2)
107     C            =0 OR IF !SUM/TMAX!**2(=SUMM2) .NE. 0 AND
108     C            REM2(=TMM2/SUMM2) .LT. TOLER2
109     C     CONTINUED FRACTION
110     C              AZR .GT. 1. RHOLS .LE. RHO .LT. RHOLC
111     C                                   RHOLC=SQRT(ONE/(TWO*TOLER))
112     C         EXP(AZ**2)*ERFC(AZ)=
113     C                    (2*AZ/SQRT(PI))*(1 I/I (2*(AZ**2)+1)-
114     C                                     1*2 I/I (2*(AZ**2)+5)-
115     C                                     3*4 I/I (2*(AZ**2)+9)-...)
```

```
C                        =(2*AZ/RTPI)*II(AM(RN) I/I EM(RN))
C                                                    RN=1,2,...,RNF
C                             AM(1)=1
C                             AM(RN+1)=-WM(RN+1)*(WM(RN+1)+1)
C                             EM(1)=2*(AZ**2)+1
C                             BM(RN+1)=BM(RN)+4
C                                  WM(1)=-1
C                                  WM(RN+1)=WM(RN)+2
C                        =(AZ*(FM/GM))*2/RTPI
C                        =(AZ*F(FN))*2/RTPI
C                     FM(-1)=1
C                     GM(-1)=0
C                      FM(0)=0
C                      GM(0)=1
C                     FM(RN)=BM(RN)*FM(RN-1)+AM(RN)*FM(RN-2)
C                     GM(RN)=BM(RN)*GM(RN-1)+AM(RN)*GM(RN-2)
C               RNF=RN IF REM2(FOR R.E.=(F(RN)-F(RN-1))/F(RN))
C                   .LT. TOL2 OR
C               RNF=RN-1 IF REM2(RN) .GE. REM2(RN-1)
C     ASYMPTOTIC EXPANSION
C               AZR .LE. 1. AELL .LE. RHO .LT. RHOLC
C               (FOR RHOLC .LE. RHO .LE. CMAX, TO PRESERVE
C                  ACCURACY AN ALTERNATIVE COMPUTATION OF
C                  THE FIRST TERM OF THE A.E. IS EMPLOYED.)
C          EXP(AZ**2)*ERFC(AZ)=(SUM(SGN(RN)*TM(RN)))/SQRT(PI)
C                                                    RN=0,1,...,RNF
C                SGN(0)=1
C                SGN(RN+1)=-SGN(RN)
C                TM(RN)=(1/AZ)*(1*3...(2*RN-1))/
C                                                 (2*(AZ**2))**RN
C                TM(0)=1/AZ
C                TM(RN+1)=DN(RN+1)*(TM(RN)*(1/(2*(AZ**2))))
C                     DN(1)=1
C                     DN(RN+1)=DN(RN)+2
C                RNF=RN IF REM2(FOR R.E.=TM/SUM) .LT. TOL2
C                RNF=RN-1 IF TMM2(RN) .GE. TMPM2(=TMM2(RN-1))
C                                                 (DIVERGENCE)
C RANGE.
C     EXP(Z**2)*ERFC(Z) IS VALID FOR ZR .GE. 0 THROUGHOUT
C     THE ENTIRE MACHINE RANGE. ERF(Z),ERFC(Z) AND
C     EXP(Z**2)*ERFC(Z)(FOR ZR .LT. 0) ARE LIMITED BY THE
C     RANGE AND ACCURACY OF THE SINE,COSINE AND/OR THE
C     EXPONENTIAL LIBRARY ROUTINES.
C ACCURACY. THE MAXIMUM RELATIVE ERROR (GENERALLY IN ERFC)
C           EXCEPT IN THE IMMEDIATE NEIGHBORHOOD OF ZEROS.
C           IS B(-E) ON THE UNIVAC 1108 FOR
C           SINGLE PRECISION COMPUTATION.  THE REAL
C           AND IMAGINARY PARTS INDEPENDENTLY AS WELL
C           AS THEIR ZEROS ENTER INTO CONSIDERATION.
C PRECISION. VARIABLE - BY SETTING A PREDETERMINED VALUE OF
C                       TOLER
C MAXIMUM      UNIVAC 1108 TIME/SHARING EXECUTIVE SYSTEM
C TIMING.        S.P.             D.P.
C (SECONDS)      .0101            .052
C STORAGE. 1171 WORDS REQUIRED BY THE UNIVAC 1108 COMPILER
C           (313 FORTRAN STATEMENTS, 95 VARIABLES)
C* THE PFORT VERIFIER,A.C.HALL AND B.G.RYDER
C (BELL LABORATORIES,MURRAY HILL, N.J.) PROC.OF THE COMPUTER
```

```
      C SCIENCE AND STATISTICS EIGHTH ANNUAL SYMPOSIUM ON THE
      C INTERFACE, UNIV. OF CALIF., LOS ANGELES, FEB.13-14,1975.
      C*****
            SUBROUTINE ERRZ(ZR,ZI,ERFZR,ERFZI,ERFCZR,ERFCZI,
           1                                  EZ2CZR,EZ2CZI,IERR)
      C           MACHINE DEPENDENT CONSTANTS
            CMAX=.17014116E39
            CMIN=.14693679E-38
            ULSC=.104857EE7
            TOLER=.745E-8
      C NOTE TOLER IS SET TO THE PRECISION OF
      C THE UNIVAC 1108 SINGLE PRECISION ARITHMETIC.
            RTPI=1.77245385090551602D0
      C           OTHER CONSTANTS
            ZERO=0
            ONE=1
            TWO=2
            THREE=3
            FOUR=4
            ONPTFV=THREE/TWO
      C           INITIALIZATION OF ERROR INDICATORS
            IERR=0
            IQ=0
      C           FUNCTION REFERENCES
      C NOTE FUNCTION REFERENCES OCCUR IN THE REGIONS OF STATEMENT
      C LABELS 5,15 AND 85 AND IN STATEMENT LABELS 110,315,515,
      C 517 AND 955.
      C           SET UP FOR Z IN FIRST QUADRANT    AZ=AZR+I AZI
          5 AZR=ABS(ZR)
            AZI=ABS(ZI)
            ARMN=AMIN1(AZR,AZI)
            ARMX=AMAX1(AZR,AZI)
            IF (ARMX .GT. ZERO) GO TO 10
      C           SPECIAL CASE, Z=0
            ERFZR=ZERO
            ERFZI=ZERO
            ERFCZR=ONE
            ERFCZI=ZERO
            EZ2CZR=ONE
            EZ2CZI=ZERO
            RETURN
      C           CONTROL VARIABLES
         10 TOLER2=TOLER*TOLER
            TOL2=TOLER2/FOUR/TWO
            RHOLS=ONPTFV
            RMNMX=ARMN/ARMX
         15 CMAXLN=ALOG(CMAX)
            CMINLN=ALOG(CMIN)
            AELL=SQRT(-ALOG(TOLER))
            RHOLC=SQRT(ONE/(TWO*TOLER))
            PRHO=SQRT(RMNMX*RMNMX+ONE)
      C           COMPUTATION OF AUXILIARY QUANTITIES
      C                COMPUTATION OF AZ**2=Z2R+I AZ2I
            IF (ARMX .LT. ONE) GO TO 60
      C                     OVERFLOW CHECK ON Z2RN=-Z2R
            TEMPB=((ONE-RMNMX)*ARMX)*(ONE+RMNMX)
            IF (TEMPB .LT. CMAX/ARMX) GO TO 20
            TEMPC=CMAX
```

```
232            GO TO 30
233         20 TEMPC=TEMPE*ARIMX
234         30 IF (AZR-ARIMX) 50,40,50
235         40 Z2RN=-TEMPC
236            GO TO 70
237         50 Z2RN=TEMPC
238            GO TO 70
239         60 Z2RN=(AZI+AZR)*(AZI-AZR)
240            GO TO 80
241       C                       OVERFLOW CHECK ON AZ2I
242         70 IF (ARIMN .LT. (CMAX/TWO)/ARIMX) GO TO 80
243            AZ2I=CMAX
244            GO TO 90
245         80 AZ2I=(TWO*ARIMN)*ARIMX
246       C                 PRELIMINARY COMPUTATIONS FOR EXP(AZ**2) AND
247       C                   EXP(-AZ**2)
248       C                       CHECK IF VALID ARGUMENT FOR SIN/COS
249            IF (AZ2I .GE. ULSC) GO TO 90
250         85 COAZ2I=COS(AZ2I)
251            SIAZ2I=SIN(AZ2I)
252       C                       EXTENDING RANGE OF EXP ROUTINE
253         90 TEMP=Z2RN/THREE
254            Z2R=-Z2RN
255       C                       OVERFLOW CHECK
256            IF (TEMP .LT. CMAXLN) GO TO 100
257            EMZ2D3=CMAX
258            EZ2R=ZERO
259            GO TO 190
260       C                       UNDERFLOW CHECK
261        100 IF (TEMP .GT. CMINLN) GO TO 110
262            EMZ2D3=ZERO
263       C                       EXP(AZ**2) OVERFLOWS (IQ=1)
264            IQ=1
265            GO TO 160
266        110 EMZ2D6=EXP(TEMP/TWO)
267            EMZ2D3=EMZ2D6*EMZ2D6
268            EZ2D6=ONE/EMZ2D6
269            IF (EZ2D6 .LE. ONE) GO TO 180
270            J=1
271            PEXP=ZERO
272            TEMP=EZ2D6
273        120   IF (TEMP .GE. CMAX/EZ2D6) GO TO 150
274              TEMP=TEMP*EZ2D6
275              J=J+1
276              IF (J-5) 120,130,140
277        130 PEXP=TEMP
278            GO TO 120
279        140 EZ2R=TEMP
280            GO TO 190
281        150 IF (PEXP) 170,160,170
282        160 PEXP=CMAX
283        170 EZ2R=CMAX
284            GO TO 190
285        180 PEXP=EZ2D6**5
286            EZ2R=PEXP*EZ2D6
287            TEZ2=(PEXP*TWO)*EZ2D6
288       C                 COMPUTATION OF RHO
289       C                       OVERFLOW CHECK
```

```
      190 IF (ARIMX .LT. CMAX/PRHO) GO TO 200
          RHO=CMAX
          GO TO 210
      200 RHO=ARIMX*PRHO
C           METHOD SELECTION
      210 IF (RHO .LT. RHOLC) GO TO 220
C                 IMPROVE ACCURACY FOR LARGE RHO
          FA=AZR/ARIMX
          FB=AZI/ARIMX
          FC=RTPI*(RMNMX*RMNMX+ONE)
          EZ2CZR=(FA/ARIMX)/FC
          EZ2CZI=-(FB/ARIMX)/FC
          GO TO 800
      220 IF (RHO .LT. RHOLS) GO TO 300
          IF (AZR .GT. ONE) GO TO 500
          IF (RHO-AELL) 300,700,700
C                 POWER SERIES FOR ERF(AZ)
C                       INITIALIZATION
      300 SUMR=ZERO
          SUMI=ZERO
          SGN=ONE
          RN=ZERO
          DN=ONE
          PTMR=AZR
          PTMI=AZI
C                       COMPUTING SUM
      310   TMR=PTMR/DN
            TMI=PTMI/DN
            SUMR=SUMR+TMR*SGN
            SUMI=SUMI+TMI*SGN
C                       SCALING TO AVOID OVERFLOW OR UNDER-
C                         FLOW IN APPROXIMATING R.E.
      315   TMAX=AMAX1(ABS(TMR),ABS(TMI),ABS(SUMR),ABS(SUMI))
            IF (TMAX) 320,360,320
      320   TMM2=(TMR/TMAX)**2+(TMI/TMAX)**2
            SUMM2=(SUMR/TMAX)**2+(SUMI/TMAX)**2
            IF (TMM2) 330,360,330
      330   IF (SUMM2) 340,350,340
      340   REM2=TMM2/SUMM2
C                       TOLERANCE CHECK
            IF (REM2 .LT. TOLER2) GO TO 360
C                       ADDITIONAL TERMS
      350   DN=DN+TWO
            RN=RN+ONE
            SGN=-SGN
            TEMP=(PTMR*Z2R-PTMI*AZ2I)/RN
            PTMI=(PTMR*AZ2I+PTMI*Z2R)/RN
            PTMR=TEMP
            GO TO 310
C                       FUNCTIONS EVALUATED IN FIRST QUADRANT
      360 ERFZR=SUMR*TWO/RTPI
          ERFZI=SUMI*TWO/RTPI
          ERFCZR=ONE-ERFZR
          ERFCZI=-ERFZI
          EZ2CZR=(COAZ2I*ERFCZR-SIAZ2I*ERFCZI)*EZ2R
          EZ2CZI=(SIAZ2I*ERFCZR+COAZ2I*ERFCZI)*EZ2R
          GO TO 840
C                 CONTINUED FRACTION FOR EXP(AZ**2)*ERFC(AZ)
```

```
C                       INITIALIZATION
  500 WM=-CNE
      BMR=TWC*Z2R+CNE
      BMI=TWC*AZ2I
      AM=CNE
      FMM2R=CNE
      FMM2I=ZERO
      GMM2R=ZERO
      GMM2I=ZERO
      FMM1R=ZERO
      FMM1I=ZERO
      GMM1R=CNE
      GMM1I=ZERO
      REPM2=CMAX
      FPR=ZERO
      FPI=ZERO
C                       RECURRENCE RELATION
  510   FMR=BMR*FMM1R-BMI*FMM1I+AM*FMM2R
        FMI=BMI*FMM1R+BMR*FMM1I+AM*FMM2I
        GMR=BMR*GMM1R-BMI*GMM1I+AM*GMM2R
        GMI=BMI*GMM1R+BMR*GMM1I+AM*GMM2I
C                       CONVERGENT F=FM/GM
C                         SCALING TO AVOID OVERFLOW IN
C                           COMPUTING CONVERGENT
  515   TMAX=AMAX1(ABS(FMR),ABS(FMI),ABS(GMR),ABS(GMI))
        SFMR=FMR/TMAX
        SFMI=FMI/TMAX
        SGMR=GMR/TMAX
        SGMI=GMI/TMAX
        TEMP=SGMR*SGMR+SGMI*SGMI
        FR=(SFMR*SGMR+SFMI*SGMI)/TEMP
        FI=(SFMI*SGMR-SFMR*SGMI)/TEMP
C                       APPROXIMATING R.E.
        TEMP=FR*FR+FI*FI
        TEMPA=FR-FPR
        TEMPB=FI-FPI
        REM2=(TEMPA*TEMPA+TEMPB*TEMPB)/TEMP
C                       TOLERANCE CHECK
        IF (REM2 .LT. TOL2) GO TO 530
        IF (REM2 .GE. REPM2) GO TO 520
C                       ADDITIONAL CONVERGENTS
        WM=WM+TWC
        BMR=BMR+FCUR
        AM=-WM*(WM+CNE)
        FMM2R=FMM1R
        FMM2I=FMM1I
        GMM2R=GMM1R
        GMM2I=GMM1I
        FMM1R=FMR
        FMM1I=FMI
        GMM1R=GMR
        GMM1I=GMI
        FPR=FR
        FPI=FI
        REPM2=REM2
C                       SCALING
C SCALING SHOULD NOT BE DELETED AS THE VALUES OF FMR,FMI
C FMR,GMI MAY OVERFLOW FOR SMALL VALUES OF REAL OF Z
```

```
      517   ABM=AMAX1(ABS(BMR),ABS(BMI))
            IF (TMAX .LT. (CMAX/FCUR)/(TWO*ABM-AM)) GO TO 510
            FMM2R=FMM2R/TMAX
            FMM2I=FMM2I/TMAX
            GMM2R=GMM2R/TMAX
            GMM2I=GMM2I/TMAX
            FMM1R=FMM1R/TMAX
            FMM1I=FMM1I/TMAX
            GMM1R=GMM1R/TMAX
            GMM1I=GMM1I/TMAX
            GO TO 510
C                       RELATIVE ERROR INCREASED-ROUNDOFFS
C                         ACCEPT PRIOR CONVERGENT
      520 FR=FPR
          FI=FPI
C                       EVALUATE EXP(AZ**2)*ERFC(AZ)
      530 EZ2CZR=(AZR*FR-AZI*FI)*TWC/RTPI
          EZ2CZI=(AZI*FR+AZR*FI)*TWC/RTPI
          GO TO 800
C                 ASYMPTOTIC EXPANSION FOR EXP(AZ**2)*ERFC(AZ)
C                       INITIALIZATION
      700 TZ2R=TWC*Z2R
          TZ2I=TWC*AZ2I
          TEMP=TZ2R*TZ2R+TZ2I*TZ2I
          RTZ2R=TZ2R/TEMP
          RTZ2I=-TZ2I/TEMP
          TMM1R=(AZR/RHC)/RHC
          TMM1I=-(AZI/RHC)/RHC
          TMPM2=TMM1R*TMM1R+TMM1I*TMM1I
          SUMR=TMM1R
          SUMI=TMM1I
          DN=ONE
          SGN=-ONE
C                       COMPUTING SUM
      710   TMR=DN*(TMM1R*RTZ2R-TMM1I*RTZ2I)
            TMI=DN*(TMM1I*RTZ2R+TMM1R*RTZ2I)
            SUMR=SGN*TMR+SUMR
            SUMI=SGN*TMI+SUMI
C                       APPROXIMATING R.E.
            SUMM2=SUMR*SUMR+SUMI*SUMI
            TMM2=TMR*TMR+TMI*TMI
            REM2=TMM2/SUMM2
C                       TOLERANCE CHECK
            IF (REM2 .LT. TOL2) GO TO 730
            IF (TMM2 .LT. TMPM2) GO TO 720
C                       DIVERGENT PATH
            SUMR=SUMR-SGN*TMR+SGN*TMM1R
            SUMI=SUMI-SGN*TMI+SGN*TMM1I
            GO TO 730
C                       ADDITIONAL TERMS
      720   SGN=-SGN
            DN=DN+TWO
            TMM1R=TMR
            TMM1I=TMI
            TMPM2=TMM2
            GO TO 710
C                       EVALUATE EXP(AZ**2)*ERFC(AZ)
      730 EZ2CZR=SUMR/RTPI
```

```
      EZ2CZI=SUMI/RTPI
C                        MAINTAINING ACCURACY IN EZ2CZR
C                          FOR SMALL AZR
      TEMP=EZ2CZR*TCLER
      IF (TEMP .GT. EZ2R) GO TO 800
      TEMP=CMIN*RHOLC
      IF (EZ2CZR .GT. TEMP) GO TO 750
      IF (EZ2R .GT. TEMP) GO TO 750
      IF (AZR) 740,750,740
C                        INDICATE RESULTING ERRORS IN ERFC
C                          (AND ERF)(IERR=2)
  740 IERR=2
  750 EZ2CZR=EZ2CZR+EZ2R*COAZ2I
C                   EVALUATE ERFC AND ERF FOR AZ IN CONTINUED
C                     FRACTION AND ASYMPTOTIC EXPANSION REGIONS
  800 IF (AZ2I .LT. ULSC) GO TO 830
C                       INVALID ARGUMENT FOR SIN/COS
C                         ERFC(AND ERF) INVALID (IERR=2)
      IF (AZR-ARIMX) 820,810,820
C                           AZR .GE. AZI
  810 ERFCZR=ZERO
      ERFCZI=ZERO
      GO TO 910
C                           AZR .LT. AZI
  820 ERFCZR=CMAX
      ERFCZI=CMAX
      GO TO 910
C                      VALID ARGUMENT FOR SIN/COS
  830 IF (RFC .GE. RHOLC) GO TO 840
C                           RHO .LT. RHOLC
      TEMPA=EZ2CZR*COAZ2I+EZ2CZI*SIAZ2I
      TEMPB=-EZ2CZR*SIAZ2I+EZ2CZI*COAZ2I
      TEMPC=EMZ2D3
      GO TO 850
C                           RFC .GE. RHOLC
  840 TEMPA=(FA*COAZ2I-FB*SIAZ2I)/FC
      TEMPB=(-FA*SIAZ2I-FB*COAZ2I)/FC
      TEMP=EMZ2D3/ARIMX
      TEMPA=TEMPA*TEMP
      TEMPB=TEMPB*TEMP
      TEMPC=CNE
  850 IF (EMZ2D3 .LE. CNE) GO TO 920
C                           EVALUATE ERFC(AZ)(AZI .GT. AZR)
      I=1
      TEMP=TEMPA
  860   J=1
        SGN=CNE
        FD=TEMPC
        IF (TEMP .GE. ZERO) GO TO 870
        SGN=-SGN
        TEMP=-TEMP
  870     IF (TEMP .LT. CMAX/FD) GO TO 880
          TEMP=CMAX
          IC=2
          GO TO 890
  880     TEMP=TEMP*FD
          J=J+1
          IF (J .GT. 3) GO TO 890
```

```
522                FD=EMZ2D3
523                GO TO 870
524          890   IF (I .GE. 2) GO TO 900
525                ERFCZR=TEMP*SGN
526                I=I+1
527                TEMP=TEMPB
528                GO TO 860
529          900 ERFCZI=TEMP*SGN
530              IF (IQ .NE. 2) GO TO 930
531        C                            ERFC(AND ERF) INVALID (IERR=2)
532        C                                OVERFLOW OF ERFC(AZ)(IQ=2)
533          910 IERR=2
534              GO TO 930
535        C                          EVALUATE ERFC(AZ)(AZI .LE. AZR)
536          920 ERFCZR=(TEMPA*EMZ2D3)*EMZ2D3*TEMPC
537              ERFCZI=(TEMPB*EMZ2D3)*EMZ2D3*TEMPC
538        C                         SPECIAL CASE (AZR=0)
539          930 IF (AZR .LE. ZERO) ERFCZR=ONE
540        C                          EVALUATE ERF(AZ)
541              ERFZR=ONE-ERFCZR
542              ERFZI=-ERFCZI
543        C           SYMMETRY RELATIONS APPLIED
544          940 IF (ZR-AZR) 950,1000,950
545        C                   REAL OF Z .LT. 0
546          950 ERFZR=-ERFZR
547              ERFCZR=TWO-ERFCZR
548              IF (AZ2I .GE. ULSC) GO TO 960
549              IF (IQ .EQ. 1) GO TO 960
550        C                   MAINTAINING ACCURACY IN 2*EXP(Z**2)
551              IF (AZR .LE. AZI) GO TO 980
552          955 TEMP=AMAX1(ABS(SIAZ2I), ABS(COAZ2I))
553              IF (TEMP .LT. ((CMAX/TWO)/PEXP)/EZ2D6) GO TO 970
554        C                   EXP(Z**2)*ERFC(Z) INVALID (IERR+1)
555          960 IERR=IERR+1
556              EZ2CZR=CMAX
557              EZ2CZI=CMAX
558              GO TO 1000
559          970 TEZ2R=((PEXP*COAZ2I)*EZ2D6)*TWO
560              TEZ2I=((PEXP*SIAZ2I)*EZ2D6)*TWO
561              GO TO 990
562          980 TEZ2R=TEZ2*COAZ2I
563              TEZ2I=TEZ2*SIAZ2I
564        C                   EVALUATE EXP(Z**2)*ERFC(Z)
565          990 EZ2CZR=TEZ2R-EZ2CZR
566              EZ2CZI=EZ2CZI-TEZ2I
567         1000 IF (ZI-AZI) 1010,1020,1010
568        C                   IMAGINARY OF Z .LT. 0
569         1010 ERFZI=-ERFZI
570              ERFCZI=-ERFCZI
571              EZ2CZI=-EZ2CZI
572         1020 RETURN
573              END
```

TABLE 1

ERFC(Z)

RHO\THETA	0°	15°	30°	37.5°	45°
.00	.100000+01 .0	.100000+01 .000000	.100000+01 .000000	.100000+01 .000000	.100000+01 .000000
.02	.977435+00 .0	.978204+00 -.583879-02	.980456+00 -.112808-01	.982095+00 -.137355-01	.984040+00 -.159556-01
.04	.954889+00 .0	.956420+00 -.116648-01	.960912+00 -.225435-01	.964183+00 -.274543-01	.968068+00 -.318984-01
.06	.932378+00 .0	.934662+00 -.174654-01	.941368+00 -.337702-01	.946257+00 -.411398-01	.952070+00 -.478156-01
.08	.909922+00 .0	.912942+00 -.232279-01	.921824+00 -.449428-01	.928310+00 -.547751-01	.936033+00 -.636943-01
.10	.887537+00 .0	.891273+00 -.289397-01	.902280+00 -.560434-01	.910337+00 -.683437-01	.919946+00 -.795217-01
.12	.865242+00 .0	.869667+00 -.345886-01	.882738+00 -.670542-01	.892330+00 -.818288-01	.903796+00 -.952846-01
.14	.843053+00 .0	.848138+00 -.401625-01	.863197+00 -.779575-01	.874283+00 -.952136-01	.887571+00 -.110970+00
.16	.820988+00 .0	.826697+00 -.456493-01	.843657+00 -.887357-01	.856190+00 -.108481+00	.871258+00 -.126564+00
.18	.799064+00 .0	.805358+00 -.510376-01	.824121+00 -.993713-01	.838045+00 -.121615+00	.854845+00 -.142053+00
.20	.777297+00 .0	.784132+00 -.563161-01	.804590+00 -.109847+00	.819844+00 -.134598+00	.838321+00 -.157424+00
.30	.671373+00 .0	.680129+00 -.806921-01	.707071+00 -.159241+00	.727824+00 -.196662+00	.753652+00 -.231995+00
.40	.571608+00 .0	.580740+00 -.100871+00	.610081+00 -.202202+00	.633845+00 -.252418+00	.664672+00 -.301347+00
.50	.479500+00 .0	.487320+00 -.115988+00	.514270+00 -.236937+00	.537866+00 -.299764+00	.570447+00 -.363359+00
.60	.396144+00 .0	.401058+00 -.125565+00	.420627+00 -.261983+00	.440342+00 -.336667+00	.470518+00 -.415645+00
.70	.322199+00 .0	.322926+00 -.129533+00	.330478+00 -.276308+00	.342317+00 -.361274+00	.365070+00 -.455585+00
.80	.257899+00 .0	.253631+00 -.128213+00	.245436+00 -.279418+00	.245465+00 -.372052+00	.255106+00 -.480414+00
.90	.203092+00 .0	.193577+00 -.122258+00	.167296+00 -.271437+00	.152078+00 -.367979+00	.142621+00 -.487404+00
1.00	.157299+00 .0	.142847+00 -.112577+00	.978859-01 -.253165+00	.649787-01 -.348749+00	.307358-01 -.474148+00
1.10	.119795+00 .0	.101201+00 -.100228+00	.388720-01 -.226077+00	-.126659-01 -.314972+00	-.762502-01 -.438939+00
1.20	.896860-01 .0	.680972-01 -.863111-01	-.844458-02 -.192259+00	-.776217-01 -.268341+00	-.172938+00 -.381252+00
1.30	.659921-01 .0	.427427-01 -.718743-01	-.433244-01 -.154271+00	-.126958+00 -.211694+00	-.253111+00 -.302268+00
1.40	.477149-01 .0	.241557-01 -.578252-01	-.657413-01 -.114934+00	-.158478+00 -.148963+00	-.310259+00 -.205369+00
1.50	.338949-01 .0	.112438-01 -.448760-01	-.764609-01 -.770708-01	-.171150+00 -.849352-01	-.338390+00 -.965018-01
1.60	.236516-01 .0	.288326-02 -.335145-01	-.770202-01 -.432136-01	-.165475+00 -.248347-01	-.333094+00 .157600-01
1.70	.162095-01 .0	-.200643-02 -.240031-01	-.696000-01 -.153368-01	-.143694+00 .262601-01	-.292775+00 .120601+00
1.80	.109095-01 .0	-.440212-02 -.164025-01	-.567976-01 .535338-02	-.109748+00 .641075-01	-.219843+00 .205946+00
1.90	.720957-02 .0	-.513475-02 -.106123-01	-.413301-01 .185261-01	-.689521-01 .859866-01	-.121580+00 .260096+00
2.00	.467773-02 .0	-.486777-02 -.641967-02	-.257133-01 .247077-01	-.273484-01 .912368-01	-.103117-01 .273926+00
2.10	.297947-02 .0	-.409504-02 -.354979-02	-.119733-01 .251347-01	.916428-02 .815039-01	.974865-01 .243355+00
2.20	.186285-02 .0	-.315468-02 -.170957-02	-.144281-02 .215037-01	.358034-01 .605788-01	.183390+00 .171536+00
2.30	.114318-02 .0	-.225377-02 -.621965-03	.531949-02 .156622-01	.497620-01 .337876-01	.230486+00 .700421-01
2.40	.688514-03 .0	-.149843-02 -.481389-04	.847425-02 .930477-02	.507367-01 .700451-02	.227631+00 -.417236-01
2.50	.406952-03 .0	-.924217-03 .201683-03	.872881-02 .372996-02	.409438-01 -.145264-01	.173531+00 -.139462+00
2.60	.236034-03 .0	-.523179-03 .266848-03	.709056-02 -.293708-03	.245557-01 -.272819-01	.792740-01 -.199249+00
2.70	.134333-03 .0	-.265334-03 .241454-03	.460569-02 -.253794-02	.664754-02 -.301636-01	-.321336-01 -.204295+00
2.80	.750132-04 .0	-.113783-03 .183127-03	.214179-02 -.321372-02	-.809354-02 -.245881-01	-.130194+00 -.151392+00
2.90	.410979-04 .0	-.339435-04 .122861-03	.256793-03 -.279917-02	-.165397-01 -.138997-01	-.185124+00 -.545715-01
3.00	.220905-04 .0	.198248-05 .741051-04	-.830403-03 -.184961-02	-.178141-01 -.225516-02	-.178018+00 .564096-01
3.50	.743098-06 .0	.383634-05 -.331302-06	.361438-04 .343118-03	.663124-02 .774278-03	.146013+00 -.667835-01
4.00	.154173-07 .0	-.506480-07 -.121829-06	-.100583-04 -.454411-04	-.206887-02 .808579-03	-.704373-01 .121816+00
4.50	.196616-09 .0	-.172664-08 .241877-08	.342245-05 .358814-05	.149447-03 -.641621-03	-.697054-01 -.103987+00
5.00	.153746-11 .0	.431344-10 -.812606-11	-.410390-06 .690194-07	.163226-03 .593711-04	.909031-01 -.666628-01
5.50	.735785-14 .0	-.401550-12 -.137042-12	-.988539-10 -.274562-07	.529439-06 .406179-04	.945377-01 .396363-01
6.00	.215197-16 .0	.222076-14 .150084-14	.136924-08 -.383336-09	-.550781-05 .636094-05	.563713-01 .752047-01
6.50	.384215-19 .0	-.905982-17 -.633184-17	.477805-10 .324007-10	-.126107-05 .886874-06	.498547-01 .710156-01
7.00	.418383-22 .0	.276523-19 .109112-19	.941894-12 .157585-11	-.164519-06 .187753-06	.710858-01 .379415-01
7.50	.277665-25 .0	-.517996-22 .562585-23	.233092-13 .393021-13	.525818-10 .356932-07	.667858-01 -.345871-01
8.00	.112243-28 .0	.396093-25 -.443759-25	.731135-15 .506747-15	.420606-08 .160997-08	-.258232-01 -.656143-01
8.50	.276232-32 .0	.111560-28 .427748-28	.130972-16 -.343079-17	.123912-09 -.485650-09	-.475602-01 .462887-01
9.00	.413703-36 .0	-.213063-31 -.174915-32	.313042-20 -.160996-18	-.462157-10 .168052-10	.623821-01 -.612171-02

ERFC(Z)

RHO\THETA	50°		60°		70°		80°		90°
.00	.100000+01	.000000	.100000+01	.000000	.100000+01	.000000	.100000+01	.000000	.1+01	.000000
.02	.985491+00	-.172863-01	.988713+00	-.195441-01	.992279+00	-.212081-01	.996080+00	-.222273-01	.1+01	-.225706-01
.04	.970967+00	-.345635-01	.977408+00	-.390882-01	.984542+00	-.424252-01	.992150+00	-.444703-01	.1+01	-.451593-01
.06	.956411+00	-.518226-01	.966067+00	-.586322-01	.976774+00	-.636604-01	.988203+00	-.667446-01	.1+01	-.677841-01
.08	.941809+00	-.690545-01	.954672+00	-.781761-01	.968959+00	-.849226-01	.984228+00	-.890659-01	.1+01	-.904633-01
.10	.927144+00	-.862497-01	.943204+00	-.977195-01	.961080+00	-.106221+00	.980217+00	-.111450+00	.1+01	-.113215+00
.12	.912401+00	-.103399+00	.931646+00	-.117262+00	.953123+00	-.127564+00	.976160+00	-.133913+00	.1+01	-.136058+00
.14	.897565+00	-.120493+00	.919978+00	-.136803+00	.945070+00	-.148961+00	.972048+00	-.156471+00	.1+01	-.159011+00
.16	.882621+00	-.137521+00	.908183+00	-.156342+00	.936906+00	-.170421+00	.967870+00	-.179140+00	.1+01	-.182093+00
.18	.867552+00	-.154473+00	.896242+00	-.175878+00	.928612+00	-.191952+00	.963617+00	-.201936+00	.1+01	-.205323+00
.20	.852345+00	-.171339+00	.884135+00	-.195409+00	.920173+00	-.213564+00	.959279+00	-.224877+00	.1+01	-.228721+00
.30	.773712+00	-.253982+00	.820454+00	-.292919+00	.875153+00	-.323124+00	.935924+00	-.342344+00	.1+01	-.348949+00
.40	.689468+00	-.332643+00	.749698+00	-.389843+00	.823615+00	-.435932+00	.908660+00	-.466099+00	.1+01	-.476625+00
.50	.598041+00	-.405420+00	.669242+00	-.485367+00	.762712+00	-.552889+00	.875613+00	-.598673+00	.1+01	-.614952+00
.60	.498195+00	-.469950+00	.576286+00	-.578076+00	.688562+00	-.674665+00	.834330+00	-.742997+00	.1+01	-.767853+00
.70	.389205+00	-.523342+00	.467898+00	-.665719+00	.598036+00	-.801524+00	.781501+00	-.902533+00	.1+01	-.940283+00
.80	.271098+00	-.562163+00	.341135+00	-.744933+00	.484501+00	-.933057+00	.712565+00	-.108143+01	.1+01	-.113867+01
.90	.144933+00	-.582512+00	.193283+00	-.810912+00	.341532+00	-.106775+01	.621138+00	-.128468+01	.1+01	-.13715+01
1.00	.131385-01	-.580211+00	.222736-01	-.857061+00	.160625+00	-.120233+01	.498184+00	-.151831+01	.1+01	-.165043+01
1.10	-.120165+00	-.551166+00	-.172655+00	-.874670+00	-.686592-01	-.133079+01	.330784+00	-.178947+01	.1+01	-.199117+01
1.20	-.248882+00	-.491928+00	-.389989+00	-.852699+00	-.358812+00	-.144298+01	.100318+00	-.210652+01	.1+01	-.241591+01
1.30	-.364829+00	-.400481+00	-.624572+00	-.777828+00	-.724161+00	-.152248+01	-.220245+00	-.247879+01	.1+01	-.295609+01
1.40	-.457890+00	-.277246+00	-.865837+00	-.635009+00	-.118000+01	-.154380+01	-.670390+00	-.291589+01	.1+01	-.365696+01
1.50	-.516623+00	-.126215+00	-.109565+01	-.408856+00	-.174051+01	-.146840+01	-.130809+01	-.342593+01	.1+01	-.458473+01
1.60	-.529455+00	.439353-01	-.128600+01	-.863300-01	-.241452+01	-.123975+01	-.221880+01	-.401186+01	.1+01	-.583773+01
1.70	-.486589+00	.219059+00	-.139708+01	.338770+00	-.319777+01	-.777391+00	-.352885+01	-.466405+01	.1+01	-.756418+01
1.80	-.382619+00	.379468+00	-.137659+01	.859011+00	-.405945+01	.291660-01	-.542509+01	-.534607+01	.1+01	-.999112+01
1.90	-.219614+00	.501081+00	-.116196+01	.144402+01	-.492009+01	.132454+01	-.818351+01	-.596797+01	.1+01	-.134718+02
2.00	-.101646-01	.558267+00	-.687539+00	.202914+01	-.561710+01	.328529+01	-.122098+02	-.633691+01	.1+01	-.185648+02
2.10	.220530+00	.528666+00	.100155+00	.250402+01	-.585370+01	.610278+01	-.180944+02	-.606686+01	.1+01	-.261677+02
2.20	.434783+00	.399806+00	.121649+01	.270506+01	-.512891+01	.993582+01	-.266833+02	-.441546+01	.1+01	-.377471+02
2.30	.586112+00	.176582+00	.260024+01	.241951+01	-.265168+01	.148074+02	-.391538+02	.862691-02	.1+01	-.557397+02
2.40	.627560+00	-.112358+00	.406480+01	.141207+01	.274334+01	.204062+02	-.570679+02	.976572+01	.1+01	-.842631+02
2.50	.524677+00	-.412231+00	.524907+01	-.511462+00	.126293+02	.257378+02	-.823162+02	.294995+02	.1+01	-.130396+03
2.60	.271303+00	-.647141+00	.559076+01	-.339050+01	.288616+02	.285642+02	-.116747+03	.675244+02	.1+01	-.206519+03
2.70	-.961516-01	-.735197+00	.436233+01	-.694257+01	.530807+02	.245883+02	-.161012+03	.138532+03	.1+01	-.334671+03
2.80	-.492661+00	-.613886+00	.827238+00	-.103663+02	.854677+02	.644245+01	-.211587+03	.268092+03	.1+01	-.554777+03
2.90	-.794447+00	-.271241+00	-.542122+01	-.121876+02	.122167+03	-.371981+02	-.253771+03	.499853+03	.1+01	-.940470+03
3.00	-.870118+00	.227570+00	-.139065+02	-.102944+02	.150602+03	-.121463+03	-.246068+03	.906353+03	.1+01	-.162999+04
3.50	.128375+01	-.438817+00	.436770+02	.609546+02	-.185185+04	-.696951+03	.126726+05	.110011+05	.1+01	-.352823+05
4.00	-.143233+01	.176970+01	-.286672+03	-.315634+03	.142504+05	.268505+05	.414164+06	-.267047+06	.1+01	-.129696+07
4.50	-.153046+01	-.394580+01	.303475+04	.899044+03	-.581405+05	-.694896+06	-.104472+08	-.211627+08	.1+01	-.801975+08
5.00	.818979+01	-.289861+01	-.236016+05	.194203+05	-.301677+05	.237891+08	-.159723+10	.902680+09	.1+01	-.829827+10
5.50	.141149+02	.136673+02	-.192298+06	-.331209+06	-.279467+09	-.117057+10	.155714+12	.170313+12	.1+01	-.143210+13
6.00	.892289+01	.480481+02	.434927+07	-.444020+07	.640472+11	.633707+11	.196750+14	-.425327+14	.1+01	-.411275+15
6.50	.767743+01	.133290+03	.130111+09	.950077+07	-.992019+13	.967322+12	-.152018+17	.205488+16	.1+01	-.196225+18
7.00	.164446+03	.364872+03	.308919+10	.172358+10	.442269+15	-.156615+16	.619376+19	.519553+19	.1+01	-.155349+21
7.50	.126058+04	.375323+03	.107926+12	.606848+11	.371118+18	.125665+18	-.143772+22	-.670033+22	.1+01	-.203882+24
8.00	.231199+04	-.413300+04	.557097+13	.462008+12	-.785527+19	.138783+21	-.257275+25	.897512+25	.1+01	-.443245+27
8.50	-.181429+05	-.441024+04	.231401+15	-.228725+15	-.624892+23	.370071+23	.115166+29	-.168785+29	.1+01	-.159530+31
9.00	.404091+05	.697050+05	-.117844+17	-.213680+17	-.554262+26	-.688648+25	-.488030+32	.526592+32	.1+01	-.950078+34

TABLE 2

EXP(Z**2)*ERFC(Z)

RHO\THETA	0°	15°	30°	37.5°	45°
.00	.100000+01 .0	.100000+01 .000000	.100000+01 .000000	.100000+01 .000000	.100000+01 .000000
.02	.977826+00 .0	.978544+00 -.564511-02	.980656+00 -.109433-01	.982202+00 -.133574-01	.984046+00 -.155619-01
.04	.956418+00 .0	.957755+00 -.109148-01	.961711+00 -.212290-01	.964623+00 -.259749-01	.968117+00 -.303494-01
.06	.935741+00 .0	.937610+00 -.158323-01	.943165+00 -.308907-01	.947276+00 -.378843-01	.952236+00 -.443878-01
.08	.915764+00 .0	.918086+00 -.204192-01	.925014+00 -.399605-01	.930171+00 -.491167-01	.936422+00 -.577025-01
.10	.896457+00 .0	.899159+00 -.246960-01	.907257+00 -.484692-01	.913315+00 -.597018-01	.920696+00 -.703184-01
.12	.877791+00 .0	.880810+00 -.286817-01	.889890+00 -.564458-01	.896717+00 -.696688-01	.905075+00 -.822605-01
.14	.859740+00 .0	.863016+00 -.323942-01	.872908+00 -.639183-01	.880383+00 -.790455-01	.889575+00 -.935532-01
.16	.842277+00 .0	.845758+00 -.358502-01	.856308+00 -.709132-01	.864318+00 -.878590-01	.874212+00 -.104221+00
.18	.825378+00 .0	.829017+00 -.390656-01	.840085+00 -.774557-01	.848526+00 -.961353-01	.858998+00 -.114286+00
.20	.809020+00 .0	.812775+00 -.420551-01	.824233+00 -.835698-01	.833010+00 -.103900+00	.843946+00 -.123774+00
.30	.734559+00 .0	.738441+00 -.540691-01	.750340+00 -.108476+00	.759640+00 -.135855+00	.771453+00 -.163319+00
.40	.670788+00 .0	.674177+00 -.621855-01	.684812+00 -.125660+00	.693269+00 -.158259+00	.704192+00 -.191604+00
.50	.615690+00 .0	.618355+00 -.674592-01	.626815+00 -.137032+00	.633647+00 -.173298+00	.642609+00 -.210932+00
.60	.567805+00 .0	.569635+00 -.706620-01	.575515+00 -.144060+00	.580342+00 -.182718+00	.586778+00 -.223250+00
.70	.525930+00 .0	.526911+00 -.723596-01	.530125+00 -.147863+00	.532829+00 -.187900+00	.536524+00 -.230166+00
.80	.489101+00 .0	.489272+00 -.729681-01	.489917+00 -.149296+00	.490547+00 -.189926+00	.491521+00 -.232989+00
.90	.456532+00 .0	.455962+00 -.727939-01	.454239+00 -.149005+00	.452940+00 -.189631+00	.451358+00 -.232766+00
1.00	.427584+00 .0	.426354+00 -.720633-01	.422513+00 -.147478+00	.419480+00 -.187662+00	.415588+00 -.230320+00
1.10	.401730+00 .0	.399923+00 -.709434-01	.394231+00 -.145081+00	.389679+00 -.184510+00	.383760+00 -.226295+00
1.20	.378537+00 .0	.376233+00 -.695576-01	.368549+00 -.142050+00	.363094+00 -.180548+00	.355440+00 -.221186+00
1.30	.357643+00 .0	.354916+00 -.679971-01	.346284+00 -.138710+00	.339332+00 -.176056+00	.330223+00 -.215369+00
1.40	.338744+00 .0	.335662+00 -.663291-01	.325905+00 -.135093+00	.318044+00 -.171244+00	.307738+00 -.209128+00
1.50	.321585+00 .0	.318209+00 -.646029-01	.307525+00 -.131350+00	.298923+00 -.166267+00	.287653+00 -.202672+00
1.60	.305953+00 .0	.302334+00 -.628545-01	.290896+00 -.127564+00	.281701+00 -.161236+00	.269672+00 -.196156+00
1.70	.291663+00 .0	.287848+00 -.611100-01	.275808+00 -.123794+00	.266147+00 -.156235+00	.253535+00 -.189690+00
1.80	.278560+00 .0	.274589+00 -.593879-01	.262075+00 -.120081+00	.252058+00 -.151319+00	.239013+00 -.183351+00
1.90	.266509+00 .0	.262415+00 -.577015-01	.249540+00 -.116455+00	.239260+00 -.146528+00	.225908+00 -.177191+00
2.00	.255396+00 .0	.251208+00 -.560596-01	.238065+00 -.112935+00	.227600+00 -.141889+00	.214048+00 -.171246+00
2.10	.245119+00 .0	.240863+00 -.544681-01	.227532+00 -.109534+00	.216948+00 -.137417+00	.203282+00 -.165535+00
2.20	.235593+00 .0	.231289+00 -.529306-01	.217837+00 -.106258+00	.207188+00 -.133122+00	.193480+00 -.160068+00
2.30	.226742+00 .0	.222408+00 -.514490-01	.208891+00 -.103112+00	.198222+00 -.129008+00	.184530+00 -.154849+00
2.40	.218499+00 .0	.214150+00 -.500239-01	.200615+00 -.100095+00	.189963+00 -.125073+00	.176334+00 -.149876+00
2.50	.210806+00 .0	.206456+00 -.486549-01	.192941+00 -.972068-01	.182336+00 -.121315+00	.168808+00 -.145143+00
2.60	.203613+00 .0	.199271+00 -.473413-01	.185809+00 -.944437-01	.175275+00 -.117730+00	.161878+00 -.140642+00
2.70	.196874+00 .0	.192549+00 -.460815-01	.179166+00 -.918020-01	.168723+00 -.114311+00	.155479+00 -.136364+00
2.80	.190549+00 .0	.186248+00 -.448740-01	.172967+00 -.892774-01	.162630+00 -.111051+00	.149556+00 -.132298+00
2.90	.184602+00 .0	.180331+00 -.437168-01	.167168+00 -.868650-01	.156950+00 -.107943+00	.144061+00 -.128434+00
3.00	.179001+00 .0	.174766+00 -.426079-01	.161735+00 -.845599-01	.151645+00 -.104980+00	.138950+00 -.124761+00
3.50	.155294+00 .0	.151281+00 -.377161-01	.139036+00 -.744669-01	.129658+00 -.920841-01	.117989+00 -.108897+00
4.00	.136999+00 .0	.133241+00 -.337346-01	.121846+00 -.663430-01	.113196+00 -.817946-01	.102526+00 -.963790-01
4.50	.122485+00 .0	.118978+00 -.304579-01	.108404+00 -.597166-01	.100432+00 -.734593-01	.906646-01 -.863253-01
5.00	.110705+00 .0	.107435+00 -.277278-01	.976147-01 -.542350-01	.902530-01 -.666012-01	.812804-01 -.781076-01
5.50	.100962+00 .0	.979088-01 -.254257-01	.887699-01 -.496392-01	.819492-01 -.608758-01	.736702-01 -.712820-01
6.00	.927766-01 .0	.899189-01 -.234628-01	.813899-01 -.457386-01	.750469-01 -.560327-01	.673730-01 -.655313-01
6.50	.858057-01 .0	.831244-01 -.217720-01	.751399-01 -.423911-01	.692192-01 -.518878-01	.620749-01 -.606252-01
7.00	.798001-01 .0	.772774-01 -.203020-01	.697797-01 -.394900-01	.642331-01 -.483034-01	.575547-01 -.563934-01
7.50	.745737-01 .0	.721940-01 -.190134-01	.651322-01 -.369532-01	.599186-01 -.451749-01	.536520-01 -.527075-01
8.00	.699852-01 .0	.677345-01 -.178753-01	.610646-01 -.347176-01	.561483-01 -.424219-01	.502479-01 -.494694-01
8.50	.659251-01 .0	.637913-01 -.168633-01	.574747-01 -.327332-01	.528254-01 -.399814-01	.472522-01 -.466031-01
9.00	.623077-01 .0	.602800-01 -.159579-01	.542832-01 -.309606-01	.498745-01 -.378036-01	.445953-01 -.440484-01

EXP(Z**2)*ERFC(Z)

RHO\THETA	50°		60°		70°		80°		90°	
.00	.100000+01	.000000	.100000+01	.000000	.100000+01	.000000	.100000+01	.000000	.100000+01	.000000
.02	.985430+00	-.168969-01	.988522+00	-.191978-01	.991980+00	-.209465-01	.995708+00	-.220828-01	.999600+00	-.225616-01
.04	.970750+00	-.330243-01	.976680+00	-.377036-01	.983379+00	-.413619-01	.990684+00	-.438614-01	.998401+00	-.450871-01
.06	.955991+00	-.484013-01	.964508+00	-.555200-01	.974228+00	-.612308-01	.984947+00	-.653065-01	.996406+00	-.675405-01
.08	.941179+00	-.630470-01	.952039+00	-.726507-01	.964559+00	-.805399-01	.978518+00	-.863902-01	.993620+00	-.898862-01
.10	.926338+00	-.769813-01	.939307+00	-.891010-01	.954404+00	-.992775-01	.971421+00	-.107086+00	.990050+00	-.112089+00
.12	.911494+00	-.902242-01	.926342+00	-.104877+00	.943794+00	-.117434+00	.963679+00	-.127369+00	.985703+00	-.134113+00
.14	.896667+00	-.102796+00	.913175+00	-.119987+00	.932761+00	-.135001+00	.955317+00	-.147215+00	.980591+00	-.155925+00
.16	.881878+00	-.114717+00	.899834+00	-.134439+00	.921336+00	-.151972+00	.946360+00	-.166602+00	.974725+00	-.177491+00
.18	.867146+00	-.126007+00	.886348+00	-.148243+00	.909551+00	-.168342+00	.936834+00	-.185511+00	.968119+00	-.198777+00
.20	.852490+00	-.136687+00	.872742+00	-.161410+00	.897434+00	-.184108+00	.926768+00	-.203921+00	.960789+00	-.219753+00
.30	.780858+00	-.181638+00	.803774+00	-.218107+00	.832921+00	-.253864+00	.869300+00	-.287964+00	.913931+00	-.318916+00
.40	.713036+00	-.214294+00	.735131+00	-.260834+00	.764351+00	-.308806+00	.802581+00	-.357672+00	.852144+00	-.406153+00
.50	.649979+00	-.236926+00	.668830+00	-.291462+00	.694712+00	-.349876+00	.730181+00	-.412479+00	.778801+00	-.478925+00
.60	.592156+00	-.251548+00	.606260+00	-.311920+00	.626410+00	-.378484+00	.655426+00	-.452678+00	.697676+00	-.535713+00
.70	.539686+00	-.259892+00	.548281+00	-.324060+00	.561255+00	-.396308+00	.581214+00	-.479263+00	.612626+00	-.576042+00
.80	.492447+00	-.263412+00	.495329+00	-.329575+00	.500496+00	-.405125+00	.509895+00	-.493727+00	.527292+00	-.600412+00
.90	.450161+00	-.263301+00	.447520+00	-.329960+00	.444890+00	-.406682+00	.443222+00	-.497872+00	.444858+00	-.610142+00
1.00	.412460+00	-.260519+00	.404741+00	-.326488+00	.394786+00	-.402602+00	.382368+00	-.493623+00	.367879+00	-.607158+00
1.10	.378934+00	-.255830+00	.366725+00	-.320215+00	.350217+00	-.394324+00	.327976+00	-.482883+00	.298197+00	-.593761+00
1.20	.349161+00	-.249826+00	.333111+00	-.311994+00	.310985+00	-.383080+00	.280243+00	-.467415+00	.236928+00	-.572397+00
1.30	.322730+00	-.242965+00	.303494+00	-.302503+00	.276740+00	-.369883+00	.239021+00	-.448772+00	.184520+00	-.545456+00
1.40	.299256+00	-.235593+00	.277452+00	-.292262+00	.247038+00	-.355543+00	.203909+00	-.428255+00	.140858+00	-.515113+00
1.50	.278384+00	-.227969+00	.254575+00	-.281666+00	.221396+00	-.340682+00	.174350+00	-.406909+00	.105399+00	-.483227+00
1.60	.259793+00	-.220280+00	.234476+00	-.271004+00	.199324+00	-.325767+00	.149701+00	-.385528+00	.773047-01	-.451284+00
1.70	.243198+00	-.212662+00	.216798+00	-.260483+00	.180352+00	-.311128+00	.129300+00	-.364688+00	.555762-01	-.420388+00
1.80	.228349+00	-.205210+00	.201224+00	-.250247+00	.164045+00	-.296992+00	.112501+00	-.344773+00	.391639-01	-.391291+00
1.90	.215025+00	-.197986+00	.187470+00	-.240389+00	.150014+00	-.283502+00	.987098-01	-.326022+00	.270518-01	-.364437+00
2.00	.203034+00	-.191033+00	.175289+00	-.230965+00	.137912+00	-.270739+00	.873971-01	-.308553+00	.183156-01	-.340026+00
2.10	.192211+00	-.184372+00	.164467+00	-.222006+00	.127441+00	-.258737+00	.781048-01	-.292400+00	.121552-01	-.318073+00
2.20	.182411+00	-.178015+00	.154819+00	-.213521+00	.118345+00	-.247499+00	.704459-01	-.277541+00	.790705-02	-.298468+00
2.30	.173510+00	-.171964+00	.146185+00	-.205507+00	.110409+00	-.237007+00	.641001-01	-.263913+00	.504176-02	-.281026+00
2.40	.165400+00	-.166214+00	.138430+00	-.197951+00	.103450+00	-.227227+00	.588065-01	-.251431+00	.315111-02	-.265522+00
2.50	.157988+00	-.160758+00	.131439+00	-.190836+00	.973162-01	-.218118+00	.543547-01	-.240002+00	.193045-02	-.251723+00
2.60	.151195+00	-.155584+00	.125111+00	-.184138+00	.918812-01	-.209636+00	.505775-01	-.229528+00	.115923-02	-.239403+00
2.70	.144950+00	-.150680+00	.119364+00	-.177833+00	.870395-01	-.201733+00	.473424-01	-.219915+00	.682328-03	-.228355+00
2.80	.139193+00	-.146031+00	.114124+00	-.171899+00	.827037-01	-.194364+00	.445450-01	-.211075+00	.393669-03	-.218399+00
2.90	.133871+00	-.141624+00	.109330+00	-.166309+00	.788013-01	-.187486+00	.421033-01	-.202926+00	.222630-03	-.209377+00
3.00	.128940+00	-.137445+00	.104930+00	-.161041+00	.752717-01	-.181058+00	.399530-01	-.195396+00	.123410-03	-.201157+00
3.50	.108892+00	-.119509+00	.874505-01	-.138780+00	.617088-01	-.154443+00	.321214-01	-.165001+00	.478512-05	-.168830+00
4.00	.942797-01	-.105481+00	.750909-01	-.121741+00	.525024-01	-.134607+00	.270928-01	-.143006+00	.112535-06	-.145954+00
4.50	.831655-01	-.942896-01	.658787-01	-.108356+00	.458048-01	-.119295+00	.235275-01	-.126308+00	.160523-08	-.128735+00
5.00	.744259-01	-.851875-01	.587346-01	-.975919-01	.406890-01	-.107125+00	.208412-01	-.113170+00	.138879-10	-.115246+00
5.50	.673700-01	-.776560-01	.530232-01	-.887581-01	.366399-01	-.972205-01	.187325-01	-.102546+00	.728772-13	-.104367+00
6.00	.615511-01	-.713293-01	.483467-01	-.813834-01	.333477-01	-.890010-01	.170271-01	-.937703-01	.231952-15	-.953962-01
6.50	.566679-01	-.659441-01	.444434-01	-.751362-01	.306137-01	-.820692-01	.156161-01	-.863935-01	.447773-18	-.878644-01
7.00	.525101-01	-.613075-01	.411335-01	-.697775-01	.283042-01	-.761436-01	.144276-01	-.801029-01	.524289-21	-.814475-01
7.50	.489261-01	-.572750-01	.382898-01	-.651309-01	.263257-01	-.710192-01	.134115-01	-.746733-01	.372336-24	-.759126-01
8.00	.458040-01	-.537368-01	.358190-01	-.610637-01	.246107-01	-.665434-01	.125322-01	-.699379-01	.160381-27	-.710891-01
8.50	.430594-01	-.506078-01	.336516-01	-.574741-01	.231091-01	-.626001-01	.117632-01	-.657709-01	.419009-31	-.668445-01
9.00	.406273-01	-.478214-01	.317343-01	-.542828-01	.217828-01	-.590993-01	.110848-01	-.620752-01	.663968-35	-.630821-01

TABLE 3

EXP(Z**2)*ERFC(-Z)

RHO\THETA	0°	15°		30°		37.5°		45°	
.00	.100000+01 .0	.100000+01	.000000	.100000+01	.000000	.100000+01	.000000	.100000+01	.000000
.02	.102297+01 .0	.102215+01	.604525-02	.101974+01	.116363-01	.101801+01	.141302-01	.101595+01	.163619-01
.04	.104678+01 .0	.104502+01	.125170-01	.103989+01	.240025-01	.103620+01	.290671-01	.103188+01	.335494-01
.06	.107147+01 .0	.106863+01	.194435-01	.106043+01	.371373-01	.105458+01	.448455-01	.104775+01	.515878-01
.08	.109708+01 .0	.109302+01	.268548-01	.108137+01	.510811-01	.107311+01	.615C09-01	.106354+01	.705024-01
.10	.112364+01 .0	.111821+01	.347829-01	.110269+01	.658763-01	.109177+01	.790701-01	.107920+01	.903181-01
.12	.115122+01 .0	.114424+01	.432622-01	.112441+01	.815669-01	.111056+01	.975904-01	.109472+01	.111059+00
.14	.117985+01 .0	.117112+01	.523294-01	.114650+01	.981992-01	.112943+01	.117100+00	.111004+01	.132751+00
.16	.120958+01 .0	.119891+01	.620234-01	.116896+01	.115821+00	.114836+01	.137638+00	.112513+01	.155415+00
.18	.124048+01 .0	.122763+01	.723862-01	.119178+01	.134483+00	.116733+01	.159244+00	.113995+01	.179075+00
.20	.127260+01 .0	.125731+01	.834622-01	.121495+01	.154237+00	.118629+01	.181958+00	.115445+01	.203753+00
.30	.145375+01 .0	.142149+01	.151332+00	.133536+01	.271371+00	.127976+01	.313595+00	.122045+01	.343076+00
.40	.167623+01 .0	.161572+01	.245769+00	.146100+01	.424910+00	.136645+01	.479143+00	.127026+01	.510240+00
.50	.195236+01 .0	.184573+01	.377084+00	.158657+01	.623876+00	.143813+01	.683551+00	.129522+01	.705740+00
.60	.229885+01 .0	.211791+01	.559713+00	.170349+01	.878536+00	.148357+01	.930808+00	.128502+01	.927798+00
.70	.273870+01 .0	.243899+01	.813903+00	.179848+01	.119994+01	.148800+01	.122283+01	.122814+01	.117142+01
.80	.330386+01 .0	.281529+01	.116807+01	.185201+01	.159889+01	.143293+01	.155787+01	.111267+01	.142738+01
.90	.403928+01 .0	.325121+01	.166206+01	.183636+01	.208415+01	.129634+01	.192846+01	.927639+00	.168134+01
1.00	.500898+01 .0	.374645+01	.235168+01	.171377+01	.265934+01	.105379+01	.231879+01	.665017+00	.191326+01
1.10	.630524+01 .0	.429102+01	.331474+01	.143482+01	.331817+01	.680682+00	.270192+01	.322278+00	.209753+01
1.20	.806285+01 .0	.485657+01	.465908+01	.938062+00	.403754+01	.156290+00	.303701+01	-.945930-01	.220410+01
1.30	.104813+02 .0	.538160+01	.653258+01	.151941+00	.476793+01	-.530066+00	.326754+01	-.568066+00	.220118+01
1.40	.138599+02 .0	.574679+01	.913501+01	-.998816+00	.542135+01	-.137052+01	.332164+01	-.106664+01	.205955+01
1.50	.186539+02 .0	.573426+01	.127298+02	-.257974+01	.585743+01	-.232809+01	.311621+01	-.154400+01	.175882+01
1.60	.255657+02 .0	.496175+01	.176520+02	-.462254+01	.587039+01	-.332543+01	.256681+01	-.194085+01	.129487+01
1.70	.356950+02 .0	.277771+01	.243017+02	-.708673+01	.518191+01	-.423536+01	.160541+01	-.219057+01	.687583+00
1.80	.507889+02 .0	-.190182+01	.331040+02	-.980423+01	.344908+01	-.487786+01	.206798+00	-.222934+01	-.131466-01
1.90	.736656+02 .0	-.108404+02	.443947+02	-.124081+02	.301777+00	-.502963+01	-.157716+01	-.201049+01	-.725740+00
2.00	.108941+03 .0	-.268411+02	.581561+02	-.142543+02	-.457055+01	-.445375+01	-.358054+01	-.152134+01	-.134236+01
2.10	.164294+03 .0	-.542404+02	.734660+02	-.143607+02	-.112629+02	-.295578+01	-.549415+01	-.798885+00	-.174372+01
2.20	.252703+03 .0	-.995202+02	.874162+02	-.114096+02	-.194032+02	-.468263+00	-.686146+01	.610500-01	-.182367+01
2.30	.396460+03 .0	-.171913+03	.930880+02	-.389141+01	-.278220+02	.284504+01	-.712231+01	.907518+00	-.152069+01
2.40	.634478+03 .0	-.283609+03	.759226+02	.950566+01	-.341808+02	.649023+01	-.572745+01	.155613+01	-.849408+00
2.50	.103581+04 .0	-.448599+03	.748935+01	.291411+02	-.347103+02	.959591+01	-.233541+01	.183009+01	.787847-01
2.60	.172508+04 .0	-.677955+03	-.164667+03	.532363+02	-.243320+02	.109818+02	.292473+01	.161505+01	.105855+01
2.70	.293094+04 .0	-.967019+03	-.532419+03	.763516+02	.239913+01	.941085+01	.919036+01	.913632+00	.182663+01
2.80	.508022+04 .0	-.126560+04	-.124780+04	.879744+02	.489857+02	.405857+01	.147289+02	-.121594+00	.213210+01
2.90	.898334+04 .0	-.141486+04	-.254465+04	.722456+02	.112885+03	-.485116+01	.171054+02	-.119568+01	.182716+01
3.00	.162060+05 .0	-.102319+04	-.474402+04	.105895+02	.179798+03	-.154399+02	.138266+02	-.196121+01	.948998+00
3.50	.417962+06 .0	.759689+05	-.127565+05	-.345002+03	-.846681+03	.352504+02	-.318118+02	.178275+01	-.513342+00
4.00	.177722+08 .0	-.303148+06	.206132+07	.165184+04	.572854+04	-.121850+03	.315751+02	-.201785+01	-.479428+00
4.50	.124593+10 .0	-.632047+08	-.532606+08	.127488+05	-.482630+05	.286262+03	.246430+03	.248394+00	.205738+01
5.00	.144010+12 .0	.504457+10	-.335304+09	-.505861+06	.179234+06	.714413+03	-.107588+04	.190113+01	-.186596+00
5.50	.274434+14 .0	-.398070+12	.262492+12	.359254+07	.647923+07	-.294447+04	-.407345+04	.714128+00	-.176703+01
6.00	.862246+16 .0	.457872+14	-.520744+14	.127587+09	-.310891+08	-.217456+05	-.476709+04	-.323300+00	-.191803+01
6.50	.446655+19 .0	-.100716+17	.118452+17	.133025+10	-.267648+10	-.112172+06	.340422+04	-.383674+00	-.191335+01
7.00	.381469+22 .0	.433489+19	-.317887+19	.207375+10	-.873217+11	-.630212+06	-.132005+06	.543630+00	-.185111+01
7.50	.537149+25 .0	-.283374+22	.426347+21	.630673+11	-.327704+13	-.252634+07	-.336114+07	.185781+01	-.535787+00
8.00	.124703+29 .0	.196497+25	.129886+25	.683728+14	-.142358+15	.165524+08	-.265076+08	.733467+00	.188952+01
8.50	.477316+32 .0	-.989764+25	-.298524+28	.943832+16	-.252614+16	.206701+09	.164806+09	-.204721+01	.598650-01
9.00	.301219+36 .0	-.549838+31	.194934+31	.397576+18	.666613+18	-.243169+10	.751742+09	.150878+01	-.121573+01

EXP(Z**2)*ERFC(-Z)

RHO\THETA	50°		60°		70°		80°		90°	
.00	.100000+01	.000000	.100000+01	.000000	.100000+01	.000000	.100000+01	.000000	.100000+01	.000000
.02	.101443+01	.176847-01	.101108+01	.198904-01	.100741+01	.214606-01	.100354+01	.223563-01	.999600+00	.225616-01
.04	.102869+01	.361748-01	.102172+01	.404727-01	.101417+01	.434163-01	.100631+01	.449542-01	.998401+00	.450871-01
.06	.104275+01	.554874-01	.103189+01	.617442-01	.102026+01	.658462-01	.100830+01	.677607-01	.996406+00	.675405-01
.08	.105656+01	.756385-01	.104154+01	.837004-01	.102564+01	.887273-01	.100949+01	.907418-01	.993620+00	.898862-01
.10	.107009+01	.966430-01	.105064+01	.106335+00	.103029+01	.112035+00	.100986+01	.113862+00	.990050+00	.112089+00
.12	.108331+01	.118515+00	.105916+01	.129639+00	.103418+01	.135743+00	.100942+01	.137086+00	.985703+00	.134113+00
.14	.109617+01	.141267+00	.106704+01	.153603+00	.103728+01	.159822+00	.100814+01	.160377+00	.980591+00	.155925+00
.16	.110862+01	.164910+00	.107424+01	.178212+00	.103956+01	.184242+00	.100603+01	.183697+00	.974725+00	.177491+00
.18	.112062+01	.189453+00	.108074+01	.203453+00	.104100+01	.208971+00	.100307+01	.207609+00	.968119+00	.198777+00
.20	.113213+01	.214906+00	.108648+01	.229307+00	.104157+01	.233974+00	.999272+00	.230273+00	.960789+00	.219753+00
.30	.118040+01	.355926+00	.110242+01	.366982+00	.103071+01	.361797+00	.967640+00	.344526+00	.913931+00	.318916+00
.40	.120806+01	.519531+00	.109341+01	.515837+00	.995593+00	.490450+00	.915655+00	.451794+00	.852144+00	.406153+00
.50	.120731+01	.703662+00	.105496+01	.670616+00	.935432+00	.614113+00	.845306+00	.547520+00	.778801+00	.478925+00
.60	.116980+01	.903774+00	.983747+00	.824347+00	.851095+00	.726620+00	.759756+00	.627812+00	.697676+00	.535713+00
.70	.108743+01	.111228+01	.878285+00	.968587+00	.745231+00	.821976+00	.663105+00	.689772+00	.612626+00	.576042+00
.80	.953336+00	.131817+01	.739549+00	.109394+01	.622230+00	.894945+00	.560035+00	.731740+00	.527292+00	.600412+00
.90	.763292+00	.150697+01	.571471+00	.119083+01	.487972+00	.941619+00	.455412+00	.753397+00	.444858+00	.610142+00
1.00	.517275+00	.166123+01	.381152+00	.125055+01	.349369+00	.959889+00	.353863+00	.755730+00	.367879+00	.607158+00
1.10	.221086+00	.176167+01	.178694+00	.126642+01	.213743+00	.949748+00	.259408+00	.740868+00	.298197+00	.593761+00
1.20	-.112292+00	.178923+01	-.234440-01	.123493+01	.881139-01	.913353+00	.175175+00	.711800+00	.236928+00	.572397+00
1.30	-.462011+00	.172780+01	-.211562+00	.115668+01	-.215044-01	.854822+00	.103231+00	.672034+00	.184520+00	.545456+00
1.40	-.799794+00	.156770+01	-.372237+00	.103688+01	-.110704+00	.779790+00	.445420-01	.625237+00	.140858+00	.515113+00
1.50	-.109192+01	.130926+01	-.494065+00	.885190+00	-.177075+00	.694764+00	-.945684-03	.574901+00	.105399+00	.483227+00
1.60	-.130302+01	.965812+00	-.569332+00	.714952+00	-.220337+00	.606395+00	-.341317-01	.524075+00	.773047-01	.451284+00
1.70	-.140154+01	.565275+00	-.595323+00	.541594+00	-.242190+00	.520751+00	-.565267-01	.475193+00	.555762-01	.420388+00
1.80	-.136640+01	.149150+00	-.574932+00	.380624+00	-.245914+00	.442725+00	-.699973-01	.429992+00	.391639-01	.391291+00
1.90	-.119347+01	-.231426+00	-.516381+00	.245402+00	-.235801+00	.375650+00	-.765256-01	.389521+00	.270518-01	.364437+00
2.00	-.900424+00	-.523642+00	-.432005+00	.145177+00	-.216510+00	.321167+00	-.780102-01	.354223+00	.183156-01	.340026+00
2.10	-.527958+00	-.682837+00	-.336258+00	.837718-01	-.192467+00	.279344+00	-.761241-01	.324056+00	.121552-01	.318073+00
2.20	-.135761+00	-.683750+00	-.243313+00	.592582-01	-.167392+00	.248596+00	-.722347-01	.298640+00	.790705-02	.298468+00
2.30	.207215+00	-.529536+00	-.164751+00	.647151-01	-.144014+00	.228112+00	-.673774-01	.277393+00	.504176-02	.281026+00
2.40	.437243+00	-.255605+00	-.107845+00	.899283-01	-.123586+00	.214327+00	-.622737-01	.259650+00	.315111-02	.265522+00
2.50	.512073+00	.744257-01	-.748106-01	.123641+00	-.107586+00	.205321+00	-.573770-01	.244750+00	.193045-02	.251723+00
2.60	.424377+00	.381557+00	-.631827-01	.155822+00	-.959278-01	.199114+00	-.529309-01	.232099+00	.115923-02	.239403+00
2.70	.207358+00	.591072+00	-.671444-01	.179408+00	-.872383-01	.194224+00	-.490308-01	.221154+00	.682328-03	.228355+00
2.80	-.711724-01	.654101+00	-.794229-01	.191148+00	-.811203-01	.189696+00	-.456768-01	.211636+00	.393669-03	.218399+00
2.90	-.326684+00	.563991+00	-.932090-01	.191421+00	-.767654-01	.185036+00	-.428169-01	.203120+00	.222630-03	.209377+00
3.00	-.483674+00	.360592+00	-.103604+00	.183219+00	-.734511-01	.180089+00	-.403769-01	.195423+00	.123410-03	.201157+00
3.50	.999905-01	.472332-02	-.891007-01	.134728+00	-.617122-01	.154611+00	-.321314-01	.164984+00	.478512-05	.168830+00
4.00	-.218410+00	.993987-01	-.749050-01	.122386+00	-.525086-01	.134600+00	-.270923-01	.143006+00	.112535-06	.145954+00
4.50	-.558352-01	.147044+00	-.658583-01	.108279+00	-.458045-01	.119295+00	-.235275-01	.126308+00	.160523-08	.128735+00
5.00	-.517307-01	.724167-01	-.587417-01	.975944-01	-.406890-01	.107125+00	-.208412-01	.113170+00	.138879-10	.115246+00
5.50	-.679421-01	.672066-01	-.530230-01	.887586-01	-.366399-01	.972205-01	-.187325-01	.102546+00	.728772-13	.104367+00
6.00	-.639612-01	.683196-01	-.483467-01	.813834-01	-.333477-01	.890010-01	-.170271-01	.937703-01	.231952-15	.953962-01
6.50	-.576053-01	.650398-01	-.444434-01	.751362-01	-.306137-01	.820692-01	-.156161-01	.863935-01	.447773-18	.878644-01
7.00	-.526816-01	.609424-01	-.411335-01	.697775-01	-.283042-01	.761436-01	-.144276-01	.801029-01	.524289-21	.814475-01
7.50	-.488796-01	.571703-01	-.382898-01	.651309-01	-.263257-01	.710192-01	-.134115-01	.746733-01	.372336-24	.759126-01
8.00	-.457747-01	.537426-01	-.358190-01	.610637-01	-.246107-01	.665434-01	-.125322-01	.699379-01	.160381-27	.710881-01
8.50	-.430626-01	.506142-01	-.336516-01	.574741-01	-.231091-01	.626001-01	-.117632-01	.657709-01	.419009-31	.668445-01
9.00	-.406279-01	.478200-01	-.317343-01	.542828-01	-.217828-01	.590993-01	-.110848-01	.620752-01	.663968-35	.630821-01